IDENTIFICATION OF POWERED PARAFOIL-VEHICLE DYNAMICS

FROM MODELLING AND FLIGHT TEST DATA

A Dissertation

by

GI-BONG HUR

Submitted to the Office of Graduate Studies of
Texas A&M University
in partial fulfillment of the requirements for the degree of

DOCTOR OF PHILOSOPHY

May 2005

Major Subject: Aerospace Engineering

IDENTIFICATION OF POWERED PARAFOIL-VEHICLE DYNAMICS

FROM MODELLING AND FLIGHT TEST DATA

A Dissertation

by

GI-BONG HUR

Submitted to Texas A&M University
in partial fulfillment of the requirements
for the degree of

DOCTOR OF PHILOSOPHY

Approved as to style and content by:

_____
John Valasek
(Chair of Committee)

_____
Donald Ward
(Member)

_____
John Junkins
(Member)

_____
John Painter
(Member)

_____
Helen Reed
(Head of Department)

May 2005

Major Subject: Aerospace Engineering

ABSTRACT

Identification of Powered Parafoil-Vehicle Dynamics from Modelling and Flight Test
Data. (May 2005)
Gi-Bong Hur, B.S.; M.S., Seoul National University, Korea
Chair of Advisory Committee: Dr. John Valasek

During the final approach and landing phase of the X-38/Crew Return Vehicle, a
steerable parafoil is used to maneuver and land at a targeted ground base under
autonomous control. To simulate and verify performance of the onboard Parafoil
Guidance, Navigation and Control system (PGNC), a commercial powered parafoil-
vehicle, called the Buckeye consisting of a parafoil and vehicle two-body system like
the X-38/CRV was modified to accommodate the avionics and scale-downed parafoil
for aerodynamic similarity and a series of flight tests were conducted.

Dynamic modelling and system identification results for the Buckeye are de-
scribed in this dissertation. The vehicle dynamics are modelled as all 8 degrees-of-
freedom system comprising 6 states for the parafoil and 2 states for the relative pitch
and yaw motion of the vehicle with respect to the parafoil. Modal analysis for the
linearized model from the nonlinear model shows the number and order of dynamic
modes as well as the system is controllable and observable. For system identifica-
tion, the overparameterized Observer/Kalman Filter Identification (OKID) method
is applied to identify a linear model of the Buckeye two-body system from the flight
data assuming that disturbances at a calm day are represented as periodic distur-
bances. The identification results show that the overparameterized OKID works well
for powered parafoil-vehicle two-body system identification under calm day condi-
tions using flight data. For the data with possible discrete gusts the OKID shows
limitation to identify a linearized model properly. Several sensor packages including
airdata and Inertial Measurement Unit are designed and installed for the parameters
for identification. The sensor packages successfully supply data of the parameters for
identification and suggest a feasible, low cost method for the parafoil-vehicle two-body
dynamic parameters.

With love,

this dissertation is dedicated to

my mother who has sacrificed all her life for her children,

my wife Eunju,

my adorable kids Yoonjung and Jaewon, and

my parents-in-law who presented me more than a lovely wife.

ACKNOWLEDGMENTS

TABLE OF CONTENTS

LIST OF TABLES

LIST OF FIGURES

FIGURE   Page

FIGURE   Page

CHAPTER I

INTRODUCTION AND BACKGROUND

Because of its low speed handling qualities and versatility of application for precision aerial delivery and recovery of payloads, the parafoil has been used in many areas from leisure to more sophisticated aerial recovery. Much research has been done at NASA Johnson Space Center to describe the dynamic behavior of the parafoil and to develop guidance and control algorithms using wind tunnel tests, ground tow tests and actual aerial drop tests.[1–4] In Europe, the Institute of Flight Research of the German Aerospace Center (DLR) has conducted research to identify the dynamic behavior of a parafoil-payload system and to investigate Guidance Navigation and Control (GNC) concepts.[5–8] They used three degrees-of-freedom (DOF) and four-DOF models for their own parafoil-payload system, ALEX(Autonomous Landing Experiment)-I and -II, to apply system identification algorithms and GNC designs.[6] The ALEX system is to be dropped from a helicopter to acquire flight data at 10 Hz. The flight data were reconstructed with constant wind assumption and used for system identification based on 3-DOF and 4-DOF model in which the relative motion was not accounted. Recently Slegers and Costello studied on the dynamic modelling of the parafoil with 9-DOF, including three inertial positions of the joint as well as the three Euler angles of the parafoil and the payload.[9] In the research both the parafoil and the payload are free to rotate about joint but are constrained by the force and the twisting torque due to relative yaw angle only at the joint. They used reduced state linear model based on a nonlinear 6-DOF parafoil and payload model to apply for the predictive control design.[10] In the research the parafoil and the payload were modelled as a single rigid body without relative motion. Meanwhile, NASA acquired a self-powered Buckeye parafoil-vehicle as a test bed, which was modified by Southwest Research

This dissertation follows the style and format of the *Journal of Guidance, Control, and Dynamics.*

Figure 1.1 Buckeye Unmanned Powered Parafoil Test Bed in Flight

Institute (SwRI) to accommodate the Parafoil Guidance, Navigation and Control (PGNC) computer (Figure 1.1) as well as other avionics instruments. Since it can climb to target altitudes repeatedly by its own power, the Buckeye is very useful and cost effective in obtaining flight data for the parafoil as well as PGNC parameters, such as PGNC commands and errors. In addition, the Buckeye can give reliable and repeatable flight data for identification provided that required parameters are acquired from proper sensor instrumentations, which could not be done in previous researches. The modified Buckeye vehicle is being evaluated using the flight test facilities of the Texas A&M University Flight Mechanics Laboratory.

The Observer/Kalman Filter Identification (OKID) methodology was selected

for identification of the longitudinal and lateral/directional dynamical models of the Buckeye parafoil-vehicle system from flight data. OKID is a time domain technique which identifies a discrete input/output mapping from known input output data records. Since first being developed by Juang in the early 1990's,[11] the method has been successfully employed to identify linear system models of flexible spacecraft structures[12–14] and aircraft.[15] Chen and Valasek applied the method for on-line system identification of six-DOF simulated aircraft dynamics, and found it is suitable for identification of linear aircraft models even without perfect trim conditions and in the presence of turbulence.[15] As the Buckeye flight is power-off gliding, it is supposed to be vulnerable to atmospheric disturbance including discrete gusts and stochastic atmospheric turbulence. To identify the system under disturbance an overparametrized OKID method[16,17] for unknown periodic disturbance was applied to calm day flight data assuming that the stochastic atmospheric disturbance at calm day can be represented by combination of a number of periodic disturbances.

In this research, the dynamics of the Buckeye vehicle are modelled with eight degrees-of-freedom: six for the parafoil, and two for the relative pitch and yaw attitudes of the vehicle. The parafoil and the vehicle are assumed as rigid bodies and the elasticity of the risers and suspension lines are ignored in modelling. Instrumentation was designed and installed to measure the states that describe eight-DOF motion of the Buckeye-vehicle, including an Inertial Measurement Unit (IMU) for attitudes and body-rate data, and a multi-function Aeroprobe flow sensor which measures angle-of-attack, sideslip angle, and static and dynamic pressures . Optical position sensing techniques such as the VisNav vision-based relative position sensor[18] and video camera imaging systems[7] were not selected for calculating the relative yaw angle because of availability and/or post processing requirements. Instead, a series of accelerometers are installed in the mid-section of the parafoil for the pitch and yaw angle of the parafoil. Relative yaw angles are then calculated by comparing the sideslip angle of the vehicle and that of the parafoil reduced from side velocity by integrating the lateral accelerometer outputs. Prior to flight testing, the OKID method was evaluated via simulation using the 8-DOF Parafoil Dynamic Simulator (PDS) , and with previously recorded Buckeye flight data. Identification results of these evaluations for

longitudinal and lateral/directional motions are presented also.

1.1   Research Objectives

Most of the researches mentioned above have been focused on the dynamics and guidance performance problem of total system in which the parafoil and the payload are regarded as one body neglecting relative motion between them. The limitation of the researches for modelling and flight test seem to be caused by the difficulty in acquiring parameters of the parafoil itself in flight data. As mentioned in some researches[7,8] the dynamic characteristics are closely related to the kinematical interaction between the two bodies. In this research a low cost, feasible sensor package is designed and installed to supply parameters of the parafoil as well as for the vehicle. As all the required parameters are available from the Buckeye flight data, the study on the dynamics of the parafoil is mainly focused other than other researches. A systematic analytical and computational study, including flight tests, was undertaken with the following objectives:

1. Develop a nonlinear analytical model of a parafoil-vehicle two-body system, verified by an identified linear model from flight test data.

2. Evaluate the suitability of the OKID method for identification of flight dynamics from flight test data.

In this research the parafoil and the vehicle are assumed as rigid bodies and the dynamics of the Buckeye-vehicle are to be modelled with eight-DOF: six for the parafoil and two for the relative pitch and yaw attitudes of the vehicle. The risers and suspension lines connecting the two bodies are of very flexible nature and nonlinearity. Nevertheless here the risers and suspension lines are regarded as rigid bodies and the assumption is justified in Ref. 8 by following reasons:

- Many possible motions are restricted or prevented by combining single lines or belts to functional units.

- Used materials offer practically no lengthening when stressed in normal operating condition; their modulus of elasticity is of the size of steel.

- Lift of the parafoil and weight of the vehicle produce an initial tension in risers and suspension lines which is increased by maneuvering loads; sagging is not to fear.

- Mechanical constraints additionally brace the connections between the parafoil and the vehicle.

As the risers and suspension lines are assumed as rigid bodies the relative roll motion between the parafoil and the vehicle can be ignored and this corresponds to observations from flight tests.

Sensors for airdata and inertial parameters for the hanging vehicle were installed, and accelerometers and remote data acquisition system for the parafoil were acquired and installed. As sensor weight can cause possible deformation of the parafoil inducing change of aerodynamic shape, sensor installation on the flexible parafoil is very limited. With the minimum installation of accelerometers and integrating those data, body rates as well as attitudes for the parafoil can be reduced. In addition to the sensors on the parafoil, 5-hole multifunction probe and Inertial Measurement Unit (IMU) installed in the hanging vehicle supply time histories of states consisting of eight-DOF of motion during the flight. Pre-flight tests for investigating the proper control inputs were done. The OKID method has been applied to the eight-DOF simulation results from the PDS and the analytical model and some flight data for system identification. Further investigation for the OKID application to actual flight test data, which include sensor noise and disturbances, are conducted. The following tasks are committed to accomplish the research objectives:

1. Deriving nonlinear and linear analytical model and conducting system analysis

2. Experiment design, including sensor selection and installation to measure observable dynamic parameters of the two-body system

3. Analytical and computational study using the nonlinear simulation for generation of test inputs to identify the parafoil-vehicle dynamics

4. Conduct flight tests and data reduction for various conditions, and apply the OKID algorithm

5. Verify the analytical model describing the parafoil-vehicle dynamics from identification of flight test data

1.2 Flight Test Vehicle Description

The flight test vehicle, Buckeye was manufactured by a Buckeye Aviation Inc. for leisure purpose. Originally it accommodates one or two pilot seats and has endurance of +3 hours with 10 gallons of fuel for fun flight. It has 65 hp water cooled Rotax 582 piston engine for powerplant, providing 600-800 fpm climb rate. (figure 1.2).

As the Buckeye system is relatively simple to operate and flexible to modify, NASA and Southwest Research Institute modified to use the vehicle as a test bed for survey of parafoil dynamics, guidance, navigation and control (PGNC) algorithms. It can provide lots of flight test chances without much cost or risk of committing the large scale parafoil drop test, and generate valuable data to feedback for aerodynamic database tuning as well as pre-check of PGNC algorithm prior to large scale model drop test with less effort. For those purposes, the pilot seats and other spaces are replaced with the PGNC computer box and avionics instruments, actuators for remote control, telemetry etc. (figure 1.3). The parafoil is replaced to a scale downed of the actual or large scale parafoil for the X-38 also. To compensate the weight increase and risk of hard landing, the landing gears are reinforced and modified also. As a result, the modified Buckeye becomes a Unmanned Aerial Vehicle (UAV) capable of self guidance, navigation, control and independent power cutoff and recovery function for safety as well.

Figure 1.2 Original Buckeye 582 Powered Parachute

Figure 1.3 Modified Buckeye Test Bed

1.3   Organization of the Dissertation

Following this introduction, Chapter II presents the development of an analytical model of the Buckeye parafoil-vehicle system as a test vehicle. Full eight degrees-of-freedom nonlinear equations of motion are derived and linearized equation of motion is presented. With the linearized model, linear system analysis was committed including controllability and observability analysis as well as modal analysis and the results are described for power-off gliding flight condition.

In chapter III, the identification method applied for the research is described. The OKID (Observer Kalman-Filter Identification) method was used to develop a linear model from the simulated and flight test data as well for the Buckeye system. Expansion of the OKID with overparameterization for identification under unknown periodic disturbances are documented.

Chapter IV presents the detail of sensors and their installation that provide the Buckeye-vehicle attitudes, speed and dynamic responses for identification applications. And the detail of experiment design that is applied to the flight test was presented. The Parafoil Dynamic Simulator (PDS) was fully used to generate the input shapes to stimulate the Buckeye dynamics prior to actual flight test.

Chapter V displays the flight test data and identification results. The identified model was described and compared to the analytical model for validation of the identified method and analytical model.

Finally, concluding remarks of this dissertation are summarized in Chapter VI and recommendations for further research are in Chapter VII.

CHAPTER II

ANALYTICAL MODEL

2.1   Introduction

Although the dynamics of conventional aircraft are generally well understood, the Buckeye has a unique configuration which results in non-standard dynamics. It has a flexible parafoil which functions as a wing, and the parafoil is attached to the payload vehicle with suspension lines and risers. Aerodynamic forces and torques are mainly on the parafoil due to it's attitudes and control inputs and those forces and torques on the vehicle are relatively small in the Buckeye-vehicle because of the vehicle's non aerodynamic shape. The forces and torques on the parafoil act through the risers and the attaching confluence point to the suspended vehicle. In the parafoil the distance between an aerodynamic center and the center of mass is much bigger than conventional aircraft. In addition to that the suspended vehicle is located far below (same order of magnitude with parafoil span) than the conventional aircraft and this causes the total system's C.G. is located far below. In this case the aerodynamic forces cause bigger effect on the rotational motion of the system than for conventional aircraft. Thus, it seems not appropriate to apply conventional aircraft dynamical models directly to the parafoil-vehicle configuration.

In this thesis the parafoil and the hanging vehicle are assumed to be rigid bodies, connected by a joint at the confluence point. The risers and suspension lines are also regarded as rigid bodies as described in Chapter I. There are 12 degrees-of-freedom based on the two-body though, the number of degrees-of-freedom can be reduced because they are bound on each other. In addition to the rigid body assumption for riser and suspension lines, it has been observed that the relative roll motion between the parafoil and the vehicle is negligible from previous flight tests, otherwise relative pitch and yaw motions are assumed to exist. So eight degrees-of-freedom model is

assumed in this research, composed of three positions and three attitudes for the parafoil, and two degrees-of-freedom for the relative pitch and yaw motions of the hanging vehicle with respect to the parafoil. All external forces and torques are restricted to be either aerodynamic or inertial.

In deriving equations of motion of the two bodies, a classical Newtonian principles or Lagrangian approach can be possible. But as described in the following sections there are holonomic and non-holonomic constraints between the two bodies and this cause derivations of extra differential equations and/or Lagrangian multipliers which must be eliminated by algebraic means. By way of contrast, the use of Kane's[19, 20] equation permits the automatic elimination of all constraint forces associated with workless constraints, and it leads to equations having simplest possible form, provided generalized speeds are selected optimally, described in following sections. In this chapter, nonlinear equations of motion for the Buckeye parafoil system are derived using Kane's equation[19, 21] which is referred as the principle of virtual velocity.[22] The Kane's equation is described briefly in the following section for the Buckeye application. Prior to deriving the equations of motion, coordinate systems in which these equations are written are described. And linearized equations of motion are derived based on appropriate assumptions made along the linearization.

2.2 Coordinate Systems

Figure 2.1 shows three axis systems: the earth fixed system X_E, Y_E, Z_E, the parafoil body fixed axis system X_P, Y_P, Z_P, and the hanging vehicle body fixed axis X_V, Y_V, Z_V. The earth fixed system is regarded as an inertial reference frame: on which Newton's laws of motion are valid. The direction cosine matrix between the basis unit vectors of the earth axis and the parafoil axis for finite rotation sequence of $3(\Psi) - 2(\Theta) - 1(\Phi)$ is as follows:
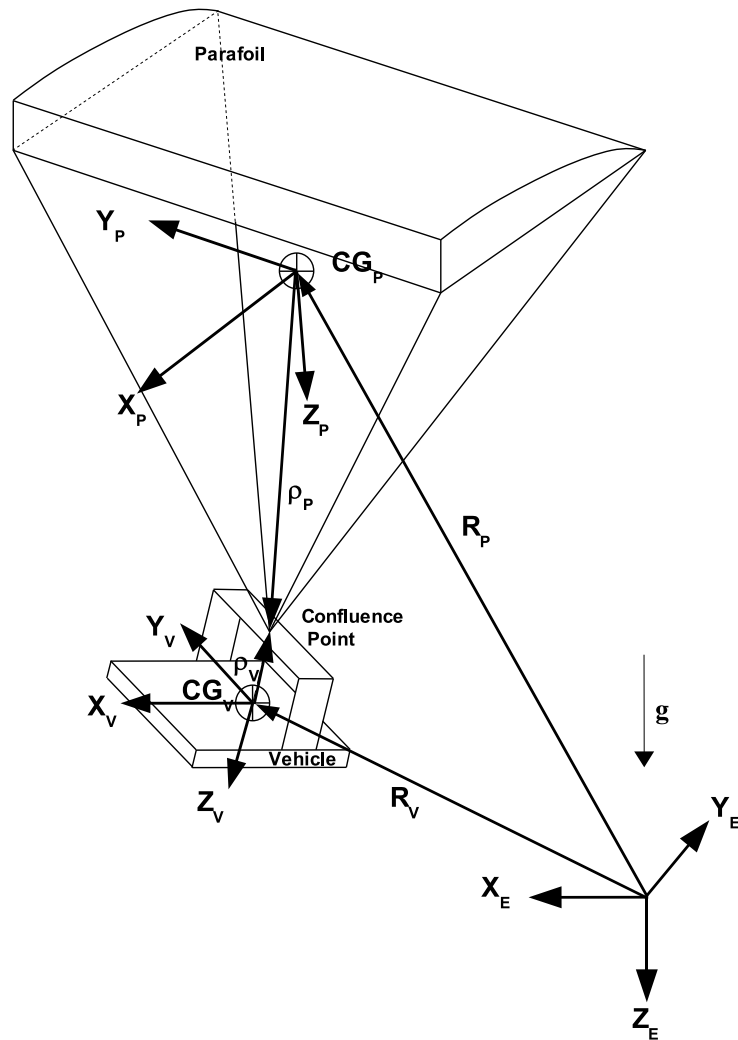
Figure 2.1 Axis System for Buckeye Parafoil-Vehicle

$$
\begin{Bmatrix} \mathbf{i} \\ \mathbf{j} \\ \mathbf{k} \end{Bmatrix} = \begin{bmatrix} c\Psi & -s\Psi & 0 \\ s\Psi & c\Psi & 0 \\ 0 & 0 & 1 \end{bmatrix} \begin{bmatrix} c\Theta & 0 & s\Theta \\ 0 & 1 & 0 \\ -s\Theta & 0 & c\Theta \end{bmatrix} \begin{bmatrix} 1 & 0 & 0 \\ 0 & c\Phi & -s\Phi \\ 0 & s\Phi & c\Phi \end{bmatrix} \begin{Bmatrix} \mathbf{i}_P \\ \mathbf{j}_P \\ \mathbf{k}_P \end{Bmatrix}
$$

$$
= \begin{bmatrix} c\Psi c\Theta & -s\Psi c\Phi + c\Psi s\Theta s\Phi & s\Psi s\Phi + c\Psi s\Theta c\Phi \\ s\Psi c\Theta & c\Psi c\Phi + s\Psi s\Theta s\Phi & -c\Psi s\Phi + s\Psi s\Theta c\Phi \\ -s\Theta & c\Theta s\Phi & c\Theta c\Phi \end{bmatrix} \begin{Bmatrix} \mathbf{i}_P \\ \mathbf{j}_P \\ \mathbf{k}_P \end{Bmatrix} \tag{2.1}
$$

$$
\triangleq [\mathbf{C}_{PI}] \begin{Bmatrix} \mathbf{i}_P \\ \mathbf{j}_P \\ \mathbf{k}_P \end{Bmatrix}
$$

where Ψ, Φ, Θ are Euler angles of the parafoil and the trigonometric functions are abbreviated as such $\cos\Psi = c\Psi$, $\sin\Psi = s\Psi$, $\cdots$ and unit vectors $\mathbf{i}, \mathbf{j}, \mathbf{k}$ are for the earth fixed inertial coordinate system X_E, Y_E, Z_E and subscripts P, V on unit vectprs are for the parafoil and the vehicle axis respectively. Similarly the direction cosine matrix of unit vectors for 3-2-1 rotation sequence between the parafoil and the vehicle is

$$
\begin{Bmatrix} \mathbf{i}_V \\ \mathbf{j}_V \\ \mathbf{k}_V \end{Bmatrix} = \begin{bmatrix} 1 & 0 & 0 \\ 0 & c\Phi_r & s\Phi_r \\ 0 & -s\Phi_r & c\Phi_r \end{bmatrix} \begin{bmatrix} c\Theta_r & 0 & -s\Theta_r \\ 0 & 1 & 0 \\ s\Theta_r & 0 & c\Theta_r \end{bmatrix} \begin{bmatrix} c\Psi_r & s\Psi_r & 0 \\ -s\Psi_r & c\Psi_r & 0 \\ 0 & 0 & 1 \end{bmatrix} \begin{Bmatrix} \mathbf{i}_P \\ \mathbf{j}_P \\ \mathbf{k}_P \end{Bmatrix}
$$

$$
= \begin{bmatrix} c\Theta_r c\Psi_r & c\Theta_r s\Psi_r & -s\Theta_r \\ s\Phi_r s\Theta_r c\Psi_r - c\Phi_r s\Psi_r & s\Phi_r s\Theta_r s\Psi_r + c\Phi_r c\Psi_r & s\Phi_r c\Theta_r \\ c\Phi_r s\Theta_r c\Psi_r + s\Phi_r s\Psi_r & c\Phi_r s\Theta_r s\Psi_r - s\Phi_r c\Psi_r & c\Phi_r c\Theta_r \end{bmatrix} \begin{Bmatrix} \mathbf{i}_P \\ \mathbf{j}_P \\ \mathbf{k}_P \end{Bmatrix} \tag{2.2}
$$

$$
\triangleq [\mathbf{C}_{PV}] \begin{Bmatrix} \mathbf{i}_P \\ \mathbf{j}_P \\ \mathbf{k}_P \end{Bmatrix}
$$

where Ψ_r, Φ_r, Θ_r are relative angles of the vehicle with respect to the parafoil measured at the confluence point as in Figure 2.2. In case of zero relative roll angle, the above direction cosine matrix equation can be rewritten as:

$$
\begin{Bmatrix} \mathbf{i}_V \\ \mathbf{j}_V \\ \mathbf{k}_V \end{Bmatrix} = \begin{bmatrix} c\Theta_r & 0 & -s\Theta_r \\ 0 & 1 & 0 \\ s\Theta_r & 0 & c\Theta_r \end{bmatrix} \begin{bmatrix} c\Psi_r & s\Psi_r & 0 \\ -s\Psi_r & c\Psi_r & 0 \\ 0 & 0 & 1 \end{bmatrix} \begin{Bmatrix} \mathbf{i}_P \\ \mathbf{j}_P \\ \mathbf{k}_P \end{Bmatrix}
$$

$$
= \begin{bmatrix} c\Theta_r c\Psi_r & c\Theta_r s\Psi_r & -s\Theta_r \\ -s\Psi_r & c\Psi_r & 0 \\ s\Theta_r c\Psi_r & s\Theta_r s\Psi_r & c\Theta_r \end{bmatrix} \begin{Bmatrix} \mathbf{i}_P \\ \mathbf{j}_P \\ \mathbf{k}_P \end{Bmatrix} \tag{2.3}
$$

$$
\triangleq [\mathbf{C}_{PV}] \begin{Bmatrix} \mathbf{i}_P \\ \mathbf{j}_P \\ \mathbf{k}_P \end{Bmatrix}
$$

As the maneuvering of the Buckeye-vehicle including relative motion does not show big attitudes changes around 90 degrees in the research, singularity in calculation is not to fear and other coordinate transformation methods preventing the singularity are not considered.

2.3   Nonlinear Equations of Motion

2.3.1   Introduction of Kane's Equation

The Kane's equation was introduced in early 80's by Thomas R. Kane and D.A.Levinson[19, 21] to develop a method to reduce the labor required for the formulation of equations of motion and/or the complexity of equations for complex dynamic system. In what follows, it is shown that how one can formulate dynamical equations of motion for $n - m$ degrees-of-freedom nonholonomic system by a using a law of motion expressed
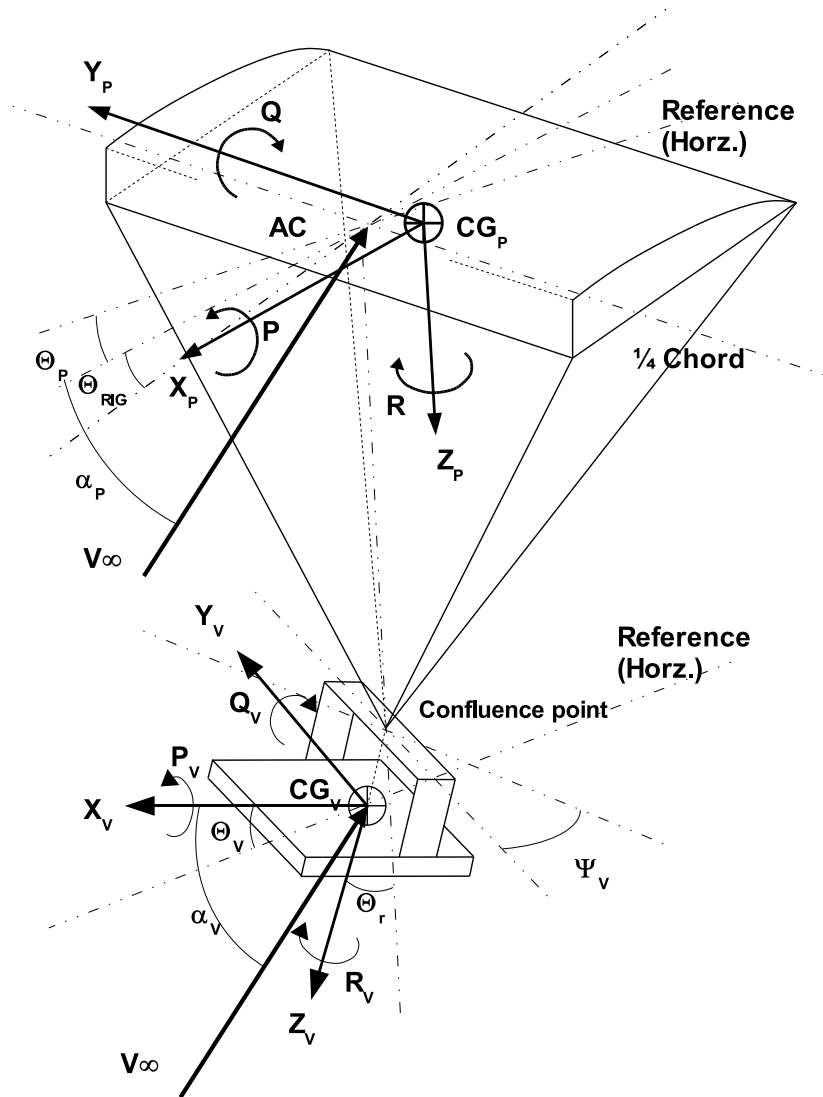
Figure 2.2 Schematic Diagram of Buckeye Parafoil-Vehicle System

as

$$F_r + F_r^* = 0 \quad (r = 1, \ldots, n - m) \tag{2.4}$$

where m is the number of nonholonomic constraints, while F_r and F_r^* are quantities that will be defined shortly, subsequent to the introduction of generalized speeds, partial angular velocities and partial velocities.

Whereas generalized coordinates, which is characterizing the configuration of a system, play a central role in Langragian mechanics,[23–25] quantities more directly associated with the motion of a system are of paramount importance in connection with the Kane's method. If generalized coordinates $q_1, \ldots, q_n$ of a system are subject to constraint equation of the form

$$\sum_{r=1}^{n} A_{sr} \dot{q}_r + B_s = 0 \quad (s = 1, \ldots, m) \tag{2.5}$$

where A_{sr} and B_s are functions of $q_1, \ldots, q_n$, and t, then one always can introduce $n - m$ quantities $u_1, \ldots, u_{n-m}$ as

$$u_r \triangleq \sum_{s=1}^{n-m} Y_{rs} \dot{q}_s + Z_r = 0 \quad (r = 1, \ldots, n - m) \tag{2.6}$$

where Y_{rs} and Z_r are functions of $q_1, \ldots, q_n$, and t, these functions being chosen such that the above equation can be solved uniquely for $\dot{q}_1, \ldots, \dot{q}_{n-m}$ and that one can satisfy Eqn. (2.5) identically for all values of $u_1, \ldots, u_{n-m}$ by expressing $\dot{q}_{n-m+1}, \ldots, \dot{q}_n$ as suitable functions of $u_1, \ldots, u_{n-m}$. The quantities $u_1, \ldots, u_{n-m}$ are called *generalized speeds*.

It can be shown that, once generalized speeds $u_1, \ldots, u_{n-m}$ have been introduced, $\boldsymbol{\omega}$, the angular velocity of a rigid body belongs to a system, and $\mathbf{v}$, the velocity of a particle belongs to a system, can be expressed uniquely as

$$\boldsymbol{\omega} \triangleq \sum_{r=1}^{n-m} \boldsymbol{\omega}_r u_r + \omega_t \tag{2.7}$$

and

$$\mathbf{v} \triangleq \sum_{r=1}^{n-m} \mathbf{v}_r u_r + \mathbf{v}_t \tag{2.8}$$

where $\boldsymbol{\omega}_r, \mathbf{v}_r, \boldsymbol{\omega}_t, \mathbf{v}_t$ are functions of $q_1, \ldots, q_n$, and t. In practice, $\boldsymbol{\omega}_r$, called the rth partial angular velocity, and $\mathbf{v}_r$, called r^{th} partial velocity, are formed by simply inspecting the coefficients of $u_1, \ldots, u_{n-m}$ in expressions having the form of the right-hand members of Eqn.(2.7) and (2.8).

Given a system S consisting of N particles $P_1, \ldots, P_N$, suppose that $n - m$ generalized speeds have been introduced, and let $\mathbf{v}_r^{P_i}$ denote the rth partial velocity of P_i. Then, if $\mathbf{R}_i$ is the resultant of all contact and body forces acting on P_i, then the $n - m$ quantities $F_1, \ldots, F_{n-m}$ defined as

$$F_r \triangleq \sum_{i=1}^{N} \mathbf{v}_r^{P_i} \cdot \mathbf{R}_i \qquad (r = 1, \ldots, n - m) \tag{2.9}$$

are called *generalized active forces* for S; if $\mathbf{R}_i^*$ denotes the inertia forces for P_i, that is , if $\mathbf{R}_i^*$ is defined as

$$\mathbf{R}_i^* \triangleq -m_i \mathbf{a}_i \qquad (i = 1, \ldots, N), \tag{2.10}$$

where m_i is the mass of P_i and $\mathbf{a}_i$ is the inertial acceleration of P_i, then the $n - m$ quantities $F_1^*, \ldots, F_{n-m}^*$ defined as

$$F_r^* \triangleq \sum_{i=1}^{N} \mathbf{v}_r^{P_i} \cdot \mathbf{R}_i^* \qquad (r = 1, \ldots, n - m) \tag{2.11}$$

are called *generalized inertia forces* for S.

If there is a rigid body B belongings to S and if a set of contact and/or body forces acting on B is equivalent to a couple of torque $\mathbf{T}$ together with a force $\mathbf{R}$ applied at a point Q of B, then $(F_r)_B$, the contribution of this set of forces to F_r, is given by

$$(F_r)_B = \boldsymbol{\omega}_r \cdot \mathbf{T} + \mathbf{v}_r \cdot \mathbf{R} \quad (r = 1, \ldots, n - m) \tag{2.12}$$

where $\boldsymbol{\omega}_r$ and $\mathbf{v}_r$ are, respectively, the rth partial angular velocity of B and the rth partial velocity of Q. Q is usually at the C.G. point of the body.

As for the contribution to the generalized inertia forces defined in Eqn. (2.11), these, too, can be easily for a rigid body. Specifically, $(F_r^*)_B$, the contribution to F_r^* of a rigid body B can be expressed as

$$(F_r^*)_B = \boldsymbol{\omega}_r \cdot \mathbf{T}^* + \mathbf{v}_r \cdot \mathbf{R}^* \quad (r = 1, \ldots, n - m) \tag{2.13}$$

where $\boldsymbol{\omega}_r$ and $\mathbf{v}_r$ are, respectively, the rth partial angular velocity of B and the rth partial velocity of the mass center of B, while $\mathbf{T}^*$ and $\mathbf{R}^*$ depend on inertial angular velocity $\boldsymbol{\omega}$ of B, the inertial angular acceleration $\boldsymbol{\alpha}$ of B, the central mass moment of inertia $\mathbf{I}$ of B, the mass M of B, and the inertial acceleration $\mathbf{a}^*$ of the mass center of B. $\mathbf{T}^*$ and $\mathbf{R}^*$ are given by

$$\mathbf{T}^* = -\boldsymbol{\alpha} \cdot \mathbf{I} - \boldsymbol{\omega} \times \mathbf{I} \cdot \boldsymbol{\omega}, \quad \mathbf{R}^* = -m\mathbf{a}^* \tag{2.14}$$

and are called, respectively, the inertia torque for B and inertia force for B.

Applying those equations to Kane's equation, equation of motion can be constructed.

$$F_r + F_r^* = 0 \quad (r = 1, \ldots, n - m)$$

Rewriting above equation with Eqn.(2.13),(2.14) for rigid body B,

$$(F_r)_B + (F_r^*)_B = \mathbf{v}_r \cdot (\mathbf{R} + \mathbf{R}^*) + \boldsymbol{\omega}_r \cdot (\mathbf{T} + \mathbf{T}^*)$$

$$= 0 \quad (r = 1, \ldots, n - m) \tag{2.15}$$

2.3.2 8-DOF Equations of Motion

As the Buckeye parafoil-vehicle is assumed as two rigid body system in the 3-D space coordinate, so the degrees-of-freedom can be $12(= 6 \times 2)$. But the two bodies are assumed to be connected through massless joint and the degrees-of-freedom reduced to $9(= 12 - 3)$ by the constraints. And from observation of flight test the roll motion of the vehicle relative to the parafoil, Φ_r is assumed to be negligible. So we can choose following 8 variables as generalized coordinates and equations of motion will be derived for the independent 8 degrees of freedom. The generalized coordinates are:

$$\{q_1 = \Phi, q_2 = \Theta, q_3 = \Psi, q_4 = X, q_5 = Y, q_6 = Z, q_8 = \Theta_r, q_9 = \Psi_r\}$$

where $q_7 = \Phi_r = 0$. To derive the equations of motion efficiently, the virtual power method[22] based on the Kane's dynamics[19, 21] was adopted.

2.3.2.1 Kinematics

From Figure 2.1 the position vectors for the parafoil and the vehicles are written as follows:

$$\mathbf{R}_P = X\mathbf{i} + Y\mathbf{j} + Z\mathbf{k}$$

$$\mathbf{R}_V = \mathbf{R}_P + \boldsymbol{\rho}_P - \boldsymbol{\rho}_V$$

(2.16)

Linear velocities of the parafoil and the vehicle are

$$\dot{\mathbf{R}}_P = \mathbf{V}_P = \dot{X}\mathbf{i} + \dot{Y}\mathbf{j} + \dot{Z}\mathbf{k}$$

$$= U\mathbf{i}_P + V\mathbf{j}_P + W\mathbf{k}_P$$

$$\dot{\mathbf{R}}_V = \mathbf{V}_V = U_V\mathbf{i}_V + V_V\mathbf{j}_V + W_V\mathbf{k}_V$$

$$= \mathbf{V}_P + \dot{\boldsymbol{\rho}}_P - \dot{\boldsymbol{\rho}}_V$$

$$= \mathbf{V}_P + \boldsymbol{\omega}_P \times \boldsymbol{\rho}_P - \boldsymbol{\omega}_V \times \boldsymbol{\rho}_V$$

(2.17)

The angular velocities of the parafoil and the vehicle are written as follows:

$$\boldsymbol{\omega}_P = P\mathbf{i}_P + Q\mathbf{j}_P + R\mathbf{k}_P$$

$$= \left(\dot{\Phi} - \dot{\Psi}s\Theta\right)\mathbf{i}_P + \left(\dot{\Theta}c\Phi + \dot{\Psi}c\Theta s\Phi\right)\mathbf{j}_P + \left(\dot{\Psi}c\Theta c\Phi - \dot{\Theta}s\Phi\right)\mathbf{k}_P$$

$$\boldsymbol{\omega}_V = P_V\mathbf{i}_V + Q_V\mathbf{j}_V + R_V\mathbf{k}_V$$

$$= \boldsymbol{\omega}_P + \boldsymbol{\omega}_{V/P}$$

(2.18)

From above equations the positions, velocities and angular velocities are considered as kinematic constraint equations. To use the Kane's equation,[19,21] we designate the generalized speeds first in the form of following equation.

$$u_1 = P, \; u_2 = Q, \; u_3 = R, \; u_4 = U, \; u_5 = V, \; u_6 = W$$

$$u_7 = P_V, \; u_8 = Q_V, \; u_9 = R_V, \; u_{10} = U_V, \; u_{11} = V_V, \; u_{12} = W_V$$

Then the kinematic relations in above equations (2.16)-(2.18) can be rewritten with the generalized coordinates and speeds in the form of kinematic differential equations.

$$
\left\{ \begin{array}{c} \dot{q}_1 \\ \dot{q}_2 \\ \dot{q}_3 \end{array} \right\} = \begin{bmatrix} 1 & s_1 t_2 & c_1 t_2 \\ 0 & c_1 & -s_1 \\ 0 & s_1/c_2 & c_1/c_2 \end{bmatrix} \left\{ \begin{array}{c} u_1 \\ u_2 \\ u_3 \end{array} \right\} \tag{2.19}
$$

$$
\left\{ \begin{array}{c} \dot{q}_4 \\ \dot{q}_5 \\ \dot{q}_6 \end{array} \right\} = \begin{bmatrix} c_3 c_2 & -s_3 c_1 + c_3 s_2 s_1 & s_3 s_1 + s_2 c_1 c_3 \\ s_3 c_2 & c_3 c_1 + s_3 s_2 s_1 & -c_3 s_1 + s_3 s_2 c_1 \\ -s_2 & s_1 c_2 & c_1 c_2 \end{bmatrix} \left\{ \begin{array}{c} u_4 \\ u_5 \\ u_6 \end{array} \right\} \tag{2.20}
$$

$$
\left\{ \begin{array}{c} \dot{q}_7 \\ \dot{q}_8 \\ \dot{q}_9 \end{array} \right\} = \begin{bmatrix} 1 & 0 & t_8 \\ 0 & 1 & 0 \\ 0 & 0 & 1/c_8 \end{bmatrix} \left\{ \begin{array}{c} u_7 \\ u_8 \\ u_9 \end{array} \right\}
$$
$$
+ \begin{bmatrix} -c_8 c_9 - s_8{}^2 c_9/c_8 & -s_9 c_8 - s_8{}^2 s_9/c_8 & 0 \\ s_9 & -c_9 & \\ -c_9 t_8 & -s_9 t_8 & -1 \end{bmatrix} \left\{ \begin{array}{c} u_1 \\ u_2 \\ u_3 \end{array} \right\} \tag{2.21}
$$

where c, s, and t represents sin, cos and tan trigonometric functions respectively and the subscript numbers are representing generalized coordinates.

Using Eqn. (2.19) to (2.21) we can derive those partial velocities and partial angular velocities. From Eqn. (2.18) it can be seen that

$$
\boldsymbol{\omega}_P = u_1 \mathbf{i}_P + u_2 \mathbf{j}_P + u_3 \mathbf{k}_P \tag{2.22}
$$

and this equation has the same form as Eqn. (2.7). The coefficients of u_1 to u_8 are the partial angular velocities of the parafoil, which are

$$
\boldsymbol{\omega}_1^P = \mathbf{i}_P, \quad \boldsymbol{\omega}_2^P = \mathbf{j}_P, \quad \boldsymbol{\omega}_3^P = \mathbf{k}_P,
$$
$$
\boldsymbol{\omega}_4^P = \boldsymbol{\omega}_5^P = \cdots = \boldsymbol{\omega}_8^P = 0 \tag{2.23}
$$

The angular velocity for the vehicle in Eqn.(2.18) is,

$$\boldsymbol{\omega}_V = u_7\mathbf{i}_V + u_8\mathbf{j}_V + u_9\mathbf{k}_V$$

From the assumption of constraint, $q_7 = 0$, $\dot{q}_7 = 0$. Using the kinematical differential equation (2.21), u_7 can be written as follows:

$$u_7 = (c_9/c_8)u_1 + (s_9/c_8)\,u_2 - t_8\,u_9 \tag{2.24}$$

So the angular velocity of the vehicle can be rewritten by representing the dependent generalized speed u_7 as function of constrained generalized speeds $u_1, u_2, \cdots, u_9$, from above nonholonomic constraint equation such as

$$\begin{aligned} \boldsymbol{\omega}_V &= u_7\mathbf{i}_V + u_8\mathbf{j}_V + u_9\mathbf{k}_V \\ &= [(c_9/c_8)u_1 + (s_9/c_8)\,u_2 - t_8\,u_9]\mathbf{i}_V \\ &\quad + u_8\mathbf{j}_V + u_9\mathbf{k}_V \end{aligned} \tag{2.25}$$

Then partial angular velocities for the vehicle are

$$\begin{aligned} \boldsymbol{\omega}_1^V &= c_9/c_8\mathbf{i}_V, \quad \boldsymbol{\omega}_2^V = s_9/c_8\mathbf{j}_V, \quad \boldsymbol{\omega}_3^V = 0, \\ \boldsymbol{\omega}_4^V &= \boldsymbol{\omega}_4^V = \boldsymbol{\omega}_6^V = 0, \\ \boldsymbol{\omega}_7^V &= \mathbf{j}_V, \quad \boldsymbol{\omega}_8^V = -t_8\mathbf{i}_V + \mathbf{k}_V. \end{aligned} \tag{2.26}$$

From Eqn (2.17), the velocity vector for the parafoil is

$$\mathbf{V}_P = u_4\,\mathbf{i}_P + u_5\,\mathbf{j}_P + u_6\,\mathbf{k}_P \tag{2.27}$$

and partial velocities for the parafoil are

$$\begin{aligned} \mathbf{v}_1^P &= \mathbf{v}_2^P = \mathbf{v}_3^P = 0, \\ \mathbf{v}_4^P &= \mathbf{i}_P, \quad \mathbf{v}_5^P = \mathbf{j}_P, \quad \mathbf{v}_6^P = \mathbf{k}_P, \\ \mathbf{v}_7^P &= \mathbf{v}_8^P = 0. \end{aligned} \tag{2.28}$$

The partial velocities for the vehicle can be derived with the same procedure for the parafoil. From Eqn.(2.17) the velocity vector of the vehicle is

$$\mathbf{V}_V = u_{10}\,\mathbf{i}_V + u_{11}\,\mathbf{j}_V + u_{12}\,\mathbf{k}_V$$

and constraint equations from kinematics are as follows:

$$u_{10} = (\rho_{x_P}s_8 + \rho_{z_P}c_8c_9)u_2 - \rho_{z_P}s_9c_8u_1 + s_9c_8u_5 + c_8c_9u_4$$

$$+ \rho_{x_P}s_9c_8u_3 - \rho_{z_V}u_8 - s_8u_6$$

$$u_{11} = c_9u_5 + \rho_{x_P}c_9u_3 + (\rho_{z_V}s_9/c_8 - \rho_{z_P}s_9)u_2 + (\rho_{z_V}c_9/c_8 - \rho_{z_P}c_9)u_1$$

$$- (\rho_{x_V} + \rho_{z_V}t_8)u_9 - s_9u_4$$

$$u_{12} = \rho_{x_V}u_8 + c_8u_6 + s_8s_9u_5 + s_8c_9u_4 + \rho_{x_P}s_8s_9u_3$$

$$+ (\rho_{z_P}s_8c_9 - \rho_{x_P}c_8)u_2 - \rho_{z_P}s_8s_9u_1$$

$$(2.29)$$

Therefore, substituting u_{10}, u_{11}, u_{12}, in the constraint equations into the velocity vector of the vehicle and making partials yields

$$\mathbf{v}_1^V = -\rho_{z_P}s_9c_8\mathbf{i}_V + (\rho_{z_V}c_9/c_8 - \rho_{z_P}c_9)\mathbf{j}_V - \rho_{z_P}s_8s_9\mathbf{k}_V,$$

$$\mathbf{v}_2^V = (\rho_{x_P}s_8 + \rho_{z_P}c_8c_9)\mathbf{i}_V + (\rho_{z_V}s_9/c_8 - \rho_{z_P}s_9)\mathbf{j}_V$$

$$+ (\rho_{z_P}s_8c_9 - \rho_{x_P}c_8)\mathbf{k}_V,$$

$$\mathbf{v}_3^V = \rho_{x_P}s_9c_8\mathbf{i}_V + \rho_{x_P}c_9\mathbf{j}_V + \rho_{x_P}s_8s_9\mathbf{k}_V,$$

$$\mathbf{v}_4^V = c_8c_9\mathbf{i}_V - s_9\mathbf{j}_V + s_8c_9\mathbf{k}_V,$$

$$(2.30)$$

$$\mathbf{v}_5^V = s_9c_8\mathbf{i}_V + c_9\mathbf{j}_V + s_8s_9\mathbf{k}_V,$$

$$\mathbf{v}_6^V = -s_8\mathbf{i}_V + c_8\mathbf{k}_V,$$

$$\mathbf{v}_7^V = -\rho_{z_V}\mathbf{i}_V + \rho_{x_V}\mathbf{k}_V,$$

$$\mathbf{v}_8^V = -(\rho_{x_V} + \rho_{z_V}t_8)\mathbf{j}_V.$$

Note that subscript numbers in Eqn.(2.23), (2.26), (2.28), (2.30) are limited to 8 because there are 8 independent variables due to 4 constraints described in Eqn.(2.24), (2.29).

2.3.2.2 Generalized Forces

Inertial Forces To obtain Kane's equations for the two-body Buckeye system, the inertial accelerations including rotational accelerations are described first. From Eqn.(2.17) and (2.18), time derivatives of velocities can be derived. The inertial translational accelerations for the parafoil and the vehicle are

$$
\mathbf{a}_P = \frac{d}{dt}\mathbf{V}_P = \frac{\partial \mathbf{V}_P}{\partial t} + \boldsymbol{\omega}_P \times \mathbf{V}_P
$$

$$
= \left(\dot{U} - VR + WQ\right)\mathbf{i}_P + \left(\dot{V} + UR - WP\right)\mathbf{j}_P + \left(\dot{W} - UQ + VP\right)\mathbf{k}_P \quad (2.31)
$$

$$
= (\dot{u}_4 - u_5 u_3 + u_6 u_2)\mathbf{i}_P + (\dot{u}_5 - u_6 u_1 + u_3 u_4)\mathbf{j}_P + (\dot{u}_6 - u_4 u_2 + u_5 u_1)\mathbf{k}_P
$$

$$
\mathbf{a}_V = \frac{d}{dt}\mathbf{V}_V = \frac{\partial \mathbf{V}_V}{\partial t} + \boldsymbol{\omega}_V \times \mathbf{V}_V
$$

$$
= \Bigg[\rho_{x_V} u_8{}^2 + \rho_{x_V} u_9{}^2 + s_8 u_2 u_4 + \rho_{z_P} s_8 u_1{}^2 + \rho_{z_P} s_8 u_2{}^2 + \rho_{z_V} t_8 u_9{}^2
$$

$$
+ (\rho_{x_P} s_8 + \rho_{z_P} c_8 c_9)\dot{u}_2 - s_8 u_1 u_5 - \rho_{x_P} s_8 u_1 u_3 - \rho_{z_V}\dot{u}_8 - s_8 \dot{u}_6
$$

$$
- \big[\rho_{z_V} c_9 u_1 u_9 + c_9 c_8{}^2 u_3 u_5 + \rho_{x_P} c_9 c_8{}^2 u_2{}^2 + \rho_{x_P} c_9 c_8{}^2 u_3{}^2 - c_9 c_8{}^2 u_2 u_6
$$

$$
- \rho_{z_P} c_9 c_8{}^2 u_1 u_3 - c_9 c_8{}^2 \dot{u}_4 - s_9(c_8{}^2 u_3 u_4 + \rho_{x_P} c_8{}^2 u_1 u_2 + \rho_{z_P} c_8{}^2 u_2 u_3
$$

$$
+ c_8{}^2 \dot{u}_5 + \rho_{x_P} c_8{}^2 \dot{u}_3 - \rho_{z_V} u_2 u_9 - c_8{}^2 u_1 u_6 - \rho_{z_P} c_8{}^2 \dot{u}_1)\big]/c_8 \Bigg]\mathbf{i}_V
$$

$$
+ \Bigg[c_9 u_3 u_4 + \rho_{x_P} c_9 u_1 u_2 + \rho_{z_P} c_9 u_2 u_3 + \rho_{x_V} t_8 u_8 u_9 + 2s_1 s_2 c_1{}^2 c_2 c_9 u_2 u_6
$$

$$
+ (2\rho_{z_V} c_9 u_2 u_9 - \rho_{z_V} u_8 u_9 - \rho_{x_V} c_8 c_9 u_1 u_8 - \rho_{z_V} c_9 c_8{}^3 u_2 u_3)/c_8{}^2
$$

$$
+ c_9 \dot{u}_5 + \rho_{x_P} c_9 \dot{u}_3 + s_9 \big[u_3 u_5 + \rho_{x_P} u_2{}^2 + \rho_{x_P} u_3{}^2 + \rho_{z_V} c_8 u_1 u_3
$$

$$
+ \rho_{z_V} s_8 \big[t_8 u_1 u_3 + (u_2 u_8 + 2c_9 u_1{}^2 + 4s_9 u_1 u_2 - 2c_9 u_2{}^2)/c_8{}^2 \big] \quad (2.32)
$$

$$
- u_2 u_6 - \rho_{z_P} u_1 u_3 - 2\rho_{z_V} u_1 u_9/c_8{}^2 - \rho_{x_V} u_2 u_8/c_8 - \dot{u}_4
$$

$$
- (\rho_{z_P} - \rho_{z_V}/c_8)\dot{u}_2 \big] - \rho_{z_V} u_8 u_9 - c_9 u_1 u_6 - \rho_{z_V} s_8 \big[c_9 t_8 u_2 u_3
$$

$$
+ u_1(2u_2 - c_9 u_8)/c_8{}^2 \big] - s_1 s_2 c_2 c_9 u_6(2s_1 c_1 u_3 + 2c_1{}^2 u_2 - 2s_1 c_1 u_3)
$$

$$
- (\rho_{x_V} + \rho_{z_V} t_8)\dot{u}_9 - c_9(\rho_{z_P} - \rho_{z_V}/c_8)\dot{u}_1 \Bigg]\mathbf{j}_V
$$

$$+\left[\rho_{z_V}u_8{}^2+\rho_{x_V}t_8u_9{}^2+\rho_{z_V}t_8^2u_9{}^2+s_8c_9u_2u_6+\rho_{z_P}s_8c_9u_1u_3+\rho_{x_V}\dot{u}_8\right.$$

$$+s_8c_9\dot{u}_4+s_9\left[s_8u_3u_4+\rho_{x_P}s_8u_1u_2+\rho_{z_P}s_8u_2u_3+s_8\dot{u}_5+\rho_{x_P}s_8\dot{u}_3\right.$$

$$-s_8u_1u_6-(\rho_{x_V}c_8u_2u_9+\rho_{z_V}s_9u_1{}^2+2\rho_{z_V}s_8u_2u_9-2\rho_{z_V}c_9u_1u_2$$

$$-\rho_{z_V}s_9u_2{}^2)/c_8{}^2-\rho_{z_P}s_8\dot{u}_1\left]-s_8c_9u_3u_5-\rho_{x_P}s_8c_9u_2{}^2-\rho_{x_P}s_8c_9u_3{}^2\right.$$

$$-(\rho_{x_P}c_8-\rho_{z_P}s_8c_9)\dot{u}_2-(c_8{}^3u_2u_4+\rho_{z_P}c_8{}^3u_1{}^2+\rho_{z_P}c_8{}^3u_2{}^2$$

$$+\rho_{x_V}c_8c_9u_1u_9+2\rho_{z_V}s_8c_9u_1u_9-\rho_{z_V}u_1{}^2-c_8{}^3u_1u_5-\rho_{x_P}c_8{}^3u_1u_3$$

$$\left.-c_8{}^3\dot{u}_6)/c_8{}^2\right]\mathbf{k}_V$$

and angular acceleration for the parafoil is

$$\boldsymbol{\alpha}_P=\dot{\boldsymbol{\omega}}_P=\frac{\partial\boldsymbol{\omega}_P}{\partial t}+\boldsymbol{\omega}_P\times\boldsymbol{\omega}_P$$

$$=\dot{P}\mathbf{i}_P+\dot{Q}\mathbf{j}_P+\dot{R}\mathbf{k}_P \tag{2.33}$$

$$=\dot{u}_1\mathbf{i}_P+\dot{u}_2\mathbf{j}_P+\dot{u}_3\mathbf{k}_P$$

and for the vehicle,

$$\boldsymbol{\alpha}_V=\dot{\boldsymbol{\omega}}_V=\frac{\partial\boldsymbol{\omega}_V}{\partial t}+\boldsymbol{\omega}_V\times\boldsymbol{\omega}_V$$

$$=\left[2c_9/c_8{}^2u_2u_9+c_9/c_8\dot{u}_1-1/c_8{}^2u_8u_9-c_8c_9u_2u_3\right.$$

$$-s_8(2/c_8{}^2u_1u_2+c_9t_8u_2u_3-c_9/c_8{}^2u_1u_8)-t_8\dot{u}_9$$

$$-s_9\left[2/c_8{}^2u_1u_9-c_8u_1u_3-s_8(t_8u_1u_3+1/c_8{}^2u_2u_8\right. \tag{2.34}$$

$$\left.\left.+2c_9/c_8{}^2u_1{}^2+4s_9/c_8{}^2u_1u_2-2c_9/c_8{}^2u_2{}^2)-1/c_8{}^2\dot{u}_2\right]\mathbf{i}_V\right.$$

$$+\dot{u}_8\,\mathbf{j}_V+\dot{u}_9\,\mathbf{k}_V$$

Using the inertial acceleration terms above, inertia torques and forces can be expressed using Eqn.(2.14).

$$\mathbf{T}^*=-\boldsymbol{\alpha}\cdot\mathbf{I}-\boldsymbol{\omega}\times\mathbf{I}\cdot\boldsymbol{\omega},\quad \mathbf{R}^*=-m\mathbf{a}^*$$

For the parafoil,

$$\mathbf{T}^{P*} = -\boldsymbol{\alpha}_P \cdot \mathbf{I}_P - \boldsymbol{\omega}_P \times \mathbf{I}_P \cdot \boldsymbol{\omega}_P, \quad \mathbf{R}^{P*} = -m_P \mathbf{a}_P \tag{2.35}$$

Expanding $\mathbf{T}^{P*}$, $\mathbf{R}^{P*}$ with acceleration terms in Eqn.(2.31),(2.33) yields

$$
\begin{aligned}
\mathbf{T}^{P*} = &-\left[I_{xx_P}\dot{u}_1 + I_{xz_P}\dot{u}_3 + I_{xz_P}u_1 u_2 + \left(I_{zz_P} - I_{yy_P} \right) u_3 u_2 \right] \mathbf{i}_P \\
&- \left[I_{yy_P}\dot{u}_2 + \left(I_{xx_P} - I_{zz_P} \right) u_1 u_3 - I_{xz_P}\left(u_1^2 - u_3^2 \right) \right] \mathbf{j}_P \\
&- \left[I_{zz_P}\dot{u}_3 + I_{xz_P}\dot{u}_1 + \left(I_{yy_P} - I_{xx_P} \right) u_1 u_2 - I_{xz_P}u_2 u_3 \right] \mathbf{k}_P
\end{aligned}
\tag{2.36}
$$

$$
\begin{aligned}
\mathbf{R}^{P*} = &-m_P\left(\dot{u}_4 - u_5 u_3 + u_6 u_2 \right)\mathbf{i}_P - m_P\left(\dot{u}_5 + u_4 u_3 - u_6 u_1 \right)\mathbf{j}_P \\
&- m_P\left(\dot{u}_6 - u_4 u_2 + u_5 u_1 \right)\mathbf{k}_P
\end{aligned}
\tag{2.37}
$$

Inertial torques and forces for the vehicle can be presented similarly as Eqn.(2.35) such as,

$$\mathbf{T}^{V*} = -\boldsymbol{\alpha}_V \cdot \mathbf{I}_V - \boldsymbol{\omega}_V \times \mathbf{I}_V \cdot \boldsymbol{\omega}_V, \quad \mathbf{R}^{V*} = -m_V \mathbf{a}_V \tag{2.38}$$

Expanding $\mathbf{T}^{V*}$ with above acceleration terms in Eqn.(2.32),(2.34) yields

$$
\begin{aligned}
\mathbf{T}^{V*} = &\left[I_{yy_V}u_8 u_9 + I_{xx_V}\left\{ s_8\left[c_9 t_8 u_2 u_3 + u_1(2u_2 - c_9 u_8)/c_8^2 \right] + t_8 \dot{u}_9 \right. \right. \\
&+ (u_8 u_9 + c_9 c_8^3 u_2 u_3 - 2c_9 u_2 u_9 - c_8 c_9 \dot{u}_1)/c_8^2 + s_9\left[2u_1 u_9/c_8^2 \right. \\
&- c_8 u_1 u_3 - s_8\left(t_8 u_1 u_3 + (u_2 u_8 + 2c_9 u_1^2 + 4s_9 u_1 u_2 - 2c_9 u_2^2)/c_8^2 \right) \\
&\left. \left. - \dot{u}_2/c_8 \right] \right\} - u_8(I_{zz_V}u_9 + I_{xz_V}u_7) - I_{xz_V}\dot{u}_9 \right] \mathbf{i}_V \\
&+ \left[u_7(I_{zz_V}u_9 + I_{xz_V}u_7) - u_9(I_{xx_V}u_7 + I_{xz_V}u_9) - I_{yy_V}\dot{u}_8 \right] \mathbf{j}_V \\
&+ \left[u_8(I_{xx_V}u_7 + I_{xz_V}u_9) + I_{xz_V}\left\{ s_8\left[c_9 t_8 u_2 u_3 + u_1(2u_2 - c_9 u_8)/c_8^2 \right] \right. \right. \\
&+ t_8 \dot{u}_9 + (u_8 u_9 + c_9 c_8^3 u_2 u_3 - 2c_9 u_2 u_9 - c_8 c_9 \dot{u}_1)/c_8^2 \\
&+ s_9\left[2u_1 u_9/c_8^2 - c_8 u_1 u_3 - s_8\left(t_8 u_1 u_3 + (u_2 u_8 + 2c_9 u_1^2 \right. \right.
\end{aligned}
\tag{2.39}
$$

$$+ 4s_9 u_1 u_2 - 2c_9 {u_2}^2)/{c_8}^2 \Big) - \dot{u}_2/c_8 \Big] \Big\} - I_{yy_V} u_7 u_8 - I_{zz_V} \dot{u}_9 \Big] \mathbf{k}_V$$

where u_7 is constraint speed in Eqn.(2.24). And $\mathbf{R}^{V*}$ can be expanded by substituting Eqn.(2.32) into Eqn.(2.38) and following equation is presented in terms of dependent variables u_{10}, u_{11} and u_{12} to save space and readability. Those dependent variables are in Eqn.2.29.

$$\begin{aligned}
\mathbf{R}^{V*} = & - m_V \Big[u_{11}(s_9 u_2 + c_9 u_1) \Big] \mathbf{k}_P \\
& + m_V \Big[u_{11}\big(u_9 + c_8 u_3\big) + u_{12}\big(s_9 u_1 - u_8 - c_9 u_2\big) - \dot{u}_{10} \Big] \mathbf{i}_V \\
& - m_V \Big[u_{10}\big(u_9 + c_8 u_3 + s_8 s_9 u_2 + s_8 c_9 u_1\big) \\
& \qquad + u_{12}\big(s_8 u_3 - s_9 c_8 u_2 - c_8 c_9 u_1\big) + \dot{u}_{11} \Big] \mathbf{j}_V \\
& + m_V \Big[s_8 u_{11} u_3 - u_{10}\big(s_9 u_1 - u_8 - c_9 u_2\big) - \dot{u}_{12} \Big] \mathbf{k}_V
\end{aligned} \qquad (2.40)$$

Active Forces Resultant (active) forces and torques for the parafoil are mainly due to aerodynamics and inertia as well as the joint force and torque due to the hanging vehicle. The aerodynamic forces act on the aerodynamic centers of the parafoil and the vehicle. The joint forces and torques are applied each other through the confluence joint and inertia forces on C.G. of the parafoil and the vehicle respectively. The inertia forces on the parafoil and the vehicle are $\mathbf{G}_P = m_P \mathbf{g}$ and $\mathbf{G}_V = m_V \mathbf{g}$ and can be

expressed in the following;

$$\mathbf{G}_P = m_P \mathbf{g} = m_P g \mathbf{k}$$

$$= -m_P s\Theta g \mathbf{i}_P + m_P c\Theta s\Phi g \mathbf{j}_P + m_P c\Theta c\Phi g \mathbf{k}_P$$

$$= -m_P g (s_2 \mathbf{i}_P - c_2 s_1 \mathbf{j}_P - c_2 c_1 \mathbf{k}_P)$$

$$\mathbf{G}_V = m_V \mathbf{g} = m_V g \mathbf{k} \tag{2.41}$$

$$= -m_V g \left(s_2 c_8 c_9 + s_8 c_1 c_2 - s_1 s_9 c_2 c_8 \right) \mathbf{i}_V$$

$$+ m_V g \left(s_2 s_9 + s_1 c_2 c_9 \right) \mathbf{j}_V$$

$$- m_V g \left(s_2 s_8 c_9 - c_1 c_2 c_8 - s_1 s_8 s_9 c_2 \right) \mathbf{k}_V$$

The aerodynamic forces and torques are expressed such as,

$$\mathbf{F}_{a_P} = F_{x_P} \mathbf{i}_P + F_{y_P} \mathbf{j}_P + F_{z_P} \mathbf{k}_P$$

$$\mathbf{T}_{a_P} = L_P \mathbf{i}_P + M_P \mathbf{j}_P + N_P \mathbf{k}_P$$

$$\mathbf{F}_{a_V} = F_{x_V} \mathbf{i}_V + F_{y_V} \mathbf{j}_V + F_{z_V} \mathbf{k}_V \tag{2.42}$$

$$\mathbf{T}_{a_V} = L_V \mathbf{i}_V + M_V \mathbf{j}_V + N_V \mathbf{k}_V$$

where $L_{P,V}, M_{P,V}, N_{P,V}$ are aerodynamic torques with respect to $X_{P,V}, Y_{P,V}, Z_{P,V}$ axis respectively. The resultant (active) forces and torques for the parafoil can be written as follows:

$$\mathbf{R}_P = F_{x_P} \mathbf{i}_P + F_{y_P} \mathbf{j}_P + F_{z_P} \mathbf{k}_P + m_P \mathbf{g} + \mathbf{F}_{cons}$$

$$\mathbf{T}_P = L_P \mathbf{i}_P + M_P \mathbf{j}_P + N_P \mathbf{k}_P + \mathbf{r}_P \times \mathbf{F}_{a_P} + \boldsymbol{\rho}_P \times \mathbf{F}_{cons} - \mathbf{T}_{cons} \tag{2.43}$$

where $\boldsymbol{\rho}_P$ is a vector from the parafoil C.G. to the confluence point and $\mathbf{r}_P$ is a vector from the C.G. to the aerodynamic center of the parafoil such as

$$\boldsymbol{\rho}_P = \rho_{x_P} \mathbf{i}_P + 0\mathbf{j}_P + \rho_{z_P} \mathbf{k}_P, \quad \mathbf{r}_P = r_{x_P} \mathbf{i}_P + 0\mathbf{j}_P + r_{z_P} \mathbf{k}_P$$

and $\mathbf{F}_{cons}$ is force term acting on the parafoil through confluence point due to the vehicle and $\mathbf{T}_{cons}$ is torque term modelled to reflect the returning torque due to the

difference between the parafoil and the vehicle heading angles. In the nominal model it is assumed to be zero at first and is described in the following paragraph. The resultant (active) forces and torques for the vehicle can be expressed also as follow;

$$\mathbf{R}_V = F_{x_V}\mathbf{i}_V + F_{y_V}\mathbf{j}_V + F_{z_V}\mathbf{k}_V + m_V\mathbf{g} - \mathbf{F}_{cons}$$

$$\mathbf{T}_V = L_V\mathbf{i}_V + M_V\mathbf{j}_V + N_V\mathbf{k}_V + \mathbf{r}_V \times \mathbf{F}_{a_V} - \boldsymbol{\rho}_V \times \mathbf{F}_{cons} + \mathbf{T}_{cons} \qquad (2.44)$$

$$= L_V\mathbf{i}_V + M_V\mathbf{j}_V + N_V\mathbf{k}_V + \mathbf{T}_{cons}$$

The hanging vehicle of the Buckeye is composed of a console box, panel, frames and struts etc. and the complexity of the shape prevents accurate modelling for aerodynamic forces and torques. The detail aerodynamic modelling is beyond this research workscope and most parts are not supposed to generate consistent aerodynamic forces or torques except drag. So only drag is taken account for the vehicle's aerodynamic terms. The vehicle's constrained motion is mainly rotational about the confluence point and the rotation torques due to drag is much less than that from weight of the vehicle. For simplification of equations of motion description, the aerodynamic center of the vehicle is assumed to be located at the C.G. of the vehicle ($\mathbf{r}_V = \mathbf{0}$) in above Eqn.(2.44). The term $\mathbf{r}_V$ is provided as an input parameter in the simulation code and can be activated with appropriate aerodynamic model of the vehicle. As described in the following paragraph $\mathbf{F}_{cons}$ is a vector parallel to $\boldsymbol{\rho}_V$ so there's no influence on the vehicle torque($\boldsymbol{\rho}_V \times \mathbf{F}_{cons} = \mathbf{0}$).

Kane's Equation   To construct the Kane's equation, substituting equations (2.43), (2.44) into Eqn. (2.12),

$$(F_r)_P = \boldsymbol{\omega}_r^P \cdot \mathbf{T}_P + \mathbf{v}_r^P \cdot \mathbf{R}_P \quad (r = 1, \ldots, 8)$$

and expanding yields

$$(F_1)_P = \boldsymbol{\omega}_1^P \cdot \mathbf{T}_P + \mathbf{v}_1^P \cdot \mathbf{R}_P = \mathbf{i}_P \cdot \mathbf{T}_P$$

$$= L_P + \rho_{z_P} \rho_{x_V} F_{cons} s_9 c_8 / l_\rho + \rho_{z_P} \rho_{z_V} F_{cons} s_8 s_9 / l_\rho - r_{z_P} F_{y_P}$$

$$(F_2)_P = M_P + r_{z_P} F_{x_P} - r_{x_P} F_{z_P} - F_{cons} \left(\rho_{x_P} s_9^2 \left(\rho_{x_V} s_8 - \rho_{z_V} c_8 \right) \right.$$

$$\left. + c_9 \left(\rho_{z_P} \rho_{x_V} c_8 + \rho_{z_P} \rho_{z_V} s_8 + \rho_{x_P} \rho_{x_V} s_8 c_9 - \rho_{x_P} \rho_{z_V} c_8 c_9 \right) \right) / l_\rho$$

$$(F_3)_P = N_P + r_{x_P} F_{y_P} + T_{cons} - \rho_{x_P} F_{cons} s_9 \left(\rho_{x_V} c_8 + \rho_{z_V} s_8 \right) / l_\rho$$

$$(F_4)_P = \boldsymbol{\omega}_4^P \cdot \mathbf{T}_P + \mathbf{v}_4^P \cdot \mathbf{R}_P = \mathbf{i}_P \cdot \mathbf{R}_P$$

$$= F_{x_P} - m_P g s_2 - \rho_{x_V} F_{cons} c_8 c_9 / l_\rho - \rho_{z_V} F_{cons} s_8 c_9 / l_\rho$$

$$(F_5)_P = F_{y_P} + m_P g s_1 c_2 - F_{cons} s_9 \left(\rho_{x_V} c_8 + \rho_{z_V} s_8 \right) / l_\rho$$

$$(F_6)_P = F_{z_P} + m_P g c_1 c_2 + F_{cons} \left(\rho_{x_V} s_8 - \rho_{z_V} c_8 \right) / l_\rho$$

$$(F_7)_P = (F_8)_P = 0$$

(2.45)

Using Eqn. (2.12) for the vehicle,

$$(F_r)_V = \boldsymbol{\omega}_r^V \cdot \mathbf{T}_V + \mathbf{v}_r^V \cdot \mathbf{R}_V \quad (r = 1, \dots, 8)$$

and expanding yields,

$$(F_1)_V = \boldsymbol{\omega}_1^V \cdot \mathbf{T}_V + \mathbf{v}_1^V \cdot \mathbf{R}_V = (c_9/c_8) \mathbf{i}_V \cdot \mathbf{T}_V$$

$$+ \left[(-\rho_{z_P} s_9 c_8) \mathbf{i}_V + c_9 \left(\rho_{z_V}/c_8 - \rho_{z_P} \right) \mathbf{j}_V - \rho_{z_P} s_8 s_9 \mathbf{k}_V \right] \cdot \mathbf{R}_V$$

$$= L_V c_9/c_8 + \rho_{z_V} F_{y_V} c_9 /c_8 + m_V g \rho_{z_V} s_1 c_2 /c_8$$

$$+ s_8 \left(T_{cons} c_9 /c_8 - \rho_{z_P} F_{z_V} s_9 - \rho_{z_P} \rho_{z_V} F_{cons} s_9 /l_\rho \right)$$

$$+ s_9 \left(m_V g \rho_{z_V} s_2 c_9 /c_8 - \rho_{z_P} F_{x_V} c_8 - \rho_{z_P} \rho_{x_V} F_{cons} c_8 /l_\rho \right.$$

$$\left. - m_V g \rho_{z_V} s_1 s_9 c_2 /c_8 \right) - \rho_{z_P} F_{y_V} c_9 - m_V g \rho_{z_P} s_1 c_8$$

$$- r_{z_V} F_{y_V} c_9 /c_8$$

(2.46a)

$$(F_2)_V = (s_9/c_8)\mathbf{j}_V \cdot \mathbf{T}_V + \left[(\rho_{x_P}s_8 + \rho_{z_P}c_8c_9)\mathbf{i}_V + (\rho_{z_V}s_9/c_8 - \rho_{z_P}s_9)\mathbf{j}_V\right.$$

$$\left. + (\rho_{z_P}s_8c_9 - \rho_{x_P}c_8)\mathbf{k}_V\right] \cdot \mathbf{R}_V$$

$$= \rho_{z_P}\, F_{x_V}\, c_8\, c_9 \;+\; \rho_{z_P}\, \rho_{x_V}\, F_{cons}\, c_8\, c_9\, /l_\rho \;+\; s_8\,(\,\rho_{x_P}\, F_{x_V}\; +\; \rho_{z_P}\, F_{z_V}\, c_9$$

$$+\; \rho_{x_P}\, \rho_{x_V}\, F_{cons}\, /l_\rho \;+\; \rho_{z_P}\, \rho_{z_V}\, F_{cons}\, c_9\, /l_\rho\,) \;-\; \rho_{x_P}\, F_{z_V}\, c_8 \qquad (2.46\text{b})$$

$$-\; m_V\, g\, \rho_{z_P}s_2 \;-\; \rho_{x_P}\, \rho_{z_V}\, F_{cons}\, c_8\, /l_\rho \;-\; m_V\, g\, \rho_{x_P}\, c_1\, c_2$$

$$-\; s_9\,(\,\rho_{z_P}\, F_{z_V}\; +\; r_{z_V}\, F_{y_V}\, /c_8 \;-\; T_{cons}\, t_8 \;-\; L_V\, /c_8 \;-\; \rho_{z_V}\, F_{y_V}\, /c_8$$

$$-\; m_V\, g\, \rho_{z_V}\, s_2\, s_9\, /c_8 \;-\; m_V\, g\, \rho_{z_V}\, s_1\, c_2\, c_9\, /c_8\,)$$

$$(F_3)_V = \left[\rho_{x_P}s_9c_8\mathbf{i}_V + \rho_{x_P}c_9\mathbf{j}_V + \rho_{x_P}s_8s_9\mathbf{k}_V\right] \cdot \mathbf{R}_V$$

$$= \rho_{x_P}\, F_{y_V}\, c_9 \;+\; m_V\, g\rho_{x_P}\, s_1\, c_2 \;+\; \rho_{x_P}\, s_9\,\big[\, F_{x_V}c_8 \qquad (2.46\text{c})$$

$$+\; \rho_{x_V}\, F_{cons}\, c_8\, /l_\rho \;+\; s_8\,(\, F_{z_V}\; +\; \rho_{z_V}\, F_{cons}\, /l_\rho\,)\,\big]$$

$$(F_4)_V = \boldsymbol{\omega}_4^V \cdot \mathbf{T}_V + \mathbf{v}_4^V \cdot \mathbf{R}_V = \left[c_8c_9\mathbf{i}_V - s_9\mathbf{j}_V + s_8c_9\mathbf{k}_V\right] \cdot \mathbf{R}_V$$

$$= F_{x_V}\, c_8\, c_9 \;+\; \rho_{x_V}\, F_{cons}\, c_8\, c_9\, /l_\rho \;+\; s_8\, c_9\,(\, F_{z_V}\; +\; \rho_{z_V}\, F_{cons}\, /l_\rho\,) \qquad (2.46\text{d})$$

$$-\; F_{y_V}\, s_9 \;-\; m_v\, g\, s_2$$

$$(F_5)_V = \left[s_9c_8\mathbf{i}_V + c_9\mathbf{j}_V + s_8s_9\mathbf{k}_V\right] \cdot \mathbf{R}_V$$

$$= F_{y_V}\, c_9 \;+\; m_V\, g\, s_1\, c_2 \;+\; s_9\,(\, F_{x_V}\, c_8 \;+\; \rho_{x_V}\, F_{cons}\, c_8\, /l_\rho \qquad (2.46\text{e})$$

$$+\; s_8\,(\, F_{z_V}\; +\; \rho_{z_V}\, F_{cons}\, /l_\rho\,)\,)$$

$$(F_6)_V = \left[-s_8\mathbf{i}_V + c_8\mathbf{k}_V\right] \cdot \mathbf{R}_V$$

$$= F_{z_V}\, c_8 \;+\; \rho_{z_V}\, F_{cons}\, c_8\, /l_\rho \;+\; m_V\, g\, c_1\, c_2 \qquad (2.46\text{f})$$

$$-\; s_8\,(\, F_{x_V}\; +\; \rho_{x_V}\, F_{cons}\, /l_\rho\,)$$

$$(F_7)_V = \mathbf{j}_V \cdot \mathbf{T}_V + \left[-\rho_{z_V} \mathbf{i}_V + \rho_{x_V} \mathbf{k}_V \right] \cdot \mathbf{R}_V$$

$$= M_V + r_{z_V} F_{x_V} + \rho_{x_V} F_{z_V} + m_V\, g\, \rho_{x_V}\, c_1\, c_2\, c_8$$

$$+ m_V\, g\, \rho_{z_V}\, s_2\, c_8\, c_9 + m_V\, g\, \rho_{z_V}\, s_8\, c_1\, c_2 + m_V\, g\, \rho_{x_V}\, s_1\, s_8\, s_9\, c_2 \qquad (2.46\mathrm{g})$$

$$- r_{x_V} F_{z_V} - \rho_{z_V} F_{x_V} - m_V\, g\, \rho_{x_V}\, s_2\, s_8\, c_9$$

$$- m_V\, g\, \rho_{z_V}\, s_1\, s_9\, c_2\, c_8$$

$$(F_8)_V = \mathbf{k}_V \cdot \mathbf{T}_V + \left[-\rho_{x_V} \mathbf{j}_V \right] \cdot \mathbf{R}_V$$

$$= N_V + r_{x_V} F_{y_V} + r_{z_V} F_{y_V}\, t_8 - \rho_{x_V} F_{y_V} - L_V\, t_8$$

$$- T_{cons}\, c_8 - \rho_{z_V} F_{y_V}\, t_8 - m_V\, g\, \rho_{x_V}\, s_2\, s_9 - T_{cons}\, s_8^2/c_8 \qquad (2.46\mathrm{h})$$

$$- m_V\, g\, \rho_{x_V}\, s_1\, c_2\, c_9 - m_V\, g\, \rho_{z_V}\, s_2\, s_9\, t_8$$

$$- m_V\, g\, \rho_{z_V}\, s_1\, c_2\, c_9\, t_8$$

Following same procedures above, the inertial torques and forces can be written in the form of Eqn.(2.13),

$$(F_r^*)_P = \boldsymbol{\omega}_r^P \cdot \mathbf{T}^*{}_P + \mathbf{v}_r^P \cdot \mathbf{R}^*{}_P \quad (r = 1, \ldots, n - m)$$

Substituting yields

$$(F_1^*)_P = \boldsymbol{\omega}_1^P \cdot \mathbf{T}^*{}_P + \mathbf{v}_1^P \cdot \mathbf{R}^*{}_P = \mathbf{i}_P \cdot \mathbf{T}^*{}_P$$

$$= -\left[I_{xx_P}\dot{u}_1 + I_{xz_P}\dot{u}_3 + I_{xz_P}u_1 u_2 + \left(I_{zz_P} - I_{yy_P} \right)u_2 u_3 \right]$$

$$(F_2^*)_P = -\left[I_{yy_P}\dot{u}_2 + \left(I_{xx_P} - I_{zz_P} \right)u_1 u_3 - I_{xz_P}\left(u_1^2 - u_3^2 \right) \right]$$

$$(F_3^*)_P = -\left[I_{zz_P}\dot{u}_3 + I_{xz_P}\dot{u}_1 + \left(I_{yy_P} - I_{xx_P} \right)u_1 u_2 - I_{xz_P}u_2 u_3 \right]$$

$$(F_4^*)_P = \boldsymbol{\omega}_4^P \cdot \mathbf{T}^*{}_P + \mathbf{v}_4^P \cdot \mathbf{R}^*{}_P = \mathbf{i}_P \cdot \mathbf{R}^*{}_P \qquad (2.47)$$

$$= -m_P\left(\dot{u}_4 - u_3 u_5 + u_2 u_6 \right)$$

$$(F_5^*)_P = -m_P\left(\dot{u}_5 - u_1 u_6 + u_3 u_4 \right)$$

$$(F_6^*)_P = -m_P \left(\dot{u}_6 - u_2 u_4 + u_1 u_5 \right)$$

$$(F_7^*)_P = (F_8^*)_P = 0$$

Using Eqn. (2.13) for the vehicle,

$$(F_r^*)_V = \boldsymbol{\omega}_r^V \cdot \mathbf{T}^*_V + \mathbf{v}_r^V \cdot \mathbf{R}^*_V \quad (r = 1, \ldots, 8)$$

Substituting yields

$$(F_1^*)_V = \boldsymbol{\omega}_1^V \cdot \mathbf{T}^*_V + \mathbf{v}_1^V \cdot \mathbf{R}^*_V$$

$$= (c_9/c_8)\mathbf{i}_V \cdot \mathbf{T}^*_V + \left[(-\rho_{z_P} s_9 c_8)\mathbf{i}_V + c_9 (\rho_{z_V}/c_8 - \rho_{z_P})\mathbf{j}_V \right.$$

$$\left. - \rho_{z_P} s_8 s_9 \mathbf{k}_V \right] \cdot \mathbf{R}^*_V$$

$$(F_2^*)_V = (s_9/c_8)\mathbf{j}_V \cdot \mathbf{T}^*_V + \left[(\rho_{x_P} s_8 + \rho_{z_P} c_8 c_9)\mathbf{i}_V + (\rho_{z_V} s_9/c_8 - \rho_{z_P} s_9)\mathbf{j}_V \right.$$

$$\left. + (\rho_{z_P} s_8 c_9 - \rho_{x_P} c_8)\mathbf{k}_V \right] \cdot \mathbf{R}^*_V$$

$$(F_3^*)_V = \left[\rho_{x_P} s_9 c_8 \mathbf{i}_V + \rho_{x_P} c_9 \mathbf{j}_V + \rho_{x_P} s_8 s_9 \mathbf{k}_V \right] \cdot \mathbf{R}^*_V$$

$$(F_4^*)_V = \boldsymbol{\omega}_4^V \cdot \mathbf{T}^*_V + \mathbf{v}_4^V \cdot \mathbf{R}^*_V$$

$$= \left[c_8 c_9 \mathbf{i}_V - s_9 \mathbf{j}_V + s_8 c_9 \mathbf{k}_V \right] \cdot \mathbf{R}^*_V \tag{2.48}$$

$$(F_5^*)_V = \left[s_9 c_8 \mathbf{i}_V + c_9 \mathbf{j}_V + s_8 s_9 \mathbf{k}_V \right] \cdot \mathbf{R}^*_V$$

$$(F_6^*)_V = \left[- s_8 \mathbf{i}_V + c_8 \mathbf{k}_V \right] \cdot \mathbf{R}^*_V$$

$$(F_7^*)_V = \mathbf{j}_V \cdot \mathbf{T}^*_V + \left[- \rho_{z_V} \mathbf{i}_V + \rho_{x_V} \mathbf{k}_V \right] \cdot \mathbf{R}^*_V$$

$$(F_8^*)_V = \mathbf{k}_V \cdot \mathbf{T}^*_V + \left[- \rho_{x_V} \mathbf{j}_V \right] \cdot \mathbf{R}^*_V$$

As the full expanded form of above equation (2.48) is too long to display, it is abbreviated without difficulty of understanding the derivation of equations.

Substituting Eqn.(2.45),(2.46a-2.46h),(2.47), (2.48) into Kane's equation (2.4), then 8-DOF nonlinear equations of motion can be constructed as following form.

$$\left[(F_r)_P + (F_r)_V \right] + \left[(F_r^*)_P + (F_r^*)_V \right] = 0 \quad (r = 1, \ldots, 8)$$

Substituting yields eight equations of motion which are long algebraic forms with double multiplication of direction cosine matrices for the parafoil and the vehicle. The full 8-DOF equations of motion were derived using a symbolic dynamic solver AUTOLEV^{TM}.[26,27] AUTOLEV^{TM} is an advanced symbolic manipulation computer program and it's purpose is to relieve the user of burdens associated with manually performing such time-consuming tasks specially for deriving multi-body dynamic equations of motion.[27] AUTOLEV^{TM} program has been validated by numerous applications and example. In Appendix A a simple two-body pendulum dynamics was solved by AUTOLEV and the resulting equations of motion are compared to those from Newtonian Mechanics.

Joint Torque Model   The torque model for the vehicle is provided to adjust the yawing moment of the vehicle in flight data identification phase. Let's define $\mathbf{F}_{cons}$ as joint force and $\mathbf{T}_{cons}$ as joint torque acting on the confluence point of the parafoil by the vehicle. The joint force for the parafoil is a fraction of the net resultant force of the vehicle, function of the relative attitudes. It is shown in following equation.

$$
\begin{aligned}
\mathbf{F}_{cons} &= -\big[(\mathbf{F}_{a_V} + \mathbf{G}_V) \cdot -\mathbf{u}\big]\, \mathbf{u} \\
&= \Big\{ [\rho_{x_V} F_{x_V} + \rho_{z_V} F_{z_V} - m_V\, g\, \rho_{x_V}(s_2 c_8 c_9 + s_8 c_1 c_2 - s_1 s_9 c_2 c_8) \\
&\quad\; - m_V\, g\, \rho_{z_V}(s_2 s_8 c_9 - c_1 c_2 c_8 - s_1 s_8 s_9 c_2)]/l_\rho \Big\}\, \mathbf{u} \\
&\triangleq -(F_{cons})\, \mathbf{u}
\end{aligned}
\tag{2.49}
$$

where $\mathbf{u}$ is a unit vector from C.G. of the vehicle to the confluence point such as:

$$
\mathbf{u} = \frac{\boldsymbol{\rho}_V}{\|\boldsymbol{\rho}_V\|} = (\rho_{x_V}/l_\rho)\mathbf{i}_V + (\rho_{z_V}/l_\rho)\mathbf{k}_V, \quad l_\rho = \|\boldsymbol{\rho}_V\|
$$

And the constraint joint torque, $\mathbf{T}_{cons}$ is caused by the difference of heading angle between the parafoil and the vehicle. The universal joint model as for longitudinal motion is not sufficient to describe the constraint torque. For lateral/directional motion the joint is modelled as a bar on which the vehicle is hanging as in Figure 2.3. As a nominal model, this torque is assumed such that there is no aerodynamic, structural or elastic torque due to twisting of risers, suspension lines or canopy shape.

H

$B\Psi r/H$ (rad)

Ψr

B

$\mathbf{F}_{cons}$

Θr

k_p

$B\Psi r/H$

$\frac{1}{2}\,\mathbf{F}_{cons}\cdot k_p$

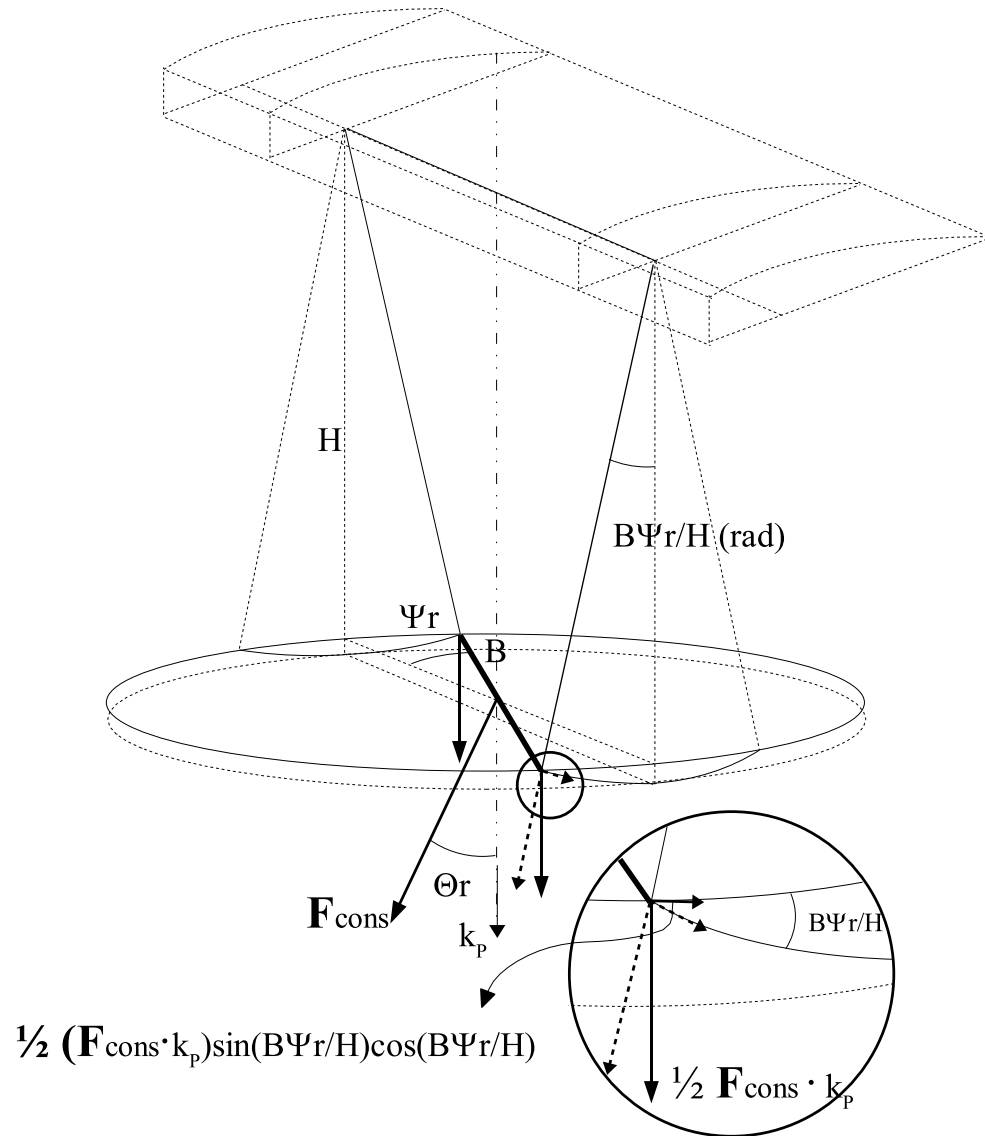$\frac{1}{2}\,(\mathbf{F}_{cons}\cdot k_p)sin(B\Psi r/H)cos(B\Psi r/H)$

Figure 2.3 Joint Model for Relative Torque

In the phase of comparing with flight data, a damping term proportional to the yaw rate change is considered to describe the motion in addition to the spring term proportional to the relative yaw angle here.

$$
\begin{aligned}
\mathbf{T}_{cons} &= -\left[(\mathbf{F}_{cons} \cdot \mathbf{k}_P)1/2 \sin\left(2(B/H)\Psi_r\right)\right]\mathbf{k}_P \\
&= -\left[-0.5B \ F_{cons} \sin\left(2(B/H)\Psi_r\right)(\rho_{x_V} \sin\Theta_r - \rho_{z_V}\cos\Theta_r)/\|\boldsymbol{\rho}_V\|\right]\mathbf{k}_P \\
&= \left[0.5B \ F_{cons} \sin\left(2B \ q_9/H\right)(\rho_{x_V}s_8 - \rho_{z_V}c_8)/l_\rho\right]\mathbf{k}_P \\
&\triangleq -(T_{cons})\,\mathbf{k}_P
\end{aligned}
\tag{2.50}
$$

where B is half width of the hanging point of the vehicle, H is height from the parafoil quarter chord to the confluence point along the Z_P ($\mathbf{k}_P$) axis as in Figure 2.3.

2.4 Linearized Equation of Motion

For stability and control analysis the 8-DOF nonlinear equations of motion are linearized. It is assumed that the motion consists of small deviations about a reference condition of steady state flight. From the nonlinear equations of motion in section 2.3, linearized equations of motion were derived using the small angle, small-perturbation theory and Taylor series expansion method.

All the variables in the equations of motion are replaced by a reference value plus a perturbation. The reference values so called trimmed values of all the variables are denoted by a subscript zero, and the small perturbations by prefix Δ as in the followings:

$$
\begin{aligned}
q_r &\approx q_{r_0} + \Delta q_r, \\
u_r &\approx u_{r_0} + \Delta u_r, \quad (r = 1, \cdots, 8)
\end{aligned}
\tag{2.51}
$$

And the forces and torques also can be represented as follows:

$$
\begin{array}{cc}
F_{x_P} \approx F_{x_{P0}} + \Delta F_{x_P}, & L_P \approx L_{P0} + \Delta L_P, \\
\vdots & \vdots \\
F_{z_V} \approx F_{z_{V0}} + \Delta F_{z_V}, & N_V \approx N_{V0} + \Delta N_V
\end{array}
\tag{2.52}
$$

In this research the reference flight is gliding without power and the condition is assumed to be symmetric and steady. Thus $V_0 = \Phi_0 = \Psi_0 = P_0 = Q_0 = R_0 = 0$ and the relative terms $\Phi_{r_0} = \Psi_{r_0} = \dot{\Phi}_{r_0} = \dot{\Theta}_{r_0} = \dot{\Psi}_{r_0} = 0$. Using the generalized coordinates and speeds defined in the previous section, zero reference values can be represented as follows:

$$q_{1_0} = \Phi_0 = 0, \quad q_{2_0} \quad = \Theta_0, \qquad q_{3_0} = \Psi_0 = 0,$$

$$q_{4_0} = X_0 = 0, \quad q_{5_0} \quad = Y_0 = 0, \quad q_{6_0} = Z_0 = -h, \qquad \text{(2.53a)}$$

$$q_{7_0} = \Phi_{r_0} = 0, \quad q_{8_0} \quad = \Theta_{r_0}, \qquad q_{9_0} = \Psi_{r_0} = 0,$$

$$u_{1_0} = P_0 = 0, \quad u_{2_0} \quad = Q_0 = 0, \quad u_{3_0} = R_0 = 0,$$

$$u_{4_0} = U_0, \qquad u_{5_0} \quad = V_0 = 0, \quad u_{6_0} = W_0,$$

$$\text{(2.53b)}$$

$$u_{7_0} = P_{V_0} = 0, \quad u_{8_0} \quad = Q_{V_0} = 0, \quad u_{9_0} = R_{V_0} = 0.$$

All the perturbation quantities and their derivatives are assumed to be small, so that their squares and products are negligible compared to first-order quantities. In dealing with the trigonometric functions in equations the small angle assumption is adopted such that $\sin\theta \approx \theta$, $\cos\theta \approx 1$ for general small angle θ in radian. In Ref. 28 these small angle approximations give quite acceptable results even for perturbed angles as large as 15 degrees. The perturbed angles of the Buckeye-vehicle are within the range. To make the complex description of 8-DOF equations of motion brief, several assumptions are made for further deriving of equations. Those assumptions are itemized as follows:

- On aerodynamics of the parafoil: In steady-state of gliding condition, the active side force and roll, yaw axis torques in the reference condition are assumed to be zeros and presented in the following equations.

$$F_{yP0} = L_{P0} = N_{P0} = 0$$

- On aerodynamics of the vehicle: The configuration of the hanging vehicle of the Buckeye doesn't have aerodynamic shape enough to show the forces and torques in general function of aerodynamic parameters. So, only drag is assumed to exist and the other aerodynamic forces and torques are neglected in deriving the linearized equations.

$$F_{y_V} = L_V = M_V = N_V = 0$$

2.4.1 Linearized Model

Following the procedures for derivations of 8-DOF nonlinear equations of motion and using the assumtions described in previous section including small angle and small-perturbation theory, the linearized equations of motion can be derived for the generalized coordinates and speeds.

Applying the small-perturbation theory to the active force equation $F_r (= (F_r)_P + (F_r)_V)$ in the Eqn.(2.45) yields

$$F_1 = \Delta L_P - r_{z_P} \Delta F_{y_P} - C_{10} m_V g c_{2_0} \Delta q_1$$

$$- [C_{T1} - C_{13} C_4 B^2 t_{8_0} / (H l_\rho^2) - C_{13} \rho_{z_P} C_3 / l_\rho^2] \Delta q_9$$

$$F_2 = \Delta M_P + r_{z_P} \Delta F_{x_P} - r_{x_P} \Delta F_{z_P} + [C_6 - \rho_{x_V} (\rho_{x_P} C_4$$

$$+ \rho_{z_P} C_3) / l_\rho^2] \Delta F_{x_V} + [C_{T2} - (C_{13} (\rho_{x_P} C_3$$

$$- \rho_{z_P} C_4) + C_2 m_V g (\rho_{x_P} C_4 + \rho_{z_P} C_3)) / l_\rho^2] \Delta q_8$$

$$- [C_5 + \rho_{z_V} (\rho_{x_P} C_4 + \rho_{z_P} C_3) / l_\rho^2] \Delta F_{z_V}$$

$$- m_V g [C_7 + C_2 (\rho_{x_P} C_4 + \rho_{z_P} C_3) / l_\rho^2] \Delta q_2$$

$$F_3 = \Delta N_P + r_{x_P} \Delta F_{y_P} + m_V g \rho_{x_P} c_{2_0} \Delta q_1 + [\rho_{x_P} C_{F1}$$

$$+ C_{13} C_4 B^2 / (H l_\rho^2) - C_{13} \rho_{x_P} C_3 / l_\rho^2] \Delta q_9$$

$$F_4 = \Delta F_{x_P} + s_{8_0} \Delta F_{z_V} + c_{8_0} \Delta F_{x_V} - C_{F2} \Delta q_8$$

$$- (m_P + m_V) g c_{2_0} \Delta q_2 \tag{2.54}$$

$$F_5 = \Delta F_{y_P} + \Delta q_1 \left(m_P + m_V \right) g\, c_{2_0} + \Delta q_9\, C_{F1}$$

$$F_6 = \Delta F_{z_P} + c_{8_0}\, \Delta F_{z_V} - C_{F1}\, \Delta q_8 - s_{8_0}\, \Delta F_{x_V}$$

$$- \left(m_P + m_V \right) g\, s_{2_0}\, \Delta q_2$$

$$F_7 = \rho_{x_V}\, \Delta F_{z_V} - \rho_{z_V}\, \Delta F_{x_V} - C_1\, m_V\, g\, \Delta q_2 - C_1\, m_V\, g\, \Delta q_8$$

$$F_8 = -C_9\, m_V\, g\, c_{2_0}\, \Delta q_1 - \left[\, C_9\, m_V\, g\, s_{2_0} + C_{13}\, C_4\, B^2 \,/(\, H\, l_\rho^2\, c_{8_0}) \,\right] \Delta q_9$$

where

$$C_1 = \left(\, \rho_{x_V}\, s_{(2_0 + 8_0)} - \rho_{z_V}\, c_{(2_0 + 8_0)} \,\right)$$

$$C_2 = \left(\, \rho_{x_V}\, c_{(2_0 + 8_0)} + \rho_{z_V}\, s_{(2_0 + 8_0)} \,\right)$$

$$C_3 = \left(\, \rho_{x_V}\, c_{8_0} + \rho_{z_V}\, s_{8_0} \,\right)$$

$$C_4 = \left(\, \rho_{x_V}\, s_{8_0} - \rho_{z_V}\, c_{8_0} \,\right)$$

$$C_5 = \left(\, \rho_{x_P}\, c_{8_0} - \rho_{z_P}\, s_{8_0} \,\right)$$

$$C_6 = \left(\, \rho_{x_P}\, s_{8_0} + \rho_{z_P}\, c_{8_0} \,\right)$$

$$C_7 = \left(\, - \rho_{x_P}\, s_{2_0} + \rho_{z_P}\, c_{2_0} \,\right)$$

$$C_8 = \left(\, \rho_{x_P}\, c_{2_0} + \rho_{z_P}\, s_{2_0} \,\right)$$

$$C_9 = \rho_{x_V} + \rho_{z_V}\, t_{8_0}$$

$$C_{10} = \rho_{z_P} - \rho_{z_V}\, c_{8_0}$$

$$C_{11} = \left(C_5 - \rho_{x_V} \right)$$

$$C_{12} = \left(C_6 - \rho_{z_V} \right)$$

$$C_{13} = \left(m_V\, g\, C_1 - \rho_{x_V}\, F_{x_V 0} - \rho_{z_V}\, F_{z_V 0} \right)$$

$$C_{T1} = \left[\, m_V\, g\, \left(C_2 + s_{2_0}\, C_4 \right) + F_{z_V 0}\, \rho_{x_V} - F_{x_V 0}\, \rho_{z_V} \right.$$

$$\left. + \rho_{z_P} \left(F_{z_V 0}\, s_{8_0} + F_{x_V 0}\, c_{8_0} \right) \right]$$

$$C_{T2} = \left[C_5\, F_{x_V 0} + C_6\, F_{z_V 0} - m_V\, g\, C_1 \right]$$

$$C_{F1} = (F_{xV0}\, c_{80} + F_{zV0}\, s_{80})$$

$$C_{F2} = (F_{xV0}\, s_{80} - F_{zV0}\, c_{80})$$

Note that above Eqn.(2.54) shows perturbed active forces from the steady-state gliding flight in the research. Based on the assumption of steady-state gliding flight of no acceleration in any axis, following equations are set to hold.

$$0 = M_{P0} + r_{zP}\, F_{xP0} - r_{xP}\, F_{zP0} + C_6\, F_{xV0} - C_5\, F_{zV0} - m_V\, g\, C_8$$
$$- C_{13}\, (\rho_{xP}\, C_4 + \rho_{zP} C_3)\, /l_\rho^2$$

$$0 = F_{xP0} + c_{80}\, F_{xV0} + s_{80}\, F_{zV0} - (m_P + m_V)\, g\, s_{20}$$

$$0 = F_{zP0} + c_{80}\, F_{zV0} - s_{80}\, F_{xV0} + (m_P + m_V)\, g\, c_{20}$$

$$0 = \rho_{xV}\, F_{zV0} - \rho_{zV}\, F_{xV0} + m_V\, g\, C_2$$

Linearization of joint force (2.49) and torque (2.50) show that they can be represented by the constants coefficients as follows:

$$F_{cons} = (C_{13} + \rho_{xV}\, \Delta F_{xV} + \rho_{zV}\, \Delta F_{zV} + m_V\, g\, C_2\,)/l_\rho\, \Delta q_2$$
$$+ m_V\, g\, C_2\, /l_\rho\, \Delta q_8 \tag{2.55}$$
$$T_{cons} = C_{13}\, C_4\, [B^2/(H\, l_\rho^2)]\, \Delta q_9$$

In the same manner linearization of inertial term $F_r^*\, (= (F_r)_P^* + (F_r)_V^*)$ can be represented as

$$F_1^* = -C_{I2}\, \Delta \dot{u}_1 - C_{I1}\, \Delta \dot{u}_3 + m_V\, C_{10}\, \Delta \dot{u}_5 - C_{I3}\, \Delta \dot{u}_9$$
$$- m_V\, C_{10}\, u_{60}\, \Delta u_1 + m_V\, C_{10}\, u_{40}\, \Delta u_3 + m_V\, C_{10}\, D_8\, \Delta u_9$$

$$F_2^* = -C_{I5}\, \Delta \dot{u}_2 + m_V\, D_9\, \Delta \dot{u}_4 + m_V\, D_{10}\, \Delta \dot{u}_6 + C_{I4}\, \Delta \dot{u}_8$$
$$- m_V\, D_{11}\, \Delta u_2$$

$$F_3^* = -C_{I1}\, \Delta \dot{u}_1 - C_{I7}\, \Delta \dot{u}_3 - m_V\, \rho_{xP}\, \Delta \dot{u}_5 + C_{I6}\, \Delta \dot{u}_9$$
$$+ m_V\, u_{60}\, \rho_{xP}\, \Delta u_1 - m_V\, u_{40}\, \rho_{xP}\, \Delta u_3 - m_V\, \rho_{xP}\, D_8\, \Delta u_9$$

$$F_4^* = m_V D_9 \Delta \dot{u}_2 - (m_P + m_V) \Delta \dot{u}_4 - m_V C_4 \Delta \dot{u}_8 + D_{13} \Delta u_2 \qquad (2.56)$$

$$F_5^* = m_V C_{10} \Delta \dot{u}_1 - m_V \rho_{x_P} \Delta \dot{u}_3 - (m_P + m_V) \Delta \dot{u}_5 + m_V C_9 \Delta \dot{u}_9$$

$$+ u_{6_0}(m_P + m_V) \Delta u_1 - u_{4_0}(m_P + m_V) \Delta u_3 - m_V D_8 \Delta u_9$$

$$F_6^* = m_V D_{10} \Delta \dot{u}_2 - (m_P + m_V) \Delta \dot{u}_6 - m_V C_3 \Delta \dot{u}_8 + D_{14} \Delta u_2$$

$$F_7^* = C_{I4} \Delta \dot{u}_2 - m_V C_4 \Delta \dot{u}_4 - m_V C_3 \Delta \dot{u}_6 - C_{I9} \Delta \dot{u}_8$$

$$+ m_V D_{12} \Delta u_2$$

$$F_8^* = -C_{I10} \Delta \dot{u}_1 + C_{I6} \Delta \dot{u}_3 + m_V C_9 \Delta \dot{u}_5 - C_{I11} \Delta \dot{u}_9$$

$$- m_V u_{6_0} C_9 \Delta u_1 + m_V u_{4_0} C_9 \Delta u_3 + m_V C_9 D_8 \Delta u_9$$

where all constant terms,

$$C_{I1} = I_{xz_P} - m_V C_{10} \rho_{x_P}$$

$$C_{I2} = I_{xx_P} + m_V C_{10}{}^2 + I_{xx_V}/c_{8_0}{}^2$$

$$C_{I3} = m_V C_{10} C_9 + (I_{xz_V} - I_{xx_V} t_{8_0})/c_{8_0}$$

$$C_{I4} = m_V (C_5 \rho_{x_V} + C_6 \rho_{z_V})$$

$$C_{I5} = I_{yy_P} + m_V (C_5{}^2 + C_6{}^2)$$

$$C_{I6} = m_V C_9 \rho_{x_P}$$

$$C_{I7} = I_{zz_P} + m_V \rho_{x_P}{}^2$$

$$C_{I9} = I_{yy_V} + m_V (\rho_{x_V}{}^2 + \rho_{z_V}{}^2)$$

$$C_{I10} = m_V C_{10} C_9 + I_{xz_V}/c_{8_0} - I_{zz_V} s_{8_0}/c_{8_0}{}^2$$

$$C_{I11} = I_{zz_V} + m_V C_9{}^2 - I_{xz_V} t_{8_0} - t_{8_0} (I_{xz_V} - I_{xx_V} t_{8_0})$$

$$D_8 = (u_{10_0} - u_{12_0} t_{8_0} - u_{4_0}/c_{8_0})$$

$$D_9 = (C_5 s_{8_0} - C_6 c_{8_0})$$

$$D_{10} = (C_5 c_{8_0} + C_6 s_{8_0})$$

$$D_{11} = C_5\, u_{10_0} + C_6\, u_{12_0}$$

$$D_{12} = \rho_{x_V}\, u_{10_0} + \rho_{z_V}\, u_{12_0}$$

$$D_{13} = m_V\, D_6 - m_P\, u_{6_0}$$

$$D_{14} = m_V\, D_7 + m_P\, u_{4_0}$$

Substituting those F_r and F_r^* in Eqn.(2.54),(2.56) into Kane's equation makes 8-DOF linear equations of motion of the Buckeye parafoil two-body system. From the linearized Kane's equations, moving all terms except accelerations terms to RHS and multiply -1 on both sides yields

$$
\begin{aligned}
C_{I2}\,\Delta\dot{u}_1 &+ C_{I1}\,\Delta\dot{u}_3 - m_V\,C_{10}\,\Delta\dot{u}_5 + C_{I3}\,\Delta\dot{u}_9 \\
&= m_V\,C_{10}\,u_{6_0}\,\Delta u_1 + m_V\,C_{10}\,u_{4_0}\,\Delta u_3 + m_V\,C_{10}\,D_8\,\Delta u_9 \\
&\quad + \Delta L_P - r_{z_P}\,\Delta F_{y_P} - \Delta q_1\,m_V\,g\,c_{2_0}\,C_{10} \\
&\quad - [C_{T1} - C_{13}\,C_4\,B^2\,t_{8_0}\,/(H\,l_\rho^2) - C_{13}\,\rho_{z_P}\,C_3\,/\,l_\rho^2]\Delta q_9
\end{aligned}
\tag{2.57a}
$$

$$
\begin{aligned}
C_{I5}\,\Delta\dot{u}_2 &- m_V\,D_9\,\Delta\dot{u}_4 - m_V\,D_{10}\,\Delta\dot{u}_6 - C_{I4}\,\Delta\dot{u}_8 \\
&= -m_V\,D_{11}\,\Delta u_2 + \Delta M_P + r_{z_P}\,\Delta F_{x_P} - r_{x_P}\,\Delta F_{z_P} \\
&\quad + [C_6 - \rho_{x_V}\,(\rho_{x_P}\,C_4 + \rho_{z_P}C_3)\,/l_\rho^2]\,\Delta F_{x_V} \\
&\quad + [C_{T2} - \big(C_{13}\,(\rho_{x_P}\,C_3 - \rho_{z_P}\,C_4) \\
&\qquad\quad + C_2\,m_V\,g\,(\rho_{x_P}\,C_4 + \rho_{z_P}C_3)\big)\,/\,l_\rho^2]\,\Delta q_8 \\
&\quad - [C_5 + \rho_{z_V}\,(\rho_{x_P}\,C_4 + \rho_{z_P}C_3)\,/l_\rho^2]\,\Delta F_{z_V} \\
&\quad - m_V\,g\,[C_7 + C_2\,(\rho_{x_P}\,C_4 + \rho_{z_P}C_3)\,/l_\rho^2]\,\Delta q_2
\end{aligned}
\tag{2.57b}
$$

$$
\begin{aligned}
C_{I1}\,\Delta\dot{u}_1 &+ C_{I7}\,\Delta\dot{u}_3 + m_V\,\rho_{x_P}\,\Delta\dot{u}_5 - C_{I6}\,\Delta\dot{u}_9 \\
&= m_V\,u_{6_0}\,\rho_{x_P}\,\Delta u_1 - m_V\,u_{4_0}\,\rho_{x_P}\,\Delta u_3 - m_V\,\rho_{x_P}\,D_8\,\Delta u_9 \\
&\quad + \Delta N_P + r_{x_P}\,\Delta F_{y_P} + \Delta q_1\,m_V\,g\,c_{2_0}\,\rho_{x_P} \\
&\quad + [\rho_{x_P}\,C_{F1} + C_{13}\,C_4\,B^2/(H\,l_\rho^2) - C_{13}\,\rho_{x_P}C_3\,/\,l_\rho^2]\Delta q_9
\end{aligned}
\tag{2.57c}
$$

$$-m_V\, D_9\, \Delta \dot{u}_2 \;+ (m_P + m_V)\, \Delta \dot{u}_4 + m_V\, C_4\, \Delta \dot{u}_8$$
$$= D_{13}\, \Delta u_2 + \Delta F_{x_P} + c_{8_0}\, \Delta F_{x_V} + s_{8_0}\, \Delta F_{z_V} - \Delta q_2\, (m_P \tag{2.57d}$$
$$+ m_V)\, g\, c_{2_0} - \Delta q_8\, C_{F2}$$

$$-m_V\, C_{10}\, \Delta \dot{u}_1 + m_V\, C_9\, \Delta \dot{u}_3 + (m_P + m_V)\, \Delta \dot{u}_5 - m_V\, \rho_{x_V}\, \Delta \dot{u}_9$$
$$= u_{6_0}(m_P + m_V)\, \Delta u_1 - u_{4_0}(m_P + m_V)\, \Delta u_3 - m_V\, D_8\, \Delta u_9 \tag{2.57e}$$
$$+ \Delta F_{y_P} + \Delta q_1\, (m_P + m_V)\, g\, c_{2_0} + \Delta q_9\, C_{F1}$$

$$-m_V\, D_{10}\, \Delta \dot{u}_2 + (m_P + m_V)\, \Delta \dot{u}_6 + m_V\, C_3\, \Delta \dot{u}_8$$
$$= D_{14}\, \Delta u_2 + \Delta F_{z_P} - s_{8_0}\, \Delta F_{x_V} + c_{8_0}\, \Delta F_{z_V} - \Delta q_2\, (m_P \tag{2.57f}$$
$$+ m_V)\, g\, s_{2_0} - \Delta q_8\, C_{F1}$$

$$-C_{I4}\, \Delta \dot{u}_2 + m_V\, C_4\, \Delta \dot{u}_4 + m_V\, C_3\, \Delta \dot{u}_6 + C_{I9}\, \Delta \dot{u}_8$$
$$= m_V\, D_{12}\, \Delta u_2 + \rho_{x_V}\, \Delta F_{z_V} - \rho_{z_V}\, \Delta F_{x_V} - \Delta q_2\, m_V\, g\, C_1 \tag{2.57g}$$
$$- \Delta q_8\, m_V\, g\, C_1$$

$$C_{I10}\, \Delta \dot{u}_1 - C_{I6}\, \Delta \dot{u}_3 - m_V\, C_9\, \Delta \dot{u}_5 + C_{I11}\, \Delta \dot{u}_9$$
$$= -m_V\, u_{6_0}\, C_9\, \Delta u_1 + m_V\, u_{4_0}\, C_9\, \Delta u_3 + m_V\, C_9\, D_8\, \Delta u_9$$
$$- \Delta q_1\, m_V\, g\, c_{2_0}\, C_9 \tag{2.57h}$$
$$- [\, C_9\, m_V\, g\, s_{2_0} + C_{13}\, C_4\, B^2 /(\, H\, l_\rho^2\, c_{8_0})\,]\, \Delta q_9$$

Note that above equations of motion are nothing but another expression of Newton's second law, $\mathbf{M}\,\mathbf{a} = \mathbf{F}$.

The linear equations of motion in Eqn.(2.57a) - (2.57h) can be represented for state-space form $\dot{x} = A\,x + B\,u$ which is used for linear system analysis. To do so all the force and torque terms are represented as function of states defined as follows:

$$\mathbf{x} = [\, \Delta u_4,\ \Delta u_6,\ \Delta u_2,\ \Delta q_2,\ \Delta u_8,\ \Delta q_8,\ \Delta u_5,\ \Delta u_1,\ \Delta u_3,\ \Delta q_1,\ \Delta u_9,\ \Delta q_9\,]$$

Those generalized coordinate and speed terms can be replaced with familiar terms with physical sense in the following respectively.

$$\mathbf{x} = [u,\ w,\ q,\ \theta,\ q_V,\ \theta_r,\ v,\ p,\ r,\ \phi,\ r_V,\ \psi_r]$$

Presenting the forces and torques with perturbed states and their stability derivatives, we can define the forces and torques as in following equations. Forces and torques can be represented by Taylor series expansion about any parameters, however, the forces and torques are represented as function of a few parameters which regarded as meaningful effect on them for very slow flight region of the Buckeye in the research. Representing the forces and torques with stability derivatives and perturbed states in body axes, subscript b, yields

$$\Delta F_{x_P} = (F_{x_u})_b \Delta u + (F_{x_w})_b \Delta w + (F_{x_q})_b \Delta q + (F_{x\,\delta e})_b \delta e$$

$$\Delta F_{y_P} = (F_{y_v})_b \Delta v + (F_{y_p})_b \Delta p + (F_{y_r})_b \Delta r + (F_{y_{\delta r}})_b \delta r$$

$$\Delta F_{z_P} = (F_{z_u})_b \Delta u + (F_{z_w})_b \Delta w + (F_{z_q})_b \Delta q + (F_{z\,\delta e})_b \delta e$$

$$\Delta L_P = (L_v)_b \Delta v + (L_p)_b \Delta p + (L_r)_b \Delta r + (L_{\delta r})_b \delta r$$

$$\Delta M_P = (M_u)_b \Delta u + (M_w)_b \Delta w + (M_q)_b \Delta q + (M_{\delta e})_b \delta e \qquad (2.58)$$

$$\Delta N_P = (N_v)_b \Delta v + (N_p)_b \Delta p + (N_r)_b \Delta r + (N_{\delta r})_b \delta r$$

$$\Delta F_{x_V} = (F_{x_u V})_b \Delta u_V + (F_{x_{\Delta \theta_r}})_b \Delta \theta_r$$

$$\Delta F_{z_V} = (F_{z_u V})_b \Delta u_V + (F_{z_{\Delta \theta_r}})_b \Delta \theta_r$$

where perturbed control input δe is symmetrical deflection of trailing edge flap of the parafoil and δr is asymmetric differential deflection of the trailing edge flap defined in the following equation.

$$\delta e \equiv \frac{\delta(flap)_{left} + \delta(flap)_{right}}{2}$$

$$\delta r \equiv \delta(flap)_{left} - \delta(flap)_{right}$$

In above equation, Δu_V can be represented from the linearized kinematic constraint

equation,

$$\Delta u_V = \cos\Theta_{r_0}\Delta u - \sin\Theta_{r_0}\Delta w + (\rho_{x_P}\sin\Theta_{r_0} + \rho_{z_P}\cos\Theta_{r_0})\Delta q$$

$$- \rho_{z_V}\Delta q_V - W_{0_V}\Delta\theta_r$$

$$U_{0_V} = U_0\cos\Theta_{r_0} - W_0\sin\Theta_{r_0}$$

$$W_{0_V} = U_0\sin\Theta_{r_0} + W_0\cos\Theta_{r_0}$$

(2.59)

Observing the linearized Equations of motion in Eqn.(2.57a)-(2.57h) reveals that the longitudinal and lateral/directional motions are not coupled. In addition, the forces and torques in Eqn.(2.58) show the parameters in one axis don't affect another axes's forces and torques. Thus we can analyze the longitudinal and the lateral/directional motion separately and respectively. Solving Eqn.(2.57a)-(2.57h) with Eqn.(2.58) for $\dot{\mathbf{x}}$ yields state-space form of $\dot{\mathbf{x}} = \mathbf{A}\mathbf{x} + \mathbf{B}\mathbf{u}$. Rearranging the longitudinal equations of motion in Eqn.(2.57b),(2.57d),(2.57f),(2.57g) and solving them about the longitudinal states shows

$$\dot{\mathbf{x}} = \mathbf{A}_{lo}\mathbf{x} + \mathbf{B}_{lo}\mathbf{u} \tag{2.60a}$$

where states $\mathbf{x} = [\Delta u, \Delta w, \Delta q, \Delta\theta, \Delta q_V, \Delta\theta_r]$, control $\mathbf{u} = \delta e$,

$$\mathbf{A}_{lo} = \begin{bmatrix} A_{1,1}^{lo} & A_{1,2}^{lo} & A_{1,3}^{lo} & A_{1,4}^{lo} & A_{1,5}^{lo} & A_{1,6}^{lo} \\ A_{2,1}^{lo} & A_{2,2}^{lo} & A_{2,3}^{lo} & A_{2,4}^{lo} & A_{2,5}^{lo} & A_{2,6}^{lo} \\ A_{3,1}^{lo} & A_{3,2}^{lo} & A_{3,3}^{lo} & A_{3,4}^{lo} & A_{3,5}^{lo} & A_{3,6}^{lo} \\ 0 & 0 & 1 & 0 & 0 & 0 \\ A_{5,1}^{lo} & A_{5,2}^{lo} & A_{5,3}^{lo} & A_{5,4}^{lo} & A_{5,5}^{lo} & A_{5,6}^{lo} \\ 0 & 0 & -1 & 0 & 1 & 0 \end{bmatrix} \tag{2.60b}$$

$$\mathbf{B}_{lo} = \begin{bmatrix} B_{1,1}^{lo} \\ B_{2,1}^{lo} \\ B_{3,1}^{lo} \\ 0 \\ B_{5,1}^{lo} \\ 0 \end{bmatrix} \tag{2.60c}$$

All matrix elements are represented in the appendix C.

Also the lateral/directional state-space equations can be represented as follows:

$$\dot{\mathbf{x}} = \mathbf{A}_{la}\,\mathbf{x} + \mathbf{B}_{la}\,\mathbf{u} \tag{2.61a}$$

where states $\mathbf{x} = [\Delta v, \Delta p, \Delta r, \Delta \phi, \Delta r_V, \Delta \psi_r]$, control $\mathbf{u} = \delta r$

$$\mathbf{A}_{la} = \begin{bmatrix} A_{1,1}^{la} & A_{1,2}^{la} & A_{1,3}^{la} & A_{1,4}^{la} & A_{1,5}^{la} & A_{1,6}^{la} \\ A_{2,1}^{la} & A_{2,2}^{la} & A_{2,3}^{la} & A_{2,4}^{la} & A_{2,5}^{la} & A_{2,6}^{la} \\ A_{3,1}^{la} & A_{3,2}^{la} & A_{3,3}^{la} & A_{3,4}^{la} & A_{3,5}^{la} & A_{3,6}^{la} \\ 0 & 1 & \tan\Theta_0 & 0 & 0 & 0 \\ A_{5,1}^{la} & A_{5,2}^{la} & A_{5,3}^{la} & A_{5,4}^{la} & A_{5,5}^{la} & A_{5,6}^{la} \\ 0 & -\tan\Theta_{r_0} & -1 & 0 & 1/\cos\Theta_{r_0} & 0 \end{bmatrix} \tag{2.61b}$$

$$\mathbf{B}_{la} = \begin{bmatrix} B_{1,1}^{la} \\ B_{2,1}^{la} \\ B_{3,1}^{la} \\ 0 \\ B_{5,1}^{la} \\ 0 \end{bmatrix} \tag{2.61c}$$

And the matrix elements are also in the appendix C.

The matrices $\mathbf{A}, \mathbf{B}$ are composed of dimensional stability derivatives and the definitions are in Table 2.1 and 2.2.[28,29] Note that the dimensional derivatives in

Eqn.(2.58) are those for body axes, otherwise those in the tables are for stability axes. To construct those system matrices in body axes, those dimensional derivatives in the table should be converted to ones for body axis with following relationships between the body axes, subscript b, and the stability axes, no subscript.[30] For the longitudinal derivatives,

$$(F_{x_u})_b = F_{x_u} \cos^2 \alpha_0 - (F_{x_w} + F_{z_u}) \sin \alpha_0 \cos \alpha_0 + F_{z_w} \sin^2 \alpha_0$$

$$(F_{x_w})_b = F_{x_w} \cos^2 \alpha_0 + (F_{x_u} - F_{z_w}) \sin \alpha_0 \cos \alpha_0 - F_{z_u} \sin^2 \alpha_0$$

$$(F_{z_u})_b = F_{z_u} \cos^2 \alpha_0 - (F_{z_w} - F_{x_u}) \sin \alpha_0 \cos \alpha_0 - F_{x_w} \sin^2 \alpha_0$$

$$(F_{z_w})_b = F_{z_w} \cos^2 \alpha_0 + (F_{z_u} + F_{x_w}) \sin \alpha_0 \cos \alpha_0 + F_{x_u} \sin^2 \alpha_0$$

$$(F_{x_q})_b = F_{x_q} \cos \alpha_0 - F_{z_q} \sin \alpha_0$$

$$(F_{z_q})_b = F_{x_q} \cos \alpha_0 + F_{x_q} \sin \alpha_0$$

$$(M_u)_b = M_u \cos \alpha_0 - M_w \sin \alpha_0$$

$$(M_w)_b = M_w \cos \alpha_0 + M_u \sin \alpha_0$$

$$(M_q)_b = M_q \tag{2.62}$$

$$(F_{x_{\delta e}})_b = F_{x_{\delta e}} \cos \alpha_0 - F_{z_{\delta e}} \sin \alpha_0$$

$$(F_{z_{\delta e}})_b = F_{z_{\delta e}} \cos \alpha_0 + F_{x_{\delta e}} \sin \alpha_0$$

$$(M_{\delta e})_b = M_{\delta e}$$

$$(F_{x_{u_V}})_b = F_{x_{u_V}} \cos^2 \alpha_0 - (F_{x_{w_V}} + F_{z_{u_V}}) \sin \alpha_0 \cos \alpha_0 + F_{x_{w_V}} \sin^2 \alpha_0$$

$$(F_{x_{w_V}})_b = F_{x_{w_V}} \cos^2 \alpha_0 + (F_{x_{u_V}} - F_{z_{w_V}}) \sin \alpha_0 \cos \alpha_0 - F_{z_{u_V}} \sin^2 \alpha_0$$

$$(F_{z_{u_V}})_b = F_{z_{u_V}} \cos^2 \alpha_0 - (F_{z_{w_V}} - F_{x_{u_V}}) \sin \alpha_0 \cos \alpha_0 - F_{x_{w_V}} \sin^2 \alpha_0$$

$$(F_{z_{w_V}})_b = F_{z_{w_V}} \cos^2 \alpha_0 + (F_{z_{u_V}} + F_{x_{w_V}}) \sin \alpha_0 \cos \alpha_0 + F_{x_{u_V}} \sin^2 \alpha_0$$

$$(F_{x_{\theta r_V}})_b = F_{x_{\alpha_V}} = U_{0_V} F_{x_{w_V}}$$

$$(F_{z_{\theta r_V}})_b = F_{z_{\alpha_V}} = U_{0_V} F_{z_{w_V}}$$

where α_0 is a trimmed angle-of-attack. For the lateral/directional derivatives,

$$(F_{y_v})_b = F_{y_v}$$

$$(F_{y_p})_b = F_{y_p} \cos \alpha_0 - F_{y_p} \sin \alpha_0$$

$$(F_{y_r})_b = F_{y_r} \cos \alpha_0 + F_{y_r} \sin \alpha_0$$

$$(F_{y_{\delta r}})_b = F_{y_{\delta r}}$$

$$(L_v)_b = L_v \cos \alpha_0 - N_v \sin \alpha_0$$

$$(L_p)_b = L_p \cos^2 \alpha_0 - (L_r + N_p) \sin \alpha_0 \cos \alpha_0 + N_r \sin^2 \alpha_0 \qquad (2.63)$$

$$(L_r)_b = L_r \cos^2 \alpha_0 - (N_r - L_p) \sin \alpha_0 \cos \alpha_0 - N_p \sin^2 \alpha_0$$

$$(L_{\delta r})_b = L_{\delta r} \cos \alpha_0 - N_{\delta r} \sin \alpha_0$$

$$(N_v)_b = N_v \cos \alpha_0 + L_v \sin \alpha_0$$

$$(N_p)_b = N_p \cos^2 \alpha_0 - (N_r - L_p) \sin \alpha_0 \cos \alpha_0 - L_r \sin^2 \alpha_0$$

$$(N_r)_b = N_r \cos^2 \alpha_0 + (L_r + N_p) \sin \alpha_0 \cos \alpha_0 + N_p \sin^2 \alpha_0$$

$$(N_{\delta r})_b = N_{\delta r} \cos \alpha_0 + L_{\delta r} \sin \alpha_0$$

2.5   Modal Analysis

With the linearized equations of motion in Eqn.(2.60a), (2.61a), one can calculate modal characteristics of the system as well as conduct controllability and observability analysis.[31,32] The nominal aerodynamic derivatives are referred from the aerodynamic dataset block in the nonlinear 8-DOF simulation tool, PDS (Parafoil Dynamic Simulator) from NASA.[33] The database was generated initially for "PARASIM"[33] program in Boeing for NASA Marshall Space Flight Center under contract NAS8-36631 and has been updated for the big parafoil for scaled X-38/CRV based on lots of empirical and experimental sources such as wind tunnel tests, tow tests, drop

Table 2.1 Summary of Longitudinal Dimensional Derivatives

$$F_{x_u} = \frac{-(C_{D_u}+2C_{D_0})QS}{U_0} \qquad F_{x_w} = \frac{-(C_{D_\alpha}-C_{L_0})QS}{U_0}$$

$$F_{z_u} = \frac{-(C_{L_u}+2C_{L_0})QS}{U_0} \qquad F_{z_w} = \frac{-(C_{L_\alpha}+C_{D_0})QS}{U_0}$$

$$F_{z_\alpha} = U_0 F_{z_w} \qquad\qquad F_{x_{\delta e}} = C_{x_{\delta e}}QS$$

$$F_{z_q} = -C_{z_q}\frac{\bar{c}}{2U_0}QS \qquad F_{z_{\delta e}} = -C_{z_{\delta e}}QS$$

$$M_u = C_{m_u}\frac{QS\bar{c}}{U_0} \qquad\qquad M_w = C_{m_\alpha}\frac{QS\bar{c}}{U_0}$$

$$M_\alpha = U_0 M_w$$

$$M_q = C_{m_q}\frac{\bar{c}}{2U_0}(QS\bar{c}) \qquad M_{\delta e} = C_{m_{\delta e}}QS\bar{c}$$

$$F_{x_{u_V}} = \frac{-(C_{D_{u\,V}}+2C_{D_{0\,V}})QS_V}{U_{0_V}} \qquad F_{z_{u_V}} = \frac{-(C_{L_{u\,V}}+2C_{L_{0\,V}})QS_V}{U_{0_V}}$$

$$F_{x_{w_V}} = \frac{-(C_{D_{\alpha\,V}}-C_{L_{0\,V}})QS_V}{U_{0_V}} \qquad F_{z_{w_V}} = \frac{-(C_{L_{\alpha\,V}}+C_{D_{0\,V}})QS_V}{U_{0_V}}$$

$$F_{x_{\theta r_V}} = F_{x_{\alpha_V}} = U_{0_V}F_{x_{w_V}} \qquad F_{z_{\theta r_V}} = F_{z_{\alpha_V}} = U_{0_V}F_{z_{w_V}}$$

Table 2.2 Summary of Lateral/Directinal Dimensional Derivatives

$$F_{y_\beta} = C_{y_\beta}QS \qquad L_\beta = C_{l_\beta}QSb \qquad N_\beta = C_{n_\beta}QSb$$

$$F_{y_p} = \frac{C_{y_p}QSb}{2U_0} \qquad L_p = \frac{C_{l_p}QSb^2}{2U_0} \qquad N_p = \frac{C_{n_p}QSb^2}{2U_0}$$

$$F_{y_r} = \frac{C_{y_r}QSb}{2U_0} \qquad L_r = \frac{C_{l_r}QSb^2}{2U_0} \qquad N_r = \frac{C_{n_r}QSb^2}{2U_0}$$

$$F_{y_{\delta r}} = C_{y_{\delta r}}QS \qquad L_{\delta r} = C_{l_{\delta r}}QSb \qquad N_{\delta r} = C_{n_{\delta r}}QSb$$

tests of the X-38/CRV.[3,4] For this research non-dimensional derivatives were referred for nominal condition of the Buckeye gliding condition at altitudes. The nominal non-dimensional derivatives used for the research are in Table 2.3. A summary of the mass, geometric, and aerodynamic characteristics of the Buckeye parafoil-vehicle were obtained from measurement and calculation as in Table 2.4.

Table 2.3 Summary of Nominal Non-Dimensional Derivatives

$$
\begin{array}{llll}
C_{L_0} & = & 0.7230 & \qquad C_{Y_\beta} & = & -0.0046/deg \\
C_{D_0} & = & 0.2309 & \qquad C_{l_\beta} & = & -0.00064/deg \\
C_{L_\alpha} & = & 0.0631/deg & \qquad C_{n_\beta} & = & 0.0001/deg \\
C_{D_\alpha} & = & 0.0182/deg & \qquad C_{Y_p} & = & 0 \\
C_{m_\alpha} & = & -0.00135/deg & \qquad C_{l_p} & = & -0.15/rad \\
C_{m_0} & = & -0.03196 & \qquad C_{n_p} & = & 0.023/rad \\
C_{L_q} & = & C_{D_q} = 0 & \qquad C_{Y_r} & = & 0 \\
C_{m_q} & = & -0.30/rad & \qquad C_{l_r} & = & 0.005/rad \\
C_{L_{\delta e}} & = & 0.0419/in & \qquad C_{n_r} & = & -0.0936/rad \\
C_{D_{\delta e}} & = & 0.0191/in & \qquad C_{Y_{\delta r}} & = & -0.00081/in \\
C_{m_{\delta e}} & = & -0.0040/in & \qquad C_{l_{\delta r}} & = & 0.00053/in \\
C_{D_{0_V}} & = & 0.3623 & \qquad C_{n_{\delta r}} & = & -0.000038/in
\end{array}
$$

2.5.1 Longitudinal Motion

Substituting all the values in Table 2.3 and 2.4 to Eqn.(2.60a), the system matrix **A** and control matrix **B** can be obtained.

$$
\dot{\mathbf{x}} = \mathbf{A}\,\mathbf{x} + \mathbf{B}\,\mathbf{u} \tag{2.64}
$$

Table 2.4 Geometric, Aerodynamic, and Mass Data for the Buckeye

Wing area, S, ft^2	500	Wing MAC chord, $\bar{c}$, ft	11.5
Wing span, b, ft	43.478	Rigging angle, Θ_{rig}, deg	7
Parafoil mass including enclosed air at sea level, m_P, $slug$	1.73	Vehicle mass with nominal 5 gallon of fuel, m_V, $slug$	19.15
Parafoil .25c location in parafoil body axis, $(r_{x_P}, r_{y_P}, r_{z_P})$, ft	(1.56, 0, -2.29)	Confluence point location in parafoil axis,$(\rho_{x_P}, \rho_{y_P}, \rho_{z_P})$, ft	(1.56, 0, 19.56)
Confluence point location in vehicle axis,$(\rho_{x_V}, 0, \rho_{z_V})$, ft	(0.178, -0.266),	Distance from vehicle C.G. to confluence point, l_ρ, ft	2.273,
Total system weight, W, lb	671.66		
Parafoil and enclosed air mass moment of inertia,		Vehicle mass moment of inertia about vehicle body axes,	
$I_{xx_P}, slug - ft^2$	257.01	$I_{xx_V}, slug - ft^2$	30.3
$I_{yy_P}, slug - ft^2$	27.97	$I_{yy_V}, slug - ft^2$	122.8
$I_{zz_P}, slug - ft^2$	252.53	$I_{zz_V}, slug - ft^2$	122.8
Reference (trim) condition gliding speed,$V_{\infty 0}$, ft/sec	39.0	U_0, ft/sec	36.8
V_0, ft/sec	0	W_0, ft/sec	10.8
Parafoil pitch angle,Θ_0, deg	-0.80	Vehicle relative pitch,Θ_{r_0}, deg	4.12

where

$$\mathbf{x} = [\Delta u, \Delta w, \Delta q, \Delta \theta, \Delta q_V, \Delta \theta_r], \qquad \mathbf{u} = [\delta e]$$

$$\mathbf{A} = \begin{bmatrix} -10.4378 & 29.4910 & -8.5769 & -32.1709 & -0.0005 & 1.1585 \\ -0.4660 & -14.9655 & 36.6555 & 0.4489 & -0.0004 & 2.0798 \\ 0.5387 & -1.5207 & -0.1376 & 0 & -0.0005 & 1.2014 \\ 0 & 0 & 1 & 0 & 0 & 0 \\ -0.0187 & 0.0618 & 0.0725 & 0 & -0.0 & -11.2972 \\ 0 & 0 & -1 & 0 & 1 & 0 \end{bmatrix} \quad (2.65)$$

$$\mathbf{B} = \begin{bmatrix} -2.0744 \\ -0.9537 \\ 0.1072 \\ 0 \\ -0.0028 \\ 0 \end{bmatrix} \quad (2.66)$$

The eigenvalues of system matrix $\mathbf{A}$ in the Table 2.5 shows the system is stable and and there are three oscillatory modes in the configuration and flight condition. Making output equation such as

$$\mathbf{y} = \mathbf{Cx}, \qquad \mathbf{C} = \mathbf{I}$$

and similarity transformation, $\mathbf{x} = M\boldsymbol{\xi}$, between state space and modal space, the real modal $\mathbf{A}, \mathbf{B}, \mathbf{C}$ matrices are determined to be

$$
\mathbf{A}_{mreal} =
\begin{bmatrix}
-12.5727 & 8.0476 & 0 & 0 & 0 & 0 \\
-8.0476 & -12.5727 & 0 & 0 & 0 & 0 \\
0 & 0 & -0.1661 & 1.0612 & 0 & 0 \\
0 & 0 & -1.0612 & -0.1661 & 0 & 0 \\
0 & 0 & 0 & & -0.0317 & 3.5143 \\
0 & 0 & 0 & 0 & -3.5143 & -0.0317
\end{bmatrix}
\tag{2.67}
$$

$$
\mathbf{B}_{mreal} =
\begin{bmatrix}
-2.1250 \\
-4.2548 \\
-0.0417 \\
-0.0866 \\
0.0081 \\
-0.0587
\end{bmatrix}
\tag{2.68}
$$

$$
\mathbf{C}_{mreal} =
\begin{bmatrix}
0.9598 & 0 & 0.9130 & 0 & 0.4477 & 0.0076 \\
-0.0810 & 0.2639 & 0.3034 & -0.1092 & 0.1839 & 0.0255 \\
-0.0509 & -0.0005 & 0.1378 & -0.0329 & 0.0782 & 0.0137 \\
0.0029 & 0.0019 & -0.0501 & -0.1220 & 0.0037 & -0.0223 \\
0.0009 & -0.0023 & 0.1545 & -0.0298 & -0.8314 & 0 \\
-0.0030 & -0.0018 & 0.0005 & -0.0158 & -0.0016 & 0.2588
\end{bmatrix}
\tag{2.69}
$$

The $\mathbf{A}_{mreal}$ matrix provides the eigenvalues, number of modes and order of modes. There are three stable oscillatory mode. With the $\mathbf{B}_{mreal}$ matrix, one can tell all three modes are controllable by the symmetrical flap input, δ_e and the input is mainly effective for the first stable oscillatory mode. And from the $\mathbf{C}_{mreal}$, forward speed

is observed strongly in the first and second stable mode, vertical speed is observable mainly in the second oscillatory mode and somewhat in the third oscillatory mode. Pitch rate of the parafoil is observable in the second stable oscillatory mode and the pitch rate of the vehicle is observed in the third oscillatory mode mainly. Pitch angle is observed in the second oscillatory mode and somewhat in the third mode. The relative pitch angle can be observed mainly in the third oscillatory mode. From observation the third stable mode is mainly related to the vehicle dynamics.

The inverse modal matrix is presented below showing the relationships between modes and states.

$$
\begin{Bmatrix} \xi_1 \\ \xi_2 \\ \xi_3 \\ \xi_4 \\ \xi_5 \\ \xi_6 \end{Bmatrix} = \begin{bmatrix} 0.7563 & -0.0149 & -4.5240 & 1.1967 & -0.0168 & 0.3220 \\ -0.0279 & 0.9982 & -2.1323 & -0.3175 & 0.0039 & -0.0120 \\ 0.2216 & 0.0184 & 4.1113 & -1.2066 & 0.5053 & -0.3300 \\ -0.0100 & 0.0053 & -0.2456 & -0.9223 & -0.0313 & -0.0666 \\ 0.0409 & -0.0069 & 0.7699 & 0.0248 & -0.9069 & -0.0392 \\ 0.0008 & 0.0073 & -0.0609 & -0.1168 & -0.0061 & 0.9924 \end{bmatrix} \begin{Bmatrix} u \\ w \\ q \\ \theta \\ q_V \\ \theta_r \end{Bmatrix}
$$

By examination:

- the first stable oscillatory mode is composed mainly of states of the parafoil, primarily pitch rate, and lesser pitch angle and to lesser extent vertical and forward speeds.
- the second oscillatory mode is composed of primarily parafoil pitch rate and lesser pitch angle and to a lesser extent vehicle pitch rate and relative pitch angle.
- the third oscillatory mode is composed of primarily relative pitch angle and pitch rate of the vehicle and lesser pitch angle of the parafoil.

Dynamic characteristics of longitudinal motion is summarized in the Table 2.5.

<div align="center">Table 2.5 Eigenvalues of Longitudinal Motion</div>

$$\lambda_{1,2} = -12.5727 \pm 8.0476\jmath\ , \quad \zeta = 0.8422\ , \quad \omega_n = 14.9277$$

$$\lambda_{3,4} = -0.1661 \pm 1.0612\jmath\ , \quad \zeta = 0.1546\ , \quad \omega_n = 1.0741$$

$$\lambda_{5,6} = -0.0317 \pm 3.5143\jmath\ , \quad \zeta = 0.0090\ , \quad \omega_n = 3.5144$$

2.5.2 Lateral/Directional Motion

Substituting all the values in Table 2.3 and 2.4 to Eqn.(2.61a), the system matrix $\mathbf{A}$ and control matrix $\mathbf{B}$ in the following equation can be obtained for lateral/directional motion.

$$\dot{\mathbf{x}} = \mathbf{A}\,\mathbf{x} + \mathbf{B}\,\mathbf{u} \tag{2.70}$$

where states $\mathbf{x} = [\Delta v, \Delta p, \Delta r, \Delta\phi, \Delta r_V, \Delta\psi_r]$, control $\mathbf{u} = \delta r$ and

$$\mathbf{A} = \begin{bmatrix} -9.0804 & 8.6462 & -37.1133 & 32.1709 & 0 & -0.2432 \\ -0.4147 & -0.1205 & -0.0279 & 0 & 0 & -0.0334 \\ -0.0971 & -0.1527 & -0.1945 & 0 & 0 & -0.7074 \\ 0 & 1.0000 & -0.0140 & 0 & 0 & 0 \\ -0.0078 & -0.0017 & -0.0004 & 0 & 0 & 1.4502 \\ 0 & -0.0719 & -1.0000 & 0 & 1.0026 & 0 \end{bmatrix} \tag{2.71}$$

$$\mathbf{B} = \begin{bmatrix} -0.1936 \\ -0.0088 \\ -0.0020 \\ 0 \\ -0.0002 \\ 0 \end{bmatrix} \tag{2.72}$$

Following the same procedure of similarity transformation for modal anaysis and

with output equation of

$$\mathbf{y} = \mathbf{Cx}, \qquad \mathbf{C} = \mathbf{I},$$

the real modal $\mathbf{A}, \mathbf{B}, \mathbf{C}$ matrices for lateral/directional motion are determined to be

$$\mathbf{A}_{mreal} = \begin{bmatrix} -12.8955 & 0 & 0 & 0 & 0 & 0 \\ 0 & -0.0044 & 1.3594 & 0 & 0 & 0 \\ 0 & -1.3594 & -0.0044 & 0 & 0 & 0 \\ 0 & 0 & 0 & -0.0417 & 0.6110 & 0 \\ 0 & 0 & 0 & -0.6110 & -0.0417 & 0 \\ 0 & 0 & 0 & 0 & 0 & -0.1601 \end{bmatrix} \tag{2.73}$$

$$\mathbf{B}_{mreal} = \begin{bmatrix} 0.2673 \\ 0.0017 \\ 0.0008 \\ 0.0003 \\ 0.0007 \\ 0.0005 \end{bmatrix} \tag{2.74}$$

$$\mathbf{C}_{mreal} = \begin{bmatrix} -0.9989 & -0.8756 & 0 & 0.0551 & -0.1291 & 0.0259 \\ -0.0456 & 0.0477 & -0.3671 & 0.1202 & 0.0500 & 0.0940 \\ -0.0114 & 0.0750 & -0.0739 & 0.0571 & -0.1196 & -0.5336 \\ 0.0035 & -0.2694 & -0.0334 & 0.0709 & -0.2003 & -0.6336 \\ -0.0009 & -0.0137 & 0.0106 & 0.0300 & 0.4066 & -0.4829 \\ -0.0011 & 0.0819 & 0.0676 & 0.8570 & 0 & -0.2668 \end{bmatrix} \tag{2.75}$$

Examining the $\mathbf{A}_{mreal}$ matrix, there are four, the first and fourth stable mode, the second and third stable oscillatory mode. As can be seen in the $\mathbf{A}_{mreal}$ matrix, the eigenvalues and dynamic properties are summarized in the Table 2.6. The $\mathbf{B}_{mreal}$

matrix shows all four modes are controllable by the asymmetrical flap input, δ_r and the input is mainly effective for the first stable mode and second stable oscillatory mode. And from the $\mathbf{C}_{m\,real}$, side speed or sideslip angle is observed mainly in the first stable and second oscillatory stable mode in almost same extent, roll rate is observable in the third stable mode and fourth stable mode and lesser in the first and second mode. Yaw rate is observed mainly in the fourth stable mode. Bank angle is observable mainly in the fourth stable mode and lesser in the third oscillatory mode. Yaw rate of the vehicle is observable in the third oscillatory and fourth stable mode and the relative yaw angle can be observed strongly in the third oscillatory mode and lesser in the fourth stable mode .

The inverse modal matrix for lateral/directional motion is presented below showing the relationships between modes and states.

$$
\begin{Bmatrix} \xi_1 \\ \xi_2 \\ \xi_3 \\ \xi_4 \\ \xi_5 \\ \xi_6 \end{Bmatrix} = \begin{bmatrix} -0.9749 & 0.3577 & -2.8732 & 2.4320 & -0.0002 & 0.0027 \\ -0.0250 & -0.3760 & 2.9618 & -2.3778 & -0.2623 & 0.0629 \\ 0.0422 & -0.9572 & 0.0397 & -0.2510 & 0.0191 & 0.1490 \\ -0.0062 & 0.2795 & -0.5952 & 0.2092 & -0.1083 & 0.9873 \\ -0.0017 & 0.1349 & -0.4936 & -0.1473 & 0.7652 & -0.0005 \\ 0.0007 & 0.1608 & -0.7311 & -0.1471 & -0.3070 & 0.0490 \end{bmatrix} \begin{Bmatrix} v \\ p \\ r \\ \phi \\ r_V \\ \psi_r \end{Bmatrix}
$$

By examination:

- the first stable mode is composed of only states of the parafoil, primarily yaw rate, bank angle and some of side speed and lesser roll rate.
- the second oscillatory stable mode is composed of primarily yaw rate and bank angle and roll rate with amount of about half of yaw rate. Also composed of almost the parafoil states.
- the third oscillatory stable mode is composed of primarily roll rate of the vehicle and relative yaw angle and yaw rate with amount of half of relative yaw angle.
- the fourth stable mode is composed mainly of yaw rate and the vehicle's yaw rate.

Table 2.6 Eigenvalues of Lateral/Directional Motion

λ_1	$=$	-12.8955
$\lambda_{2,3}$	$=$	$-0.0044 \pm 1.3594\jmath$, $\quad \zeta = 0.0680$, $\quad \omega_n = 0.6124$
$\lambda_{4,5}$	$=$	$-0.0417 \pm 0.6110\jmath$, $\quad \zeta = 0.0032$, $\quad \omega_n = 1.3595$
λ_6	$=$	-0.1601

The nominal linear model dynamics shows that the relative yaw motion of the vehicle is oscillatory and slightly stable. For the nominal model with modified U-joint in Section 2.3.2.2, it is assumed that yaw torque proportional to relative yaw angle exists and restoring torque model from other factors such as twisted canopy, elastic suspension lines and risers as well as aerodynamics of the vehicle is not modelled. The yaw torque model is updated and described at the phase of identification of flight data to match the time responses between the model and flight data in Chapter V. The identified model has all the combined effect not accounted in the analytical model as well as from the relative yaw angle. In general the lateral/directional motion of the parafoil-vehicle shows the system is stable and oscillatory stable yawing motion of the hanging vehicle.

2.6   Conclusion

With the approach of Kanian dynamics and using Kane's equation, 8-DOF nonlinear equations of motion were derived for the Buckeye parafoil two-body system. To get neater equations of motion several assumptions were made within the physically acceptable limitations for practical application. Based on the nonlinear equations of motion linearized ones were derived for stability and control analysis. The linearized model was used as a reference model for system identification for flight data later.

CHAPTER III

SYSTEM IDENTIFICATION METHOD

3.1 Introduction

For identification of the parafoil-vehicle Buckeye system, the Observer/Kalman Filter Identification (OKID) method was used. OKID, a time domain technique, identifies a discrete input-output mapping from known input-output data records. Since first being developed by Juang[11,13,14,34] in the early 1990's, the method has been successfully employed to identify flexible spacecraft structures[12] and aircraft.[15] Chen and Valasek[15] applied the method for on-line system identification of six DOF simulated aircraft dynamics, and found it is suitable for identification of linear aircraft models even without perfect trim conditions and in the presence of sensor noise. A variant of this OKID algorithm was applied here to the simulation and the flight test data of the parafoil-vehicle.

3.2 Observer Kalman-Filter Identification Formulation

The Observer/Kalman Filter Identification (OKID) is an extension of Eigen System Realization (ERA) which was developed to permit efficient identification of large flexible space structures. The ERA algorithm was extended by Juang and Pappa[35] from Ho and Kalman's approach[36] to system identification using the concept of minimum realization. The time domain ERA algorithm solves for sampled pulse response histories which is called system Markov parameters. It has been used successfully on flexible structures,[37] and for system with sensor noise.[38] But there are two basic limitations of the ERA technique, one is that the initial conditions of the system states and controls must be zero, and the other is that the perturbed system must decay to zero in steady-state. Those limitation causes difficulty in practical applications such

as aircraft system identification. In practical environment of airborne vehicle, the trim states are usually imperfect with even small atmospheric disturbances like gusts and turbulence. Additionally, the latter requirement results in not only excessive input-output data record and storage requirements but also long computing time or failure to process to invert the large input matrix caused by the long time to decay to steady-state.

Based on the concept of stochastic Kalman filter estimation and the techniques of deterministic Markov parameter identification, OKID generates a state-space discrete linear model representation of the nonlinear system in the time-domain. For lightly damped systems, like the phugoid mode in the aircraft longitudinal motion, OKID can artificially improve system damping, thereby making the system deadbeat after a small number of steps. This significantly reduces the required data record, storage space, and computation time, features which make OKID applicable to lightly damped system as well as online identification. Nonzero initial conditions on the states and controls can be easily accommodated with OKID, so the technique is applicable to flight vehicles. In practice system identification must often contend with external disturbances. For the specific case of flight vehicle identification the external disturbances are typically discrete gusts and stochastic atmospheric turbulence. As mentioned ideal linear system identification is almost impossible in practice because external disturbances, often unknown, act on the system. So the accuracy of the identified model using OKID will depend upon how closely the stochastic disturbance approximates the modelled disturbance in OKID. Figure 3.1 shows the process of OKID algorithm.[39]

This section starts by reviewing the basic formulation of OKID algorithm. The discrete-time linear state-space perturbation model of the trimmed nonlinear parafoil-vehicle dynamics can be represented in the general discrete state-space form:

$$x(k + 1) = Ax(k) + Bu(k)$$
$$y(k) = Cx(k) + Du(k)$$

(3.1)

where $x(k) \in R^n, y(k) \in R^m, u(k) \in R^r$ are states, outputs and control inputs with dimension of n, m, and r respectively. Following Juang,[14] solving for the output

Road Map for Identification of an Open-Loop System
(general input/output data)

```
┌─────────────────────────────────────────────┐
│      Input and Output Time Histories          │
└─────────────────────────────────────────────┘
                     │ arx_bat
                     ▼
        ┌──────────────────────┐
        │   Observer Markov     │
        │     Parameters        │
        └──────────────────────┘
                │ mar_com
     OKID   ┌───┴───────────────┐
            ▼                   ▼
┌──────────────────┐  ┌──────────────────────┐
│  System Markov    │  │   Observer Gain       │
│   Parameters      │  │  Markov Parameters    │
└──────────────────┘  └──────────────────────┘
            │       m2p        │
            └────────┬─────────┘
              era │ eradc
                  ▼
      ┌──────────────────────────────┐
      │  System Matrices A,B,C,D      │
      │   Observer Gain Matrix G      │
      └──────────────────────────────┘
```
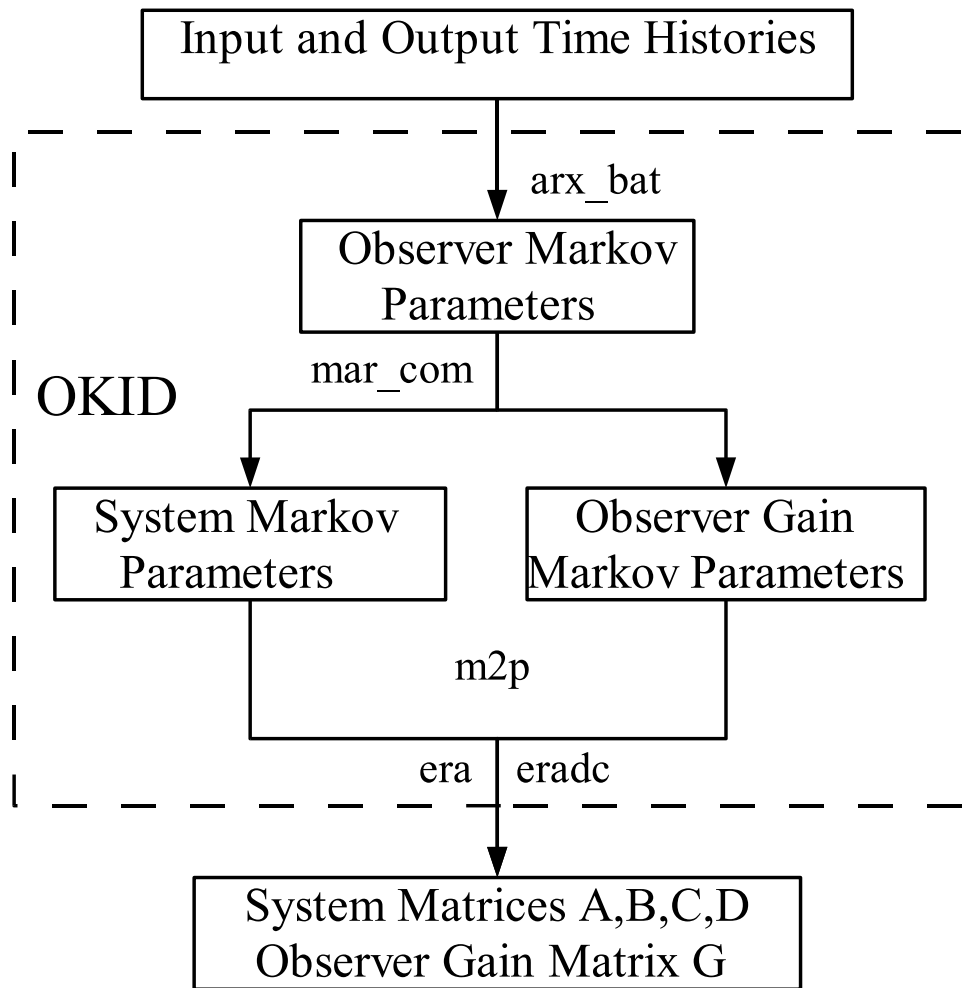
Figure 3.1 OKID Program Flowchart

with zero initial condition $x(0) = 0$ from Eqn. (3.1) in terms of the previous inputs $u(k)$ $(k = 0, 1, 2, \cdots, l - 1)$, yields

$$x(0) = 0,$$

$$y(0) = D\,u(0);$$

$$x(1) = B\,u(0),$$

$$y(1) = CB\,u(0) + D\,u(1); \qquad (3.2)$$

$$x(2) = AB\,u(0) + B\,u(1),$$

$$y(2) = CAB\,u(0) + CB\,u(1) + Du(2);$$

$$\vdots$$

$$x(l - 1) = \sum_{i=1}^{l-1} A^{i-1}B\,u(l - 1 - i),$$

$$y(l - 1) = \sum_{i=1}^{l-1} CA^{i-1}B\,u(l - 1 - i) + Du(l - 1)$$

Eqn.(3.2) can be grouped in a matrix form to yield

$$\overset{m \times l}{y} = \underset{m \times rl}{Y} \overset{rl \times l}{U} \qquad (3.3)$$

where

$$y = [y(0) \ y(1) \ y(2) \ \cdots \ y(l - 1)]$$

$$Y = [D \ CB \ CAB \ \cdots \ CA^{l-2}B]$$

and

$$U = \begin{bmatrix} u(0) & u(1) & u(2) & \cdots & u(l - 1) \\ & u(0) & u(1) & \cdots & u(l - 2) \\ & & u(0) & \cdots & u(l - 3) \\ & & & \ddots & \vdots \\ & & & & u(0) \end{bmatrix}$$

Eqn.(3.3) is a matrix representaion of the relationship between the input and output time histories. The matrix y is an $m \times l$ output data matrx where m is the number of outputs and l is the number of data samples. The matrix Y, of dimension $m \times rl$ with r the number of inputs, contains all the Markov parameters $D, CB, CAB, \cdots, CA^{l-2}B$, which is to be determined and are commonly used as the basis to identify mathematical models for linear dynamic systems. Linear state-space model can then be generated from Markov parmeters using the relation with Hankel matrix[14, 15] U. For lightly damped system, however, the slow decaying response may produce too large Hankel matrix to solve for its inverse numerically in practice, and therefore impractically long computation time. The OKID method overcomes this problem by introducing an observer into the system, which places eigenvalues as desired. Adding and subtracting an observer term $Gy(k)$ in right side of the Eqn.(3.1) yields

$$x(k+1) = Ax(k) + Bu(k) + Gy(k) - Gy(k)$$

$$= (A + GC)x(k) + (B + GD)u(k) - Gy(k)$$

which can be written compactly as

$$x(k + 1) = \bar{A}x(k) + \bar{B}v(k) \tag{3.4}$$

where

$$\bar{A} = A + GC$$

$$\bar{B} = [B + GD, -G]$$

$$v(k) = \begin{bmatrix} u(k) \\ y(k) \end{bmatrix}$$

and G is an $n \times m$ arbitrary matrix chosen to make the matrix $\bar{A}$ as stable as desired, i.e. place the eigenvalues of $\bar{A}$ to any desired values. Although Eqn.(3.4) is mathematically identical to Eqn.(3.1), it is expressed using different system matrices and has a different input. In fact, Eqn.(3.4) is an observer equation if the states $x(k)$ is considered as an observer state vector. Therefore, the Markov parameters of the

system in Eqn.(3.4) will be referred to as the observer Markov parameters. Because the $n \times m$ matrix G can be arbitrarily chosen, the eigenvalues of $\bar{A}$ may be arbitrarily assigned for an observable system. The mathematical development here can be interpreted from the point of view of Ref.14,34 as attempting to place all eigenvalues of $\bar{A}$ at the origin, i.e., a deadbeat observer. This ensures that $C\bar{A}^{k-1}\bar{B} \approx 0$ for $k \geq p$ in real data including noise, where p is the number of independent Markov parameters and sufficiently large integer. Note that $v(k)$ is the input vector for the new observer system in Eqn.(3.4) and is composed of the nominal system inputs and outputs of Eqn.(3.1).

For non-zero initial conditions for imperfect trim condition of airborne vehicle system, the following derivation is used. From Eqn.(3.4), it is easy to show that

$$
\begin{aligned}
x(k+1) &= \bar{A}x(k) + \bar{B}v(k), \\
x(k+2) &= \bar{A}x(k+1) + \bar{B}v(k+1) \\
&= \bar{A}^2 x(k) + \bar{A}\bar{B}v(k) + \bar{B}v(k+1), \\
&\vdots \\
x(k+p) &= \bar{A}x(k+p-1) + \bar{B}v(k+p-1) \\
&= \bar{A}^p x(k) + \bar{A}^{p-1}\bar{B}v(k) + \bar{A}^{p-2}\bar{B}v(k+1) \\
&\quad + \cdots + \bar{B}v(k+p-1)
\end{aligned}
\tag{3.5}
$$

Using the measurement equation in Eqn.(3.2), yields

$$
\begin{aligned}
y(k+p) &= Cx(k+p) + Du(k+p) \\
&= C\bar{A}^p x(k) + C\bar{A}^{p-1}\bar{B}v(k) + C\bar{A}^{p-2}\bar{B}v(k+1) + \cdots \\
&\quad + C\bar{B}v(k+p-1) + Du(k+p)
\end{aligned}
\tag{3.6}
$$

The set of these equations for a sequence of $k = 0, \cdots, l-1$ can be written as

$$
\bar{y} = C\bar{A}^p x + \bar{Y}\bar{V}
\tag{3.7}
$$

where

$$\bar{y} = [y(p) \quad y(p+1) \quad \cdots \quad y(l-1)]$$

$$\bar{Y} = [D \quad C\bar{B} \quad C\bar{A}\bar{B} \quad \cdots \quad C\bar{A}^{(p-1)}\bar{B}]$$

$$\bar{V} = \begin{bmatrix} u(p) & u(p+1) & \cdots & u(l-1) \\ v(p-1) & v(p) & \cdots & v(l-2) \\ v(p-2) & v(p-1) & \cdots & v(l-3) \\ \vdots & \vdots & \ddots & \vdots \\ v(0) & v(1) & \cdots & v(l-p-1) \end{bmatrix} \tag{3.8}$$

Note that $D \quad C\bar{B} \quad C\bar{A}\bar{B} \quad \cdots \quad C\bar{A}^{(p-1)}\bar{B}$ are observer Markov parameters, and $\bar{V}$ is a Hankel matrix. The first term in Eqn.(3.7) represents the effect of the preceding $p-1$ time steps. For the case where $\bar{A}^p$ is sufficiently small and all the states in x are bounded, Eqn.(3.7) can be approximated by neglecting the first term on the right-hand side,

$$\overset{m \times l}{\bar{y}} = \underset{m \times [(r+m)p+r]}{\bar{Y}} \overset{[(r+m)p+r] \times l}{\bar{V}} \tag{3.9}$$

which has following least-squares solution:

$$\bar{Y} = \bar{y}\,\bar{V}^T [\bar{V}\,\bar{V}^T]^{-1} \quad or \quad \bar{Y} = \bar{y}\,\bar{V}^\dagger \tag{3.10}$$

provided that $[\bar{V}\,\bar{V}^T]^{-1}$ exists, otherwise $\bar{V}^T [\bar{V}\,\bar{V}^T]^{-1}$ should be replaced by $\bar{V}^\dagger$, pseudo inverse of the matrix $\bar{V}$. For nonzero unknown initial conditions, Eqn.(3.9) must be used in order to eliminate the effect of initial conditions because the initial conditions become negligible when they are multiplied by $\bar{A}^p$. In other words, the initial conditions have little effect on the measured data after p time steps.

Now the Markov parameters include the system Markov parameters and the observer gain Markov parameters. The system Markov parameters are used to compute the system matrices $A, B, C,$ and D whereas the observer gain Markov parameters are used to determine the observer gain matrix G. System Markov parameters Y can then be recovered from the observer Markov parameters $\bar{Y}$ through partition of $\bar{Y}$ as:

$$\bar{Y} = [D \ C\bar{B} \ C\bar{A}\bar{B} \cdots C\bar{A}^{(p-1)}\bar{B}] = [\bar{Y}_0 \ \bar{Y}_1 \ \bar{Y}_2 \cdots \bar{Y}_p] \tag{3.11}$$

from which we get observer Markov parameters

$$\bar{Y}_0 = D$$

$$\begin{aligned}
\bar{Y}_k &= C\bar{A}^{(k-1)}\bar{B} \\
&= [C(A+GC)^{k-1}(B+GD) \quad -C(A+GC)^{k-1}G] \\
&\triangleq [\bar{Y}_k^{(1)} \quad -\bar{Y}_k^{(2)}]; \quad k = 1,\ 2,\ 3,\ \cdots
\end{aligned}$$

$$(3.12)$$

Based on the definition of system Markov parameters, we have system Markov parameters

$$\begin{aligned}
Y_1 &= CB = C(B+GD) - (CG)D \\
&= \bar{Y}_1^{(1)} - \bar{Y}_1^{(2)}D \\
Y_2 &= CAB \\
&= \bar{Y}_2^{(1)} - \bar{Y}_1^{(2)}Y_1 - \bar{Y}_2^{(2)}D \\
&\vdots
\end{aligned}$$

$$(3.13)$$

By induction, the general relationship between the actual system Markov parameters and the observer Markov parameters is

$$\begin{aligned}
D &= Y_0 = \bar{Y}_0 \\
Y_k &= \bar{Y}_k^{(1)} - \sum_{i=1}^{k} \bar{Y}_i^{(2)} Y_{(k-i)} \quad for\ k = 1,\ \cdots,\ p \\
Y_k &= -\sum_{i=1}^{p} \bar{Y}_i^{(2)} Y_{(k-i)} \quad for\ k = p+1,\ \cdots,\ \infty
\end{aligned}$$

$$(3.14)$$

Now the desired discrete system realization $[A, B, C, D]$ is obtained from the system

Markov parameters using singular value decomposition (SVD) of the Hankel matrix:

$$
H(k-1) = \begin{bmatrix}
Y_k & Y_{k+1} & \cdots & Y_{k+\beta-1} \\
Y_{k+1} & Y_{k+2} & \cdots & Y_{k+\beta} \\
\vdots & \vdots & \ddots & \vdots \\
Y_{k+\alpha-1} & Y_{k+\alpha} & \cdots & Y_{k+\alpha+\beta-2}
\end{bmatrix}
$$

$$
= \begin{bmatrix}
CA^{k-1}B & CA^kB & \cdots & CA^{\beta-1}B \\
CA^kB & CA^{k+1}B & \cdots & CA^\beta B \\
\vdots & \vdots & \ddots & \vdots \\
CA^{\alpha-1}B & CA^\alpha B & \cdots & CA^{\alpha+\beta-2}B
\end{bmatrix}
\tag{3.15}
$$

It can be proved by observing the Hankel matrix that

$$
H(k-1) = P_\alpha A^{k-1} Q_\beta \tag{3.16}
$$

where

$$
P_\alpha = \begin{bmatrix} C \\ CA \\ \vdots \\ CA^{\alpha-1} \end{bmatrix} \quad and \quad Q_\beta = \begin{bmatrix} B & AB & \cdots & A^{\beta-1}B \end{bmatrix} \tag{3.17}
$$

For $k=1$, using a singular value decomposition yields

$$
H(0) = P_\alpha Q_\beta
$$

where block matrix P_α is the observability matrix, whereas the block matrix Q_β is the controllability matrix. If the order of the system is n, then the minimum dimension of the state matrix is $n \times n$. Therefore, the Hankel matrix $H(0)$ is of rank n. Based on the properties of the Hankel matrix composed of the Markov parameters (pulse-response samples), the ERA is used to compute the three matrices A, B, and C. The ERA process starts with the factorization of the Hankel matrix by use of SVD:

$$
H(0) = P_\alpha Q_\beta = R \Sigma S^T \tag{3.18}
$$

where the columns of matrix R and S are orthonormal, and is a rectangular matrix composed of singular values of the Hankel matrix:

$$\Sigma = \begin{bmatrix} \Sigma_n & 0 \\ 0 & 0 \end{bmatrix} \quad \text{and} \quad \Sigma_n = diag\ [\sigma_1,\ \sigma_2,\ \cdots,\ \sigma_n]$$

where n is the system order and σ_i's are singlar values.

Let R_n, S_n be the matrix formd by the first n columns of R and S respectively. Hence, the matrix $H(0)$ becomes

$$H(0) = R_n \Sigma_n S_n, \tag{3.19}$$

where $R_n^T R_n = I = S_n^T S_n$. We can write the equality

$$H(0) = \left[R_n \Sigma_n^{1/2}\right]\left[\Sigma_n^{1/2} S_n\right] \cong P_\alpha Q_\beta$$

Therefore we obtain

$$B = \text{the first } r \text{ columns of } Q_\beta$$
$$C = \text{the first } m \text{ rows of } P_\alpha \tag{3.20}$$

With $k = 2$ in the Hankel matrix,

$$H(1) = P_\alpha A Q_\beta = R_n \Sigma_n^{1/2} A \Sigma_n^{1/2} S_n^T$$

One obvious solution for the state matrix A becomes

$$A = \Sigma_n^{-1/2} R_n^T H(1)\, S_n \Sigma_n^{-1/2} \tag{3.21}$$

As in equations (3.19),(3.20),(3.21), the procedure requires computation of two Hankel matrices, $H(0)$ and $H(1)$. The identfied system matrices are

$$A = \Sigma_n^{-1/2} R_n^T H(1) S_n \Sigma_n^{-1/2}$$
$$B = \text{the first } r \text{ columns of } Q_\beta = \Sigma_n^{1/2} S_n^T E_r$$
$$C = \text{the first } m \text{ rows of } P_\alpha = E_m^T R_n \Sigma_n^{1/2} \tag{3.22}$$
$$D = Y_0$$

where $E_m^T = [I_m\ 0_m\ \cdots\ 0_m], \quad E_r^T = [I_r\ 0_r\ \cdots\ 0_r]$ and $I_i, 0_i$ are identity and null matrix of order i respectively.

3.3   OKID under Disturbance

In practical applications such as the aerial vehicle system identification in this flight test research, the outputs usually include sensor noises and disturbance effects as well as pure system outputs produced by given inputs. For identification from disturbance contaminated input-output time responses, Juang, Phan and Goodzeit et al.[16,17,40] expanded OKID for system identification with unknown disturbances. Valasek and Chen[15] applied this version to nonlinear aircraft with disturbances. Consequently Goodzeit's approaches converge to a result saying that "despite the unknown disturbances altering the autoregressive moving average model with exogenous input (ARX) model coefficients, the system Markov parameters can still be recovered exactly as if the disturbances were not present". From these Markov parameters one can obtain a minimum-order state-space realization then can predict the disturbance-free response to arbitrary inputs.

From the derivation in Section 3.2, the system input and output relationship can be expressed by the following recursive finite-difference equation, known as the autoregresive model with exogenous input (ARX):

$$
\begin{aligned}
y(k) = {} & -\bar{Y}_1^{(2)} y(k-1) - \bar{Y}_2^{(2)} y(k-2) - \cdots - \bar{Y}_p^{(2)} y(k-p) \\
& + \bar{Y}_0\, u(k) + \bar{Y}_1^{(1)}\, u(k-1) + \cdots + \bar{Y}_p^{(1)}\, u(k-p)
\end{aligned}
\tag{3.23}
$$

where $\bar{Y}_i^{(1)}, \bar{Y}_i^{(2)}$ are defined as in Eqn.(3.12). This equation says the current output $y(k)$ can be expressed by the current input $u(k)$, p past control inputs $u(k-1), \cdots, u(k-p)$ and system outputs $y(k-1), \cdots, y(k-p)$. Following Juang and Goodzeit's approach, we define the periodic disturbance effect term $\eta(k)$ and it's auto-regressive model with order τ,

$$
\eta(k) = \gamma_1\, \eta(k-1) + \gamma_2\, \eta(k-2) + \cdots + \gamma_\tau\, \eta(k-\tau)
\tag{3.24}
$$

where the disturbance order τ is arbitrary to express the disturbance effect assuming that all periodic disturbance can be represented as combinations of a simple periodic disturbance such as sine wave. If there are f distinct frequencies present in the disturbances, then τ is $2f$ or $2f + 1$, depending on whether any disturbance has

nonzero mean. Current output with the periodic disturbance becomes:

$$
\begin{aligned}
y(k) &= -\bar{Y}_1^{(2)}y(k-1) - \bar{Y}_2^{(2)}y(k-2) - \cdots - \bar{Y}_p^{(2)}y(k-p) \\
&\quad + \bar{Y}_0\, u(k) + \bar{Y}_1^{(1)}u(k-1) + \cdots + \bar{Y}_p^{(1)}u(k-p) + \eta(k) \\
&\triangleq \alpha_1\, y(k-1) + \alpha_2\, y(k-2) + \cdots + \alpha_p\, y(k-p) \\
&\quad + \beta_0\, u(k) + \beta_1\, u(k-1) + \cdots + +\beta_p\, u(k-p) + \eta(k)
\end{aligned}
\tag{3.25}
$$

By substituting Eqn.(3.24) into Eqn.(3.25), we have

$$
\begin{aligned}
&y(k) - \gamma_1\, y(k-1) - \gamma_2\, y(k-2) - \cdots - \gamma_\tau\, y(k-\tau) \\
&= \alpha_1\, y(k-1) + \alpha_2\, y(k-2) + \cdots + \alpha_p\, y(k-p) \\
&\quad + \beta_0\, u(k) + \beta_1\, u(k-1) + \cdots + \beta_p\, u(k-p) + \eta(k) \\
&\quad - \gamma_1[\alpha_1\, y(k-2) + \alpha_2\, y(k-3) + \cdots + \alpha_p\, y(k-p-1) \\
&\quad\quad + \beta_0\, u(k-1) + \beta_1\, u(k-2) + \cdots + \beta_p\, u(k-p-1)] - \gamma_1\, \eta(k-1) \\
&\quad - \gamma_2[\alpha_1\, y(k-3) + \alpha_2\, y(k-4) + \cdots + \alpha_p\, y(k-p-2) \\
&\quad\quad + \beta_0\, u(k-2) + \beta_1\, u(k-3) + \cdots + \beta_p\, u(k-p-2)] - \gamma_2\, \eta(k-2) \\
&\quad\ \vdots \\
&\quad - \gamma_\tau[\alpha_1\, y(k-\tau-1) + \alpha_2\, y(k-\tau-2) + \cdots + \alpha_p\, y(k-p-\tau) \\
&\quad\quad + \beta_0\, u(k-\tau) + \beta_1\, u(k-\tau-1) + \cdots + \beta_p\, u(k-p-\tau)] - \gamma_\tau\, \eta(k-\tau)
\end{aligned}
\tag{3.26}
$$

Expanding above equation yields

$$y(k) = (\alpha_1 + \gamma_1)\, y(k-1) + (\alpha_2 + \gamma_2 - \gamma_1\,\alpha_1)\, y(k-2)$$

$$+ (\alpha_3 + \gamma_3 - \gamma_1\,\alpha_2 - \gamma_2\,\alpha_1)\, y(k-2) + \cdots$$

$$+ (\alpha_p + \gamma_p - \cdots - \gamma_{p-2}\,\alpha_2 - \gamma_{p-1}\,\alpha_1)\, y(k-p)$$

$$+ (\gamma_{p+1} - \gamma_1\,\alpha_p - \gamma_2\,\alpha_{p-1} - \cdots - \gamma_p\,\alpha_1)\, y(k-p-1)$$

$$+ (\gamma_{p+2} - \gamma_2\,\alpha_p - \gamma_3\,\alpha_{p-1} - \cdots - \gamma_{p+1}\,\alpha_1)\, y(k-p-2) + \cdots$$

$$+ (-\gamma_{\tau-1}\,\alpha_p - \gamma_\tau\,\alpha_{p-1})\, y(k-p-\tau+1) \qquad (3.27)$$

$$+ (-\gamma_\tau\,\alpha_p)\, y(k-p-\tau)$$

$$+ \beta_0\, u(k) + (\beta_1 - \gamma_1\,\beta_0)\, u(k-1) + (\beta_2 - \gamma_1\,\beta_1 - \gamma_2\,\beta_0)\, u(k-2) + \cdots$$

$$+ (\beta_p - \gamma_1\,\beta_{p-1} - \gamma_2\,\beta_{p-2} - \cdots - \gamma_p\,\beta_0)\, u(k-p)+$$

$$+ (-\gamma_1\,\beta_p - \gamma_2\,\beta_{p-1} - \cdots - \gamma_{p-1}\,\beta_0)\, u(k-p-1) + \cdots$$

$$+ (-\gamma_\tau\,\beta_p)\, u(k-p-\tau)$$

Note that the disturbance terms $\eta(k), \cdots, \eta(k-\tau)$ were cancelled out, so we don't need to worry about the disturbance term from now on. From above derivation, one obtains the input-output model of the following form

$$y(k) = \bar{\alpha}_1\, y(k-1) + \bar{\alpha}_2\, y(k-2) + \cdots + \bar{\alpha}_{p+\tau}\, y(k-p-\tau)$$

$$+ \bar{\beta}_0\, u(k) + \bar{\beta}_1\, u(k-1) + \cdots + \bar{\beta}_{p+\tau}\, u(k-p-\tau)$$

$$(3.28)$$

where the output coefficients are

$$\bar{\alpha}_1 = \alpha_1 + \gamma_1$$

$$\bar{\alpha}_2 = \alpha_2 + \gamma_2 - \gamma_1\,\alpha_1$$

$$\vdots$$

$$\bar{\alpha}_p = \alpha_p + \gamma_p - \cdots - \gamma_{p-2}\,\alpha_2 - \gamma_{p-1}\,\alpha_1 \tag{3.29}$$

$$\vdots$$

$$\bar{\alpha}_{p+\tau} = -\gamma_\tau\,\alpha_p$$

and the input coefficients are

$$\bar{\beta}_0 = \beta_0$$

$$\bar{\beta}_1 = \beta_1 - \gamma_1\,\beta_0$$

$$\vdots$$

$$\bar{\beta}_p = \beta_p - \gamma_1\,\beta_{p-1} - \cdots - \gamma_p\,\beta_0 \tag{3.30}$$

$$\vdots$$

$$\bar{\beta}_{p+\tau} = -\gamma_\tau\,\beta_p$$

By assuming that measurements of $u(k)$ and $y(k)$ are available for $k = 0, 1, \cdots, l-1$ and defining $\zeta = p + \tau$, the model coefficients matrices can be calculated by following the same procedures in Section 3.2. Note that the order of the system increases from p to $\zeta = p + \tau$. Let the $(m+r) \times l$ vector $v(k)$ be defined as

$$v(k) = \begin{bmatrix} y(k) \\ u(k) \end{bmatrix}, \quad k = 0, 1, \cdots, l-1 \tag{3.31}$$

Equation (3.28) produces the following matrix equation:

$$[y_0 \quad y] = \theta[V_0 \quad V] \tag{3.32}$$

where

$$y_0 = [y(0) \quad y(1) \quad \cdots \quad y(\zeta - 1)],$$

$$y = [y(\zeta) \quad y(\zeta + 1) \quad \cdots \quad y(l - 1)],$$

$$\theta = \left[\bar{\beta}_0 \quad (\bar{\alpha}_1 \quad \bar{\beta}_1) \quad \cdots \quad (\bar{\alpha}_{\zeta-1} \quad \bar{\beta}_{\zeta-1}) \quad (\bar{\alpha}_\zeta \quad \bar{\beta}_\zeta) \right],$$

$$V_0 = \begin{bmatrix} u(0) & u(1) & \cdots & u(\zeta - 1) \\ 0 & v(0) & \cdots & v(\zeta - 2) \\ \vdots & \vdots & \ddots & \vdots \\ 0 & 0 & \cdots & v(0) \\ 0 & 0 & \cdots & 0 \end{bmatrix}, \tag{3.33}$$

$$V = \begin{bmatrix} u(\zeta) & u(\zeta + 1) & \cdots & u(l - 1) \\ v(\zeta - 1) & v(\zeta) & \cdots & v(l - 2) \\ \vdots & \vdots & \ddots & \vdots \\ v(1) & v(2) & \cdots & v(l - \zeta) \\ v(0) & v(1) & \cdots & v(l - \zeta - 1) \end{bmatrix}.$$

For tests starting with some transient response, y_0 and V_0 are deleted under the same condition for identifying the observer Markov parameters with a deadbeat observer as in Eqn.(3.7),(3.8), and the observer Markov parameter θ from disturbance-corrupted input-output data can be

$$\theta = y \, \bar{V}^+ \tag{3.34}$$

The data set must be sufficiently long so that one has at least as many equations as the number of unknowns, and more to average out the effect of noise. Furthermore, the excitation input must be sufficiently rich so that the rows of the input data in V are full rank.

From the definitions in Eqn.(3.12), (3.25) and the observer Markov parameters θ in Eqn.(3.29), (3.30), one can derive the system Markov parameters and the state-space model as follows: Since the first input coefficient is simply the direct transmission term in the equivalent state-space model, and thus is equal to the system

input-output matrix D:

$$D = Y_0 = \beta_0 = \bar{\beta}_0 = \bar{Y}_0 \tag{3.35}$$

Now the system Markov parameters can be fully recovered from the observer Markov parameters in the same way described in Section 3.2 by replacing p to $\zeta = p + \tau$. In the following equations, Y_i denotes system Markov parameters, $[\bar{\beta}_i \quad \bar{\alpha}_i]$ are disturbance-corrupted observer Markov parameters, and $[\bar{Y}_i^{(1)} \quad -\bar{Y}_i^{(2)}] \triangleq [\beta_i \quad \alpha_i]$ are the disturbance-free observer Markov parameters. From Eqn.(3.13),(3.14),(3.29) and (3.30) one can find the relationship between the Markov parameters such that

$$
\begin{aligned}
Y_1 &= \bar{Y}_1^{(1)} - \bar{Y}_1^{(2)} Y_0 \\
&= \beta_1 + \alpha_1 Y_0 \\
&= (\bar{\beta}_1 + \gamma_1 \bar{Y}_0) + (\bar{\alpha}_1 - \gamma_1) Y_0 \\
&= \bar{\beta}_1 + \bar{\alpha}_1 Y_0
\end{aligned}
\tag{3.36}
$$

where the terms involving the disturbance coefficients γ_i cancel themselves out and thus makes the expression for the system Markov parameters from the disturbance-corrupted coefficients be identical with those from the disturbance-free coefficients. In the same fashion, one obtains the expression for the system Markov parameters in the general case,

$$
\begin{aligned}
D = Y_0 &= \bar{Y}_0 = \bar{\beta}_0 \\
Y_k &= \bar{Y}_k^{(1)} - \sum_{i=1}^{k} \bar{Y}_i^{(2)} Y_{(k-i)} \\
&= \bar{\beta}_i + \sum_{i=1}^{k} \bar{\alpha}_i Y_{(k-i)} \qquad for \quad k = 1, \cdots, \zeta \\
Y_k &= -\sum_{i=1}^{p} \bar{Y}_i^{(2)} Y_{(k-i)} \\
&= \sum_{i=1}^{p} \bar{\alpha}_i Y_{(k-i)} \qquad for \quad k = \zeta + 1, \cdots, \infty
\end{aligned}
\tag{3.37}
$$

From the derivations above, despite unknown disturbances altering the ARX model coefficients, the system Markov parameters can still be recovered exactly as if

the disturbances were not exist. Once we get the system Markov parameters we can get a minimum-order state-space realization by following the same ERA procedure described in Section 3.2.

If we approximate a random disturbance as a very large order periodic disturbance, we can apply periodic disturbance OKID method to system identification with an arbitrary disturbance.

3.4   Conclusion

In this chapter, equations for a time-domain identification algorithm OKID have been presented. This algorithm has been shown to be useful and effective for identifying linear system matrices from input-output time histories of nonlinear systems under disturbance in several research applications. The main features of OKID are:

- Time domain method

- Nonzero initial conditions

- Arbitrary multiple inputs and outputs

- Observer effectively increases damping

  - Permits shorter data record

  - Compresses number of required Markov parameters

  - Smaller Hankel matrix $\rightarrow$ Reduced computational effort

- Works well for lightly damped systems (full decay not necessary)

- Observer gain G is obtained directly, and can be used to arbitrarily place system poles

And the derivation of periodic disturbance OKID shows that the system Markov parameters can be recovered from disturbance-corrupted input-output data and then minimum-order state-space realization can be achieved.

CHAPTER IV

EXPERIMENT DESIGN

4.1 Introduction

Testing airborne vehicle is a complex and interrelated process. Generally there are three main factors in flight test planning, which are safety, cost and schedule mentioned in Ward's.[41] As the flight tests for identification are inserted between PGNC tests all the PGNC standard operation procedures are complied for safety and efficiency. And there are not enough data parameters with high sample rate for the identification test, necessary data acquisition subsystems are chosen and acquired at minimal cost for the test. As the identification test has lower priority than PGNC test the test schedule depends on that of NASA's PGNC test. Several clean runs are expected for the identification test.

To accomplish the research objectives of modelling and it's verification from flight tests, all states used to define the analytical model should be recorded from flight tests. From Chapter II, there are 12 of states and two control inputs to construct longitudinal and lateral/directional linear models of the Buckeye. Some of them are measured directly from flight tests, and some are calculated by kinematic equations using measured ones. In this chapter, all the prerequisite work and analysis prior to flight test for proper data acquisition is described. It can be categorized in three broad areas as follows: sensors provision for data acquisition systems description; validation of OKID algorithm on the simulated data; and flight test design using a simulation study.

4.2   Data Acquisition System and Installation

To describe the dynamics of the airborne vehicle from flight test, appropriate data set representing the dynamic behavior should be acquired through the tests. It means that the dynamic description should be observable, and appropriate sensors should be provided for the data acquisition. Necessary hardware provisions (including sensor installations) are limited because the existing hardware capability for data handling should impact the test vehicle as little as possible.

As shown in Chapter II all longitudinal and lateral/directional modes are observable and controllable in the Buckeye parafoil-vehicle's two-body dynamics. Natural frequencies of oscillatory modes of each motion are 14.93 rad/sec and 1.36 rad/sec for longitudinal and lateral/directional respectively. Thus the frequency of the highest oscillatory motion is 2.38 Hz. To avoid aliasing and to detect all the motion including un-modelled or unexpected dynamics with the existing hardware capability, nominal data acquisition frequency of 25 Hz - greater than 10 times the highest frequency - was used.

The data types to be acquired from the Buckeye can be categorized by data properties and required sensor types as follows.

- air data: static and dynamic pressure; airspeed; angle-of-attack; and sideslip angle of the hanging vehicle
- inertial measurements: attitudes; accelerations; and body rates of the hanging vehicle
- parafoil inertial measurements: attitudes; accelerations; and body rates of the parafoil
- vehicle status: control inputs; engine rpm; and positions on Earth including altitude etc.

For the identification three data acquisition subsystems were added to the existing system. Position data from existing Global Positioning System (GPS) and other vehicle status data at low sampling rates for PGNC tests are not used for identification. Thus the added three subsystems are described in the following subsections.

4.2.1   Air Data sensor

There is a pitot tube in the original Buckeye system to provide speed data as a PGNC parameter. It is located at about 5 inches in front of the computer box where the flow is affected by the interference with the box and other strut and frames. Thus it's reduced speed can be affected by the attitude change of the vehicle. It is determined not suitable to be used for identification. It's data acquisition rate is about 5 Hz and it is much less than the required acquisition rate which should reflect dynamics for identification purpose. Practically the angle-of-attack and sideslip angle are required to measure and extra vanes are needed if the probe is used. So a Multifunction probe was acquired to provide accurate data at high sampling rate. The original pitot tube was used for initial calibration stage of the multifunction probe.

To prevent additional cost and efforts for a hardware provision such as a vane type or differential pressure type for flow angles, a 5-hole multifunction probe[42] manufactured by Aeroprobe Corporation (Figure 4.1) was used. It can measure pressure data as well as flow angles at the same time. In addition to the multifunction capability, it avoids much of the time-delay caused by the pneumatic delay inside the probe. It gives a quick response time for flow property variations at frequencies up to 100 Hz.[42] It was modified for the Buckeye application and installed in front of the hanging vehicle so as to clear the aerodynamic interference of the vehicle (Figure 4.2). The closeup of the probe tip in the inset of Figure 4.2 shows the 5-hole locations. The technical specification is summarized in Table 4.1.

In general the multifunction probe is calibrated in a wind tunnel varying flow speed and angles at the manufacturing stage. The calibration data is used for reduction of flow magnitude and direction, total and static pressures, Mach and Reynold's number ad fluid properties like density and viscosity from the recorded data.[43] Once it is calibrated, there is no need to recalibrate unless the aerodynamic shape of the tip is altered.[43] To use the probe for the Buckeye test, several in the field calibration tests were conducted for the verification of sensor performance and the operational temperature effects.[44] The initial conditions for every test are recorded at the very first stage of each test for the ambient pressure and temperature. The data is used

Table 4.1 Technical Specification of Multifunction Aeroprobe

		Range		Operational	
Sample Rate	Speed	Flow Direction		Vibration	Temperature
100 Hz	20 - 60 Kts	$\pm 60 deg$		$\pm 4g$	20-100 $^\circ F$

during the reduction later. The data from the probe is saved in the onboard Flight Computer (ACP) and downloaded after flight tests. Depending upon workload of the ACP, the data is saved at a variable update rate of 55-60 Hz. To protect the probe from unexpected roll-over incidents during take-off and landing, a roll-bar and dorsal beam were installed to provide clearance from the ground (Figure 4.2).

4.2.2   Inertial Measurement Unit

To measure attitudes and body rates, an Inertial Measurement Unit (IMU)[45] manufactured by Watson Industries, Inc. was installed near the C.G. on the floor of the hanging vehicle of the Buckeye (Figure 4.3). The weight of the IMU is less than 4 lbs and it can survive in 600 g's shock. Operational temperature ranges from -30 $^\circ C$ to 71 $^\circ C$. The sensor technical specification of the IMU is summarized in Table 4.2. The data is saved in the ACP at 35 to 37 Hz depending on the workload of the ACP.

Table 4.2 Technical Specification of IMU

	Angular Rates	Accelerations	Attitude
Range	$\pm 100^\circ/sec$	± 2 g's	$\pm 60^\circ$
Resolution	$< 0.02^\circ/sec$	1 mg	0.09°
Bandwidth	> 70 Hz		
Bias	$< 0.1^\circ/sec$	< 20 mg	
Frequency Response		20 Hz	20 Hz

Figure 4.1 5-Hole Multifunction Aeroprobe, Courtesy of Aeroprobe Corp.

Figure 4.2 5-Hole Multifunction Aeroprobe Installed on Buckeye
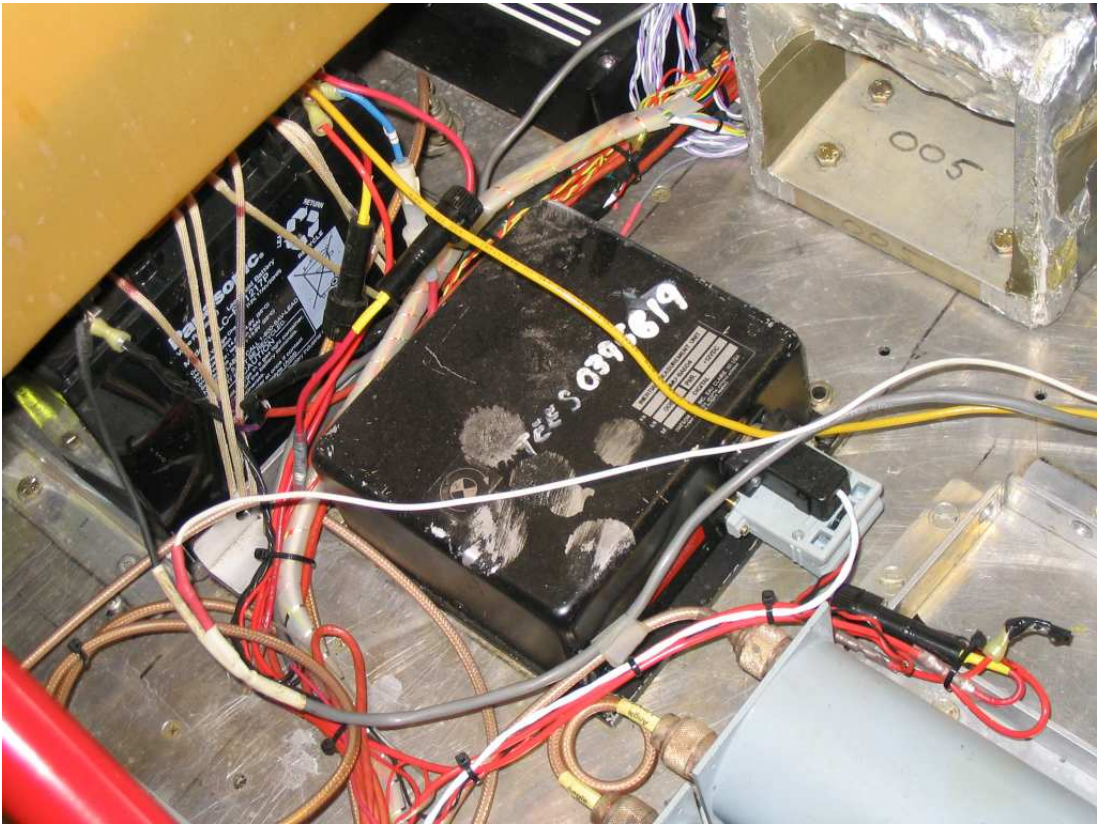
Figure 4.3 Inertial Measurement Unit Installed on Buckeye

4.2.3   Sensors for Parafoil Motion

The multifunction probe and IMU installed on the vehicle are limited to providing data for the parafoil itself. Since it is essential to measure parameters of the parafoil in this research, several techniques were investigated. Measuring the parameters of the parafoil was challenging because the parafoil is made of fabric cloth. Some proposed techniques for measuring the relative heading angle between the parafoil and hanging vehicle were an optical data acquisition system such as a video camera[7,8] and the VisNav[18] sensor. The former was not adopted as it requires special video analysis software with excessive post processing and limited usage (it supplies only relative heading). The VisNav sensor can produce both pitch and yaw information simultaneously but, a unit was not available for testing. Therefore a new data acquisition system was considered and installed in the parafoil prior to the flight tests.

Four main requirements were considered to design the system. First of all, as it must be installed in the parafoil it must weigh as little as possible. Thus number of units and weight should be minimized, and the configuration shouldn't deform the aerodynamic shape when the parafoil is opened. Second, as there are no hard places to install the sensors, a special installation technique is required. Third, the system should survive repeated possible impacts when the Buckeye lands and the parafoil falls down on the ground. Last, data acquisition rate should be high enough to supply sufficient data for analysis.

4.2.3.1   Accelerometers

Based on the requirements, small Crossbow® accelerometers and a Bluetooth® wireless data acquisition system including the Valitec® ReadyDAQ AD2000 Data Logger was selected for the parafoil data acquisition. The onboard sensor package is composed of two 1-axis (CXL02LF1) and two 3-axis (CXL01LF3) accelerometers and a remote transmitter (Figure 4.4) that weighs 2.7 lbs including cables, connectors and two batteries. Accelerometers were carefully sewn in the canopy of the parafoil (Figure 4.5). The sensitive axes of the accelerometers were aligned to directions of the
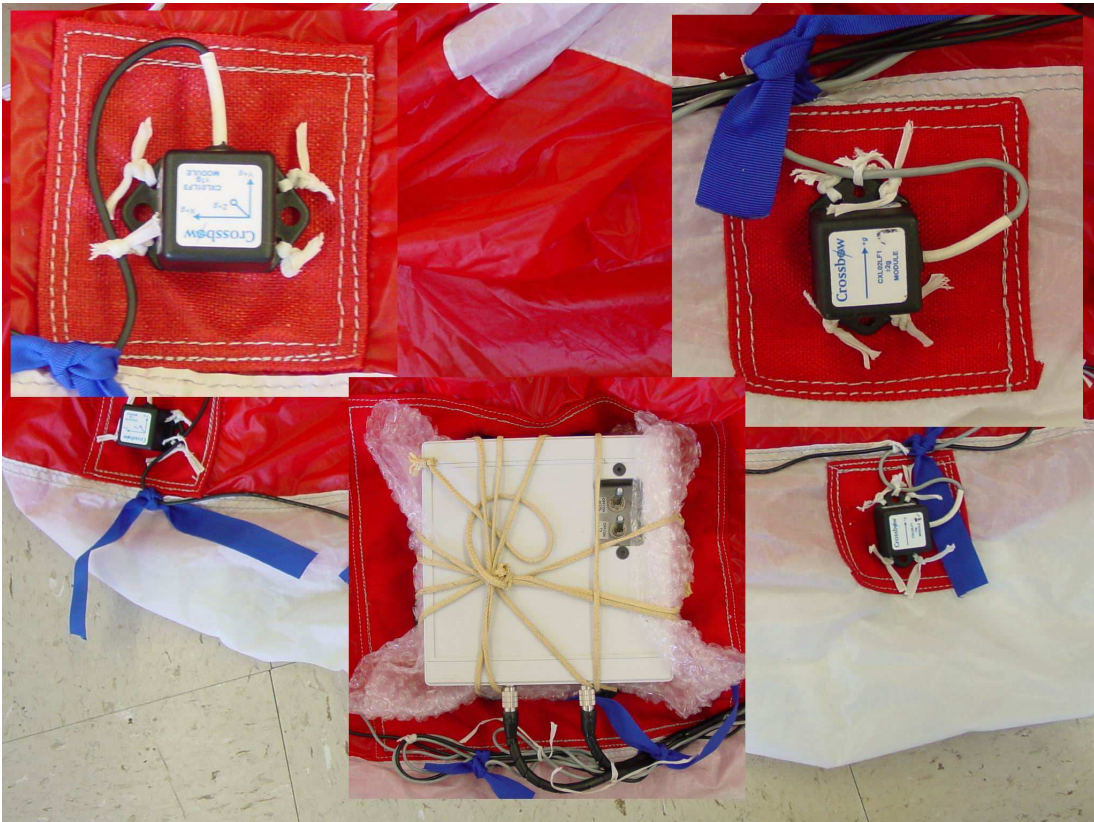
Figure 4.4 Accelerometers and Remote Data Transmitter on the Parafoil
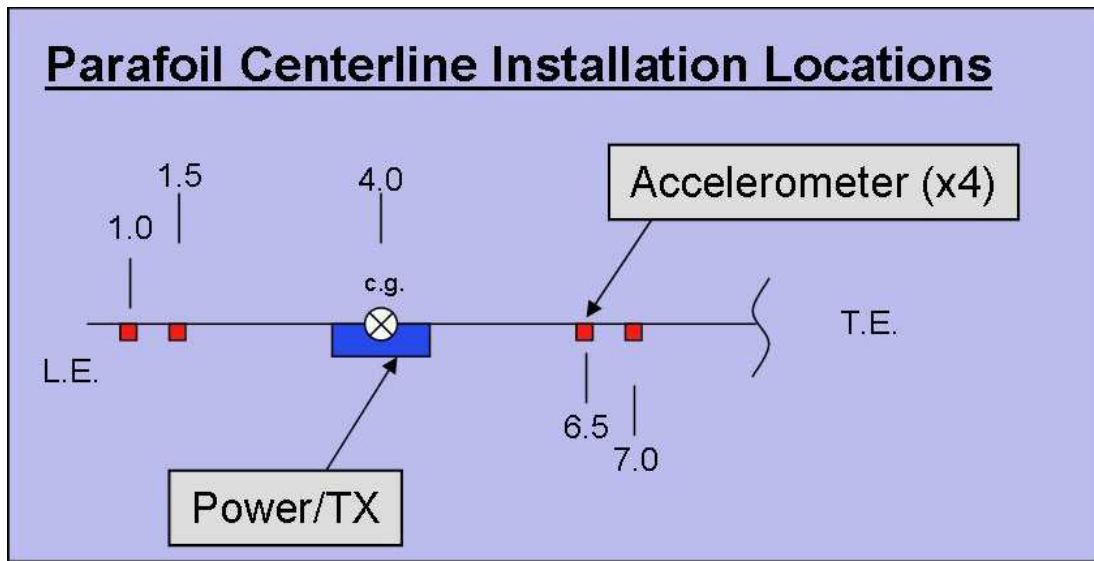
Figure 4.5 Accelerometers and Data Transmitter Locations on the Parafoil

parafoil body axes. To minimize the dynamic effect due to weight increase of the parafoil, the box housing remote transmitter and power supplier was installed at the C.G. of the parafoil. The remote data receiver and logger were installed on the vehicle to save data from possible crashes during take-offs and landings for repeated tests. The accelerometer outputs are 3-axes accelerations which are integrated to 3-axes velocities of the parafoil. The specifications of the CXL01LF3 and two CXL02LF1 Crossbow accelerometers are given in Table 4.3.

4.2.3.2 Wireless Data Acquisition System

Since it is not practical to connect wires from the sensors on the parafoil to data acquisition system on the Buckeye vehicle, a wireless data acquisition system was designed. Because the existing hardware capacity is limited for further data acquisition expansion, an independent data acquisition system was adopted. It is composed of a Crossbow WSC-100 wireless transmitter, receiver, and Valitec data logger. The

Table 4.3 Technical Specification of Accelerometers on the Parafoil

Specifications		CXL01LF1 CXL01LF1Z CXL01LF3	CXL02LF1 CXL02LF1Z CXL02LF3	Remarks
Performance				
Input Range (g)		±1	±2	±5%
Zero g Drift (mV)		±30	±30	0°C to +70°C
Sensitivity (V/g)		2	1	±5%
Transverse Sensitivity (%FS)		±5	±5	Max
Non-Linearity (%FS)		±3	±2	Typical
Alignment Error (deg)		±2	±2	Typical
Noise Density (µg/Hz½)		70	140	Typical
Noise (mg rms)		0.5	1.0	Typical
Bandwidth (Hz)		DC-50	DC-50	±5%
Environment				
Temperature Range (°C)		-40 to +85	-40 to +85	
Shock (g)		2000	2000	
Electrical				
Supply Voltage (Volts)		+5 ± 0.25	+5 ± 0.25	
Zero g Output (Volts)		+2.5 ± 0.15	+2.5 ± 0.15	@ +25°C
Supply Voltage -R option (Volts)		+6 to +30V	+6 to +30V	Unregulated
Supply Current (mA)		4/axis	4/axis	Typical
Span Output (Volts)		± 2.0 ± 0.1	± 2.0 ± 0.1	@ +25°C
Output Loading		>20kΩ, <30 nF	>20kΩ, <30 nF	
Physical				
Size	Standard package	0.75" x 1.875" x 1.00 (1.90 cm x 4.76 cm x 2.54 cm)		
	Aluminum package	0.95" x 2.00" x 1.20" (2.41 cm x 5.08 cm x 3.05 cm)		
Weight	Standard package	1.62 oz (46 gm)		

Notes
All frequency break points are -3 dB, single pole, -6 dB per octave roll-off. Non-linearity is the deviation from a best fit straight line at full scale. Transverse sensitivity is error measured in the primary axis output created by forces induced in the orthogonal axis. Transverse sensitivity error is primarily due to the effects of misalignment (i.e., much of it can be tuned out by adjusting the package orientation). Zero g drift is specified as the typical change in 0 g level from its initial value at +25 °C to its worst case value at Tmin or Tmax.

wireless smart I/O modules provide 8 channels of data stream with a range of 100 ft across a 2.4 GHz Frequency Hopping Spread Spectrum to prevent frequency interference. The I/O module can transmit at a maximum rate of 100 Hz with 12-bit resolution. The Valitec AD2000 data logger, can save data at rates up to 500 Hz with a serial cable connected to the receivers. In the configuration used in this research, the acquisition rate was set to 25 Hz considering for reasons of the flight time, power consumption of remote sensor package, and saving capability of the logger.

4.2.4 *Multi-rate Data Acquisition*

As described in above, data acquisition systems were added to the existing Buckeye data acquisition system which was originally designed for NASA's PGNC testing, which required only a low rate data stream and small data storage. Nominal data acquisition rates are 5 Hz for PGNC parameters, and 1 or 2 Hz for general vehicle parameters and GPS data. For these reasons data acquisition systems for the purpose of system ID were designed and added within the limits of the expandable capacity of the existing hardware. This situation mandated different rates for each subsystem and the need for synchronization for later use. The synchronization of the data stream is described in Chapter V. The subsystems sample rates are summarized below:

- Air Data: around 59 Hz depending on the ACP workload
- IMU: around 36 Hz depending on the ACP workload
- Parafoil accelerometers: 25 Hz constant
- Control input 5 Hz, GPS: 2 Hz from nominal system

4.3 OKID Application for Nonlinear Simulation Data

A nonlinear, non real-time eight DOF simulation for the Buckeye parafoil-vehicle is used to generate appropriate input amounts for flight test applications, and to generate time histories for the OKID identification routine. During the simulation states and controls are integrated at 50 Hz and stored at 25 Hz like flight data with inputs. The input amplitudes and durations must excite the dynamics modes, but

prevent the system from going unstable. A controllability and observability analysis was done using an identified state-space linear model to confirm and verify the result with the analytical model. The nonlinear simulation code used in this research is Parafoil Dynamic Simulator (PDS) supplied from NASA. A full descriptions of the PDS nonlinear simulation is provided in Appendix D.

4.3.1 Identified Linear Model and Time Histories

As shown in the following figures, the PDS nonlinear simulation starts at some feasible arbitrary initial flight conditions and settles to steady-state after some time. After it stabilizes, a small amount of input (symmetric for longitudinal and asymmetric for lateral/directional) is applied for two seconds to excite the dynamic modes. The resulting inputs and outputs are then fed to the OKID routine. The following figures show the accuracy of the identified linear model by comparing the nonlinear simulation histories and linear model simulation with the same inputs. Results from the longitudinal identification in Figure 4.6 demonstrate that the OKID local linear model approximates the nonlinear dynamics very well. Figure 4.7 shows that the lateral/directional identification results of the OKID model follow the responses of the nonlinear model quite closely.

4.3.2 Input Survey through Simulation Analysis

Figure 4.8 shows that the identified linear model comes short of representing the large input nonlinear dynamic responses because the applied input is beyond the linear range of the identified model. Figure 4.9 shows the effect of an excitation control input for the same flight condition. It implies that inputs causing large perturbations can adversely affect the fidelity of identified linear model. For flight test application, the magnitude of the inputs should be scaled properly for better identification.
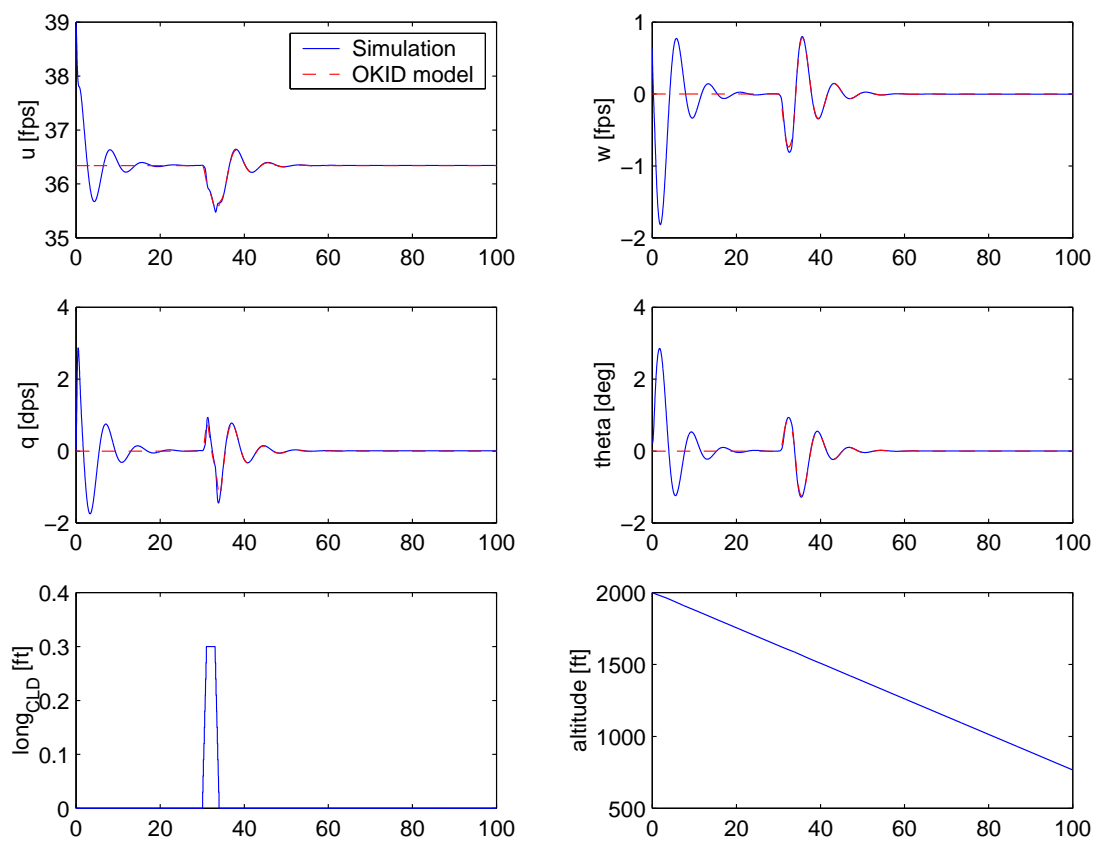
Figure 4.6 Comparison of Longitudinal Model Identification Responses to Nonlinear Simulation
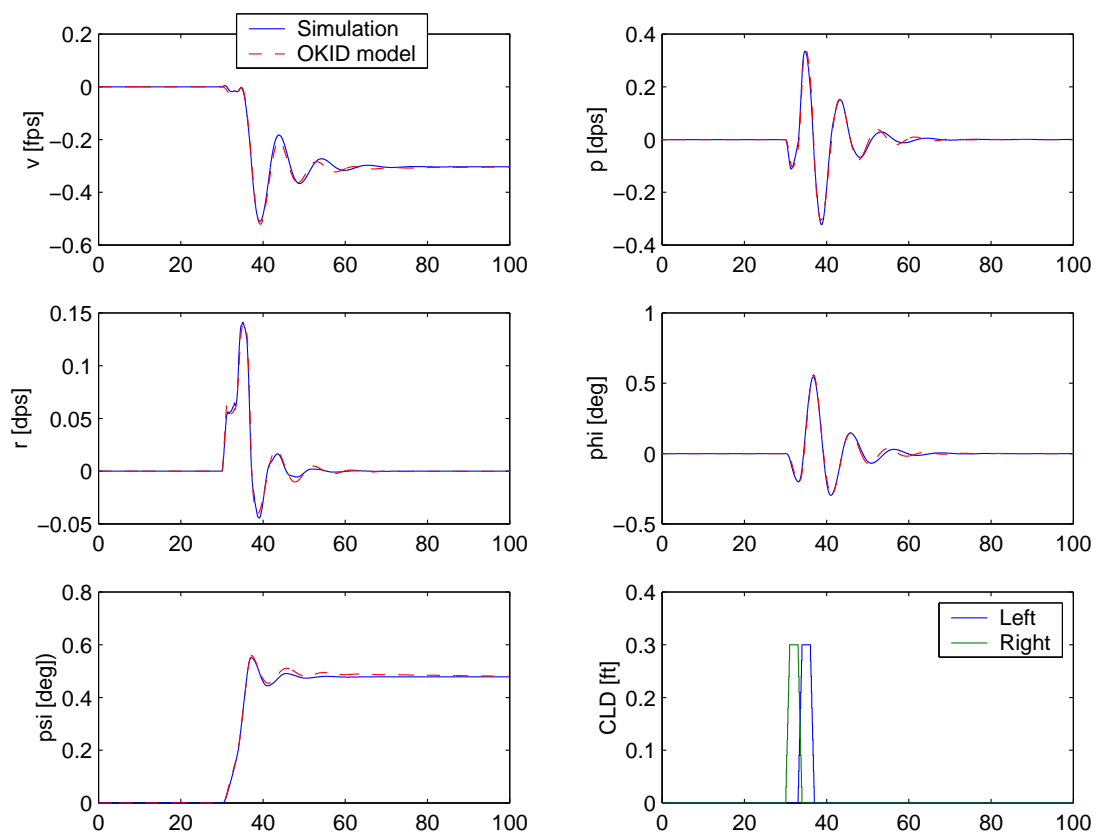
Figure 4.7 Comparison of Lateral/Directional Model Identification Responses to Non-linear Simulation
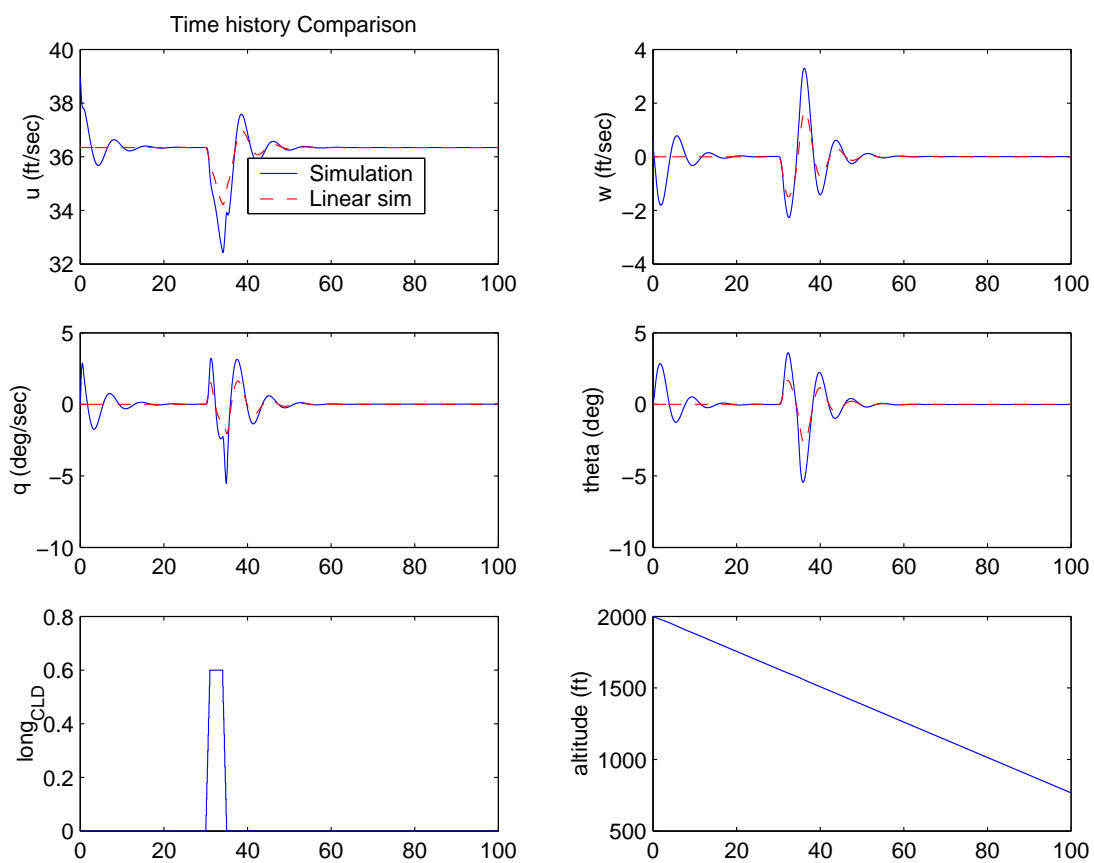
Figure 4.8 Comparison of Responses of Identified Longitudinal Linear Model and Non-linear Simulation for Large Input
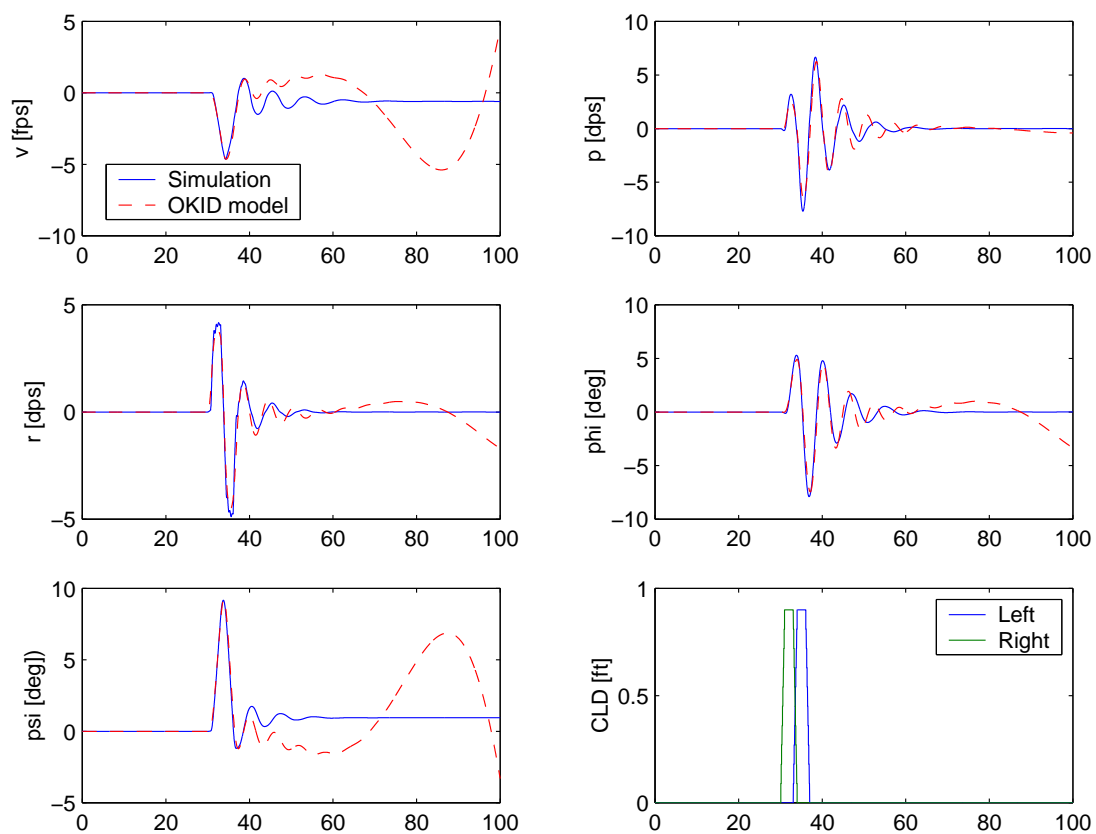
Figure 4.9 Comparison of Responses of Identified Lateral/Directional Linear Model and Nonlinear Simulation for Large Input

4.4 Flight Test Design

All information from the simulation study and previous flight testing experience was considered to design the test. Simulation study of the Buckeye parafoil-vehicle enables us to validate the performance of OKID, help select appropriate inputs for flight test, and indicates flight characteristics of the parafoil-vehicle. As described previously the Buckeye has only three control devices consisting of this left and right trailing edge flaps and engine rpm. For gliding flight dynamics to be identified, only two controls are available, the left and right trailing edge flaps. These controls are not sufficient to stabilize the Buckeye at desired trim point as for conventional aircraft. With change of the flaps the gliding attitude and corresponding sink rate can be controlled. For the Buckeye flight test the flaps are set to zero at initial and the parameters for trimming converges to a trim point for given weight and C.G. condition while gliding without input change. As noted from the simulation study, long stabilized flight is required before input initiation even without atmospheric disturbance. As atmospheric disturbance can affect the equilibrium state significantly, test date and time should be chosen carefully with long stabilization flight for test. In designing the flight test several assumptions are made as follows:

- Parafoil is a rigid body; No elastic effect

- Vehicle starts perfectly trimmed condition

- No distortion effect from location of aeroprobe

- Parafoil sideslip angle is calculated from speeds integrated from accelerations

- Multi-rate sampling will be sufficient

- IMU is located at C.G. of the vehicle as close as possible

- Number of accelerometers on the parafoil are sufficient; Two for X, Y axis, 4 for Z axis

- 25 Hz of the parafoil sensor sampling rate is enough based on analytical model

- 5 Hz of control input sampling rate is enough

4.4.1   Test Procedures

The identification flight tests were conducted during routine PGNC tests, all PGNC standard operating procedures for operation were used.[44]   General procedures for PGNC test flights are as follows:

1. Preflight check

2. Take-off and climb for altitudes. Usually 1500 to 2000 ft AGL.

3. Engine off gliding for PGNC test with "Auto" or "Manual"

4. At predetermined safe altitude, engine restart and climb

5. Repeat step 2 to 4 for tests within the endurance limit

6. Land and data archiving

The identification flight tests were inserted between step 2 to 4 in place of the PGNC flight. Procedures for identification tests consisted of the following:

1. *Stabilization flight*
   At altitude with engine-off, let it glide for a while enough to be stabilized. Based on the simulation study it should be at least 30 seconds without disturbance and any input. In practice with disturbance 50 seconds looked appropriate. Longer time limits maneuvering altitudes.

2. *Input commands*
   After stabilization flight, put predetermined inputs at the PGNC input notebook computer in the ground station manually. Automatic input was not provided due to resource limit of computing power.

3. *Input commands for validation data for ID*
   About 20 seconds following *Input commands*, apply another small inputs. This tie histories used to validate the linear model identified from the first input command.

4.4.2 Test Inputs

An infinite number of inputs could be used for the test but one must consider how open loop dynamics can be excited first.[41] There mentioned three types of control inputs for airplane dynamic flight test in Ref.41. Unlike for airplanes the control input of the parafoil is limited to only downward deflection of the trailing edge flap. Thus step input or pulse (singlet) input are candidates for control input. During flight tests the input commands are exerted by discrete key stroke command with ground station notebook computer manually. From the nonlinear simulation study and OKID applications small pulse inputs of less than 30 percentage of full control authority appear good enough to stimulate dynamic modes. It is supposed to generate responses be distinguished from those due to small disturbance excitation and stimulate the open loop dynamic without much of nonlinear effect. For longitudinal motion a symmetric flap input of two to three seconds were applied and asymmetric left pulse flap followed by right pulse flap inputs were applied for lateral/directional motion. A typical input history is shown in Figure 4.10.

4.4.3 Flight Tests

For NASA's PGNC tests there have been more than 35 flights since Oct. 18th, 2001 in the Flight Test Facility of Flight Mechanics Laboratory of Texas A&M University.[44] As part of the flight tests, 7 system identification flights were conducted from July 2003 to July 2004.

The Buckeye-parafoil system does not fly like other powered airplanes or powered ultralights during gliding. While gliding it is very vulnerable to atmospheric disturbances and the gliding speed is almost the same order of magnitude as most atmospheric disturbances. To remove any unexpected/undesirable disturbance effects including turbulence, test flights were supposed to be conducted during calm conditions. But despite of careful selection of the test date, it was inevitable to have disturbances, and this resulted in disturbance-corrupted data on most of the flights.

On the Buckeye there are only two control inputs, symmetrical trailing edge flap
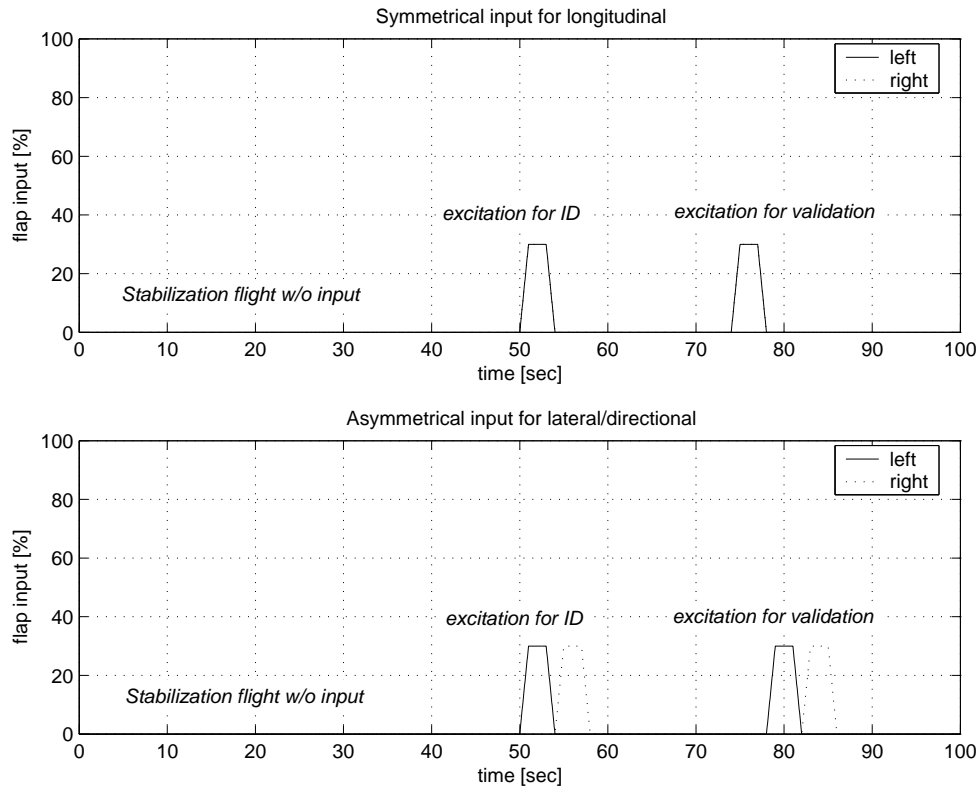
Figure 4.10 Typical Input Shapes for Identification Test

for longitudinal, and asymmetrical trailing edge flap for lateral/directional motion respectively during power-off gliding. Precise trim for general aircraft requires many parameters to be steady-state and can be achieved with 3-axis controls and power. But for gliding Buckeye, there are limited trim points which can be achieved with two controls. With zero deflection of flaps and no power with given weight and C.G. condition, there is one trim point during gliding flight. At the trim point, all body rates are zero, all three axis speeds are constant. With it's slow flight speed it is very sensitive to atmospheric disturbance, which can prevent the Buckeye from being trimmed in short time. So unusual trimming technique was adopted for the Buckeye and it was allowed to dynamically settle before committing input commands. The settling time depends upon atmospheric conditions, and was selected to be around 30 to 50 seconds based on the nonlinear simulation and previous flight experience with the Buckeye.

All test runs are summarized in Table 4.4. There are 42 runs of test maneuvers,

including 19 longitudinal and 23 of lateral/directional shots during the tests. From the flight data most of runs are corrupted by disturbances and in many cases the flight histories show bigger responses even without control inputs than those due to inputs and can not be stabilized within a reasonable time. It is supposed to be corrupted by disturbance such as discrete gusts which can not be represented by combinations of periodic disturbance in OKID routine. Showing all the time histories determined not to be suitable for inputs for identification in this dissertation are lengthy and tedious, comments are put in the "Remarks" column in the table. Additionally malfunctions of the sensor packages occurred on some flights. In Table 4.4 the run ID's are designated as three digit numbers. The first digit of the run ID is 1 for longitudinal and 2 for lateral/directional test and the rest two digits are numbered sequentially.

4.5   Conclusions

Data acquisition system for identification of the Buckeye system were designed and described in detail. Being composed several independent subsystem, it provides useful data stream for the dynamic parameters of the Buckeye system. It is noteworthy that relatively simple and low cost system was constructed as data acquisition system for the parafoil parameters.

Computational simulations were performed to evaluate proposed OKID routine for identification of the Buckeye parafoil-vehicle. The various simulation analyses prove that the identified linear model follows the nonlinear results very well for given input commands even for large inputs which can cause nonlinear responses not implemented in the OKID linear model. The results proves that OKID routine is suitable for identification of the linear system from nonlinear dynamic motions of the Buckeye parafoil-vehicle.

The OKID application study for the simulation results with various input shapes gives intuitions on the input shape. Typical input commands are designed for the identification test.

Table 4.4 Flight Test Log for Identification

Flight ID (Date)	Run ID	Run Time (sec)			Input	Remarks
		Start	Input	Stop		
B34	101	1781.5	1793	1820	pulse	
(7/24/03)	201	2322	2340	2356	-	
	202	2381		2404	pulse	
	203	3011	3026	3045	-	
	102	3062	3072	3077	-	
	103	3077	3083	3087	-	
	204	3087	3093	3112	-	
	205	3124	3130	3145	-	
	104	3936	3944	3949	pulse	
	206	3949	3956	3972	-	
	105	4002	4009	4014	pulse	
	207	4015	4020	4031	pulse	
	208	4031	4038	4047	pulse	
	209	4048	4054	4066	-	
B35a	106	5346	5373	5385	pulse	
(8/1/03)	107	6446	6470	6507	pulse	

Table 4.4 Continued

Flight ID (Date)	Run ID	Run Time (sec)			Input	Remarks
		Start	Input	Stop		
	108	6540	6560	6570	pulse	
	210	7575		7620	-	
	109	7650		7705	-	
	110	7700		7720	-	
B35b	211	2112		2210	pulse	
(8/1/03)	111	2197		2230	-	
	212	3746		3780	-	
	213	3780		3805	-	
	214	3835		3865	-	
	215	3887		3915	-	
	112	3945		3975	-	9", 5sec
	113	4736		4765	-	8", 5sec
B37	114	1733 1780	1765	1780 1790	-	
(10/1/03)	216	2385	2415	2430	pulse	
	217	3257	3310 3330	3325 3342	-	
	115	3362	3396 3411	3405 3420	-	
	218	4320	4381	4392	6" pulse	

Table 4.4 Continued

Flight ID (Date)	Run ID	Run Time (sec)			Input	Remarks
		Start	Input	Stop		
	219		4402	4422	4" pulse	
	116	4412	4422	4480	6" step	
		4480		4520	-	no input
B41	-	2328	2379	2420	pulse	
(12/19/03)	-	3266	3318	3363	pulse	probe
	-	3800	3853	3895	pulse	mal-function
	-	4610	4665	4708	pulse	
	-	5142	4192	5230	pulse	
			5232	5258	10.5" pulse	
B43	117	2922	2930	2936	pulse	
(7/19/04)	118	2936	2949	2985	random	
	119	3004	3028	3049	pulse	
	220	3870	3924	3945	random	
	221	3945	3953	3965	pulse	
	222	3965	3975	3987	pulse	
	223	3987	4010	4047	pulse	
B44	-	10690	-	13458	-	probe mal-function

CHAPTER V

IDENTIFICATION RESULTS FROM FLIGHT TEST DATA

5.1   Introduction

In this chapter, flight test preparations, actual tests, and data saving are described including data reductions. Reduced data were applied to identification routines and its results are presented in the form of mathematical models, descriptions and figures. Finally the identified model from flight data is compared with the analytical model.

5.2   Data Reduction

To construct data sets for identification tests, all of the raw data was reduced by postprocess consisting of filtering and interpolation. All reduction was performed as carefully as possible so as not to affect the original dynamic properties of the data. Reduction procedures are described in following in detail in subsections.

5.2.1   Air Data

Air data including speeds and flow angles were constructed by postprocessing raw pressures of the 5-hole multifunction probe. The postprocessing code and calibration equations for of the multifunction probe were provided by the manufacturer, Aeroprobe Inc. Technical development and calibration methods are described in detail in Johansen's thesis[43,46] and paper.[47] Reduction procedures in Ref. 44 are followed.

The raw pressure data was converted to velocity and flow angle data with engineering units through the reduction code Multiprobe®. As can be seen in Figure 5.1, typical airdata has noise and must be filtered to be useful for identification. The converted probe parameters in the legend box are defined in Figure 5.2 representing the
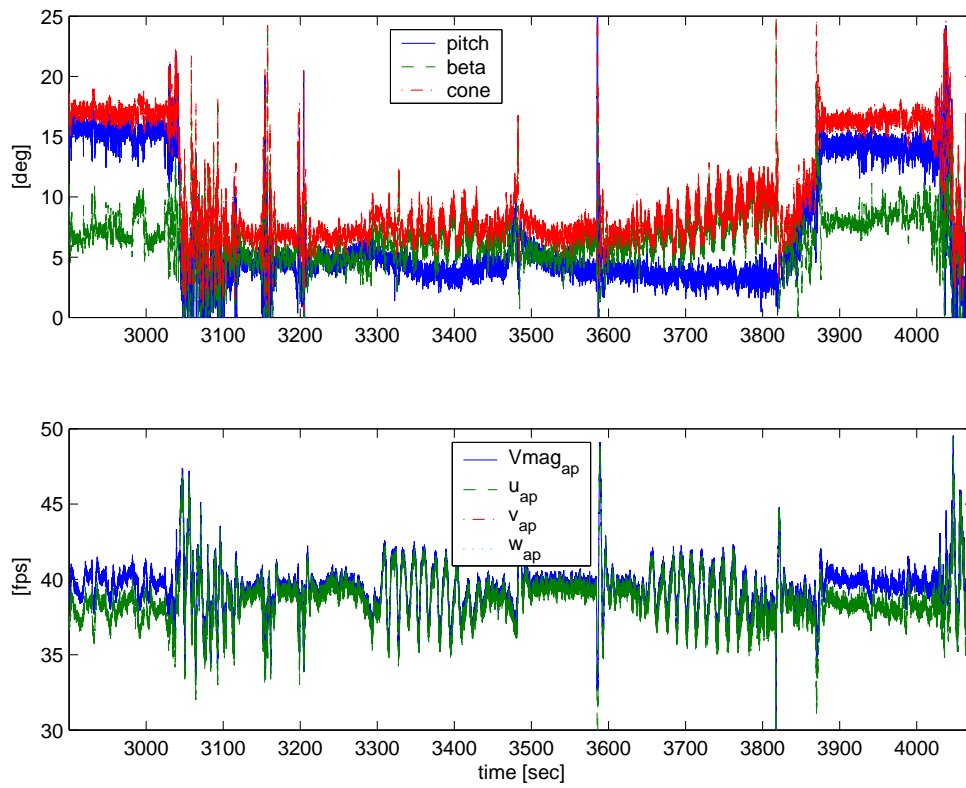
Figure 5.1 Raw Data from Multifunction Probe

pitch, sideslip, roll, cone angles and 3-axis speed u, v, w with total velocity $Vmag_{ap}$.[42] The subscript "ap" says it is a probe data.
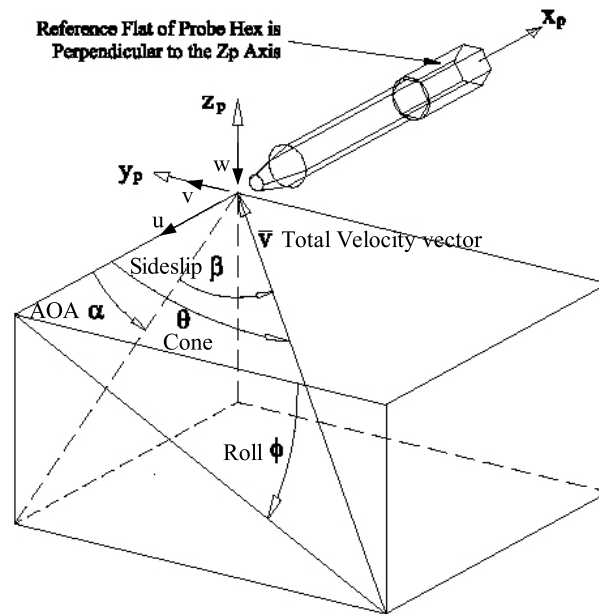
Figure 5.2 Coordinate Definition for Multifunction Probe

To remove high frequency noise we need a low pass filter that removes all the data points that respond at frequencies higher than the cutoff frequency while keeping the response with lower frequencies than the cutoff frequency.[48] The cutoff frequency was selected from the analysis of the data's power spectral density. A power spectral density from Fast Fourier Transform of a typical data stream reveals that how much of the data responds at a particular frequency[48] (Figure 5.3). One can decide significant frequencies to be included in the filtered data. From Figure 5.3, the aeroprobe data is almost near the very low frequency and magnitudes of the spectral density over bigger frequencies are very small (around 10^{-4} times) with respect to the magnitude at the very low frequency. It means that most of signals are coming from noise except
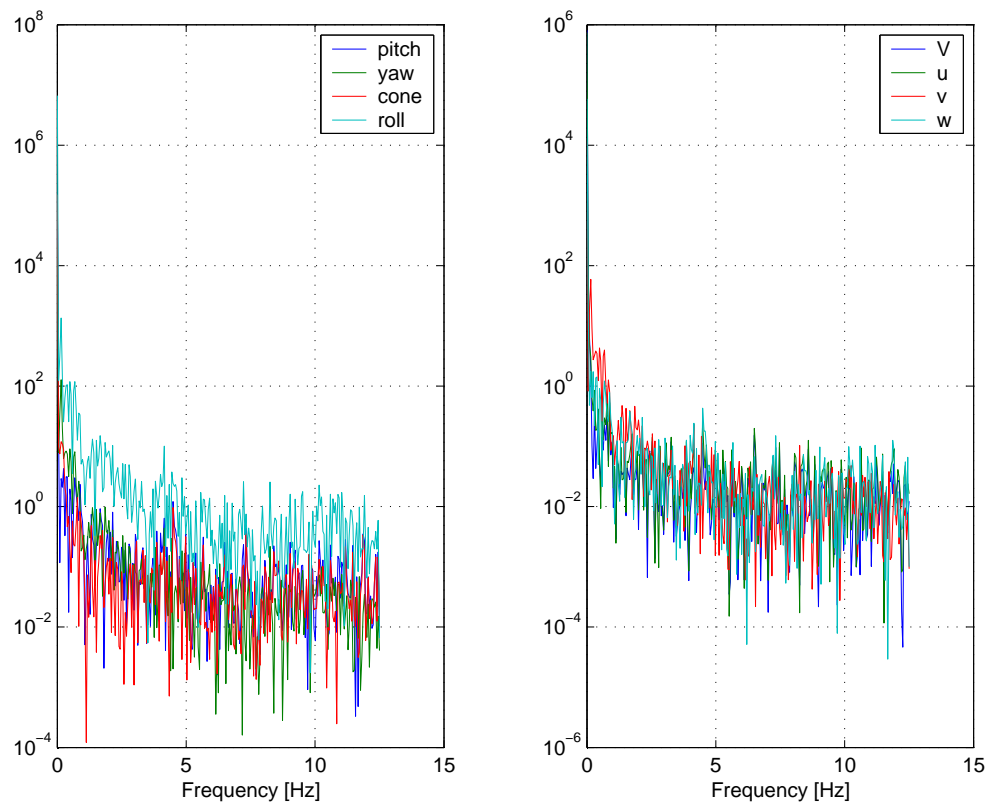
Figure 5.3 Power Spectral Density from Fourier Transform of Multifunction Probe Data

system's dynamic response. Thus the cutoff frequency for the low pass filter is selected to remove high frequency noise. The cut-off frequency was selected by trial and error method with "buttord.m" in Matlab$^{®}$ to have minimal distortion for filtered data with respect to original ones. For the probe data the cut-off frequency 0.3 Hz as 3 dB frequency was selected. There are several low pass filters such as Chebyshev type I, type II, Butterworth, Elliptic etc. and a Butterworth filter used for parafoil data processing during the parafoil tow test in Ref.49 was selected because it smoothed the data with minimal distortion as well as is convenient to use. As the filter is to be used for off-line signal processing, mathematical complexity such as higher order of the filter was allowed. To remove the undesirable time shift that typically occurs during filtering, the Matlab$^{®}$ command "filtfilt.m" which filters data forward and backward to remove time shift was used.[48] The designed filter properties in frequency domain are shown in Figure 5.4. In Figure 5.5 the filtered data stream shows good matches compared to the unfiltered ones. The roll angle histories from the probe shows some peaks after 3040 seconds and it corresponds to fluctuation by power-on of the Buckeye. Power-on data were not used for identification. The power effect can be seen clearly from probe pitch angle (vehicle's angle-of-attack, refer definition in Fig.5.2) which decreases on the first chart in Figure 5.5. No saturation was observed from gliding flight data for identification. Note that the roll angle in Figure 5.5 is not the roll attitude of the parafoil or vehicle. The definition is in Figure 5.2.

5.2.2 IMU Data

The IMU data of accelerations, attitudes, and body rates of the vehicle are saved in binary form in the harddisk of ACP. The DOS (Disk Operating System)$^{®}$ based conversion code "IMU-TAMU.EXE" was supplied by NASA and gives 3-axis body accelerations, body rates, and attitudes from saved binary data in the ACP. The data stream has noise and is supposed to be filtered out also. The noise level of IMU accelerometers is relatively small compared to the parafoil data as seen in Figure 5.6. The accelerometers of IMU and the parafoil have full range of $+2 \sim -2g$. The noise of the IMU data is almost negligible compared with that from the parafoil data. In the
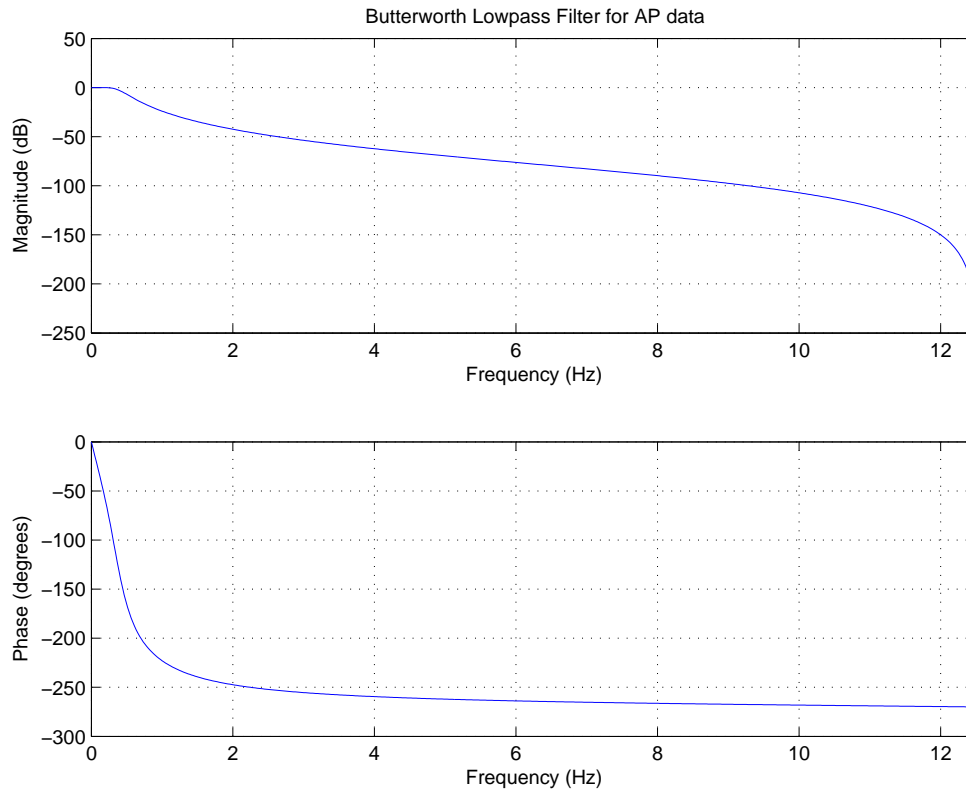
Figure 5.4 Bode Plot of Butterworth Filter for Probe Data

figure "pf" represents parafoil data and "IMU" does IMU data in the legend. The power spectral density by Fourier transformation can be seen in Figure 5.7. As can be seen in the figure significant responses exist at around 3 Hz and the responses disappears as frequency increases. A Butterworth filter was designed with cutoff frequency of 3 Hz for passband for 3 dB and stopband 5 Hz for 60 dB attenuation as in Figure 5.8. In Figure 5.9 the filtered data stream shows good matches compared to the unfiltered ones. The full range of accelerometers are $\pm$ 2 g's and the full range of bodyrates are $\pm$ 100 deg/sec.
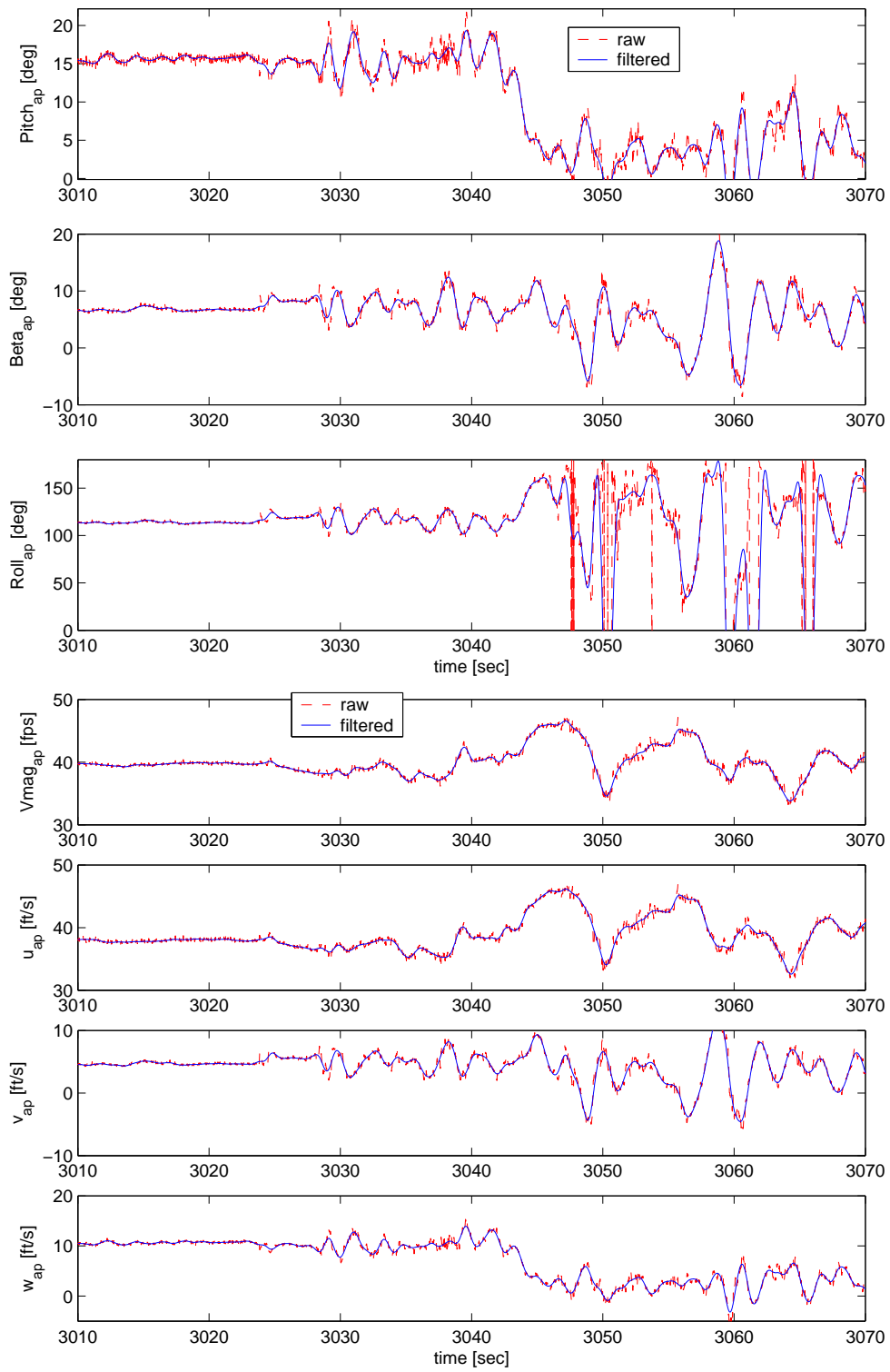
Figure 5.5 Filtered and Unfiltered Time Histories of Probe Data
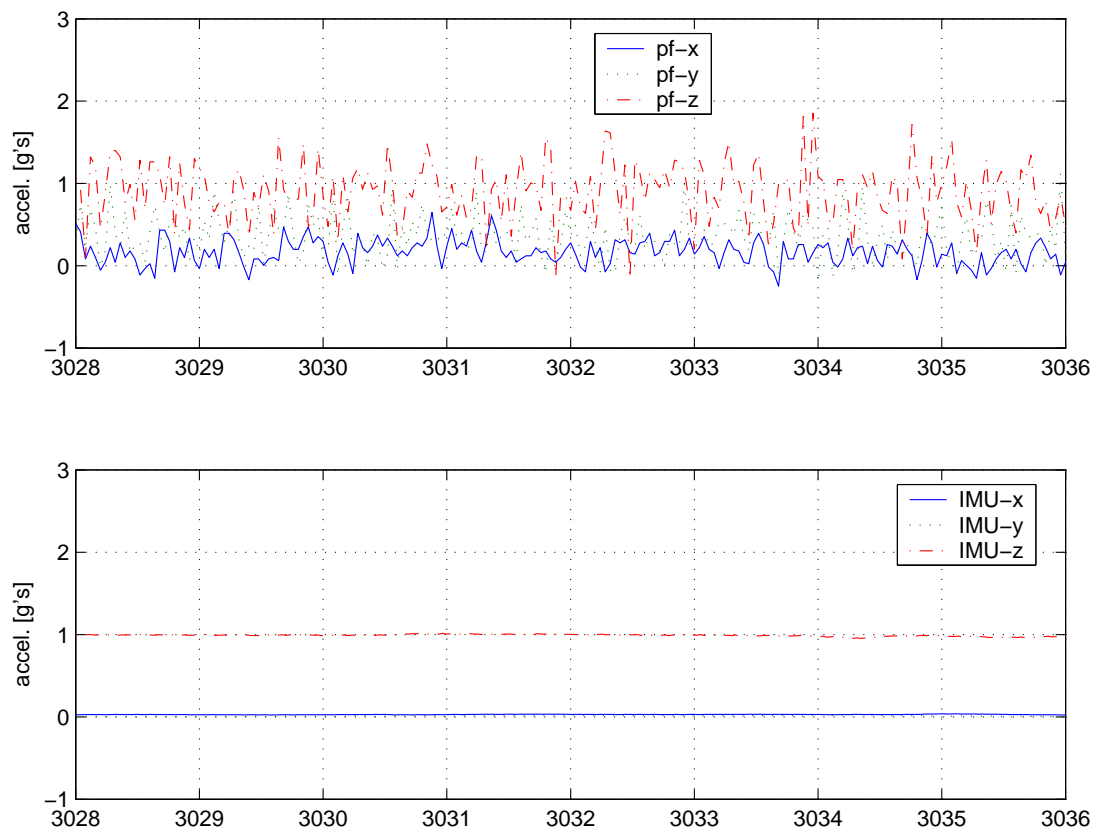
Figure 5.6 Raw Data from IMU and Parafoil Accelerometers
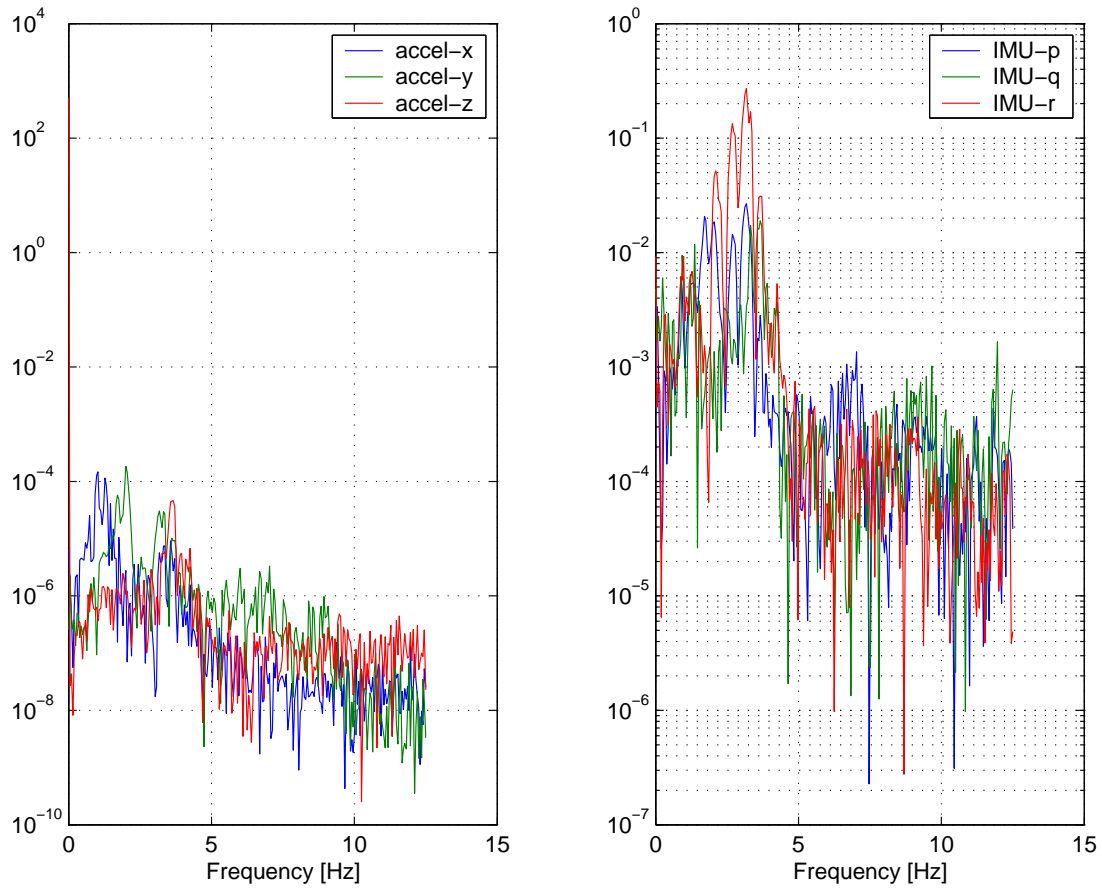
Figure 5.7 Power Spectral Density from Fourier Transform of IMU Data
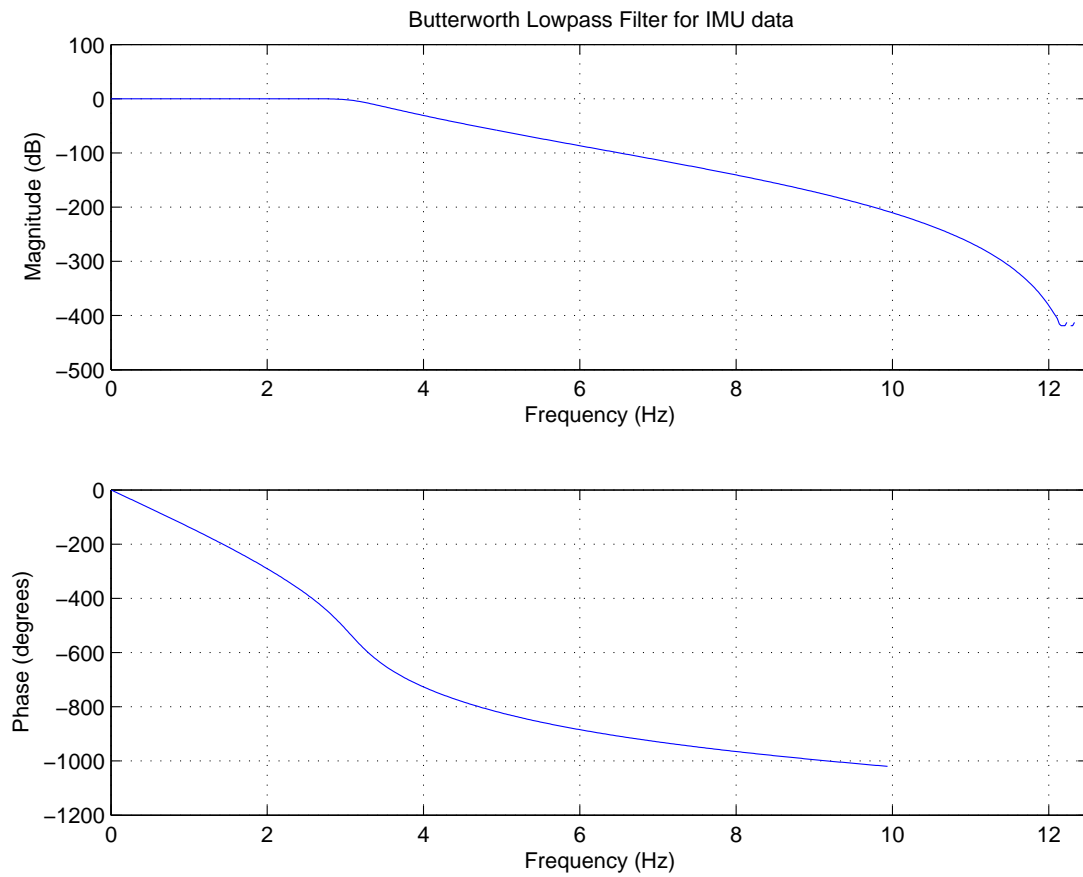
Figure 5.8 Bode Plot of Butterworth Filter for IMU Data
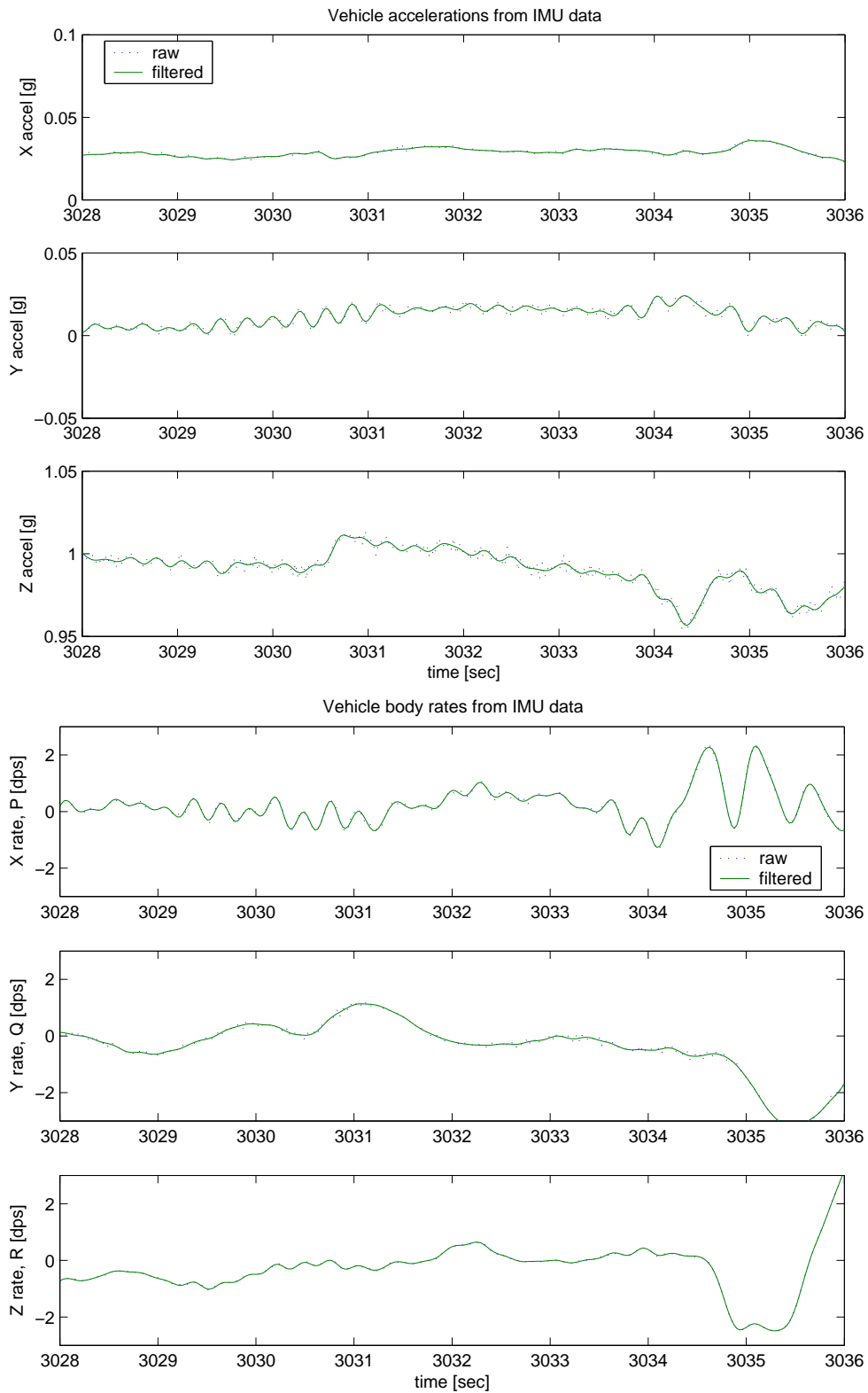
Figure 5.9 Filtered and Unfiltered Time Histories of IMU Data

5.2.3   Parafoil Accelerometers

Since there is no rigid structure in the parafoil, it was challenging to install sensors on the fabric body and get useful data from them. As described in chapter IV, a minimum number of small accelerometers were installed and aligned to the parafoil body axis as close as possible. As expected, the accelerometer had to cope with the noisy environment and fabric vibration, as well as sensor noise itself during flight (Figure 5.6). Typical power spectral density of parafoil data stream from Fourier Transformation is shown in Figure 5.10. From the figure there is no dominant frequencies in the data stream. A Butterworth filter was designed with cutoff frequency of 0.2 Hz (Figure 5.11) and applied for the accelerometer data (Figure 5.12).
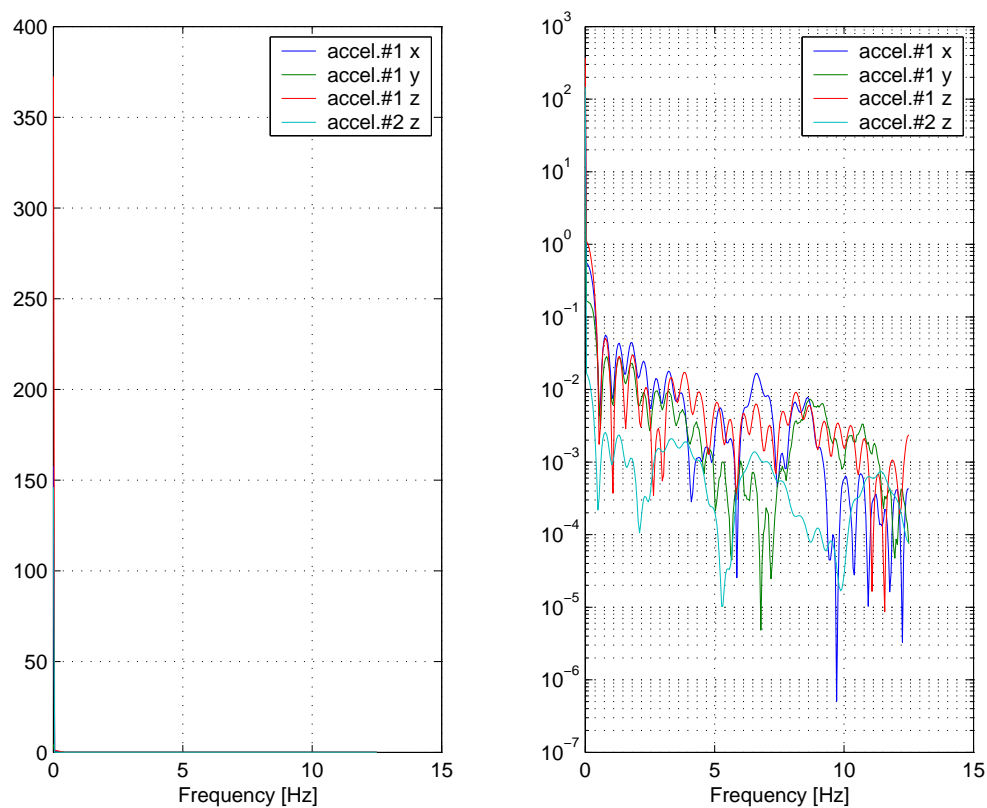
Figure 5.10 Power Spectral Density from Fourier Transform of Parafoil Data
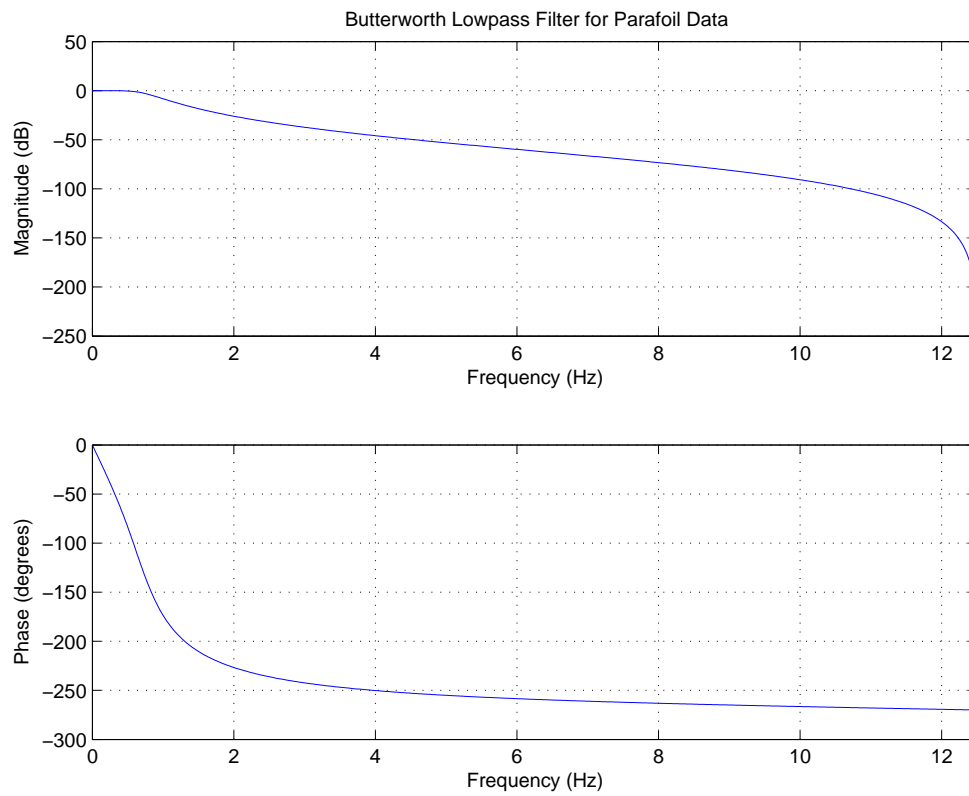
Figure 5.11 Bode Plot of Butterworth Filter for Parafoil Data
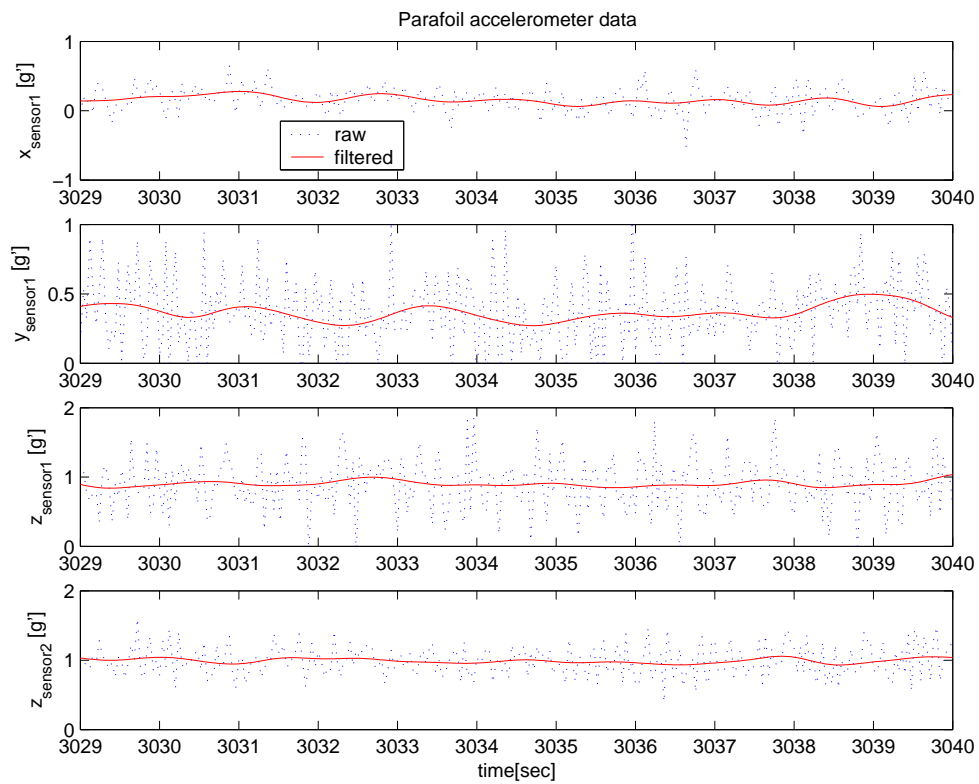
Figure 5.12 Filtered and Unfiltered Time Histories of Parafoil Data

Because of the physical constraints of a parafoil, only light and small accelerometers were installed. Three axis velocities are reduced by integrating the three axis acceleration data. Pitch and roll attitudes are converted directly from accelerations, and pitch and roll rates of the parafoil are reduced by differentiating attitude data with respect to time. Sideslip angle was calculated from reduced velocities, and yaw rate was reduced by differentiation of sideslip angle.

5.2.4   Synchronization of Multi-rate Sensor Outputs

As described earlier, the data acquisition system is composed of four subsystems with different acquisition frequencies. To apply the OKID routine, the data set should be prepared at a common sample rate. Extrapolation of coarse data for higher rate data could generate unknown dynamics, so high rate data was interpolated for the slower rate. The slowest data stream comes from the parafoil accelerometers at 25 Hz, and the 5 Hz of control input data in PGNC parameters.

Being different from normal technique of continuous control stick input for aircraft flight test with various input frequencies, the input commands in this research were exerted through a notebook computer by pressing keyboard discretely at about 4-6 Hz. In addition the control inputs for identification were put monotonously for increase and decrease and hold 2 to 4 seconds at maximum for pulse input shape as in Figure 4.10 and Figure 5.13. As can be seen from Figure 5.13, there is little possibility of aliasing. As the control input histories were recorded from the potentiometers of control winch motors and the recorded data were used for inputs for identification directly, the dynamics of winch from the keyboard input to the flap deflection was not modelled with the assumption for rigid riser and strings for tension. As in Figure 5.13 the flap positions are converted from raw data and extrapolated for 25 Hz. No extra instrumentation for high frequency input sensing was provided for cost minimization.

From analytical data, natural frequencies of oscillatory modes of each motion are 14.93 rad/sec and 1.36 rad/sec for longitudinal and lateral/directional respectively. Thus the frequency of the highest oscillatory motion is 2.38 Hz. To avoid aliasing and to detect all the motion including un-modelled or unexpected dynamics with the
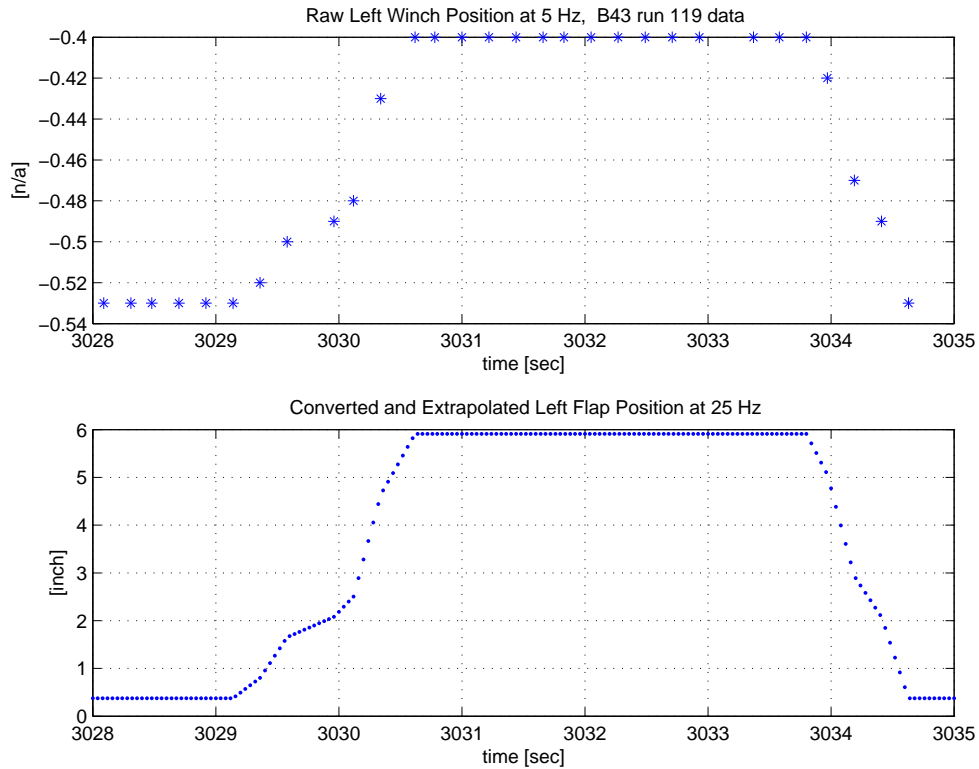
Figure 5.13 Raw Data at 5 Hz and Extrapolated/Converted Control Input Data at 25
Hz

existing hardware capability, nominal data acquisition frequency of 25 Hz - greater
than 10 times the highest frequency - was used. Higher rates of multifunction probe
and IMU data were reconstructed by interpolating at 25 Hz. The time histories for
original and interpolated are compared in Figure 5.14, and shows that the interpolated
trajectory represents the original one very well.

5.3   OKID Application to Flight Test Data

Figures 5.15 to 5.20 show filtered flight data for a typical stabilized flight B35a, B37,
and B43. Much of the data seems to be corrupted by disturbances. After 50 seconds
of flight without any inputs, all states should be stabilize to steady-state values.
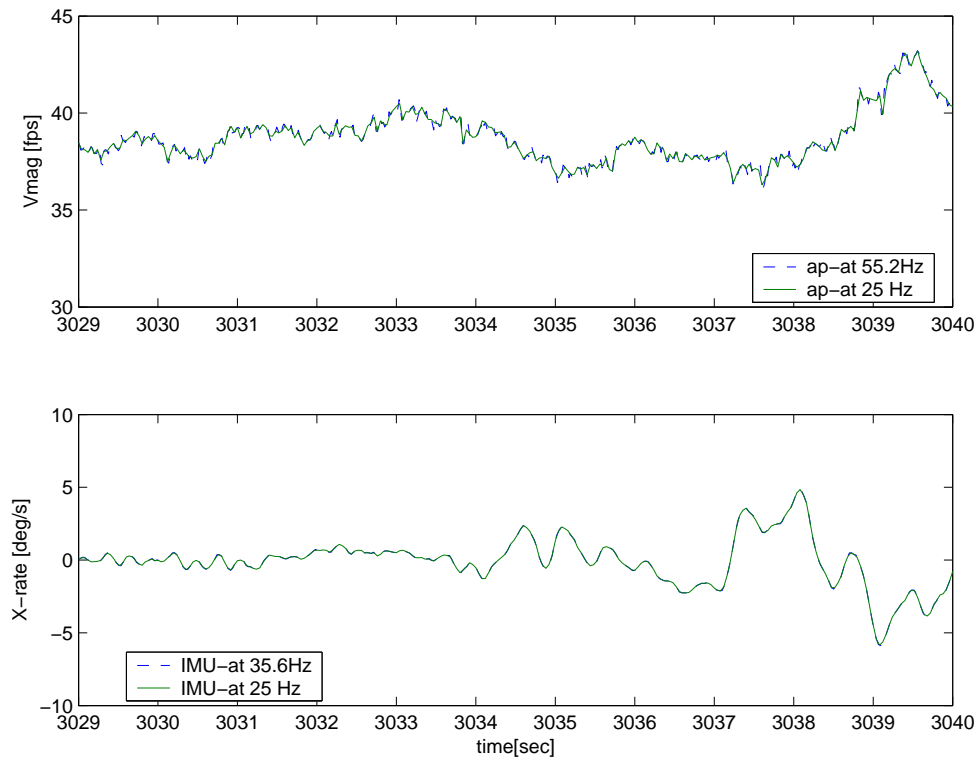
Figure 5.14 Interpolated IMU and Probe Data at 25 Hz

However the time histories show that the states are not stabilized with no input. The B43 flight conducted on July 19th, 2004 showed the best shot ever, and it was this data that was applied to OKID routine for identification (Fig. 5.19, 5.20).
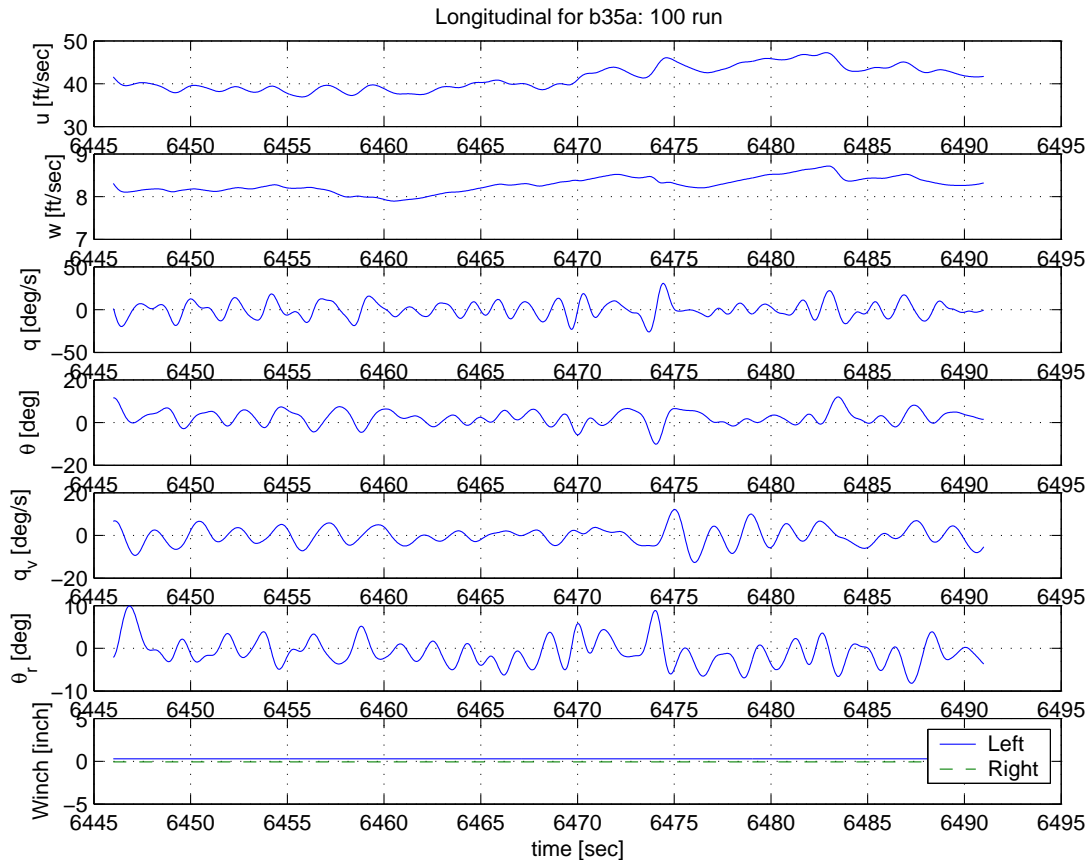
Figure 5.15 Stabilization Flight of B35a - Longitudinal States

5.3.1 Identified Linear System Model

As described above in section 5.2 all data of B43 flight are reduced and synchronized at 25 Hz and applied to the OKID routine. The order of the system Markov parameters is set to large enough to cover all expected periodic disturbances - it is called as
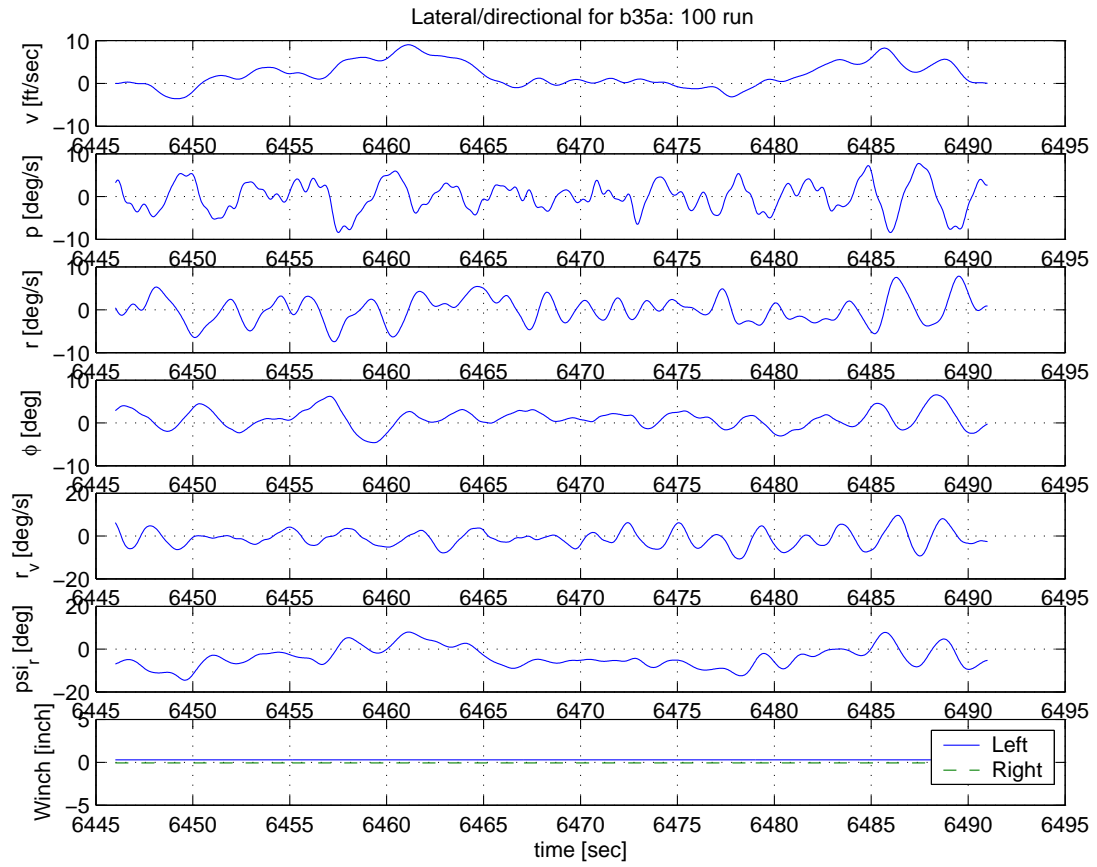
Figure 5.16 Stabilization Flight of B35a - Lateral/Directional States
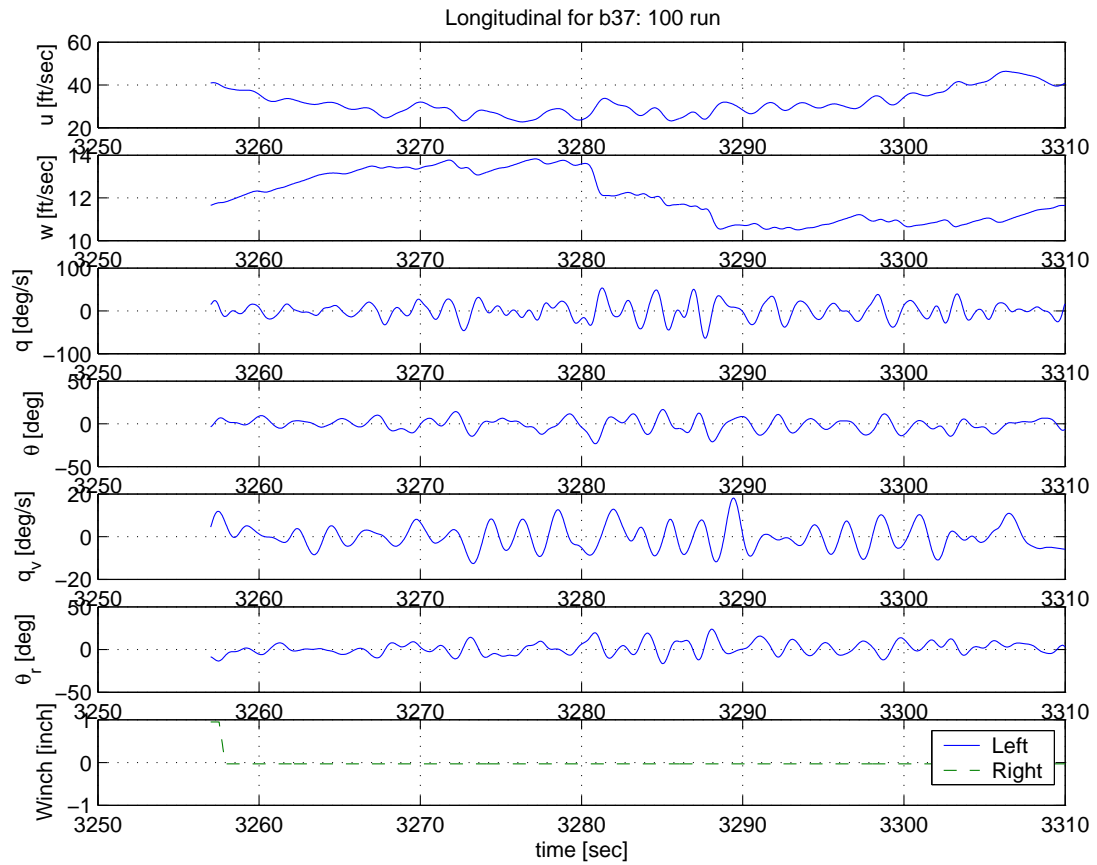
Figure 5.17 Stabilization Flight of B37 - Longitudinal States
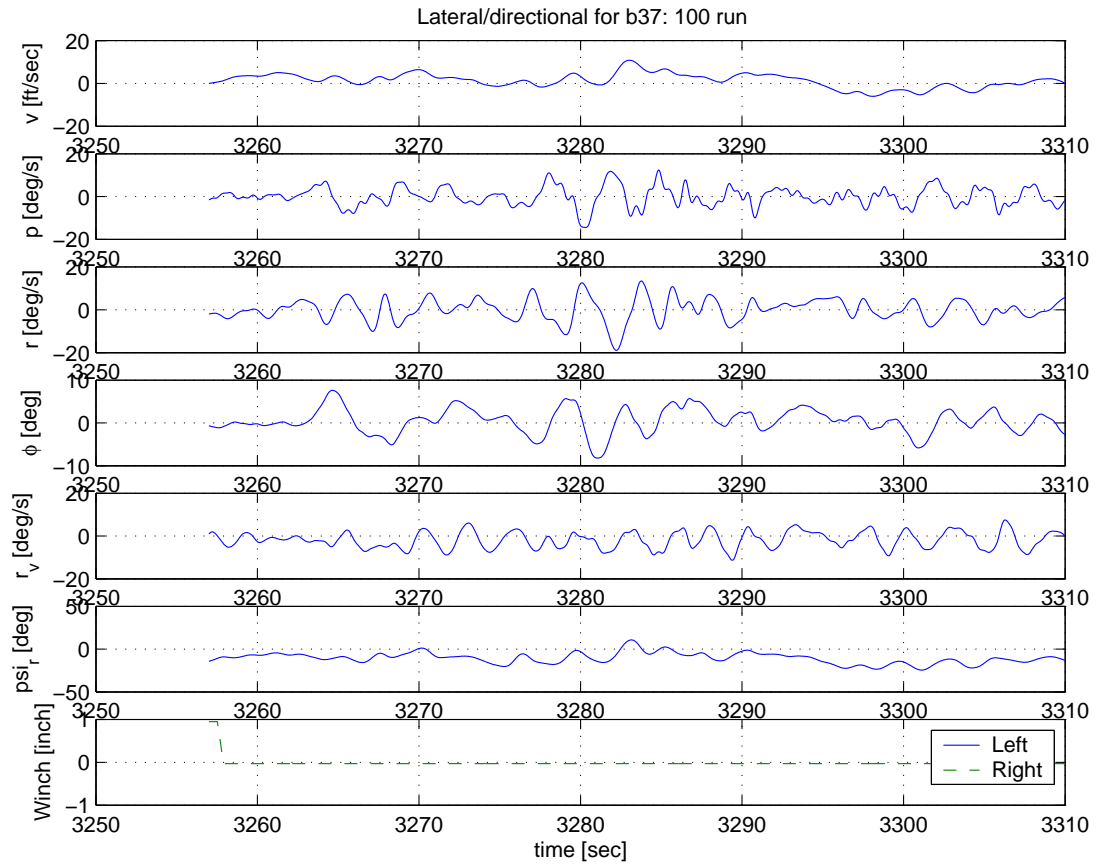
Figure 5.18 Stabilization Flight of B37 - Lateral/Directional States
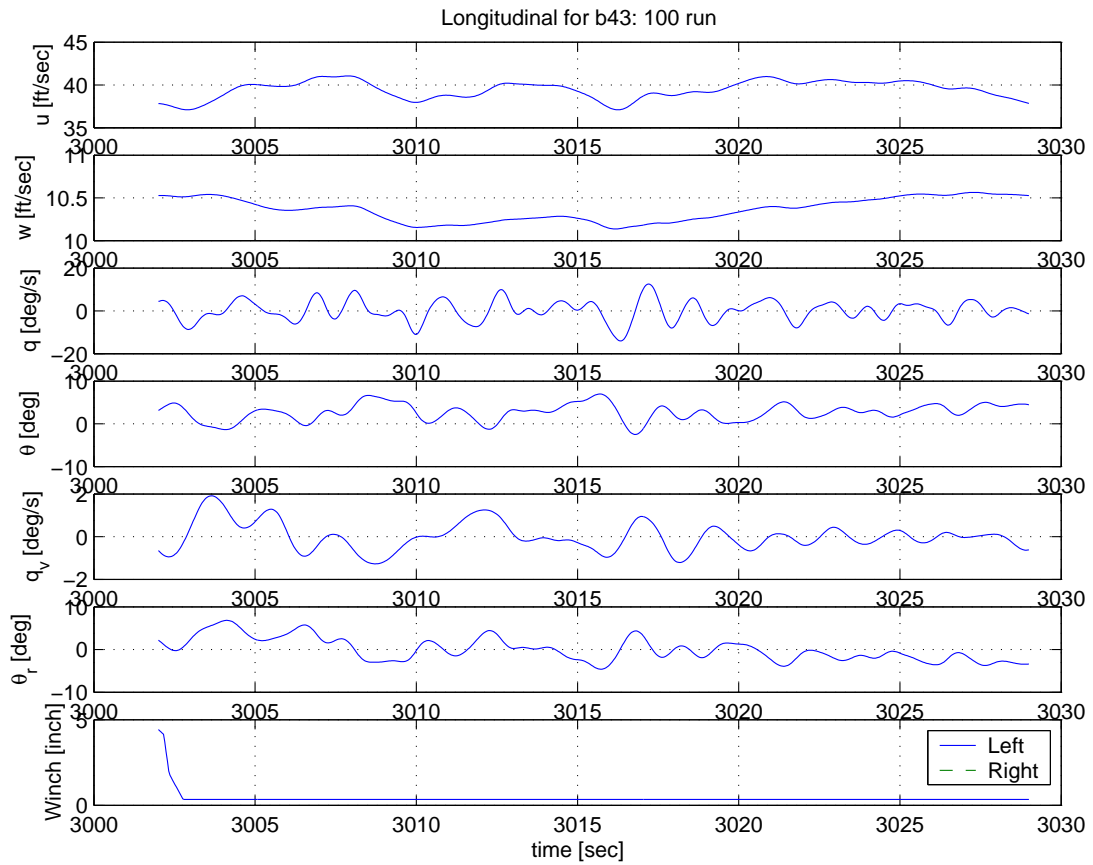
Figure 5.19 Stabilization Flight of B43 - Longitudinal States
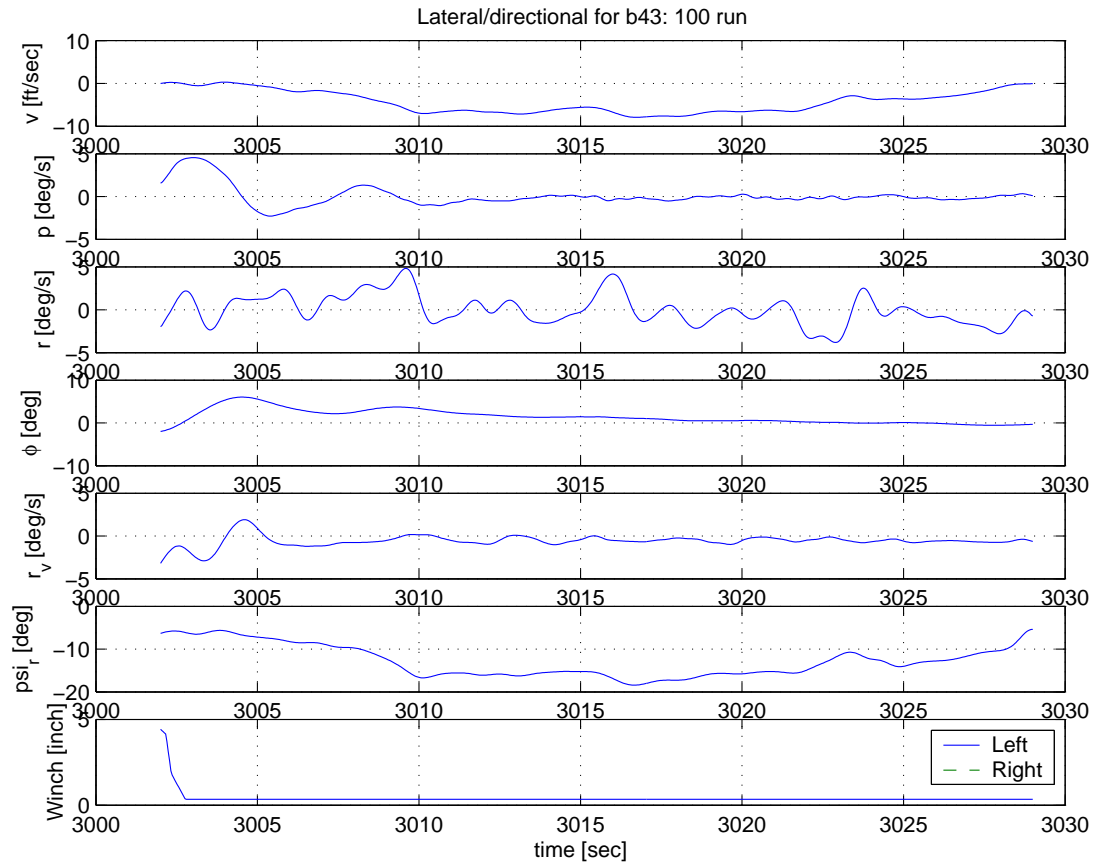
Figure 5.20 Stabilization Flight of B43 - Lateral/Directional States

overparameterization in Ref. 16. The system Markov parameters are related to the data length, which should be greater than the number of parameters to be identified. Large numbers of system Markov parameters results in a high computational burden, but it doesn't matter for the off-line identification of this Buckeye identification research. With system Markov parameter larger than the order of the system to be identified, there are extra singular values of the which do not belongs to the system. From Figure 5.21 one can select the order of the system from the dominant singular values. The system order was picked to be 10 for the case in which we don't know the system order, and the modal singular values are calculated and plotted. One can tell easily from the modal singular values in Figure 5.21 that the system order to be identified is 6, because the other singular values have much less significance than those for the system. In general the singular values of the Hankel matrix include true identifiable dynamic modes of the system, uncontrollable disturbance modes, and uncontrollable modes from overparameterization.[16]

5.3.1.1 Longitudinal Model

Applying the input and output time histories of flight B43 to the OKID routine, a linear system with matrices A, B, C, D and an observer gain G were identified. With the deadbeat observer gain G and overparameterization, the OKID find sinular values of the large system including internal models of disturbance from the overparameteriation. The OKID routine sums all the singular values and compare it with the sum of significant singular values of system which can be picked from the Hankel singular value chart in Figure 5.21. As can be seen in Figure 5.21 the order of magnitudes of singular values for unknown disturbances are much less than those of the system. With the singular value ratio of following equation the OKID routine determines whether the model with the picked order describes the system well or not
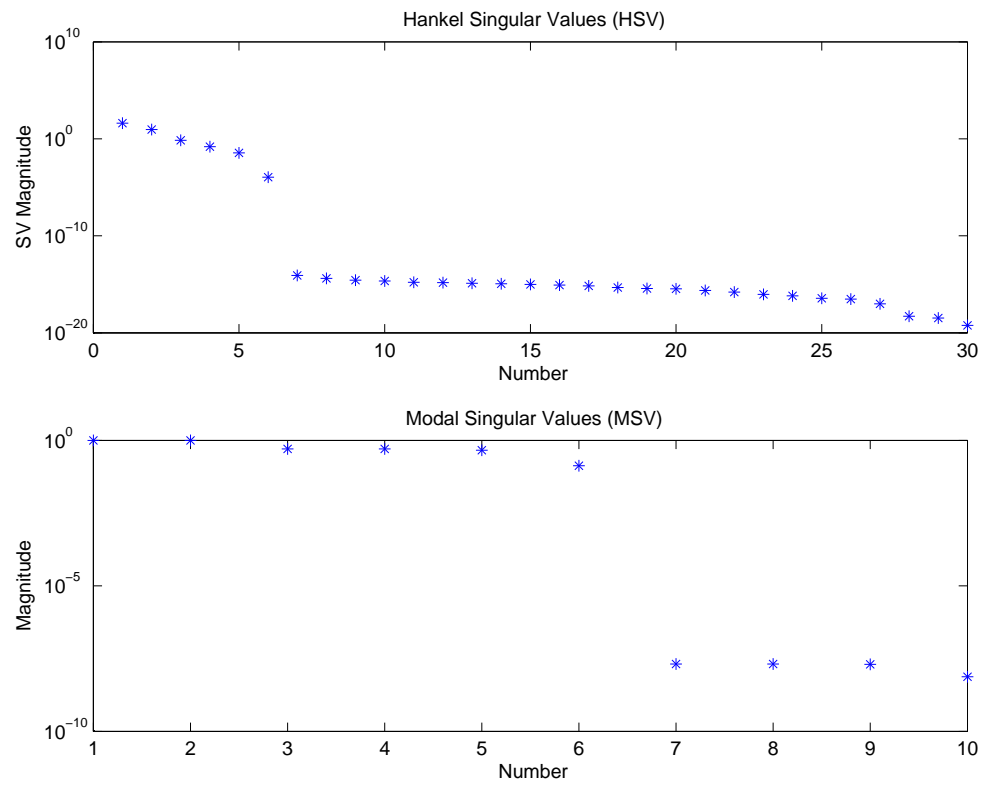
Figure 5.21 Hankel Singular Values and Modal Singular Values

quantitatively.

$$singular\ value\ ratio = \ \frac{\sum\limits_{i=1}^{n} \sigma_n}{\sum\limits_{j=1}^{N} \sigma_N} \times \ 100$$

$$where\ \ N = system\ order\ from\ overparameterization$$

$$n = system\ order\ picked\ from\ large\ singular\ values$$

$$\sigma_{i,j} = singular\ values$$

Figure 5.22 shows that the model of picked order of system with observer gain could estimate and track the flight test output time histories quite well. In this case the singular value ratio was 100% because a lot of singular values from the overparameterization were much less significant ($\approx 10^{-10}$). In Figure 5.22, the sequentially
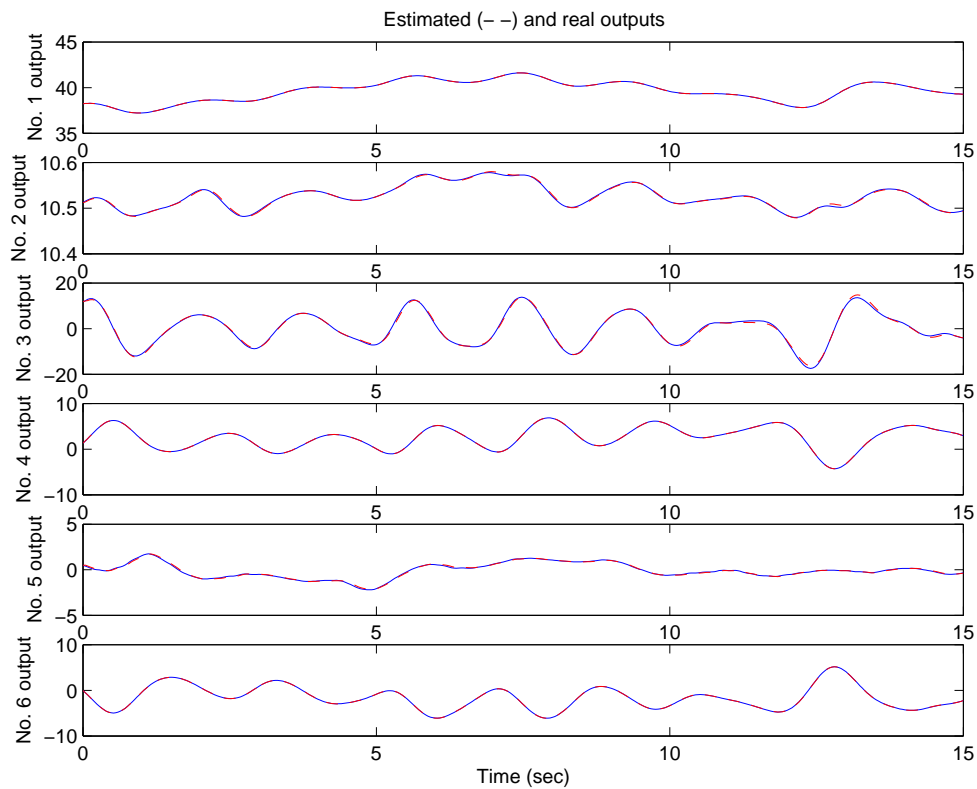
Figure 5.22 Estimated Trajectory by OKID with Observer Gain G

numbered outputs are matched to parafoil forward velocity u, parafoil vertical veloc-

ity w, parafoil pitch rate q, parafoil pitch angle θ, vehicle's pitch rate q_v, and vehicle's relative pitch angle θ_r respectively. As described in Chapter III the system matrices without observer gain can be found from the estimated system matrices from distinguishing the system Markov parameters from the observer Markov parameters. Figure 5.23 shows responses of the linear model with system matrices distinguished from the augmented system matrices with observer gain. That is the identified linear model from OKID. Comparing those two figures one can say that the OKID has great advantage to the ERA algorithm because the time histories does not show quick fading to steady state. The responses in Figure 5.23 are for the identified system only without the internal models of disturbance in OKID. The disturbance effects are shown prominently after the control input ended, when the identified model doesn't follow the disturbed trajectories. The differences between estimated trajectory in Figure 5.22 and model trajectory in Figure 5.23 are caused by the observer gain for the output histories to follows exact track (deadbeat). Identified model are shown in Table 5.1. There are two stable oscillatory modes and two real stable modes in the motion. Detail description are in Section 5.4.

Table 5.1 Eigenvalues of Identified Longitudinal Model

$$\lambda_{1,2} = -0.0757 \pm 3.0689\jmath \;, \quad \zeta = 0.0247 \;, \quad \omega_n = 3.0698$$

$$\lambda_{3,4} = -0.1025 \pm 0.9130\jmath \;, \quad \zeta = 0.1116 \;, \quad \omega_n = 0.9188$$

$$\lambda_5 = -0.1062$$

$$\lambda_6 = -0.0002$$

5.3.1.2 Lateral/Directional Model

Following the same process as the longitudinal model identification, a set of synchronized time histories with lateral/directional inputs was applied to the OKID routine. The estimated time histories with observer gain in Figure 5.24 shows that the identified model with observer gain can describe the flight data well. Also the singular
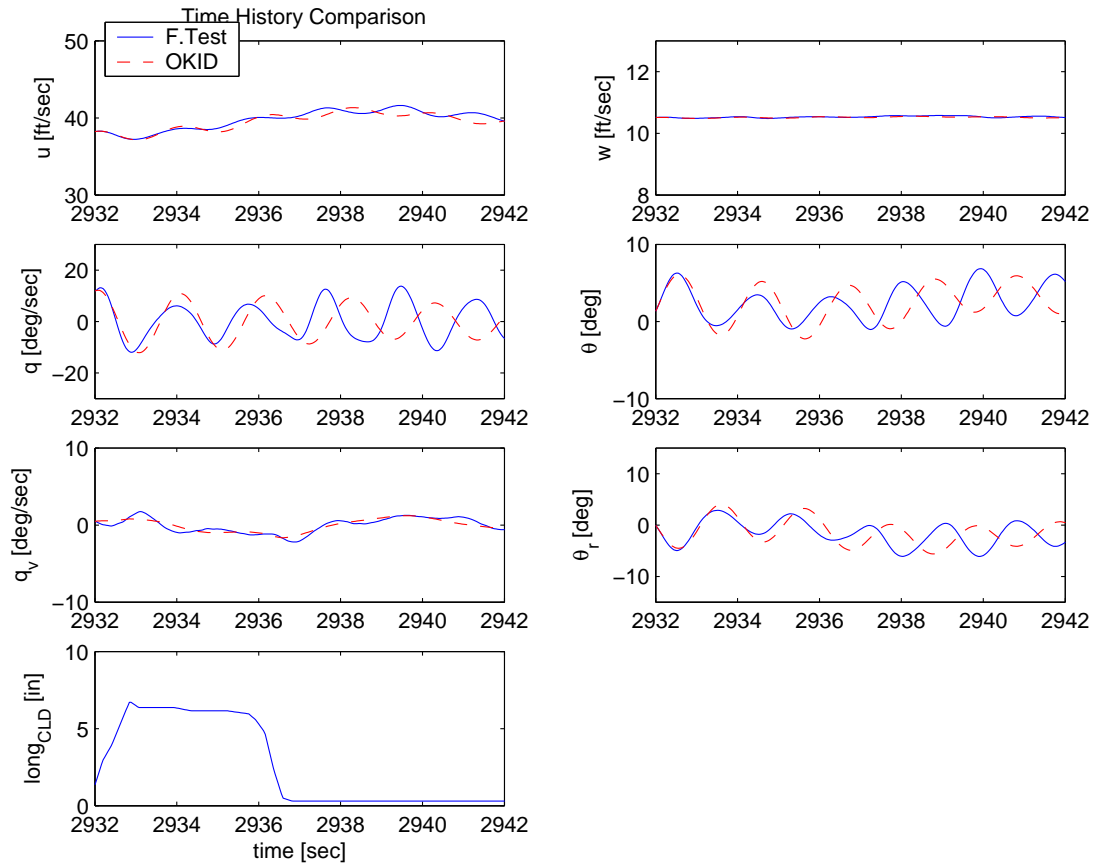
Figure 5.23 Comparison of OKID Identified Longitudinal Model Trajectory and Flight Data from Run 117

value ratio was 100% here. Variable names in the figure represents the same states as in Figure 5.25 with the same order. In Figure 5.25, the identified linear model by OKID shows trajectories for the same input of flight data. One can see the disturbance effect in Figure 5.25. Identified model properties from OKID are shown in Table 5.2. There are two stable oscillatory modes and two real stable modes in the motion. Modal analysis results are describe in Section 5.4.

Table 5.2 Eigenvalues of Identified Lateral/Directional Model

$$\lambda_{1,2} = -0.1010 \pm 2.8619\jmath \,, \quad \zeta = 0.0353 \,, \quad \omega_n = 2.8636$$

$$\lambda_{3,4} = -0.3661 \pm 0.3627\jmath \,, \quad \zeta = 0.7104 \,, \quad \omega_n = 0.5153$$

$$\lambda_5 = -0.0765$$

$$\lambda_6 = -0.0019$$

5.3.2   Time History Comparison

To verify the identified linear model, the trajectories from several flight runs at similar flight conditions are compared to the linear model trajectory with the same flight test inputs. But since the flight trajectories do not start from the stabilized initial values because of disturbances and they are unknown, the comparison of the linear simulation histories of the identified model with unknown initial values is less meaningful. In the following there are several figures for trajectory comparison as reference test cases.

5.3.2.1   Longitudinal Motion

Figure 5.26 and Figure 5.27 are constructed with the assumption that the initial conditions of both Run 118 and Run 119 are the same as those of Run 117 since they were recorded during the same flight, B43. Figure 5.26 shows that there are mismatches in the trajectories due to apparent data shifting while the frequencies
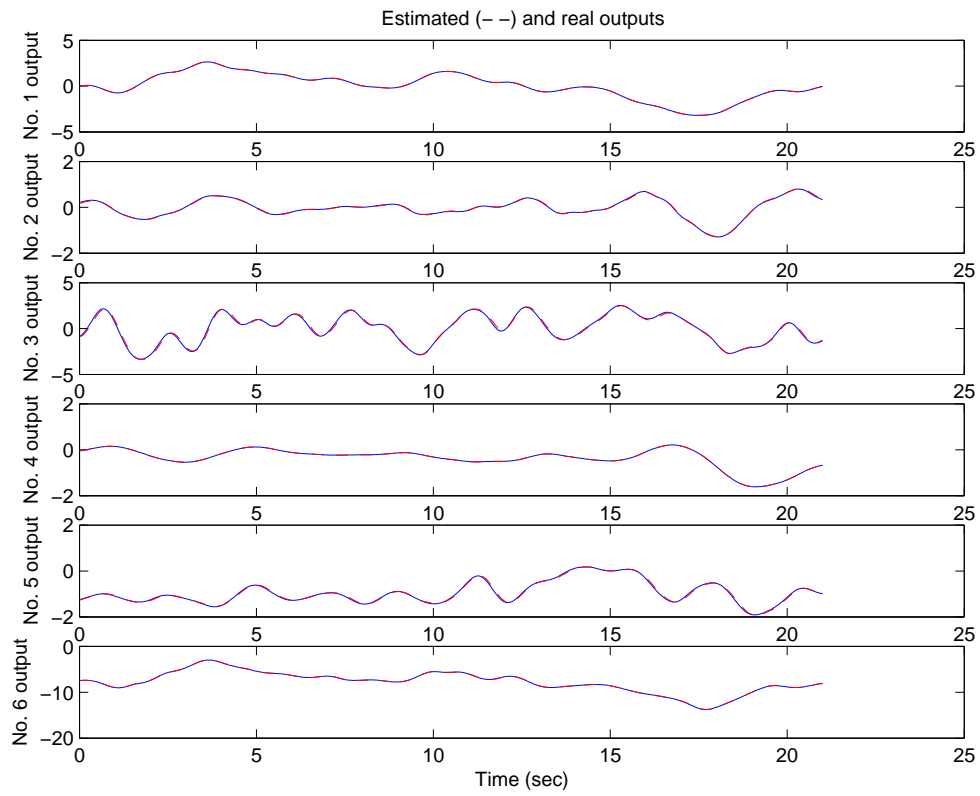
Figure 5.24 Estimated Trajectory by OKID with Observer Gain G
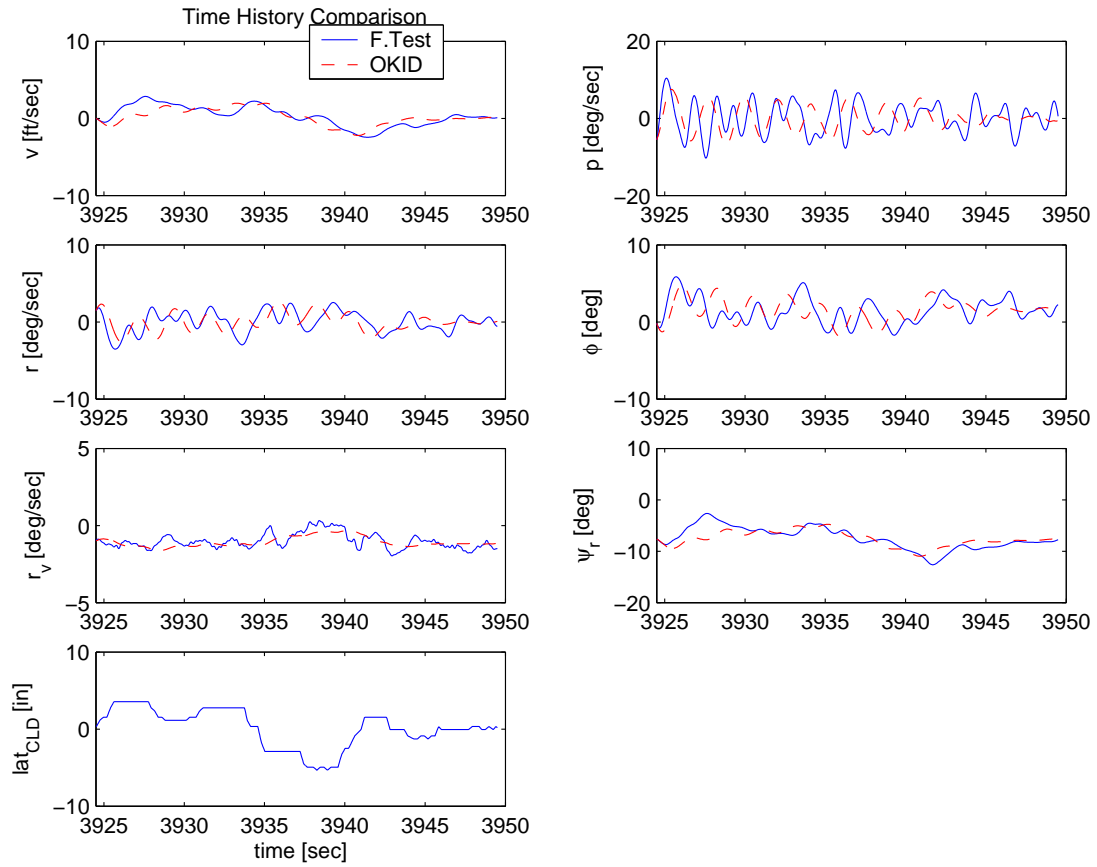
Figure 5.25 Comparison of OKID Identified Lateral/Directional Model Trajectory and Flight Run 220

appear to be very close and the magnitudes from OKID are amplified. Figure 5.27 also shows that the frequencies of the identified model are close to those of the flight data, but in this case the OKID amplitudes are attenuated instead of amplified as they were in Figure 5.27. The responses from flight data are getting bigger after control input ends. It shows the responses are affected by atmospheric disturbance and the order of magnitude is as big as that due to input command. During input commands, the linear model responses seem to be shifted with similar frequencies from flight data. It can be caused by initial condition difference.
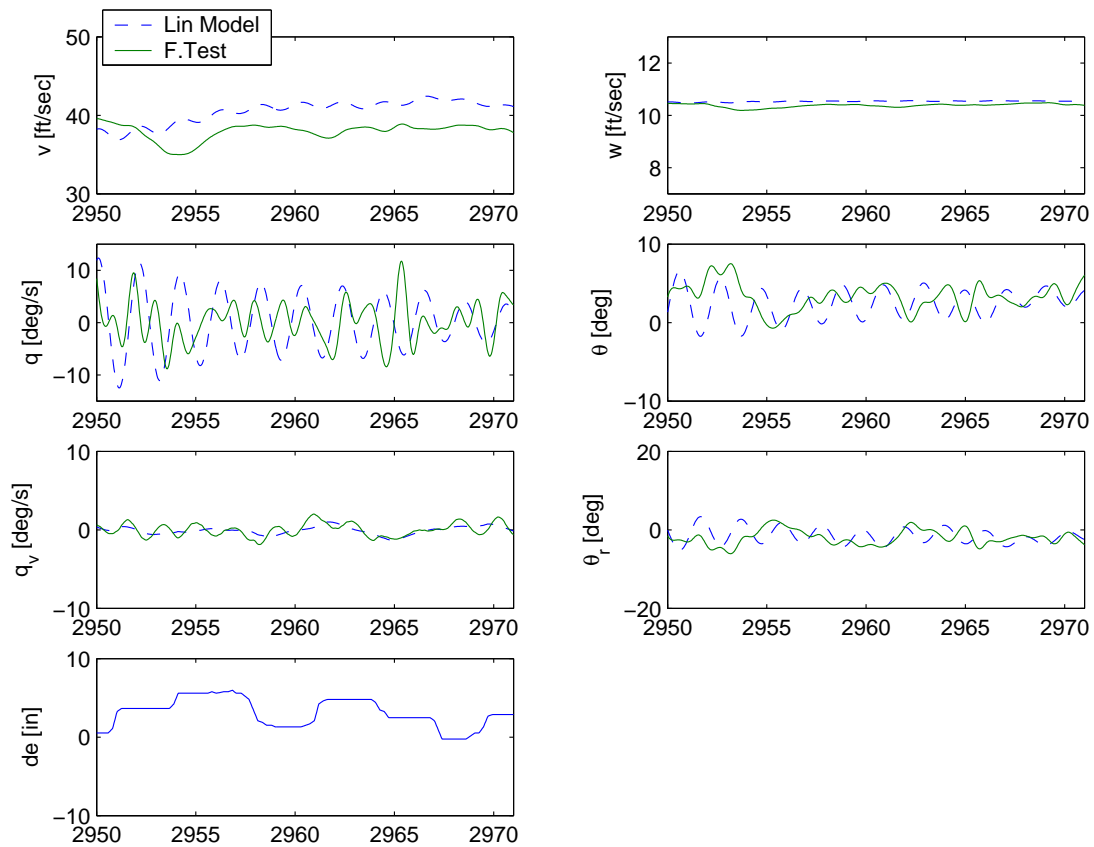
Figure 5.26 Comparison of Identified Model Trajectory and Flight Run 118 for Longitudinal Motion
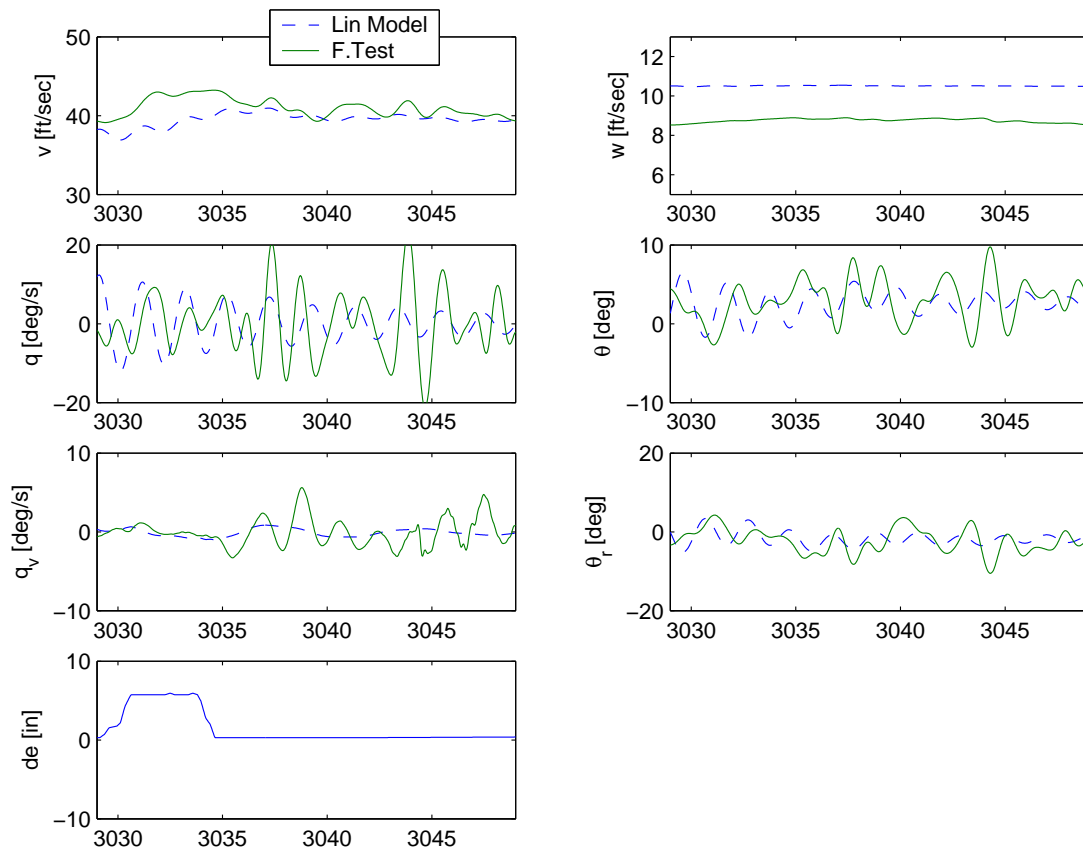
Figure 5.27 Comparison of Identified Model Trajectory and Flight Run 119 for Longitudinal Motion

5.3.2.2   Lateral/Directional Motion

For the lateral/directional motion, the identified model from flight B43, Run 220 was used for trajectory comparison in an attempt to minimize unknown initial condition difference. Run 221, 222 of the same flight were chosen for comparison. The same input used in the flight was used for the linear model, and then the trajectories are compared as in Figures 5.28, 5.29. Similar to the longitudinal cases, the trajectories from input commands show some phase shift with similar frequencies.
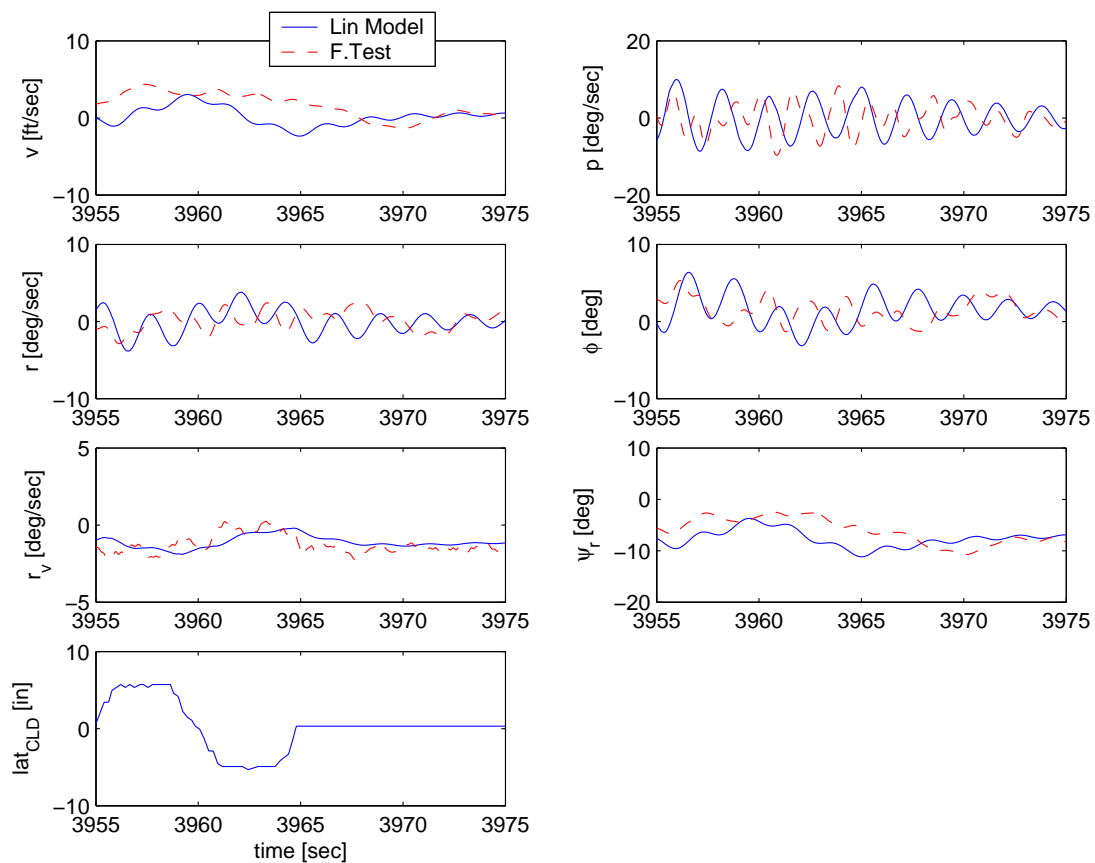
Figure 5.28 Comparison of Identified Model Trajectory and Flight Run 221 for Lateral/Directional Motion
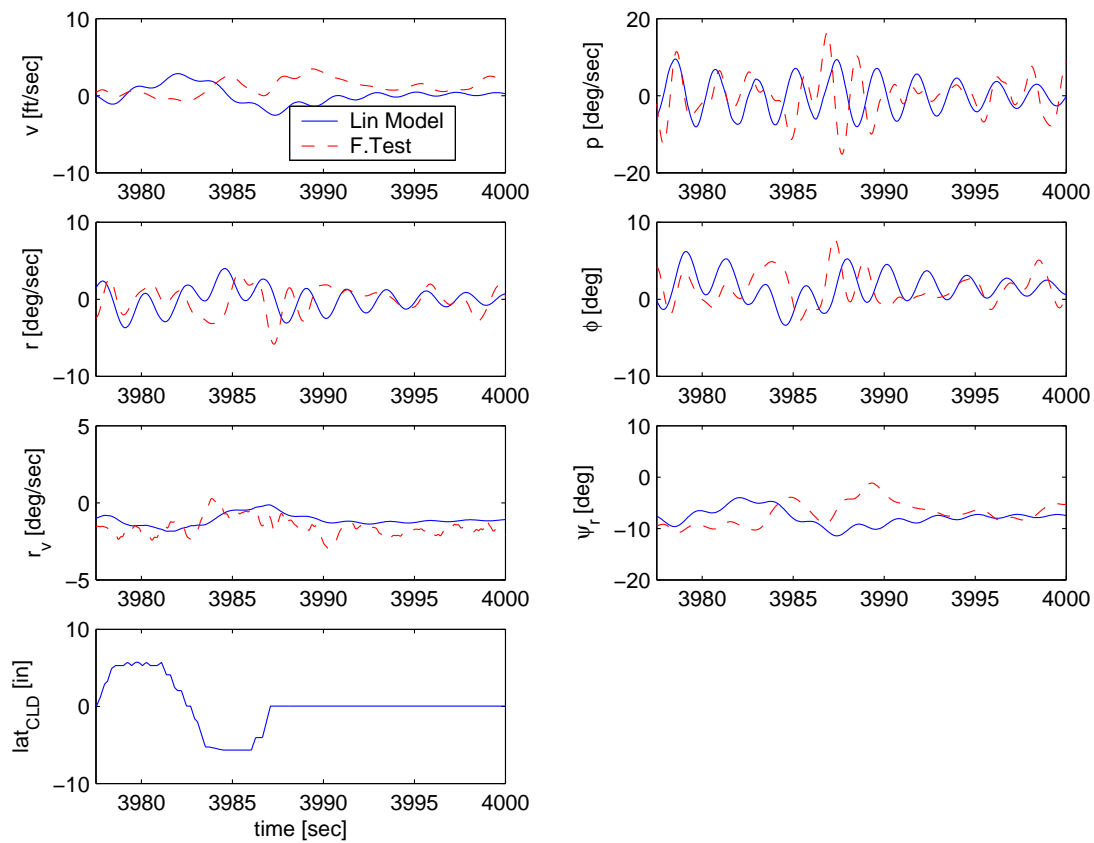
Figure 5.29 Comparison of Identified Model Trajectory and Flight Run 222 for Lateral/Directional Motion

5.4   Modal Analysis of Identified Model

To compare the identified model with the analytical model, modal analysis was conducted for the identified linear model. Comparing the modal properties, dynamic characteristics of the analytical model in Chapter II can be verified.

5.4.1   Longitudinal

After examining several OKID models, the identified model from Run 117 is picked as a nominal system because it's trajectories are matched better with flight data. As the trajectories are disturbed by disturbances the "match" means there were lesser disturbance at the test. As there are few flight data available not disturbed much, the choice was limited to runs of B43. As shown in Figures 5.15 to 5.20, B43 flight shows responses with less atmospheric disturbance. Clean flight data could give good identification results and the trajectories would be well matched for the case. The model for better match (assuming clearer, calmer flight data) was chosen as a nominal model. The identified continuous longitudinal system matrices from flight Run117 are shown in the following:

$$\mathbf{x} = [\Delta u, \Delta w, \Delta q, \Delta \theta, \Delta q_V, \Delta \theta_r], \qquad \mathbf{u} = [\delta e]$$

$$\mathbf{A} = \begin{bmatrix} -0.1227 & -3.1390 & -0.2884 & -0.1804 & 0.1068 & -0.0012 \\ 2.9784 & -0.0271 & 0.1017 & 0.1021 & 0.0276 & -0.0000 \\ 0.1835 & -0.1683 & -0.0224 & -0.3488 & 0.6493 & -0.0011 \\ 0.2113 & -0.1072 & 0.3610 & 0.0044 & 0.6268 & 0.0000 \\ 0.2862 & 0.1818 & -0.4831 & -0.6524 & -0.2922 & 0.0008 \\ -0.2091 & -0.2312 & -0.0928 & 0.0734 & 0.4246 & -0.0029 \end{bmatrix} \quad (5.1)$$

control distribution matrix

$$
\mathbf{B} = \begin{bmatrix} 2.5137 \\ 1.4498 \\ 1.0675 \\ -0.2192 \\ -3.8425 \\ 2.5134 \end{bmatrix} \tag{5.2}
$$

and output matrix

$$
\mathbf{C} = \begin{bmatrix} -0.0313 & -0.0090 & 0.0437 & -0.0226 & -0.0111 & 0.0000 \\ -0.0010 & -0.0003 & 0.0009 & -0.0003 & -0.0003 & -0.0001 \\ -0.4997 & -0.1278 & -0.0139 & -0.0056 & 0.0055 & -0.0000 \\ 0.0411 & -0.1642 & -0.0077 & 0.0059 & -0.0248 & 0.0000 \\ -0.0028 & 0.0042 & 0.0242 & 0.0413 & -0.0040 & -0.0000 \\ -0.0438 & 0.1688 & -0.0151 & -0.0013 & -0.0226 & -0.0000 \end{bmatrix} \tag{5.3}
$$

and carry through matrix

$$
\mathbf{D} = \begin{bmatrix} -0.0001 \\ 0.0021 \\ -0.0477 \\ -0.0033 \\ 0.1530 \\ 0.0018 \end{bmatrix} \tag{5.4}
$$

The eigenvalues of this system in Table 5.1 shows that it is stable, as there are two oscillatory and two real stable modes. From the output equation and similarity transformation, $\mathbf{x} = M\boldsymbol{\xi}$, between state space and modal space, the real modal

$\mathbf{A}, \mathbf{B}, \mathbf{C}$ matrices are determined to be

$$\mathbf{A}_{mreal} = \begin{bmatrix} -0.0757 & 3.0689 & 0 & 0 & 0 & 0 \\ -3.0689 & -0.0757 & 0 & 0 & 0 & 0 \\ 0 & 0 & -0.1025 & 0.9130 & 0 & 0 \\ 0 & 0 & -0.9130 & -0.1025 & 0 & 0 \\ 0 & 0 & 0 & & -0.1062 & 0 \\ 0 & 0 & 0 & 0 & 0 & -0.0002 \end{bmatrix} \tag{5.5}$$

$$\mathbf{B}_{mreal} = \begin{bmatrix} 3.3064 \\ -2.5216 \\ -4.8758 \\ 0.9982 \\ 6.4485 \\ -3.4137 \end{bmatrix} \tag{5.6}$$

$$\mathbf{C}_{mreal} = \begin{bmatrix} -0.0208 & 0.0063 & 0.0043 & -0.0158 & 0.0190 & -0.0005 \\ -0.0006 & 0.0002 & 0.0000 & -0.0004 & 0.0003 & -0.0001 \\ -0.3546 & 0.0890 & 0.0116 & -0.0218 & -0.0002 & 0.0000 \\ 0.0319 & 0.1152 & -0.0251 & -0.0099 & 0.0036 & -0.0000 \\ -0.0010 & -0.0056 & -0.0104 & -0.0303 & 0.0000 & 0.0000 \\ -0.0336 & -0.1148 & -0.0076 & 0.0205 & -0.0047 & 0.0000 \end{bmatrix} \tag{5.7}$$

The $\mathbf{A}_{mreal}$ matrix provides the eigenvalues, number of modes and order of modes. There are two stable oscillatory modes and two stable real modes. With the $\mathbf{B}_{mreal}$ matrix, one can tell that all modes are controllable by the symmetrical flap input, δ_e and the input is effective almost evenly for all modes. From the $\mathbf{C}_{mreal}$, forward speed is observed strongly in the first oscillatory mode and third stable mode, vertical

speed is observable mainly in the first, second oscillatory mode and somewhat in the third real mode. Pitch rate of the parafoil is observable in the first stable oscillatory mode and the pitch rate of the vehicle is observed in the second oscillatory mode and lesser in the first oscillatory mode. Pitch angle is observed mainly in the first oscillatory mode and some in the second oscillatory mode. The relative pitch angle can be observed mainly in the first oscillatory mode and one fifth lesser in the second oscillatory mode.

The inverse modal matrix is presented below showing the relationships between modes and states.

$$
\begin{Bmatrix} \xi_1 \\ \xi_2 \\ \xi_3 \\ \xi_4 \\ \xi_5 \\ \xi_6 \end{Bmatrix} = \begin{bmatrix} 0.9988 & -0.0096 & 0.0506 & 0.0345 & 0.0489 & -0.0001 \\ -0.0142 & -0.9938 & -0.0942 & -0.0722 & 0.0476 & -0.0004 \\ 0.0156 & -0.0665 & 0.2195 & -0.2872 & 0.8442 & -0.0005 \\ 0.0219 & 0.0888 & -0.4805 & -0.6351 & -0.1883 & 0.0003 \\ -0.0734 & 0.1398 & 1.4392 & -1.8062 & -1.0310 & 0.0233 \\ 0.0225 & -0.0305 & -1.6439 & 1.4992 & 0.9883 & 0.9769 \end{bmatrix} \begin{Bmatrix} u \\ w \\ q \\ \theta \\ q_V \\ \theta_r \end{Bmatrix}
$$

By examination:

- the first stable oscillatory mode is composed mainly of forward and vertical speed of the parafoil and one tenth lesser of pitch rate of the parafoil.

- the second stable oscillatory mode is composed of primarily vehicle's pitch rate and lesser parafoil pitch rate and pitch angle.

- the third stable mode is composed of primarily vehicle pitch rate and pitch attitude and lesser vehicle's pitch rate.

- the fourth stable mode is composed of primarily states of the parafoil pitch rate and angle and lesser of vehicle's pitch rate and angle.

Even though most of the flight data is corrupted by disturbances, several favorable runs are applied to the OKID routine. Although OKID performs well for system

identification under periodic disturbance, it can not produce accurate models if there are discrete disturbances like gusts common in the real world. In that case, the OKID model trajectories will not matched well with flight data, and it's eigenvalues will not show close match either. As in Figure 5.30, the analytical model has very stable mode compared to the identified eigenvalues. In that case the longitudinal motion damps out quickly as can be seen in Figure 4.6. The rest of the flight modes are similar to identified ones from flight data. In Figure 5.30 eigenvalues identified from flight
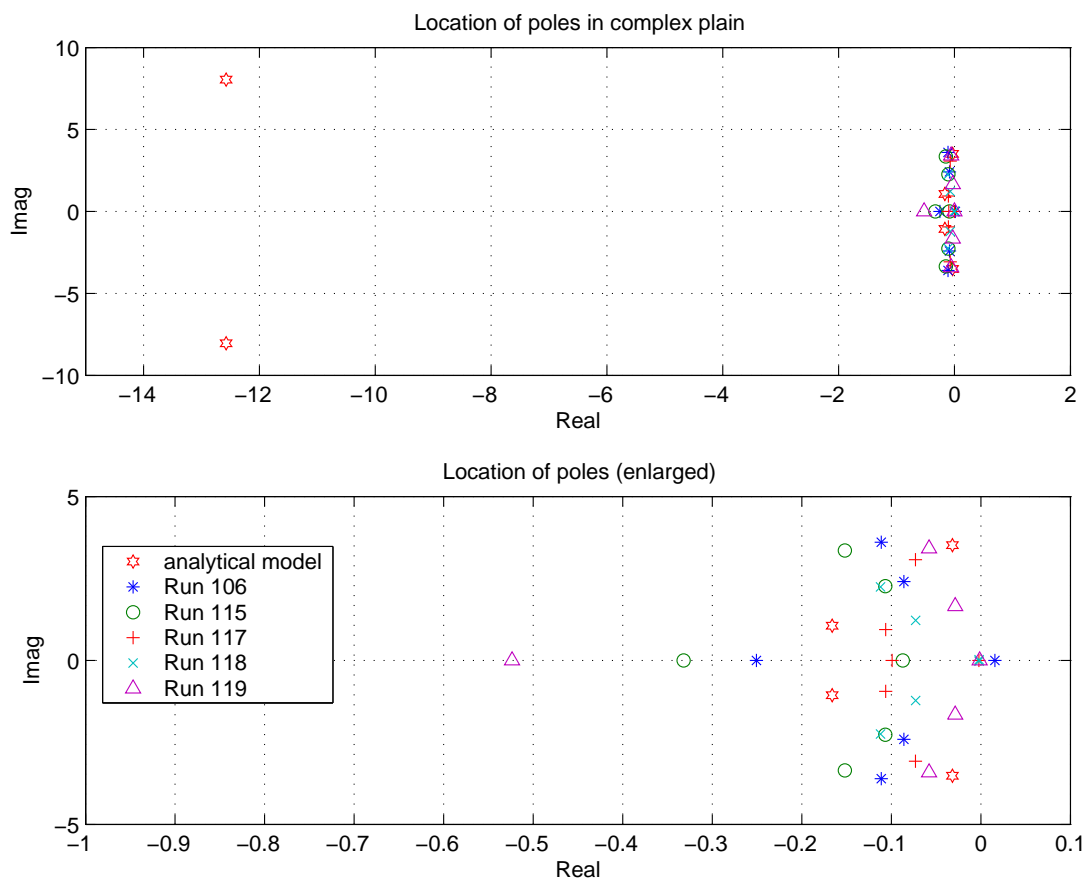
Figure 5.30 Comparison of Longitudinal Eigenvalues from OKID Model and Analytical Model

data are seen to be consistent and agree with flight observation. The number of flight modes and order of modes agree with those from the analytical model except that one

pair of conjugate poles are divided into two real poles. The dynamic characteristics from the analytical model seem to represent the actual motions of the Buckeye system except for the fast stable oscillatory mode. The nonlinear aerodynamic database used for the analytical model has been constructed and amended mainly by using flight test data of a large (around more than ten times larger) parafoil which was used for a scaled X-38 flight test. The large parafoil does not seem to correctly represent the aerodynamic characteristics of the small parafoil of the Buckeye.

Generally speaking, based on the flight data the identified parafoil-vehicle system is longitudinally stable. Comparing to the general dynamics of airplanes, the first oscillatory mode is similar to the phugoid mode related to forward and vertical speed and the second is similar to the short period mode related to pitch rate and pitch angle. The third and fourth real modes are mainly related to pitch responses between the parafoil and the hanging vehicle, and they are additional modes due to the hanging vehicle which are not in general aircraft dynamics.

5.4.2   Lateral/Directional

Flight Run 220 was chosen as a nominal identified model from several runs applied to OKID. It's trajectories are in Figure 5.25. Identified system matrices are as follows:

$$\mathbf{x} = [\Delta v, \Delta p, \Delta r, \Delta \phi, \Delta r_V, \Delta \psi_r], \qquad \mathbf{u} = [\delta r]$$

$$\mathbf{A} = \begin{bmatrix} -0.1698 & -2.787 & 0.0181 & 0.0077 & 0.0038 & -0.00018 \\ 2.936 & -0.0293 & 0.0094 & -0.00074 & -0.0034 & -0.00019 \\ -0.3517 & 0.1293 & -0.1592 & 0.0353 & 0.0789 & -0.0011 \\ -0.5165 & 0.2281 & -0.5404 & -0.3797 & 0.0558 & 0.01997 \\ -0.43 & 0.1762 & -0.4807 & -0.7036 & -0.2521 & 0.01937 \\ -0.251 & 0.1399 & -0.2818 & -0.3757 & -0.3994 & -0.0226 \end{bmatrix} \qquad (5.8)$$

control distribution matrix

$$\mathbf{B} = \begin{bmatrix} 2.9155 \\ -1.2649 \\ 2.8469 \\ 4.3784 \\ 3.6272 \\ 2.2233 \end{bmatrix} \tag{5.9}$$

output matrix

$$\mathbf{C} = \begin{bmatrix} -0.0711 & -0.0154 & 0.0626 & 0.0050 & -0.0074 & 0.0016 \\ 1.0912 & 0.2609 & -0.0050 & -0.0117 & -0.0049 & 0.0003 \\ 0.0799 & -0.2934 & 0.0156 & -0.0072 & -0.0097 & 0.0002 \\ -0.0977 & 0.3687 & -0.0186 & 0.0090 & 0.0088 & 0.0004 \\ 0.0097 & -0.0149 & -0.0073 & -0.0181 & 0.0037 & 0.0012 \\ -0.1093 & -0.0292 & 0.0944 & -0.0104 & -0.0077 & -0.0005 \end{bmatrix} \tag{5.10}$$

and carry through matrix

$$\mathbf{D} = \begin{bmatrix} -0.0032 \\ -0.7238 \\ 0.0104 \\ -0.0151 \\ 0.0427 \\ -0.0079 \end{bmatrix} \tag{5.11}$$

Following the same procedure of the similarity transformation for the longitudinal modal analysis, the real modal $\mathbf{A}, \mathbf{B}, \mathbf{C}$ matrices for lateral/directional motion are

determined to be

$$\mathbf{A}_{mreal} = \begin{bmatrix} -0.1010 & 2.8619 & 0 & 0 & 0 & 0 \\ 2.8619 & -0.1010 & 0 & 0 & 0 & 0 \\ 0 & 0 & -0.3661 & 0.3627 & 0 & 0 \\ 0 & 0 & 0.3627 & -0.3661 & 0 & 0 \\ 0 & 0 & 0 & 0 & -0.0765 & 0 \\ 0 & 0 & 0 & 0 & 0 & -0.0019 \end{bmatrix} \tag{5.12}$$

$$\mathbf{B}_{mreal} = \begin{bmatrix} -1.8652 \\ 4.2465 \\ -4.8988 \\ -18.8278 \\ 9.8825 \\ -4.0700 \end{bmatrix} \tag{5.13}$$

$$\mathbf{C}_{mreal} = \begin{bmatrix} -0.0150 & -0.0503 & -0.0110 & -0.0035 & 0.0057 & 0.0003 \\ 0.1660 & 0.7449 & -0.0013 & 0.0049 & 0.0000 & -0.0000 \\ -0.2063 & 0.0554 & -0.0081 & 0.0044 & 0.0006 & 0.0000 \\ 0.2593 & -0.0676 & 0.0084 & -0.0047 & -0.0005 & 0.0010 \\ -0.0083 & 0.0079 & 0.0028 & 0.0051 & 0.0022 & -0.0007 \\ -0.0250 & -0.0759 & -0.0176 & -0.0006 & 0.0074 & -0.0046 \end{bmatrix} \tag{5.14}$$

Examining the $\mathbf{A}_{mreal}$ matrix, there are two stable oscillatory modes and two stable real modes. The eigenvalues can be seen in the $\mathbf{A}_{mreal}$ matrix. The $\mathbf{B}_{mreal}$ matrix shows that all modes are controllable by the asymmetrical flap input, δ_r, and the input is mainly effective for the second oscillatory mode and to less extent for the third real mode. From the $\mathbf{C}_{mreal}$, side speed or sideslip angle is observed mainly in the first oscillatory mode. Roll rate, yaw rate and bank angle are mainly observable in the

first oscillatory mode. Yaw rate of the vehicle and relative yaw angle are observable over all modes but primarily in the first oscillatory mode. Note that the parafoil's variables are hardly observable in real modes and two variables, relative yaw angle and vehicle's yaw rate which are related to the vehicle are hardly observable in the two real modes as well as in oscillatory modes.

The inverse modal matrix for lateral/directional motion is presented below showing the relationships between modes and states.

$$
\begin{Bmatrix} \xi_1 \\ \xi_2 \\ \xi_3 \\ \xi_4 \\ \xi_5 \\ \xi_6 \end{Bmatrix} = \begin{bmatrix} -0.0009 & 0.9985 & -0.0067 & -0.0031 & -0.0016 & 0.0001 \\ 1.0000 & 0.0246 & 0.0041 & 0.0003 & -0.0013 & -0.0001 \\ -0.0153 & -0.1837 & -1.7423 & -0.2823 & 0.7340 & 0.0363 \\ -0.1400 & -0.2248 & -0.7389 & -0.7580 & -0.1077 & 0.0297 \\ 0.1598 & 0.4225 & 4.5675 & -1.4752 & 0.6478 & 0.4091 \\ -0.0449 & -0.1868 & -2.8251 & 1.7574 & -1.3820 & 0.5547 \end{bmatrix} \begin{Bmatrix} v \\ p \\ r \\ \phi \\ r_V \\ \psi_r \end{Bmatrix}
$$

By examination of the inverse modal matrix:

- the first oscillatory stable mode is composed of primarily roll rate and side speed, and one hundredth times lesser yaw rate. It is composed almost entirely of the parafoil states.

- the second stable mode is composed of states of the parafoil and the vehicle, primarily yaw rate and lesser bank angle of the parafoil and vehicle's yaw rate to the same extent of the bank angle. It is a combined mode for the parafoil and the vehicle.

- the third stable mode is composed of primarily yaw rate and side speed, bank angle with one third the amount of yaw rate.

- the fourth stable mode is composed of mainly yaw rate, lesser bank angle and vehicle's yaw rate of about half of yaw rate.

Even though most of the flight data is corrupted by disturbances, several favorable runs performed at relatively calm condition were applied to the OKID routine.

The identified eigenvalues are compared to those of the analytical model in Figure
5.31. Note that the analytical model has a very stable mode compared to the identi-
fied eigenvalues. As in the longitudinal motion, the lateral/directional motion damps
out quickly as can be seen in Figure 4.7. The rest of the flight modes are similar
to ones identified from flight data. In Figure 5.31 eigenvalues identified from flight
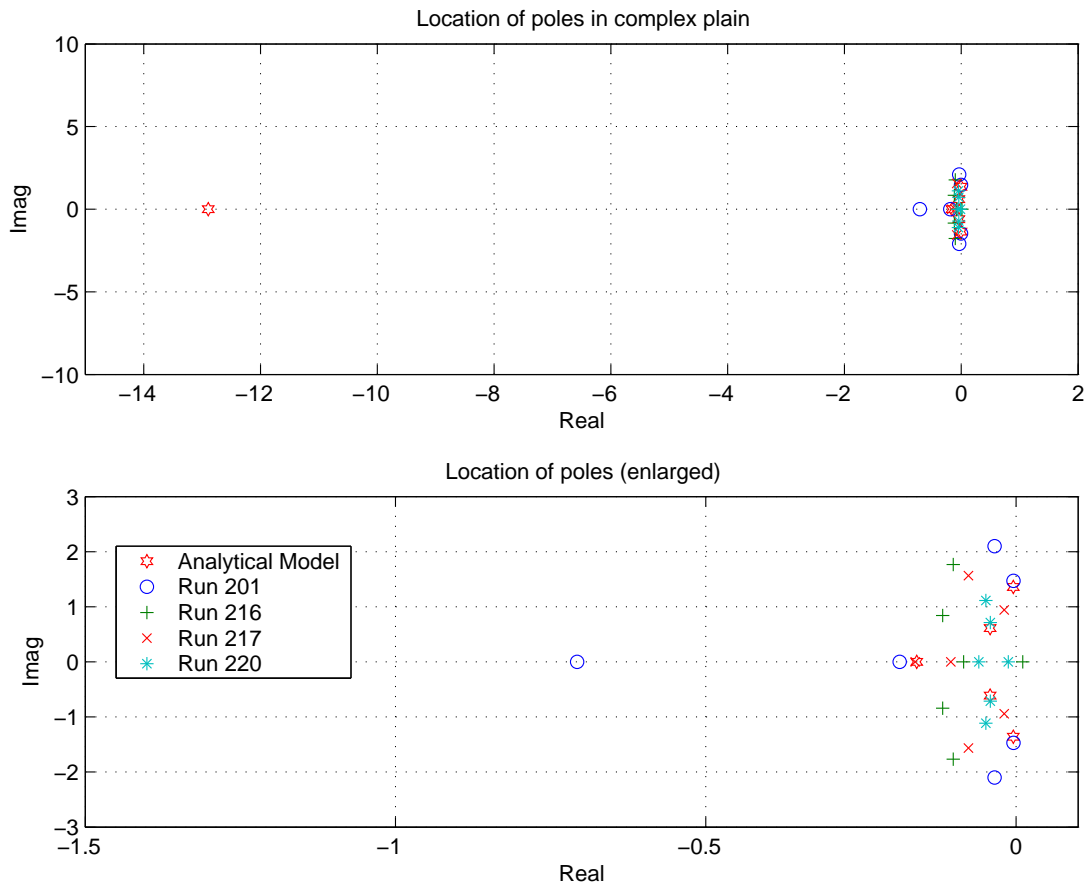
Figure 5.31 Comparison of Lateral/Directional Eigenvalues from OKID Model and
Analytical Model

data are consistent over several runs. The number of flight modes and the order of
modes agree with those from the analytical model. The dynamic characteristics of
the analytical model seem to represent the actual motions of the Buckeye system,

except fast stable mode just like in the longitudinal motion. As mentioned earlier the nonlinear database seems to not correctly represent aerodynamic characteristics of the small parafoil of the Buckeye.

In summary, the identified parafoil-vehicle system is lateral/directionally stable also. The flight modes exhibited by the identified model show some different modes from the general motion of airplanes. The two real stable modes are strongly related to yaw rate, which is different from the roll and spiral modes in typical airplane dynamics. Other than longitudinal motion, the hanging vehicle's states are related to every mode. That means that the vehicle motion is closely coupled to the parafoil motion in lateral/directionally, since the joint between the parafoil and the vehicle is not modelled as universal joint such as it is for the longitudinal motion analysis.

5.5   Comparison of Trajectories between Analytical and Identified Model

As can be seen in Figure 5.30 and 5.31, the identified model has different pole locations for both axes. Observing the figures one can tell that the frequencies are similar but the damping terms are different than the analytical model's, even though the number of modes are the same and stable. Simulation trajectories from the nonlinear analytical model are compared with those from linear simulation with the identified model in Figures 5.32, 5.33, and 5.34. To verify the analytical model, the PDS simulation trajectories using the same aero database as the analytical model are plotted in the same figures for comparison. In the figures legend "TAMU" is the nonlinear simulation code programmed from the 8-DOF analytical model.

Assuming that the trajectory from flight data contains extra nonlinear dynamic effects not included in the analytical model, the trajectory can not be tracked exactly by the analytical model. For pitch rate responses in Figure 5.32, while the identified model shows oscillation with fast frequency, the analytical model responses show combined phugoid and short period modes, with speed and pitch angle changes at relatively slow frequency. The difference is suspected to come from unmodelled dynamics such as flexibility and elasticity of the parafoil, risers and suspension strings.
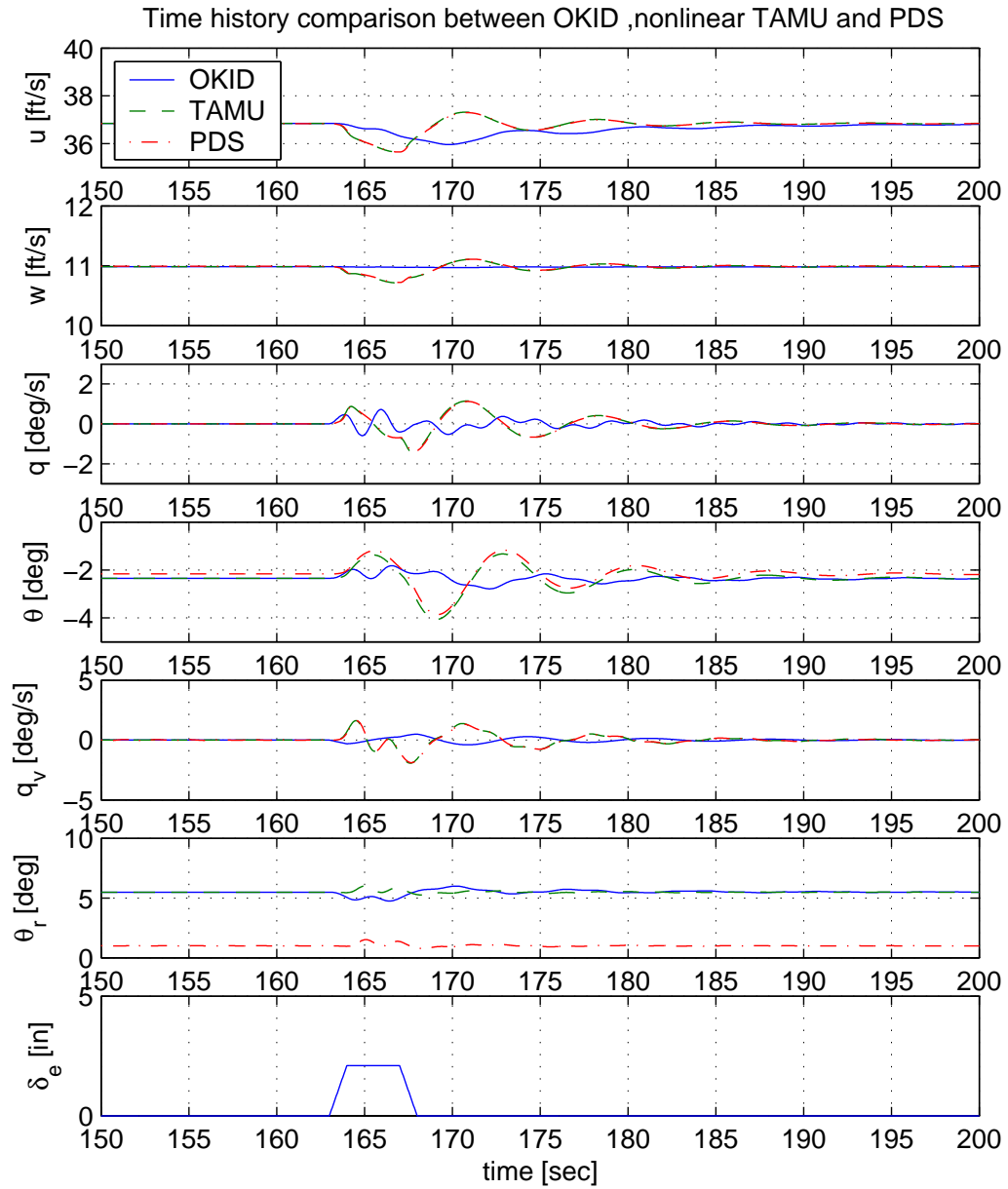
Figure 5.32 Comparison of Trajectories from OKID Model, Nonlinear Analytical Model and NASA's PDS - Longitudinal
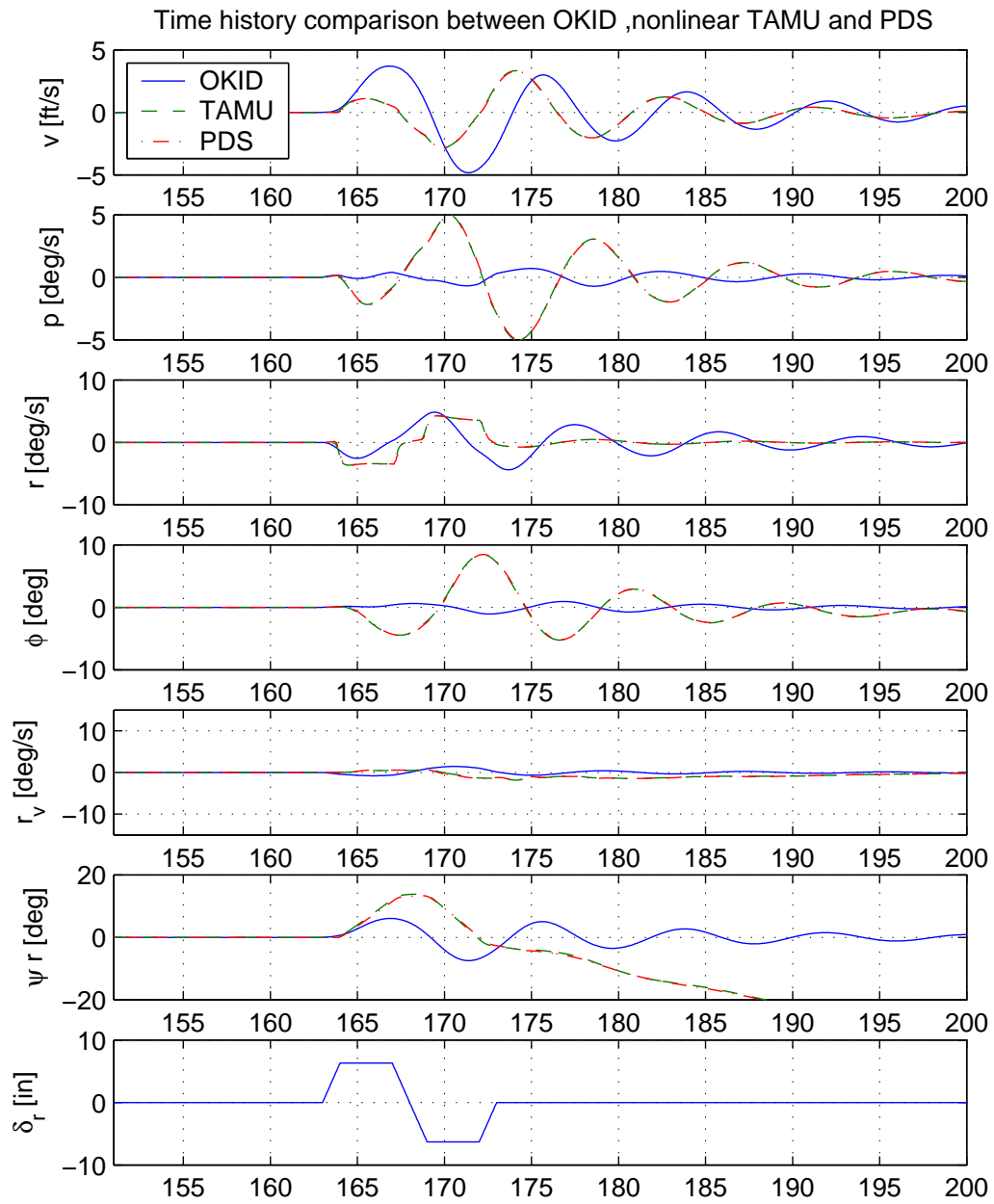
Figure 5.33 Comparison of Trajectories from OKID Model, Nonlinear Analytical Model and NASA's PDS without Torque Model - Lateral/Directional
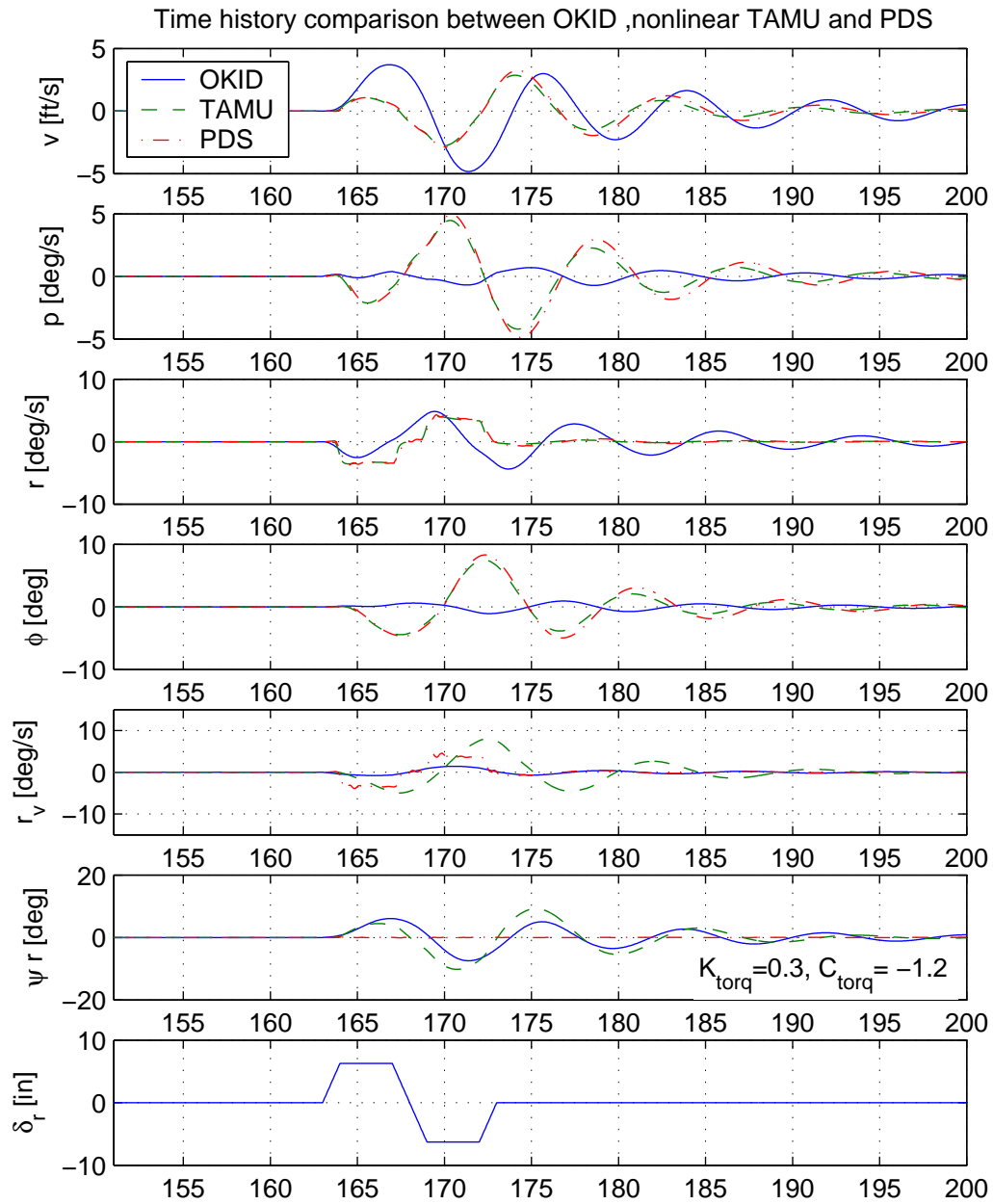
Figure 5.34 Comparison of Trajectories from OKID Model, Nonlinear Analytical Model and NASA's PDS with Torque Model - Lateral/Directional

Note that the vehicle attitudes are tracked better. Using the same aerodynamic database and geometry PDS and "TAMU" trajectories are identical except minor trimmed value difference.

For lateral/directional trajectories in Figure 5.33, sideslip and yaw rates match better than other states with some phase shift, while roll rate and bank angle changes are much less than the analytical model's. Note that the vehicle's relative yaw angles are not limited in the analytical model without the joint torque model. The joint torque model is adjusted to accommodate the flight responses of the vehicle from basic model in Eqn. (2.50), as Eqn. (5.15). The joint torque model is composed of spring effect proportional to relative yaw angle and damping term proportional to relative yaw rate. With trial and error, the model coefficients are chosen as $K_{torq} = 0.3$, $C_{torq} = -1.2$ to match the relative yaw angle trajectory as in Figure 5.34. The joint torque model in PDS doesn't work for the Buckeye parafoil-vehicle motion (Fig. 5.34).

$$
\begin{aligned}
\mathbf{T}_{cons} = \Big\{ & K_{torq} \left[0.5B\ F_{cons} \sin\left(2B\ q_9/H\right)(\rho_{x_V} s_8 - \rho_{z_V} c_8)/l_\rho \right] \\
& + C_{torq}\left(u_9 - u_3\right) \frac{b_V}{2\,V_\infty}\ q_{DYN}\ S_V\ b_V \Big\}\ \mathbf{k}_P
\end{aligned}
\tag{5.15}
$$

For both axes, identified model trajectories of relative vehicle motion are matched well to those of analytical model. In analytical modelling of the vehicle, there exists only drag as an aerodynamic term and gravitational force has major effect on it and it's good enough for modelling the vehicle.

5.6 Error Analysis

Doing experiments like flight test in practice result in unexpected errors which can effect the results. In this section some possible errors are summarized and their effects are discussed.

- Missing a degree-of-freedom in making an analytical model: One degree-of-freedom of relative roll motion between the parafoil and the vehicle was ignored

in the analytical model to simplify the dynamics. Based on the assumption on the rigidity of risers and suspension lines when they have tension in flight it is reasonable to remove the degree-of-freedom as the Buckeye vehicle is connected directly to the lines with the assumption that the parafoil is rigid wing. If there is a detail dynamic model of flexible curved shaped parafoil then the roll degree-of-freedom should be provided for relative roll motion in addition to degrees-of-freedom from the flexible parafoil dynamics.

- Sensor noise: Typically sensor noise has property of very high frequency. In this dissertation a low pass filter was used to remove them using power spectral density analysis not to reject possible high frequency dynamics of the system. To minimize the noise effect selection and maintenance of sensors during operations should be well controlled and noise property must be considered in designing the experiment.

- The vehicle not being trimmed exactly: Theoretically the inputs for identification excite dynamics from trimmed condition. But in practice it is very difficult to trim perfectly and even worse in UAV (Unmanned Aerial Vehicle). Possible deviation from the trimmed initial condition can cause transient response in addition to the response due to control input. It can cause the identification routine's performance and require more tests to get correct results. In the dissertation the time shifts between the response of identified model and flight test response can be seen because of the imperfect trimmed flight test and initial condition mismatch between test response and those from identified model response.

- Aero dataset used for nonlinear simulation: It would be very good to assure of identification results if there is a reference model to be compared with identified ones. In this dissertation a nonlinear model was used as a nominal reference model. It was generated by linearization of nonlinear aero database made for large parafoil ten times bigger than that of the Buckeye. From analysis it has typical pole locations different from several identified ones. As those of identified models coincide each other, the nominal linearized model was not considered to

represent the Buckeye's dynamics well. The aero database should be modified to be used for scale-downed parafoil dynamics simulation. Global performance variables such as gliding path, position, altitudes were well represented by simulation with the aero database though.

- Weather effect in flight testing: As the parafoil flight is actually gliding through air with same magnitude of wind speed, it is very vulnerable to wind gust, turbulence and disturbance. Because of adverse wind effect, some precious flight test results turned to useless for identification. As it can not be controlled by any means in the field, the flight date and time must be picked for calm day. The author considered this as the biggest issue to perform flight tests of low speed UAV.

CHAPTER VI

SUMMARY AND CONCLUSIONS

In this dissertation, an analytical and simulation study on the Buckeye parafoil-vehicle system and experimental research work for flight test are presented. They are summarized in the following.

An 8-DOF analytical model was developed for the Buckeye parafoil-vehicle two-body system. Using an empirical aerodynamic database constructed for X-38/CRV parafoil, nonlinear 8-DOF simulation can be done for given control inputs. A linear model was derived by linearization of the 8-DOF nonlinear model. It was used to investigate stability and control of the system. It describes the linear dynamics of the Buckeye parafoil-vehicle system well. For identification of the Buckeye parafoil-vehicle system, the Observer/Kalman Filter Identification (OKID) method was used. OKID, a time domain technique, identifies a discrete input-output mapping from known input-output data records. The formulation for identification under disturbance are developed and documented. To acquire parameters to be usable for identification, several data acquisition systems including 5-hole multifunction probe, Inertial Measurement Unit and accelerometer package on the parafoil were designed and installed on the Buckeye. They supplied all the parameters required for system identification with high sampling rates. For identification purpose a detail flight test procedure was planned and executed without any safety concern. All 7 sorties were completed under atmospheric disturbances and several sets of good data were applied to the OKID routine for identification.

Before giving conclusions evaluations for assumptions made in the flight test design are summarized:

- Parafoil is a rigid body: Globally yes, but OKID model shows some of unmodelled responses

- Vehicle starts perfectly trimmed condition: No,Very difficult

- No distortion effect from location of aeroprobe: Yes

- Parafoil sideslip angle calculated from speeds integrated from accelerations: effectively represent the sideslip angle

- Multi-rate sampling will be sufficient: yes

- IMU is located at C.G. of the vehicle as close as possible: yes, no extra dynamic effect on the vehicle motion

- Number of accelerometers on the parafoil are sufficient: yes, but the more the better if weight is OK

- 25 Hz of the parafoil sensor sampling rate is enough based on analytical model: yes, ID model shows slow responses

- 5 Hz of control input sampling rate is enough: yes, no dynamic effects

Based upon the analysis and results presented in this dissertation, the following conclusions are made:

- The OKID routine successfully identifies linear model under light and moderate disturbances, and the modal properties of the identified model show that dynamic modes and it's order are consistent for the test cases presented. By overparameterization the OKID routine can identify a linear model from disturbance-corrupted flight data successfully. This says that the OKID is suitable for identifying a linear model from flight data of parafoil-vehicle two-body system.

- The 8-DOF analytical model was verified by comparing the response with PDS's for the same inputs. This model seems to be valuable to describe the dynamics of the parafoil-vehicle with appropriate database. The large number of stable eigenvalues in both axes are considered to be coming from the X-38's big parafoil database used for analytical modelling. The database seems not represents the aerodynamics of the small parafoil correctly.

- The data acquisition subsystems have worked well to provide usable set of data for identification and proved they are sufficient for data acquisition for identification. Specially the accelerometer package for the parafoil was a suitable method for obtaining the parafoil parameters with minimum cost. If a weight increase is allowed for the parafoil, more sensors are preferable for better measurement averaging for the flexible parafoil.

CHAPTER VII

RECOMMENDATIONS

1. During the test we found that the unmanned aerial vehicle (UAV) Buckeye with 2 minimal control inputs can not be perfectly trimmed for identification test under disturbance. Under disturbance, even a longer trim settling time does not help to effectively stabilize the Buckeye for testing. To minimize the disturbance effect, careful selection of test dates and conditions are recommended.

2. The discrepancy between the analytical model and the identified is mainly due to the aerodynamic database used for the analytical model. For scaling down the database for the small parafoil of the Buckeye system, further investigations of sensitivity and a parametric study with more flight data is needed.

3. If time histories from the big parafoil are available for all of the parameters being identified, OKID can identify the linear model for the big parafoil from the time histories. In that case the aerodynamic database can be verified too. To increase the order of the parafoil dynamics to account for elastic effects, more accelerometers distributing strategically on the parafoil are needed. This could increase the weight of the parafoil, so it is most suitable for use on the big parafoil.

4. As mentioned above the dynamics of the parafoil have nonlinearities which can not be modelled precisely in the linear dynamic model. Applying nonlinear identification methods can be helpful to identify the dynamics of the parafoil including embedded nonlinearity.

5. Goodzeit and al. suggest that the disturbance effect can be discriminated from the identified overparameterization model by checking modal damping and the contribution factor.[16] The embedded disturbance effect can be identified from the input-output data and the disturbance response can be calculated and used

as a feedforward control signal to compensate it's effect. Once the feedforward controller is designed, it will be good for systems vulnerable to disturbances like parafoils.

6. Three independent data acquisition subsystems have caused an extra burden for preparing identification data sets. Synchronization, separate data reductions as well as casting a sampling frequency bottle-neck limited by the slowest frequency of a subsystem are issues. For better identification a unified and synchronized data acquisition system with high sampling rate will help.

REFERENCES

[1] Iacomini, C. and Madsen, C., "Investigation of Large Scale Parafoil Rigging Angles: Analytical and Drop Test Results," American Institude of Aeronautics and Astronautics, Inc., 1999, AIAA-99-1752.

[2] Smith, J. and Bennet, T., "Development of NASA X-38 Parafoil Landing System," AIAA, 1999, AIAA-99-1704.

[3] Iacomini, C. S. and Cerimele, C., "Longitudinal Aerodynamics From A Large Scale Parafoil Test Program," AIAA, 1999, AIAA-99-1732.

[4] Iacomini, C. S. and Cerimele, C., "Lateral-Directional Aerodynamics From A Large Scale Parafoil Test Program," AIAA, 1999, AIAA-99-1731.

[5] Jann, T., Doherr, K.-F., and Gockel, W., "Parafoil Test Vehicle ALEX - Further Development and flight Test Results," AIAA, 1999, AIAA-99-1751.

[6] Jann, T., "Aerodynamic Model Identification and GNC Design for the Parafoil-Load System ALEX," AIAA, 2001, AIAA-2001-2015.

[7] Strickert, G. and Jann, T., "Determination of the Relative Motion between Parafoil Canopy and Load Using Advanced Video Image Processing Techniques," AIAA, 1999, AIAA-99-1754.

[8] Strickert, G. and Witte, L., "Analysis of the Relative Motion in a Parafoil-Load System," AIAA, 2001, AIAA-2001-2013.

[9] Slegers, N. and Costello, M., "Comparison of Measured and Simulated Motion of a Controllable Parafoil and Payload System," AIAA, 2003, AIAA-2003-5611.

[10] Slegers, N. and Costello, M., "Model Predictive Control of a Parafoil and Payload System," AIAA, 2004, AIAA-2004-4822.

[11] Phan, M., Juang, J.-N., and Longman, R. W., "Identification of Linear Multivariable System by Identification of Observer with Assigned Real Eigenvalues," *The Journal of the Astronautical Sciences*, Vol. 40, No. 2, April-June 1992, pp. 261–279.

[12] Chen, C.-W., Huang, J.-K., Phan, M., and Juang, J.-N., "Integrated System Identification and State Estimation for Control of Flexible Space Structures," *Journal of Guidance, Control, and Dynamics*, Vol. 15, No. 1, 1992, pp. 88–95.

[13] Juang, J.-N., Phan, M., Horta, L. G., and Longman, R. W., "Identification of Observer/Kalman Filter Markov Parameters: Theory and Experiments," *Journal of Guidance, Control, and Dynamics*, Vol. 16, No. 2, March-April 1993, pp. 320–329.

[14] Juang, J.-N., *Applied System Identification*, PTR Prentice Hall, Englewood Cliffs, New Jersey, 1994.

[15] Valasek, J. and Chen, W., "Observer/Kalman Filter Identification for On-Line System Identification of Aircraft," *Journal of Guidance, Control, and Dynamics*, Vol. 26, No. 2, March-April 2003, pp. 347–353.

[16] Phan, M. Q. and Goodzeit, N. E., "System Identification in the presence of Completely Unknown Periodic Disturbances," *Journal of Guidance , Control, and Dynamics*, Vol. 23, No. 2, March-April 2000, pp. 251–259.

[17] Phan, M. Q. and Goodzeit, N. E., "System and Disturbance Indentification for Feedforward and Feedback COntrol Applications," *Journal of Guidance , Control, and Dynamics*, Vol. 23, No. 2, March-April 2000, pp. 260–268.

[18] Junkins, J. L., Ward, D. T., and Valasek, J., "Vision-Based Navigation and Adaptive Control of Nonlinear Dynamical System," Technical report, Department of Aerospace Engineering, Texas A&M University, 1998.

[19] Kane, T. R., "Formulation of Dynamical Equations of Motion," *American Journal of Physics*, Vol. 51, November 1983, pp. 974–977.

[20] Kane, T. R. and Levinson, D. A., "Multibody Dynamics," *Journal of Applied Mechanics*, Vol. 50, December 1983, pp. 1071–1078.

[21] Kane, T. R. and Levinson, D. A., *Dynamics: Theory and Applications*, McGraw-Hill, New York, 1985.

[22] Moon, F. C., *Applied Dynamics: With Applications to Multibody and Mechatronic Systems*, John Wiley & Sons, Inc., New York, 1998.

[23] Greenwood, D. T., *Classical Dynamics*, Dover Publications, Inc., Mineola, New York, 1977.

[24] Greenwood, D. T., *Principles of Dynamics*, 2nd ed., Prentice-Hall, Inc., Englewood Cliffs, New Jersey, 1988.

[25] Junkins, J. L. and Schaub, H., *Analytical Mechanics of Aerospace Systems*, American Institute of Aeronautics and Astronautics, Inc., Washington, DC, 2003.

[26] Kane, T. R. and Levinson, D. A., *Dynamics Online: Theory and Implementation with AUTOLEV^{TM}*, Online Dyamics, Inc., Sunnyvale, California, 2000.

[27] Kane, T. R. and Levinson, D. A., *AUTOLEV 4 User's Manual*, Online Dynamics, Inc., 2004.

[28] Roskam, J., *Airplane Flight Dynamics and Automatic Flight Control*, DARcorporation, Lawrence, Kansas, 1995.

[29] Etkin, B. and Reid, L. D., *Dynamics of Flight: Stability and Control,* 3rd ed., John Wiley & Sons, Inc., New York, 1996.

[30] McRuer, D., Ashkenas, I., and Graham, D., *Aircraft Dynamics and Automatic Control*, Princeton Univ. Press, Princeton, New Jersey, 1973.

[31] Chen, C.-T., *Linear System Theory and Design,* 3rd ed., Oxford University Press, Inc., New York, 1999.

[32] Valasek, J., "Digital Control of Aerospace Systems," Lecture Notes, Texas A&M University, 2000.

[33] Jessick, M., "PARASIM Program Document," Tech. Rep. Boeing D180-32581-1, Boeing, Huntsville, Alabama, September 1990.

[34] Phan, M. Q., Horta, L. G., Juang, J.-N., and Longman, R. W., "Identfication of Linear System by an Asymtotically Stable Observer," NASA Technical Paper 3164, NASA, Hampton, Virginia, 1992.

[35] Juang, J.-N. and Pappa, R. S., "An Eigensystem Realization Algorithm for Modal Parameter Identification and Modal Reduction," *The Journal of Guidance, Control and Dynamics*, Vol. 8, No. 5, 1985, pp. 620–627.

[36] Ho, B. L. and Kalman, R. E., "Effective Construction of Linear State-Variable Models from Input-output Data," *Proceedings of the 3rd Annual Allerton Conference on Circuit and System Theory*, Monticello, Illinois, October 1965, pp. 449–459.

[37] Pappa, R. S., Schenk, A., and Noll, C., "Some Experiences with the Eigensystem Realization Algorithm," *Sound and Vibration*, Vol. 22, No. 1, January 1988, pp. 30–35.

[38] Juang, J.-N. and Pappa, R. S., "Effects of Noise on Modal Parameters Identfied by the Eigensystem Realization Algorithm," *The Journal of Guidance, Control and Dynamics*, Vol. 9, No. 3, 1986, pp. 294–303.

39 Juang, J.-N., Horta, L. G., and Phan, M. Q., "User's Guide for System/Observer/Controller Identification Toolbox," NASA Technical Memorandum 107566, NASA, Hampton, Virginia, 1992.

40 Phan, M. Q., Goodzeit, N. E., and Juang, J.-N., "Identification of System and Periodic Disturbances," ASME Design Engineering Technical Conferences, DETC97/VIB-4256, Sacramento, California, September 1997.

41 Ward, D. T. and Stragnac, T. W., *Introduction to Flight Test Engineering,* 2nd ed., Kendal/Hunt Publishing Co., Dubuque, Iowa, 1998.

42 Aeroprobe Corporation, 1700 Kraft Drive, Suite 2413, Blacksburg, VA 24060, *Multi-Hole Probe Information Packet*, edition 1.5 ed., October 2001.

43 Johansen, E., *Development Of A Fast-Response Multi-Hole Probe For Unsteady And Turbulent Flowfields*, Ph. D. Dissertation, Texas A&M University, 2001.

44 Lund, D. W., Ward, D. T., Pollock, T. L., Valasek, J., Hur, G.-B., and Wilkey, J., "Flight Tests of an Unmanned Powered Parachute: A Validation Tool for GN&C Algorithms - Stage II," Technical Report Flight Mechanics Laboratory Report 2003-1, Flight Mechanics Laboratory,Texas Engineering Experiment Station, Texas A&M University, December 2003.

45 Watson Industries, Inc., 3041 Melby Road, Eau Claire, WI 54703, *Inertial Measurement Unit Owner's Manual, Part Number: IMU-BA604*, revision g ed., June 1997.

46 Johansen, E., *Steady and Unsteady Calibration of Multi-Hole Probes*, M.S. Thesis, Texas A&M University, 1998.

47 Johansen, E. S., Rediniotis, O., and Jones, G., "The Compressible Calibration of Miniature Multi-Hole Probes," *Transactions of the ASME*, Vol. 123, No. 1, March 2001, pp. 128–138.

48 Krauss, T. P., Shure, L., and Little, J. L., *Signal Processing Toolbox*, The Mathworks, Inc., South Natick, Massachusetts, 1994.

49 Caicedo, E., Hur, G.-B., Lund, D. W., Strelec, J., and Ward, D. T., "Aerodynamic Tow Tests: X-38 Subscale Parafoil (750 ft^2)," Technical Report Flight Mechanics Laboratory Report 2001-1, Flight Mechanics Laboratory,Texas Engineering Experiment Station, Texas A&M University, July 2001.

[50] The Boeing Company, Huntsville, Alabama, *User manual for PARASIM*, October 1990.

APPENDIX A

SAMPLE APPLICATION OF KANE'S DYNAMICS

As mentioned in Chapter II, the Kane's equation was introduced in early 80's by Thomas R. Kane and D. A. Levinson[19,21] to develop a method to reduce the labor required for the formulation of equations of motion and/or the complexity of equations for complex dynamic system. For assisting engineers and scholars to develop model for complex multibody dynamic systems in practice, a symbolic dynamic solver for dynamic systems has been developed by Kane and Levinson.[26,27] The symbolic dynamic solver is AUTOLEV^{TM} and it has been used for developing the 8-DOF model of the Buckeye. It is quite well documented and has been validated from numerous examples in Reference 26, 27.

To assure the validity and to apply AUTOLEV^{TM} to this research an example of "Cart-Pendulum" in Reference 25 was applied to AUTOLEV^{TM} and the resulting equations of motion were compared to those from Newtonian dynamics. It is two-body system and can be regarded as a simplified system representing the parafoil-vehicle two-body system.

The "Cart-Pendulum" system consists of a cart moving on an axis and a pendulum hanging on the cart as in Figure 7.1. Following the notations in Ref. 25, the kinematic equations can be derived as follows:

Kinematics of m_1:

$$\mathbf{R}_1 = x\mathbf{n}_1, \ \dot{\mathbf{R}}_1 = \mathbf{V}_1 = \dot{x}\mathbf{n}_1, \ \ddot{\mathbf{R}}_1 = \dot{\mathbf{V}}_1 = \ddot{x}\mathbf{n}_1 \tag{A.1}$$

Kinematics of m_2:

$$\mathbf{R}_2 = x\mathbf{n}_1 + r\mathbf{e}_r = (x + r\sin\theta)\mathbf{n}_1 + (-r\cos\theta)\mathbf{n}_2$$

$$\dot{\mathbf{R}}_2 = \mathbf{V}_2 = \dot{x}\mathbf{n}_1 + r\dot{\theta}\mathbf{e}_\theta = (\dot{x} + r\dot{\theta}\cos\theta)\mathbf{n}_1 + (r\dot{\theta}\sin\theta)\mathbf{n}_2$$

$$\ddot{\mathbf{R}}_2 = \dot{\mathbf{V}}_2 = \ddot{x}\mathbf{n}_1 - r\dot{\theta}^2\mathbf{e}_r + r\ddot{\theta}\mathbf{e}_\theta \tag{A.2}$$

$$= (\ddot{x} - r\dot{\theta}^2\sin\theta + r\ddot{\theta}\cos\theta)\mathbf{n}_1 + (r\dot{\theta}^2\cos\theta + r\ddot{\theta}\sin\theta)\mathbf{n}_2$$

$$= (\ddot{x}\sin\theta - r\dot{\theta}^2)\mathbf{e}_r + (\ddot{x}\cos\theta + r\ddot{\theta})\mathbf{e}_\theta$$
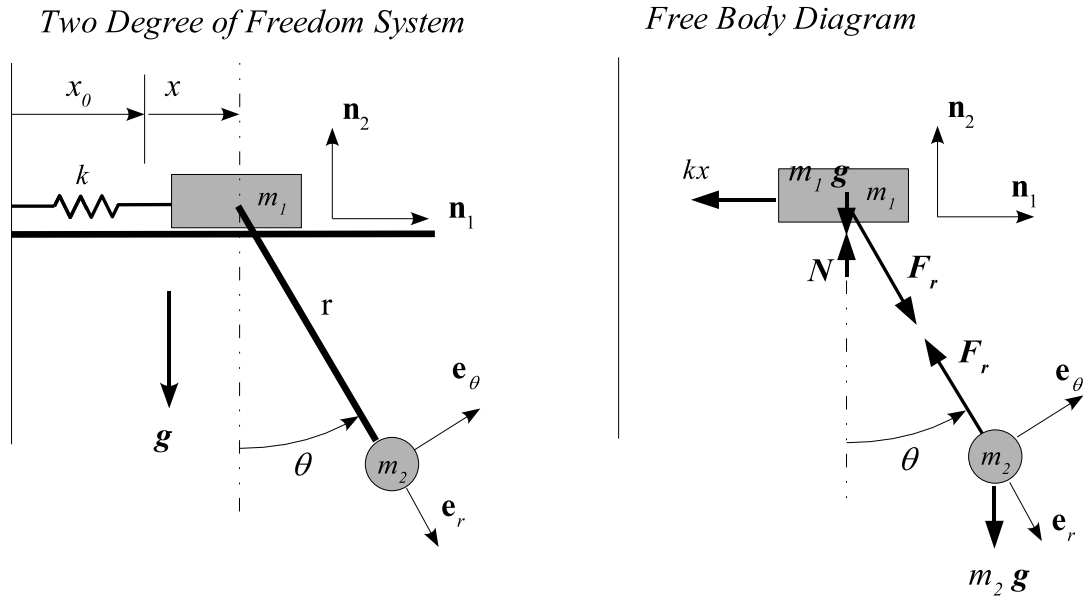
Figure 7.1 Cart-Pendulum Two-Body System

Making use of Newton's second law, we have the vector equations of motion

$$m_i \ddot{\mathbf{R}}_i = m_i \dot{\mathbf{V}}_i = \mathbf{F}_i \tag{A.3}$$

Referring to the free body diagram on the right side of Figure 7.1, and making use of Eqn.(A.1) and (A.2) to obtain

$$m_1 \ddot{x} = -kx + F_r \sin\theta$$
$$0 = N - m_1 g - F_r \cos\theta \tag{A.4}$$

and for the m_2 equations, taking components of Eqn.(A.3) in the $\mathbf{e}_r$, $\mathbf{e}_\theta$ basis

$$m_2(\ddot{x}\sin\theta - r\dot{\theta}^2) = -F_r + m_2\cos\theta$$
$$m_2(\ddot{x}\cos\theta + r\ddot{\theta}) = -m_2 g\sin\theta \tag{A.5}$$

Solvng the first of Eqn.(A.5) for the constraint force (pendulum tension) F_r, we obtain

$$F_r = m_2 g\cos\theta - m_2(\ddot{x}\sin\theta - r\dot{\theta}^2) \tag{A.6}$$

which, substituting into the first of Eqn.(A.4) and the second of Eqn.(A.5) eliminates the constraint force F_r and leads to the pair of differential equations of motion that govern the system dynamics:

$$(m_1 + m_2 \sin^2 \theta)\ddot{x} - m_2 r \dot{\theta}^2 \sin \theta = -kx + m_2 g \sin \theta \cos \theta$$

$$(m_2 \cos \theta)\ddot{x} + (m_2 r)\ddot{\theta} = -m_2 g \sin \theta$$

(A.7)

Derivng differential equations via Kane's equation uses same concept of the virtual power form of D'Alembert's Principle mentioned in the Ref. 25. Both method derive the equations of motion via a path that does not require us to first introduce the constraint forces (N, F_r), then eliminate them. This is very effective approach for multibody problems that usually have lots of constraint forces between them and causes tedious derivation and elimination of the constraint forces. Here we make use of equations in Section2.3.1 to derive equations of motion via Kane's equation. For the initial development we choose general coordinates $q_1 = x$, $q_2 = \theta$. And we define generalized speeds $u_1 \triangleq \dot{x}$, $u_2 \triangleq \dot{\theta}$. From positions and velocities in Eqn.(A.1) and Eqn.(A.2)

$$\mathbf{R}_1 = q_1 \mathbf{n}_1, \ \dot{\mathbf{R}}_1 = \mathbf{V}_1 = \dot{q}_1 \mathbf{n}_1 = u_1 \mathbf{n}_1$$

$$\mathbf{R}_2 = q_1 \mathbf{n}_1 + r \mathbf{e}_r$$

$$\dot{\mathbf{R}}_2 = \mathbf{V}_2 = \dot{q}_1 \mathbf{n}_1 + r\dot{q}_2 \mathbf{e}_\theta = u_1 \mathbf{n}_1 + r u_2 \mathbf{e}_\theta$$

$$= (u_1 \cos q_2 + r u_2)\mathbf{e}_\theta + u_1 \sin q_2 \mathbf{e}_r$$

(A.8)

Partial velocities,

$$v_1^1 \triangleq \frac{\partial \mathbf{V}_1}{\partial u_1} = \mathbf{n}_1, \quad v_2^1 \triangleq \frac{\partial \mathbf{V}_1}{\partial u_2} = 0$$

$$v_1^2 \triangleq \frac{\partial \mathbf{V}_2}{\partial u_1} = \mathbf{n}_1, \quad v_2^2 \triangleq \frac{\partial \mathbf{V}_2}{\partial u_2} = r\mathbf{e}_\theta$$

(A.9)

Resultant forces for m_1 and m_2:

$$\mathbf{Q_1} = -kq_1 \mathbf{n}_1 + (N - m_1 g)\mathbf{n}_2 + F_r \mathbf{e}_r$$

$$\mathbf{Q_2} = -m_2 g \mathbf{n}_2 - F_r \mathbf{e}_r$$

(A.10)

Using the definitions in Eqn.(2.9), generalized active forces are:

$$F_1 = v_1^1 \cdot \mathbf{Q_1} + v_1^2 \cdot \mathbf{Q_2}$$

$$= \mathbf{n_1} \cdot \{-kq_1\mathbf{n_1} + (N - m_1g)\mathbf{n_2} + F_r\mathbf{e}_r\} + \mathbf{n_1} \cdot \{-m_2g\mathbf{n_2} - F_r\mathbf{e}_r\}$$

$$= -kq_1$$

$$F_2 = v_2^1 \cdot \mathbf{Q_1} + v_2^2 \cdot \mathbf{Q_2}$$ (A.11)

$$= r\mathbf{e}_\theta \cdot \{-m_2g\mathbf{n_2} - F_r\mathbf{e}_r\}$$

$$= -rm_2g\sin q_2$$

Calculate accelerations:

$$\ddot{\mathbf{R}}_1 = \dot{\mathbf{V}}_1 = \dot{u}_1\mathbf{n_1} = \ddot{q}_1\mathbf{n_1}$$

$$\ddot{\mathbf{R}}_2 = \dot{\mathbf{V}}_2 = \ddot{q}_1\mathbf{n_1} - r\dot{q}_2^2\mathbf{e}_r + r\ddot{q}_2\mathbf{e}_\theta$$ (A.12)

Inertia forces for m_1 and m_2:

$$\mathbf{Q_1^*} \triangleq -m_1\dot{\mathbf{V}}_1 = -m_1\ddot{q}_1\mathbf{n_1}$$

$$\mathbf{Q_2^*} \triangleq -m_2\dot{\mathbf{V}}_2$$ (A.13)

$$= -m_2\{\ddot{q}_1\mathbf{n_1} - r\dot{q}_2^2\mathbf{e}_r + r\ddot{q}_2\mathbf{e}_\theta\}$$

Using the definitions in Eqn.(2.11), generalized inertia forces are:

$$F_1^* = v_1^1 \cdot \mathbf{Q^*}_1 + v_1^2 \cdot \mathbf{Q^*}_2$$

$$= \mathbf{n_1} \cdot \{-m_1\ddot{q}_1\mathbf{n_1}\} + \mathbf{n_1} \cdot \{-m_2(\ddot{q}_1\mathbf{n_1} - r\dot{q}_2^2\mathbf{e}_r + r\ddot{q}_2\mathbf{e}_\theta)\}$$

$$= -m_1\ddot{q}_1 - m_2\ddot{q}_1 + m_2r\dot{q}_2^2\sin q_2 - m_2r\ddot{q}_2\cos q_2$$

$$= -(m_1 + m_2)\ddot{q}_1 + m_2r\dot{q}_2^2\sin q_2 - m_2r\ddot{q}_2\cos q_2$$ (A.14)

$$F_2^* = v_2^1 \cdot \mathbf{Q^*}_1 + v_2^2 \cdot \mathbf{Q^*}_2$$

$$= r\mathbf{e}_\theta \cdot -m_2\{\ddot{q}_1\mathbf{n_1} - r\dot{q}_2^2\mathbf{e}_r + r\ddot{q}_2\mathbf{e}_\theta\}$$

$$= -m_2r\ddot{q}_1\cos q_2 - m_2r^2\ddot{q}_2$$

Substituting Eqn.(A.11),(A.14) into Kane's equation in Eqn.(2.4) leads to the system of differential equations:

$$0 = F_1 + F_1^*$$
$$= -kx - (m_1 + m_2)\ddot{q}_1 + m_2 r \dot{q}_2^2 \sin q_2 - m_2 r \ddot{q}_2 \cos q_2$$
$$0 = F_2 + F_2^*$$
$$= -m_2 gr \sin q_2 - m_2 r \ddot{q}_1 \cos q_2 - m_2 r^2 \ddot{q}_2$$
$$= -m_2 gr \sin q_2 - m_2 r \ddot{q}_1 \cos q_2 - m_2 r \ddot{q}_2$$

(A.15)

Rearranging above equation yields

$$(m_1 + m_2)\ddot{q}_1 + (m_2 r \cos q_2)\ddot{q}_2 - m_2 r \dot{q}_2^2 \sin q_2 = -kx$$
$$(m_2 r \cos q_2)\ddot{q}_1 + (m_2 r)\ddot{q}_2 = -m_2 gr \sin q_2$$

(A.16)

This Kane's approach is mentioned in Ref. 25 as *virtual power form of D'Alembert's principle*. Comparing Eqn.(A.16) to those (Eqn.(A.7)) obtained from Newton's second law, these equations have different forms. The more elegant form of Eqn.(A.16) is preferred due to the symmetry of acceleration coefficients ("mass matrix"). Both sets of equations are correct and it is easy to rearrange Eqn.(A.7) via linear combinations of the two equations to obtain the form of Eqn.(A.16)

As can be seen from the derivations from both methods, the Kane's approach (or *virtual power form of D'Alembert's Principle*) saves efforts to derive the constraint equations to be canceled at last. For multibody problems with more degrees of freedom and more constraints, the Kane's approach can save time and effort much to derive equations of motion.

2-DOF equations of motion for the cart-pendulum system were derived using a symbolic dynamic solver AUTOLEV^{TM}. The symbols used for AUTOLEV are summarized as follows:

MA:	m_1	MB:	m_2
X:	x	R:	r
THETA:	θ		
Q1:	x	Q1':	$\dot{x}$
Q2:	θ	Q2':	$\dot{\theta}$
U1:	$\dot{x}$	U2:	$\dot{\theta}$

The procedure for symbolic calculation and the 2-DOF equations of motion in text form are appended. The equations of motion at line (51) and (52) are same as derived by hand for the simple 2-DOF cart-pendulum system in Eqn.(A.16).

```
(1) %degrees off

(2) AUTOZ off

(3) % Newtonian, bodies, frames, points

(4) Newtonian N

(5) Bodies A,B

(6) Points O

(7) % variables, constants

(8) Variables U{2}'

(9) Variables X', THETA'

(10) Constants R

(11) Constants G

(12) Constants K %spring constant

(13) %

(14) Mass A=MA, B=MB

(15) Inertia B, 0, 0, 0

-> (16) I_B_BO>> = 0>*0>


(17) %
```

```
   (18) Simprot(N,B,3,1.5*pi+THETA)
-> (19) N_B = [SIN(THETA), COS(THETA), 0; -COS(THETA), SIN(THETA),
0; 0, 0, 1]


   (20) % position vectors
   (21) P_O_Ao>=X*N1>
-> (22) P_O_AO> = X*N1>


   (23) P_Ao_Bo>=R*B1>
-> (24) P_AO_BO> = R*B1>


   (25) % kineamatic differential eqn
   (26) X'=U1
-> (27) X' = U1


   (28) THETA'=U2
-> (29) THETA' = U2


   (30) % angular velocities
   (31) W_A_N>=0>
-> (32) W_A_N> = 0>


   (33) W_B_N>=THETA'*B3>
-> (34) W_B_N> = U2*B3>


   (35) % velocities
   (36) V_Ao_N>=DT(P_O_Ao>,N)
-> (37) V_AO_N> = U1*N1>
```

```
    (38) V2pts(N,B,Ao,Bo)
-> (39) V_BO_N> = R*U2*B2> + U1*N1>


    (40) % forces
    (41) Gravity(-G*N2>)
-> (42) FORCE_AO> = -G*MA*N2> -> (43) FORCE_BO> = -G*MB*N2>


    (44) Force_Ao>+= -K*X*N1>
-> (45) FORCE_AO> = -K*X*N1> - G*MA*N2>


    (46) % Equations of motion
    (47) Zero=Fr()+Frstar()
-> (48) ZERO[1] = MB*R*SIN(THETA)*U2^2 - K*X - (MA+MB)*U1' -
MB*R*COS(THETA)*U2'
-> (49) ZERO[2] =
-MB*R*(G*SIN(THETA)+R*U2'+COS(THETA)*U1')


    (50) Kane()
-> (51) ZERO[1] = MB*R*SIN(THETA)*U2^2 - K*X - (MA+MB)*U1' -
MB*R*COS(THETA)*U2'
-> (52) ZERO[2] =
-MB*R*(G*SIN(THETA)+R*U2'+COS(THETA)*U1')
```

APPENDIX B

8-DOF EQUATIONS OF MOTION FOR THE BUCKEYE PARAFOIL-VEHICLE
IN AUTOLEV SYMBOLIC FORM

Full 8-DOF equations of motion for two-body parafoil-vehicle were derived using a symbolic dynamic solver AUTOLEV^{TM}. The variable names are the same as used in chapter II except some greek symbols such as OMEGA for ω, RHO for ρ etc. The symbols used for AUTOLEV are summarized as follows:

FAP1:	F_{x_P}	FAP2:	F_{y_P}	FAP3:	F_{z_P}
TAP1:	L_P	TAP2:	M_P	TAP3:	N_P
RAP1:	r_{x_P}	RAP2:	r_{y_P}	RAP3:	r_{z_P}
RHOPX:	ρ_{x_P}	RHOPY:	ρ_{y_P}	RHOPZ:	ρ_{z_P}
FAV1:	F_{x_V}	FAP2:	F_{y_V}	FAP3:	F_{z_V}
TAV1:	L_V	TAP2:	M_V	TAP3:	N_V
RAV1:	r_{x_V}	RAP2:	r_{y_V}	RAP3:	r_{z_V}
RHOVX:	ρ_{x_V}	RHOPY:	ρ_{y_V}	RHOPZ:	ρ_{z_V}
MP:	m_P	MV:	m_V		
IP1:	I_{xx_P}	IP2:	I_{yy_P}	IP3:	I_{zz_P}
IV1:	I_{xx_V}	IV2:	I_{yy_V}	IV3:	I_{zz_V}
Q1:	q_1	...	Q1':	$\dot{q}_1$	...
U1:	u_1	...	U1':	$\dot{u}_1$	...

The 8-DOF equations of motion in text form are as follows:

```
ZERO1[1] = TAP1 + IP2*U2*U3 + MV*RHOPZ*SIN(Q9)^2*U3*U4 +

MV*RHOPZ*COS( Q9)^2*U3*U4 + MV*RHOPX*RHOPZ*SIN(Q9)^2*U1*U2 +

MV*RHOPX*RHOPZ*COS(Q9)^ 2*U1*U2 + MV*RHOPZ^2*SIN(Q9)^2*U2*U3 +
```

MV*RHOPZ^2*COS(Q9)^2*U2*U3 + IV1*COS(Q9)^2*TAN(Q8)^2*U2*U3 +

MV*RHOPZ*RHOVX*COS(Q9)*TAN(Q8)*U8*U9

 + MV*RHOVZ^2*COS(Q9)^2*TAN(Q8)^2*U2*U3 + MV*RHOPZ*SIN(Q2)*COS(Q1)*COS

(Q2)*SIN(2*Q1)*COS(Q9)^2*U2*U6 +

2*MV*RHOPZ*SIN(Q2)*COS(Q1)*COS(Q2)* SIN(Q1)^2*COS(Q9)^2*U3*U6 +

MV*RHOPZ*U5' + MV*RHOPX*RHOPZ*U3' + MV*RH

OPZ^2*SIN(Q9)*COS(Q9)*U2' +

SIN(Q8)*((CONTOR*COS(Q9)*COS(Q8)^2+2*IV1*

COS(Q9)*U1*U2+MV*RHOPZ*RHOVZ*COS(Q8)*U1*U8+2*MV*RHOVZ^2*COS(Q9)*U1*U2-

IV1*U1*U8-MV*RHOVZ^2*U1*U8-IV1*SIN(Q8)*COS(Q8)*U2*U3-2*MV*RHOPZ*RHOVZ*

COS(Q8)*COS(Q9)*U1*U2-MV*RHOVX*RHOVZ*COS(Q8)*COS(Q9)*U8*U9-MV*RHOVZ^2*

SIN(Q8)*COS(Q8)*U2*U3)/COS(Q8)^3-SIN(Q9)*(RHOPZ*FAV3-MV*RHOPZ*RHOVZ*

U8^2-MV*RHOPZ*RHOVX*TAN(Q8)*U9^2-MV*RHOPZ*RHOVZ*COS(Q9)*TAN(Q8)*U1*U3-

(2*IV1*U2^2+2*MV*RHOVZ^2*U2^2+MV*RHOPZ*RHOVZ*COS(Q8)*U9^2+3*MV*RHOPZ*

RHOVZ*COS(Q8)*U1^2+MV*RHOPZ*RHOVZ*COS(Q8)*COS(Q9)*U2*U8-2*IV1*U1^2-2*

MV*RHOVZ^2*U1^2-IV1*COS(Q9)*U2*U8-2*MV*RHOPZ*RHOVZ*COS(Q8)*U2^2-MV*RH

OVZ^2*COS(Q9)*U2*U8-SIN(Q9)*(2*IV1*SIN(Q9)*U2^2+4*IV1*COS(Q9)*U1*U2+

MV*RHOPZ*RHOVZ*COS(Q8)*U1*U8+2*MV*RHOVZ^2*SIN(Q9)*U2^2+4*MV*RHOVZ^2*

COS(Q9)*U1*U2+MV*RHOPZ*RHOVX*COS(Q8)^2*U2*U9+2*MV*RHOPZ*RHOVZ*SIN(Q8)*

COS(Q8)*U2*U9+3*MV*RHOPZ*RHOVZ*SIN(Q9)*COS(Q8)*U1^2-IV1*U1*U8-MV*RHOVZ

^2*U1*U8-2*IV1*SIN(Q9)*U1^2-2*MV*RHOVZ^2*SIN(Q9)*U1^2-IV1*SIN(Q8)*COS(

Q8)*U2*U3-6*MV*RHOPZ*RHOVZ*COS(Q8)*COS(Q9)*U1*U2-3*MV*RHOPZ*RHOVZ*SIN(

Q9)*COS(Q8)*U2^2-MV*RHOVZ^2*SIN(Q8)*COS(Q8)*U2*U3))/COS(Q8)^3-MV*RHOPZ

*RHOVX*U8')) - RAP3*FAP2 - RHOPZ*FAV2*COS(Q9) -

G*MV*RHOPZ*SIN(Q1)*COS (Q2)*SIN(Q9)^2 -

G*MV*RHOPZ*SIN(Q1)*COS(Q2)*COS(Q9)^2 - IP3*U2*U3 - IP6*U1*U2 -

MV*RHOPZ*SIN(Q9)^2*U1*U6 - MV*RHOPZ*COS(Q9)^2*U1*U6 - MV*

RHOPZ*RHOVZ*COS(Q9)*U8*U9 - MV*RHOPZ*RHOVZ*SIN(Q9)^2*U2*U9 -

MV*RHOPZ* RHOVZ*SIN(Q9)*COS(Q9)*U1*U9 −

MV*RHOPZ*RHOVX*SIN(Q9)*COS(Q9)*TAN(Q8)* U1*U9 −

2*MV*RHOPZ*RHOVZ*SIN(Q9)*COS(Q9)*TAN(Q8)^2*U1*U9 − 2*MV*RHOPZ*

SIN(Q1)*SIN(Q2)*COS(Q2)*COS(Q1)^2*COS(Q9)^2*U2*U6 −

MV*RHOPZ*SIN(Q1)* SIN(Q2)*COS(Q2)*SIN(2*Q1)*COS(Q9)^2*U3*U6 −

IP1*U1' − IP6*U3' − MV*RH OPZ*RHOVX*COS(Q9)*U9' −

MV*RHOPZ^2*SIN(Q9)^2*U1' − MV*RHOPZ*RHOVZ*COS(Q9)*TAN(Q8)*U9' −

MV*COS(Q9)^2*(RHOPZ-RHOVZ/COS(Q8))^2*U1' − MV*SIN(

Q9)*COS(Q9)*(RHOPZ-RHOVZ/COS(Q8))^2*U2' −

(RAV3*FAV2*COS(Q9)*COS(Q8)^2

+RHOPZ*FAV1*SIN(Q9)*COS(Q8)^4+2*IV1*COS(Q9)^2*U2*U9+IV3*COS(Q9)*COS(

Q8)^2*U8*U9+IV6*COS(Q9)*COS(Q8)^2*U7*U8+2*MV*RHOVZ^2*COS(Q9)^2*U2*U9+

MV*RHOPZ*RHOVZ*COS(Q8)*COS(Q9)*U8*U9+IV1*SIN(Q9)*COS(Q8)*COS(Q9)*U1*

U3+MV*RHOVZ*COS(Q8)^2*COS(Q9)^2*U3*U4+MV*RHOPX*RHOVZ*COS(Q8)^2*COS(Q9)

^2*U1*U2+MV*RHOPZ*RHOVX*COS(Q8)^2*COS(Q9)^2*U1*U8+MV*RHOVZ*SIN(Q9)*COS

(Q9)*COS(Q8)^2*U3*U5+MV*RHOVZ^2*SIN(Q9)*COS(Q8)*COS(Q9)*U1*U3+2*MV*RH

OPZ*RHOVZ*COS(Q8)^2*COS(Q9)^2*U2*U3+2*MV*RHOPZ*RHOVZ*SIN(Q9)*COS(Q8)*

COS(Q9)*U1*U9+MV*RHOPX*RHOVZ*SIN(Q9)*COS(Q9)*COS(Q8)^2*U2^2+MV*RHOPX*

RHOVZ*SIN(Q9)*COS(Q9)*COS(Q8)^2*U3^2+MV*RHOPZ*RHOVX*SIN(Q9)*COS(Q9)*

COS(Q8)^2*U2*U8+MV*RHOVZ*SIN(Q2)*COS(Q1)*COS(Q2)*SIN(2*Q1)*COS(Q8)^2*

COS(Q9)^2*U2*U6+IV1*COS(Q8)*COS(Q9)^2*U1'+IV6*COS(Q9)*COS(Q8)^2*U9'+

IV1*SIN(Q9)*COS(Q8)*COS(Q9)*U2'+MV*RHOPZ*RHOVZ*SIN(Q9)*COS(Q8)^4*U8'+

MV*RHOVZ*COS(Q8)^2*COS(Q9)^2*U5'+MV*RHOPX*RHOVZ*COS(Q8)^2*COS(Q9)^2*

U3'-TAV1*COS(Q9)*COS(Q8)^2-RHOVZ*FAV2*COS(Q9)*COS(Q8)^2-G*MV*RHOVZ*SIN

(Q2)*SIN(Q9)*COS(Q9)*COS(Q8)^2-IV1*COS(Q9)*U8*U9-MV*RHOVZ^2*COS(Q9)*

U8*U9-2*IV1*SIN(Q9)*COS(Q9)*U1*U9-IV1*COS(Q8)*COS(Q9)^2*U2*U3-IV2*COS(

Q9)*COS(Q8)^2*U8*U9-2*MV*RHOVZ^2*SIN(Q9)*COS(Q9)*U1*U9-2*MV*RHOPZ*RHO

VZ*COS(Q8)*COS(Q9)^2*U2*U9-MV*RHOPZ*RHOVX*SIN(Q9)*COS(Q8)^4*U8^2-MV*

RHOPZ*RHOVX*SIN(Q9)*COS(Q8)^4*U9^2-MV*RHOVX*RHOVZ*COS(Q8)*COS(Q9)^2*
U1*U8-MV*RHOVZ*COS(Q8)^2*COS(Q9)^2*U1*U6-MV*RHOVZ^2*COS(Q8)*COS(Q9)^2*
U2*U3-MV*RHOVZ^2*COS(Q9)*COS(Q8)^2*U8*U9-MV*RHOVX*RHOVZ*SIN(Q9)*COS(
Q8)*COS(Q9)*U2*U8-MV*RHOVZ*SIN(Q9)*COS(Q9)*COS(Q8)^2*U2*U6-MV*RHOPZ*
RHOVZ*SIN(Q9)*COS(Q9)*COS(Q8)^2*U1*U3-MV*RHOPZ*RHOVZ*SIN(Q9)*COS(Q9)*
COS(Q8)^4*U1*U3-MV*RHOVZ*SIN(Q1)*COS(Q2)*COS(Q8)^2*COS(Q9)^2*(G+SIN(
Q2)*SIN(2*Q1)*U3*U6+2*SIN(Q2)*COS(Q1)^2*U2*U6-2*SIN(Q1)*SIN(Q2)*COS(
Q1)*U3*U6)-IV1*SIN(Q8)*COS(Q8)*COS(Q9)*U9'-MV*RHOVX*RHOVZ*COS(Q9)*COS(
Q8)^2*U9'-MV*RHOVZ*SIN(Q9)*COS(Q9)*COS(Q8)^2*U4'-MV*RHOVZ^2*SIN(Q8)*
COS(Q8)*COS(Q9)*U9')/COS(Q8)^3

ZERO1[2] = TAP2 + RAP3*FAP1 + RHOPZ*FAV1*COS(Q8)*COS(Q9) +
IP3*U1*U3
 + IP6*U1^2 + MV*RHOPX*U1*U5 + MV*RHOPZ*U3*U5 + MV*RHOPX*RHOPZ*U3^2 +
MV*RHOPX^2*U1*U3 + MV*RHOPZ*RHOVZ*U1*U9 +
MV*RHOPX*RHOVZ*COS(Q8)*U8^2 + MV*RHOPZ*RHOVX*TAN(Q8)*U1*U9 +
MV*RHOPX*RHOVZ*U1^2/COS(Q8) + 2*MV* RHOPZ*RHOVZ*TAN(Q8)^2*U1*U9 +
MV*RHOPX*U6' + MV*RHOPX*RHOVX*COS(Q8)* U8' +
MV*RHOPZ*RHOVZ*COS(Q8)*COS(Q9)*U8' + SIN(Q8)*(RHOPX*FAV1+RHOPZ*
FAV3*COS(Q9)+MV*RHOPX*RHOVZ*U8'-MV*RHOPX*RHOVX*U8^2-MV*RHOPZ*RHOVZ*COS
(Q9)*U8^2-MV*RHOPZ*RHOVX*COS(Q9)*TAN(Q8)*U9^2-MV*RHOPZ*RHOVZ*COS(Q9)*(
U1^2+U9^2)/COS(Q8)^2-MV*RHOPZ*RHOVX*COS(Q9)*U8') - RAP1*FAP3 -
RHOPX* FAV3*COS(Q8) - G*MV*RHOPZ*SIN(Q2) -
G*MV*RHOPX*COS(Q1)*COS(Q2) - IP1* U1*U3 - IP6*U3^2 -
MV*RHOPX*U2*U4 - MV*RHOPZ*U2*U6 - MV*RHOPX*RHOPZ* U1^2 -
MV*RHOPZ^2*U1*U3 - MV*RHOPX*RHOVX*COS(Q9)*U1*U9 - MV*RHOPX*RHO
VZ*COS(Q9)*TAN(Q8)*U1*U9 - MV*RHOPZ*RHOVX*COS(Q8)*COS(Q9)*U8^2 -
MV* RHOPZ*RHOVX*COS(Q8)*COS(Q9)*U9^2 - IP2*U2' - MV*RHOPZ*U4' -

MV*(RHOPX* SIN(Q8)+RHOPZ*COS(Q8)*COS(Q9))^2*U2' -

MV*(RHOPX*COS(Q8)-RHOPZ*SIN(Q8) *COS(Q9))^2*U2' -

SIN(Q9)*(RHOPZ*FAV2+MV*RHOPX*RHOVX*U2*U9+MV*RHOPZ*

RHOVZ*U8*U9+MV*RHOPX*RHOVZ*TAN(Q8)*U2*U9+MV*RHOPZ*RHOVZ*SIN(Q9)*U1*U9+

MV*RHOPZ*RHOVX*SIN(Q9)*TAN(Q8)*U1*U9+2*MV*RHOPZ*RHOVZ*SIN(Q9)*TAN(Q8)^

2*U1*U9+MV*SIN(Q1)*COS(Q2)*COS(Q9)*(2*RHOPZ*SIN(Q2)*U2*U6+RHOPZ*SIN(

Q2)*SIN(2*Q1)*U3*U6-RHOVZ*(G+2*SIN(Q2)*U2*U6+SIN(Q2)*SIN(2*Q1)*U3*U6)/

COS(Q8)-2*SIN(Q1)*SIN(Q2)*U6*(RHOPZ*SIN(Q1)*U2+RHOPZ*COS(Q1)*U3-RHOVZ*

(SIN(Q1)*U2+COS(Q1)*U3)/COS(Q8)))+MV*RHOPZ*RHOVX*U9'+MV*RHOPZ*RHOVZ*

TAN(Q8)*U9'+MV*SIN(Q9)*(RHOPZ-RHOVZ/COS(Q8))^2*U2'+MV*COS(Q9)*(RHOPZ-

RHOVZ/COS(Q8))^2*U1'-CONTOR*TAN(Q8)-MV*RHOPZ*RHOVX*TAN(Q8)*U8*U9-MV*

RHOPZ*RHOVZ*COS(Q9)*U2*U9-MV*RHOPZ*RHOVX*COS(Q9)*TAN(Q8)*U2*U9-2*MV*

RHOPZ*RHOVZ*COS(Q9)*TAN(Q8)^2*U2*U9-MV*RHOPZ*SIN(Q2)*COS(Q1)*COS(Q2)*

COS(Q9)*SIN(2*Q1)*U2*U6-MV*RHOPZ^2*COS(Q9)*U1'-SIN(Q8)*(SIN(Q9)*(MV*

RHOPZ*RHOVZ*TAN(Q8)*U1*U3+(2*IV1*COS(Q9)*U2^2+MV*RHOPZ*RHOVZ*COS(Q8)*

U2*U8+2*MV*RHOVZ^2*COS(Q9)*U2^2+3*MV*RHOPZ*RHOVZ*COS(Q8)*COS(Q9)*U1^2+

6*MV*RHOPZ*RHOVZ*SIN(Q9)*COS(Q8)*U1*U2-IV1*U2*U8-MV*RHOVZ^2*U2*U8-4*

IV1*SIN(Q9)*U1*U2-2*IV1*COS(Q9)*U1^2-4*MV*RHOVZ^2*SIN(Q9)*U1*U2-2*MV*

RHOVZ^2*COS(Q9)*U1^2-3*MV*RHOPZ*RHOVZ*COS(Q8)*COS(Q9)*U2^2)/COS(Q8)^3)

-MV*RHOPZ*RHOVZ*COS(Q9)*TAN(Q8)*U2*U3-(IV1*COS(Q9)*U1*U8+MV*RHOVX*RHO

VZ*COS(Q8)*U8*U9+MV*RHOVZ^2*COS(Q9)*U1*U8+4*MV*RHOPZ*RHOVZ*COS(Q8)*U1*

U2-2*IV1*U1*U2-2*MV*RHOVZ^2*U1*U2-MV*RHOPZ*RHOVZ*COS(Q8)*COS(Q9)*U1*

U8-IV1*COS(Q8)*U9'-MV*RHOVZ^2*COS(Q8)*U9')/COS(Q8)^3)-(TAV1*COS(Q8)^2+

RHOVZ*FAV2*COS(Q8)^2+G*MV*RHOVZ*SIN(Q2)*SIN(Q9)*COS(Q8)^2+IV1*U8*U9+

MV*RHOVZ^2*U8*U9+2*IV1*SIN(Q9)*U1*U9+IV2*COS(Q8)^2*U8*U9+IV1*COS(Q8)*

COS(Q9)*U2*U3+2*MV*RHOVZ^2*SIN(Q9)*U1*U9+MV*RHOVZ^2*COS(Q8)^2*U8*U9+

MV*RHOVX*RHOVZ*SIN(Q9)*COS(Q8)*U2*U8+MV*RHOVX*RHOVZ*COS(Q8)*COS(Q9)*

U1*U8+MV*RHOVZ*SIN(Q9)*COS(Q8)^2*U2*U6+MV*RHOVZ*COS(Q9)*COS(Q8)^2*U1*

U6+MV*RHOVZ^2*COS(Q8)*COS(Q9)*U2*U3+2*MV*RHOPZ*RHOVZ*COS(Q8)*COS(Q9)*

U2*U9+MV*RHOPX*RHOVZ*COS(Q9)*COS(Q8)^2*U1*U2+MV*RHOPZ*RHOVZ*SIN(Q9)*

COS(Q8)^2*U1*U3+MV*RHOPZ*RHOVZ*SIN(Q9)*COS(Q8)^4*U1*U3+MV*RHOVX*RHOVZ*

COS(Q8)^2*U9'+MV*RHOVZ*SIN(Q9)*COS(Q8)^2*U4'-RAV3*FAV2*COS(Q8)^2-2*IV1

*COS(Q9)*U2*U9-IV3*COS(Q8)^2*U8*U9-IV6*COS(Q8)^2*U7*U8-2*MV*RHOVZ^2*

COS(Q9)*U2*U9-MV*RHOPZ*RHOVZ*COS(Q8)*U8*U9-IV1*SIN(Q9)*COS(Q8)*U1*U3-2

*MV*RHOPZ*RHOVZ*SIN(Q9)*COS(Q8)*U1*U9-MV*RHOVZ*SIN(Q9)*COS(Q8)^2*U3*

U5-MV*RHOVZ*COS(Q9)*COS(Q8)^2*U3*U4-MV*RHOVZ^2*SIN(Q9)*COS(Q8)*U1*U3-

MV*RHOPX*RHOVZ*SIN(Q9)*COS(Q8)^2*U1^2-MV*RHOPX*RHOVZ*SIN(Q9)*COS(Q8)^2

*U3^2-MV*RHOPZ*RHOVX*SIN(Q9)*COS(Q8)^2*U2*U8-MV*RHOPZ*RHOVX*COS(Q9)*

COS(Q8)^2*U1*U8-MV*RHOPZ*RHOVZ*COS(Q9)*COS(Q8)^2*U2*U3-MV*RHOPZ*RHOVZ*

COS(Q9)*COS(Q8)^4*U2*U3-MV*RHOVZ*SIN(Q2)*COS(Q1)*COS(Q2)*COS(Q9)*SIN(2

*Q1)*COS(Q8)^2*U2*U6-IV6*COS(Q8)^2*U9'-IV1*SIN(Q9)*COS(Q8)*U2'-IV1*COS

(Q8)*COS(Q9)*U1'-MV*RHOVZ*COS(Q9)*COS(Q8)^2*U5'-MV*RHOPX*RHOVZ*COS(Q9)

*COS(Q8)^2*U3')/COS(Q8)^3

ZERO1[3] = CONTOR + TAP3 + RAP1*FAP2 + RHOPX*FAV2*COS(Q9) +

IP1*U1*U2 + IP6*U2*U3 + MV*RHOPX*U1*U6 +

MV*RHOPX*RHOVZ*COS(Q9)*U8*U9 + MV*RHOPX

*SIN(Q1)*COS(Q2)*(G+SIN(Q2)*SIN(2*Q1)*U3*U6+2*SIN(Q2)*COS(Q1)^2*U2*U6-

2*SIN(Q1)*SIN(Q2)*COS(Q1)*U3*U6) + MV*RHOPX*RHOPZ*U1' +

MV*RHOPX*RHOVX *COS(Q9)*U9' + MV*RHOPX*RHOVZ*COS(Q9)*TAN(Q8)*U9' +

MV*RHOPX*(RHOVX*

COS(Q8)*U1*U8+RHOVZ*COS(Q8)*U2*U3+RHOVZ*COS(Q9)*U8*U9-2*RHOVZ*U2*U9-

RHOVZ*COS(Q8)*U1')/COS(Q8)^2 - IP2*U1*U2 - MV*RHOPX*U3*U4 -

MV*RHOPX* RHOPZ*U2*U3 - MV*RHOPX^2*U1*U2 -

MV*RHOPX*RHOVX*COS(Q9)*TAN(Q8)*U8*U9 -

MV*RHOPX*SIN(Q2)*COS(Q1)*COS(Q2)*SIN(2*Q1)*U2*U6 - IP3*U3' -

IP6*U1' - MV*RHOPX*U5' - MV*RHOPX^2*U3' -

RHOPX*SIN(Q8)*(MV*RHOVZ*U1*(U8-2*COS

(Q9)*U2)/COS(Q8)^2-SIN(Q9)*(FAV3-MV*RHOVZ*U8^2-MV*RHOVX*TAN(Q8)*U9^2-

MV*RHOVZ*COS(Q9)*TAN(Q8)*U1*U3-MV*(RHOVZ*U9^2+3*RHOVZ*U1^2+RHOVZ*COS(

Q9)*U2*U8-2*RHOVZ*U2^2-SIN(Q9)*(RHOVZ*U1*U8+RHOVX*COS(Q8)*U2*U9+2*RHO

VZ*SIN(Q8)*U2*U9+3*RHOVZ*SIN(Q9)*U1^2-6*RHOVZ*COS(Q9)*U1*U2-3*RHOVZ*

SIN(Q9)*U2^2))/COS(Q8)^2-MV*RHOVX*U8')) -

RHOPX*SIN(Q9)*(MV*SIN(Q1)*

SIN(Q2)*SIN(Q9)*COS(Q2)*U6*(SIN(2*Q1)*U3+2*COS(Q1)^2*U2-2*SIN(Q1)*COS(

Q1)*U3)-MV*RHOVZ*SIN(Q9)*U2*U9-MV*RHOVZ*COS(Q9)*U1*U9-MV*RHOVX*COS(Q9)

*TAN(Q8)*U1*U9-2*MV*RHOVZ*COS(Q9)*TAN(Q8)^2*U1*U9-MV*SIN(Q2)*SIN(Q9)*

COS(Q1)*COS(Q2)*SIN(2*Q1)*U2*U6-(FAV1*COS(Q8)^3+2*MV*RHOVZ*SIN(Q9)*U2*

U9+2*MV*RHOVZ*COS(Q9)*U1*U9+MV*RHOVX*COS(Q8)*COS(Q9)*U2*U8+MV*RHOVZ*

COS(Q8)^3*U8'+MV*RHOVZ*SIN(Q9)*COS(Q8)*U1'-MV*RHOVX*COS(Q8)^3*U8^2-MV*

RHOVX*COS(Q8)^3*U9^2-MV*RHOVX*SIN(Q9)*COS(Q8)*U1*U8-MV*RHOVZ*SIN(Q9)*

COS(Q8)*U2*U3-MV*RHOVZ*COS(Q9)*COS(Q8)^3*U1*U3-MV*RHOVZ*COS(Q8)*COS(

Q9)*U2')/COS(Q8)^2)

ZERO1[4] = FAP1 + FAV1*COS(Q8)*COS(Q9) + MP*U3*U5 + MV*U3*U5 +

MV*RHO PX*U2^2 + MV*RHOPX*U3^2 + MV*RHOVZ*U1*U9 +

MV*RHOVX*TAN(Q8)*U1*U9 + 2* MV*RHOVZ*TAN(Q8)^2*U1*U9 +

MV*RHOVZ*COS(Q8)*COS(Q9)*U8' + SIN(Q8)*COS(

Q9)*(FAV3-MV*RHOVZ*U8^2-MV*RHOVX*TAN(Q8)*U9^2-MV*RHOVZ*(U1^2+U9^2)/COS

(Q8)^2-MV*RHOVX*U8') +

SIN(Q9)*(MV*RHOVX*TAN(Q8)*U8*U9+MV*RHOVZ*COS(

Q9)*U2*U9+MV*RHOVX*COS(Q9)*TAN(Q8)*U2*U9+2*MV*RHOVZ*COS(Q9)*TAN(Q8)^2*

U2*U9-FAV2-MV*RHOVZ*U8*U9-MV*RHOVZ*SIN(Q9)*U1*U9-MV*RHOVX*SIN(Q9)*TAN(

Q8)*U1*U9-2*MV*RHOVZ*SIN(Q9)*TAN(Q8)^2*U1*U9-MV*RHOVX*U9'-MV*RHOVZ*TAN

(Q8)*U9'-MV*(RHOVZ*U8*U9+2*RHOVZ*SIN(Q9)*U1*U9+RHOVX*SIN(Q9)*COS(Q8)*
U2*U8+RHOVX*COS(Q8)*COS(Q9)*U1*U8+RHOVZ*COS(Q9)*COS(Q8)^3*U2*U3-2*RHO
VZ*COS(Q9)*U2*U9-RHOVZ*SIN(Q9)*COS(Q8)^3*U1*U3-RHOVZ*SIN(Q8)*(SIN(Q9)*
U2*U8+COS(Q9)*U1*U8+6*SIN(Q9)^2*U1*U2+3*SIN(Q9)*COS(Q9)*U1^2+SIN(Q8)*
SIN(Q9)*COS(Q8)*U1*U3-4*U1*U2-3*SIN(Q9)*COS(Q9)*U2^2-SIN(Q8)*COS(Q8)*
COS(Q9)*U2*U3)-RHOVZ*SIN(Q9)*COS(Q8)*U2'-RHOVZ*COS(Q8)*COS(Q9)*U1')/
COS(Q8)^2) - MP*U2*U6 - MV*U2*U6 - MV*RHOPZ*U1*U3 -
MV*RHOVX*COS(Q8)* COS(Q9)*U8^2 - MV*RHOVX*COS(Q8)*COS(Q9)*U9^2 -
SIN(Q2)*(G*MP+G*MV-MV*
SIN(Q9)*COS(Q2)*COS(Q9)*U6*(COS(Q1)*SIN(2*Q1)*U2-SIN(Q1)*(SIN(2*Q1)*
U3+2*COS(Q1)^2*U2-2*SIN(Q1)*COS(Q1)*U3))) - MP*U4' - MV*U4' -
MV*RHOPZ *U2'

ZERO1[5] = FAP2 + FAV2*COS(Q9) + MP*U1*U6 + MV*U1*U6 +
MV*RHOVZ*COS(Q9)*U8*U9 +
SIN(Q1)*COS(Q2)*(G*MP+G*MV*SIN(Q9)^2+G*MV*COS(Q9)^2+MV*SIN
(Q2)*SIN(2*Q1)*COS(Q9)^2*U3*U6+2*MV*SIN(Q2)*COS(Q1)^2*COS(Q9)^2*U2*U6-
G*MV*SIN(Q1)*SIN(Q2)*COS(Q2)*SIN(Q3)^2*SIN(Q8)^2*(SIN(2*Q9)-2*SIN(Q9)*
COS(Q9))-2*MV*SIN(Q1)*SIN(Q2)*COS(Q1)^3*COS(Q9)^2*U3*U6-2*MV*COS(Q1)*
SIN(Q1)^3*SIN(Q2)^3*COS(Q9)^2*U3*U6-2*MV*SIN(Q2)*COS(Q1)*SIN(Q1)^3*COS
(Q2)^2*COS(Q9)^2*U3*U6) + MV*RHOPZ*U1' + MV*RHOVX*COS(Q9)*U9' +
MV*RH OVZ*COS(Q9)*TAN(Q8)*U9' +
MV*(RHOVX*COS(Q8)*U1*U8+RHOVZ*COS(Q8)*U2*U3+
RHOVZ*COS(Q9)*U8*U9-2*RHOVZ*U2*U9-RHOVZ*SIN(Q8)*U1*(U8-2*COS(Q9)*U2)-
RHOVZ*COS(Q8)*U1')/COS(Q8)^2 +
SIN(Q9)*(MV*RHOVZ*SIN(Q9)*U2*U9+MV*RHO
VZ*COS(Q9)*U1*U9+MV*RHOVX*SIN(Q9)*TAN(Q8)*U2*U9+MV*RHOVX*COS(Q9)*TAN(
Q8)*U1*U9+2*MV*RHOVZ*SIN(Q9)*TAN(Q8)^2*U2*U9+2*MV*RHOVZ*COS(Q9)*TAN(

Q8)^2*U1*U9+MV*SIN(Q2)*SIN(Q9)*COS(Q1)*COS(Q2)*SIN(2*Q1)*U2*U6+SIN(Q8)
*(FAV3+MV*RHOVZ*(2*U2^2-3*U1^2-U9^2-COS(Q9)*U2*U8)/COS(Q8)^2-MV*RHOVZ*
U8^2-MV*RHOVX*TAN(Q8)*U9^2-MV*RHOVZ*COS(Q9)*TAN(Q8)*U1*U3-MV*RHOVZ*SIN
(Q9)*(TAN(Q8)*U2*U3-(U1*U8+3*SIN(Q9)*U1^2-6*COS(Q9)*U1*U2-3*SIN(Q9)*
U2^2)/COS(Q8)^2)-MV*RHOVX*U8')+(FAV1*COS(Q8)^3+2*MV*RHOVZ*SIN(Q9)*U2*
U9+2*MV*RHOVZ*COS(Q9)*U1*U9+MV*RHOVX*COS(Q8)*COS(Q9)*U2*U8+MV*RHOVZ*
COS(Q8)^3*U8'+MV*RHOVZ*SIN(Q9)*COS(Q8)*U1'-MV*RHOVX*COS(Q8)^3*U8^2-MV*
RHOVX*COS(Q8)^3*U9^2-MV*RHOVX*SIN(Q9)*COS(Q8)*U1*U8-MV*RHOVZ*SIN(Q9)*
COS(Q8)^3*U2*U3-MV*RHOVZ*COS(Q9)*COS(Q8)^3*U1*U3-MV*RHOVZ*COS(Q8)*COS(
Q9)*U2')/COS(Q8)^2) - MP*U3*U4 - MV*U3*U4 - MV*RHOPX*U1*U2 -
MV*RHOPZ* U2*U3 - MV*RHOVX*COS(Q9)*TAN(Q8)*U8*U9 -
MV*SIN(Q2)*COS(Q1)*COS(Q2)* SIN(2*Q1)*U2*U6 - MP*U5' - MV*U5' -
MV*RHOPX*U3'

-> (454) ZERO1[6] = FAP3 + FAV3*COS(Q8) + G*MP*COS(Q1)*COS(Q2) +
G*MV*COS(Q1)* COS(Q2) + MP*U2*U4 + MV*U2*U4 + MV*RHOPZ*U1^2 +
MV*RHOPZ*U2^2 + MV*RH OVX*COS(Q9)*U1*U9 +
MV*RHOVZ*COS(Q9)*TAN(Q8)*U1*U9 + MV*SIN(Q9)*(RHOVX
*U2*U9+RHOVZ*TAN(Q8)*U2*U9+RHOVZ*(SIN(Q9)*U1^2-2*COS(Q9)*U1*U2-SIN(Q9)
*U2^2)/COS(Q8)) + MV*RHOPX*U2' +
SIN(Q8)*(MV*RHOVX*U8^2-FAV1-MV*RHOVZ* U8') - MP*U1*U5 - MV*U1*U5 -
MV*RHOPX*U1*U3 - MV*RHOVZ*COS(Q8)*U8^2 - MV*RHOVZ*U1^2/COS(Q8) -
MP*U6' - MV*U6' - MV*RHOVX*COS(Q8)*U8'

ZERO1[7] = TAV2 + RAV3*FAV1 + RHOVX*FAV3 +
G*MV*RHOVZ*SIN(Q8)*COS(Q1)* COS(Q2) + IV3*U7*U9 + IV6*U7^2 +
MV*RHOVX*RHOVZ*U9^2 + MV*RHOVZ*SIN(Q8)*U2*U4 +
MV*RHOPZ*RHOVZ*SIN(Q8)*U1^2 + MV*RHOPZ*RHOVZ*SIN(Q8)*U2^2 +

```
MV*RHOVZ^2*TAN(Q8)*U9^2 + MV*RHOVX*SIN(Q8)*COS(Q9)*U3*U5 +

MV*RHOPX* RHOVX*SIN(Q8)*COS(Q9)*U2^2 +

MV*RHOPX*RHOVX*SIN(Q8)*COS(Q9)*U3^2 + MV* RHOPX*RHOVZ*SIN(Q8)*U2'

- RAV1*FAV3 - RHOVZ*FAV1 - G*MV*RHOVX*SIN(Q2)* SIN(Q8)*COS(Q9) -

IV1*U7*U9 - IV6*U9^2 - MV*RHOVZ*SIN(Q8)*U1*U5 - MV*

RHOPX*RHOVZ*SIN(Q8)*U1*U3 - MV*RHOVX^2*TAN(Q8)*U9^2 -

MV*RHOVX*RHOVZ* TAN(Q8)^2*U9^2 - MV*RHOVX*SIN(Q8)*COS(Q9)*U2*U6 -

MV*RHOPZ*RHOVX*SIN( Q8)*COS(Q9)*U1*U3 - IV2*U8' - MV*RHOVX^2*U8' -

MV*RHOVZ^2*U8' - MV*RH OVZ*SIN(Q8)*U6' -

MV*RHOVX*SIN(Q8)*COS(Q9)*U4' - MV*RHOPZ*RHOVX*SIN( Q8)*COS(Q9)*U2'

- MV*SIN(Q9)*(RHOVX*SIN(Q8)*U3*U4+RHOPX*RHOVX*SIN(Q8)*

U1*U2+RHOPZ*RHOVX*SIN(Q8)*U2*U3+RHOVX*SIN(Q8)*U5'+RHOPX*RHOVX*SIN(Q8)*

U3'-G*RHOVX*SIN(Q1)*SIN(Q8)*COS(Q2)-RHOVX*SIN(Q8)*U1*U6-RHOPZ*RHOVX*

SIN(Q8)*U1'-(RHOVX*RHOVZ*SIN(Q9)*U1^2+RHOVX^2*COS(Q8)*U2*U9+RHOVZ*COS(

Q8)^3*U3*U4+2*RHOVX*RHOVZ*SIN(Q8)*U2*U9+RHOPX*RHOVZ*COS(Q8)^3*U1*U2+

RHOPZ*RHOVZ*COS(Q8)^3*U2*U3+RHOVZ*COS(Q8)^3*U5'+RHOPX*RHOVZ*COS(Q8)^3*

U3'-G*RHOVZ*SIN(Q1)*COS(Q2)*COS(Q8)^3-2*RHOVX*RHOVZ*COS(Q9)*U1*U2-RHO

VX*RHOVZ*SIN(Q9)*U2^2-RHOVZ*COS(Q8)^3*U1*U6-RHOVZ^2*COS(Q8)*U2*U9-RHO

PZ*RHOVZ*COS(Q8)^3*U1')/COS(Q8)^2) -

MV*(RHOVX*RHOVZ*U1^2+RHOVX*COS(

Q8)^3*U1*U5+RHOPX*RHOVX*COS(Q8)^3*U1*U3+RHOVZ*COS(Q9)*COS(Q8)^3*U3*U5+

RHOVZ^2*COS(Q8)*COS(Q9)*U1*U9+RHOPX*RHOVZ*COS(Q9)*COS(Q8)^3*U2^2+RHOPX

*RHOVZ*COS(Q9)*COS(Q8)^3*U3^2+RHOVX*COS(Q8)^3*U6'-G*RHOVX*COS(Q1)*COS(

Q2)*COS(Q8)^3-G*RHOVZ*SIN(Q2)*COS(Q9)*COS(Q8)^3-RHOVX*COS(Q8)^3*U2*U4-

RHOPZ*RHOVX*COS(Q8)^3*U1^2-RHOPZ*RHOVX*COS(Q8)^3*U2^2-2*RHOVX*RHOVZ*

SIN(Q8)*COS(Q9)*U1*U9-RHOVX^2*COS(Q8)*COS(Q9)*U1*U9-RHOVZ*COS(Q9)*COS(

Q8)^3*U2*U6-RHOPZ*RHOVZ*COS(Q9)*COS(Q8)^3*U1*U3-RHOPX*RHOVX*COS(Q8)^3*

U2'-RHOVZ*COS(Q9)*COS(Q8)^3*U4'-RHOPZ*RHOVZ*COS(Q9)*COS(Q8)^3*U2')/COS
```

(Q8)^2

ZERO1[8] = TAV3 + RAV1*FAV2 + RAV3*FAV2*TAN(Q8) + IV1*U7*U8 +

IV6*U8* U9 + IV3*TAN(Q8)*U8*U9 + IV6*TAN(Q8)*U7*U8 +

MV*RHOVX*SIN(Q9)*U3*U5 + MV*RHOVX*COS(Q9)*U3*U4 +

MV*RHOPX*RHOVX*SIN(Q9)*U2^2 + MV*RHOPX*RHOVX* SIN(Q9)*U3^2 +

MV*RHOPX*RHOVX*COS(Q9)*U1*U2 + MV*RHOPZ*RHOVX*COS(Q9)* U2*U3 +

MV*RHOVX^2*TAN(Q8)*U8*U9 + MV*RHOVX*RHOVZ*TAN(Q8)^2*U8*U9 +

MV*RHOVZ*SIN(Q9)*TAN(Q8)*U3*U5 + MV*RHOVZ*COS(Q9)*TAN(Q8)*U3*U4 +

MV* RHOPX*RHOVZ*SIN(Q9)*TAN(Q8)*U2^2 +

MV*RHOPX*RHOVZ*SIN(Q9)*TAN(Q8)*U3^2 +

MV*RHOPX*RHOVZ*COS(Q9)*TAN(Q8)*U1*U2 + MV*RHOPZ*RHOVZ*COS(Q9)*TAN(

Q8)*U2*U3 +

MV*RHOVX*SIN(Q2)*COS(Q1)*COS(Q2)*COS(Q9)*SIN(2*Q1)*U2*U6

 + MV*RHOVZ*SIN(Q2)*COS(Q1)*COS(Q2)*COS(Q9)*TAN(Q8)*SIN(2*Q1)*U2*U6 +

2*IV6*TAN(Q8)*U9' + MV*RHOVX*COS(Q9)*U5' +

MV*RHOPX*RHOVX*COS(Q9)*U3' + MV*RHOVZ*COS(Q9)*TAN(Q8)*U5' +

MV*RHOPX*RHOVZ*COS(Q9)*TAN(Q8)*U3' – RHOVX*FAV2 – TAV1*TAN(Q8) –

RHOVZ*FAV2*TAN(Q8) – G*MV*RHOVX*SIN(Q2)* SIN(Q9) –

G*MV*RHOVZ*SIN(Q2)*SIN(Q9)*TAN(Q8) – IV2*U7*U8 – MV*RHOVX*

RHOVZ*U8*U9 – IV2*TAN(Q8)*U8*U9 – MV*RHOVX*SIN(Q9)*U2*U6 –

MV*RHOVX* COS(Q9)*U1*U6 – MV*RHOPZ*RHOVX*SIN(Q9)*U1*U3 –

MV*RHOVZ^2*TAN(Q8)*U8* U9 – MV*RHOVZ*SIN(Q9)*TAN(Q8)*U2*U6 –

MV*RHOVZ*COS(Q9)*TAN(Q8)*U1*U6

 – MV*RHOPZ*RHOVZ*SIN(Q9)*TAN(Q8)*U1*U3 – MV*SIN(Q1)*COS(Q2)*COS(Q9)*(

G*RHOVX+G*RHOVZ*TAN(Q8)+2*RHOVX*SIN(Q2)*U2*U6+2*RHOVZ*SIN(Q2)*TAN(Q8)*

U2*U6+RHOVX*SIN(Q2)*SIN(2*Q1)*U3*U6+RHOVZ*SIN(Q2)*TAN(Q8)*SIN(2*Q1)*

U3*U6-2*SIN(Q1)*SIN(Q2)*U6*(RHOVX*SIN(Q1)*U2+RHOVX*COS(Q1)*U3+RHOVZ*

```
SIN(Q1)*TAN(Q8)*U2+RHOVZ*COS(Q1)*TAN(Q8)*U3)) - IV3*U9' -

IV1*TAN(Q8)^ 2*U9' - MV*RHOVX*SIN(Q9)*U4' -

MV*RHOPZ*RHOVX*SIN(Q9)*U2' - MV*RHOPZ* RHOVX*COS(Q9)*U1' -

MV*RHOVZ*SIN(Q9)*TAN(Q8)*U4' - MV*(RHOVX+RHOVZ*TAN (Q8))^2*U9' -

MV*RHOPZ*RHOVZ*SIN(Q9)*TAN(Q8)*U2' - MV*RHOPZ*RHOVZ*COS(

Q9)*TAN(Q8)*U1' -

(CONTOR*COS(Q8)^4+MV*RHOVX*RHOVZ*COS(Q8)*U8*U9+MV*

RHOVZ^2*SIN(Q8)*U8*U9+2*IV6*COS(Q8)*COS(Q9)*U2*U9+IV6*SIN(Q9)*COS(Q8)^

4*U1*U3+2*MV*RHOVX*RHOVZ*SIN(Q9)*COS(Q8)*U1*U9+2*MV*RHOVZ^2*SIN(Q8)*

SIN(Q9)*U1*U9+MV*RHOVX*RHOVZ*COS(Q9)*COS(Q8)^4*U2*U3+MV*RHOVX^2*SIN(

Q9)*COS(Q8)^2*U2*U8+MV*RHOVX^2*COS(Q9)*COS(Q8)^2*U1*U8+MV*RHOVX*RHOVZ*

SIN(Q8)*SIN(Q9)*COS(Q8)*U2*U8+MV*RHOVX*RHOVZ*SIN(Q8)*COS(Q8)*COS(Q9)*

U1*U8+IV6*SIN(Q9)*COS(Q8)^2*U2'+IV6*COS(Q9)*COS(Q8)^2*U1'-IV6*COS(Q8)*

U8*U9-2*IV6*SIN(Q9)*COS(Q8)*U1*U9-IV6*COS(Q9)*COS(Q8)^4*U2*U3-2*MV*RH

OVX*RHOVZ*COS(Q8)*COS(Q9)*U2*U9-2*MV*RHOVZ^2*SIN(Q8)*COS(Q9)*U2*U9-MV*

RHOVX*RHOVZ*SIN(Q9)*COS(Q8)^4*U1*U3-MV*RHOVX*RHOVZ*SIN(Q9)*COS(Q8)^2*

U2'-MV*RHOVX*RHOVZ*COS(Q9)*COS(Q8)^2*U1'-MV*RHOVZ^2*SIN(Q8)*SIN(Q9)*

COS(Q8)*U2'-MV*RHOVZ^2*SIN(Q8)*COS(Q8)*COS(Q9)*U1')/COS(Q8)^3 -

SIN(

Q8)*(CONTOR*TAN(Q8)+MV*RHOVX*RHOVZ*COS(Q9)*TAN(Q8)*U2*U3+(IV1*U8*U9+2*

IV1*SIN(Q8)*U1*U2+IV1*COS(Q8)*COS(Q9)*U2*U3+IV6*COS(Q8)*COS(Q9)*U1*U8+

2*MV*RHOVX*RHOVZ*COS(Q8)*U1*U2+2*MV*RHOVZ^2*SIN(Q8)*U1*U2+MV*RHOVZ^2*

COS(Q8)*COS(Q9)*U2*U3-2*IV1*COS(Q9)*U2*U9-2*IV6*COS(Q8)*U1*U2-IV1*SIN(

Q8)*COS(Q9)*U1*U8-MV*RHOVX*RHOVZ*COS(Q8)*COS(Q9)*U1*U8-MV*RHOVZ^2*SIN(

Q8)*COS(Q9)*U1*U8-IV1*COS(Q8)*COS(Q9)*U1')/COS(Q8)^3-IV6*COS(Q9)*TAN(

Q8)*U2*U3-SIN(Q9)*(MV*RHOVX*RHOVZ*TAN(Q8)*U1*U3-IV6*TAN(Q8)*U1*U3-(2*

IV1*U1*U9+IV6*COS(Q8)*U2*U8+2*IV1*SIN(Q8)*COS(Q9)*U2^2+2*IV6*COS(Q8)*

COS(Q9)*U1^2+4*IV6*SIN(Q9)*COS(Q8)*U1*U2+2*MV*RHOVX*RHOVZ*COS(Q8)*COS(
```

Q9)*U2^2+2*MV*RHOVZ^2*SIN(Q8)*COS(Q9)*U2^2-IV1*SIN(Q8)*U2*U8-IV1*COS(

Q8)*U1*U3-MV*RHOVX*RHOVZ*COS(Q8)*U2*U8-MV*RHOVZ^2*SIN(Q8)*U2*U8-MV*RH

OVZ^2*COS(Q8)*U1*U3-4*IV1*SIN(Q8)*SIN(Q9)*U1*U2-2*IV1*SIN(Q8)*COS(Q9)*

U1^2-2*IV6*COS(Q8)*COS(Q9)*U2^2-4*MV*RHOVX*RHOVZ*SIN(Q9)*COS(Q8)*U1*

U2-4*MV*RHOVZ^2*SIN(Q8)*SIN(Q9)*U1*U2-2*MV*RHOVX*RHOVZ*COS(Q8)*COS(Q9)

*U1^2-2*MV*RHOVZ^2*SIN(Q8)*COS(Q9)*U1^2-IV1*COS(Q8)*U2')/COS(Q8)^3))

APPENDIX C

MATRIX ELEMENTS OF THE STATE-SPACE EQUATIONS

The elements of the state-space equations are presented here. They are solved using the symbolic tool AUTOLEV. The variable's and constants name are symbolized as in the appendix B. All the constants symbols are same as in the body of the dissertation.

For longitudinal matrices:

```
ALONG[1,1] =
(MV^2*(C4*CI4*D10-CI9*D10*D9-C3*(C4*CI5-CI4*D9))*(FZU+COS
        (NQ8)^2*FZUV-SIN(NQ8)*COS(NQ8)*FXUV)+(C3*MV^2*(C3*CI5-CI4*D10)-CI4*(
        C3*D10*MV^2-CI4*(MP+MV))-CI9*(CI5*(MP+MV)-D10^2*MV^2))*(FXU+COS(NQ8)^2
        *FXUV+SIN(NQ8)*COS(NQ8)*FZUV)-MV*COS(NQ8)*(CI4*D9*(MP+MV)-C4*CI5*(MP+
        MV)-D10*MV^2*(C3*D9-C4*D10))*(RHOVX*FZUV-RHOVZ*FXUV)-MV*(CI9*D9*(MP+
        MV)-C4*CI4*(MP+MV)-C3*MV^2*(C3*D9-C4*D10))*(MU+RAP3*FXU+COS(NQ8)*(C6+
        RHOVX*(RHOPX*RHOVZ*COS(NQ8)-RHOPX*RHOVX*SIN(NQ8)-RHOPZ*RHOVX*COS(NQ8)-
        RHOPZ*RHOVZ*SIN(NQ8))/(RHOVX^2+RHOVZ^2))*FXUV-RAP1*FZU-COS(NQ8)*(C5-
        RHOVZ*(RHOPX*RHOVZ*COS(NQ8)-RHOPX*RHOVX*SIN(NQ8)-RHOPZ*RHOVX*COS(NQ8)-
        RHOPZ*RHOVZ*SIN(NQ8))/(RHOVX^2+RHOVZ^2))*FZUV))/CDEN1


ALONG[1,2] =
(MV*SIN(NQ8)*(CI4*D9*(MP+MV)-C4*CI5*(MP+MV)-D10*MV^2*(C3*
        D9-C4*D10))*(RHOVX*FZUV-RHOVZ*FXUV)+MV^2*(C4*CI4*D10-CI9*D10*D9-C3*(
        C4*CI5-CI4*D9))*(FZW+SIN(NQ8)^2*FXUV-SIN(NQ8)*COS(NQ8)*FZUV)+(C3*MV^2*
        (C3*CI5-CI4*D10)-CI4*(C3*D10*MV^2-CI4*(MP+MV))-CI9*(CI5*(MP+MV)-D10^2*
        MV^2))*(FXW-SIN(NQ8)^2*FZUV-SIN(NQ8)*COS(NQ8)*FXUV)+MV*(CI9*D9*(MP+MV)
        -C4*CI4*(MP+MV)-C3*MV^2*(C3*D9-C4*D10))*(RAP1*FZW+SIN(NQ8)*(C6+RHOVX*(
```

```
RHOPX*RHOVZ*COS(NQ8)-RHOPX*RHOVX*SIN(NQ8)-RHOPZ*RHOVX*COS(NQ8)-RHOPZ*
RHOVZ*SIN(NQ8))/(RHOVX^2+RHOVZ^2))*FXUV-MW-RAP3*FXW-SIN(NQ8)*(C5-RHOVZ
*(RHOPX*RHOVZ*COS(NQ8)-RHOPX*RHOVX*SIN(NQ8)-RHOPZ*RHOVX*COS(NQ8)-RHOPZ
*RHOVZ*SIN(NQ8))/(RHOVX^2+RHOVZ^2))*FZUV))/CDEN1


ALONG[1,3] =

((C3*MV^2*(C3*CI5-CI4*D10)-CI4*(C3*D10*MV^2-CI4*(MP+MV))-
       CI9*(CI5*(MP+MV)-D10^2*MV^2))*(D13+FXQ+C6*SIN(NQ8)*FZUV+C6*COS(NQ8)*
       FXUV)-MV*(CI4*D9*(MP+MV)-C4*CI5*(MP+MV)-D10*MV^2*(C3*D9-C4*D10))*(D12*
       MV+C6*RHOVX*FZUV-C6*RHOVZ*FXUV)-MV^2*(C4*CI4*D10-CI9*D10*D9-C3*(C4*CI5
       -CI4*D9))*(C6*SIN(NQ8)*FXUV-D14-FZQ-C6*COS(NQ8)*FZUV)-MV*(CI9*D9*(MP+
       MV)-C4*CI4*(MP+MV)-C3*MV^2*(C3*D9-C4*D10))*(MQ+RAP3*FXQ+C6*(C6+RHOVX*(
       RHOPX*RHOVZ*COS(NQ8)-RHOPX*RHOVX*SIN(NQ8)-RHOPZ*RHOVX*COS(NQ8)-RHOPZ*
       RHOVZ*SIN(NQ8))/(RHOVX^2+RHOVZ^2))*FXUV-D11*MV-RAP1*FZQ-C6*(C5-RHOVZ*(
       RHOPX*RHOVZ*COS(NQ8)-RHOPX*RHOVX*SIN(NQ8)-RHOPZ*RHOVX*COS(NQ8)-RHOPZ*
       RHOVZ*SIN(NQ8))/(RHOVX^2+RHOVZ^2))*FZUV))/CDEN1


ALONG[1,4] =

-G*(MV^2*SIN(NQ2)*(MP+MV)*(C4*CI4*D10-CI9*D10*D9-C3*(C4*
       CI5-CI4*D9))+COS(NQ2)*(MP+MV)*(C3*MV^2*(C3*CI5-CI4*D10)-CI4*(C3*D10*
       MV^2-CI4*(MP+MV))-CI9*(CI5*(MP+MV)-D10^2*MV^2))-C1*MV^2*(CI4*D9*(MP+
       MV)-C4*CI5*(MP+MV)-D10*MV^2*(C3*D9-C4*D10))-MV^2*(CI9*D9*(MP+MV)-C4*
       CI4*(MP+MV)-C3*MV^2*(C3*D9-C4*D10))*(RHOPZ*COS(NQ2)-RHOPX*SIN(NQ2)-C2*
       (RHOPX*RHOVZ*COS(NQ8)-RHOPX*RHOVX*SIN(NQ8)-RHOPZ*RHOVX*COS(NQ8)-RHOPZ*
       RHOVZ*SIN(NQ8))/(RHOVX^2+RHOVZ^2)))/CDEN1


ALONG[1,5] =

-RHOVZ*((C3*MV^2*(C3*CI5-CI4*D10)-CI4*(C3*D10*MV^2-CI4*(
```

```
        MP+MV))-CI9*(CI5*(MP+MV)-D10^2*MV^2))*(SIN(NQ8)*FZUV+COS(NQ8)*FXUV-

        MV^2*(C4*CI4*D10-CI9*D10*D9-C3*(C4*CI5-CI4*D9))*(SIN(NQ8)*FXUV-COS(NQ8

        )*FZUV)-MV*(CI4*D9*(MP+MV)-C4*CI5*(MP+MV)-D10*MV^2*(C3*D9-C4*D10))*(

        RHOVX*FZUV-RHOVZ*FXUV)-MV*(CI9*D9*(MP+MV)-C4*CI4*(MP+MV)-C3*MV^2*(C3*

        D9-C4*D10))*((C6+RHOVX*(RHOPX*RHOVZ*COS(NQ8)-RHOPX*RHOVX*SIN(NQ8)-RHO

        PZ*RHOVX*COS(NQ8)-RHOPZ*RHOVZ*SIN(NQ8))/(RHOVX^2+RHOVZ^2))*FXUV-(C5-

        RHOVZ*(RHOPX*RHOVZ*COS(NQ8)-RHOPX*RHOVX*SIN(NQ8)-RHOPZ*RHOVX*COS(NQ8)-

        RHOPZ*RHOVZ*SIN(NQ8))/(RHOVX^2+RHOVZ^2))*FZUV))/CDEN1


ALONG[1,6] =

-(MV^2*(C4*CI4*D10-CI9*D10*D9-C3*(C4*CI5-CI4*D9))*(CF1+

        SIN(NQ8)*(FXTHERV-NU12*FXUV)-COS(NQ8)*(FZTHERV-NU12*FZUV))+MV*(CI4*D9*

        (MP+MV)-C4*CI5*(MP+MV)-D10*MV^2*(C3*D9-C4*D10))*(RHOVX*(FZTHERV-NU12*

        FZUV)-C1*G*MV-RHOVZ*(FXTHERV-NU12*FXUV))+(C3*MV^2*(C3*CI5-CI4*D10)-CI4

        *(C3*D10*MV^2-CI4*(MP+MV))-CI9*(CI5*(MP+MV)-D10^2*MV^2))*(CF2-SIN(NQ8)

        *(FZTHERV-NU12*FZUV)-COS(NQ8)*(FXTHERV-NU12*FXUV))+MV*(CI9*D9*(MP+MV)-

        C4*CI4*(MP+MV)-C3*MV^2*(C3*D9-C4*D10))*(CT2+(C6+RHOVX*(RHOPX*RHOVZ*COS

        (NQ8)-RHOPX*RHOVX*SIN(NQ8)-RHOPZ*RHOVX*COS(NQ8)-RHOPZ*RHOVZ*SIN(NQ8))/

        (RHOVX^2+RHOVZ^2))*(FXTHERV-NU12*FXUV)-(C13*RHOPX*RHOVX*COS(NQ8)+C13*

        RHOPX*RHOVZ*SIN(NQ8)+C13*RHOPZ*RHOVZ*COS(NQ8)-C13*RHOPZ*RHOVX*SIN(NQ8)

        -C2*G*MV*(RHOPX*RHOVZ*COS(NQ8)-RHOPX*RHOVX*SIN(NQ8)-RHOPZ*RHOVX*COS(

        NQ8)-RHOPZ*RHOVZ*SIN(NQ8)))/(RHOVX^2+RHOVZ^2)-(C5-RHOVZ*(RHOPX*RHOVZ*

        COS(NQ8)-RHOPX*RHOVX*SIN(NQ8)-RHOPZ*RHOVX*COS(NQ8)-RHOPZ*RHOVZ*SIN(NQ8

        ))/(RHOVX^2+RHOVZ^2))*(FZTHERV-NU12*FZUV)))/CDEN1


ALONG[2,1] =

(MV^2*(C3*CI4*D9-CI9*D10*D9-C4*(C3*CI5-CI4*D10))*(FXU+COS

        (NQ8)^2*FXUV+SIN(NQ8)*COS(NQ8)*FZUV)+MV*COS(NQ8)*(C3*CI5*(MP+MV)-CI4*
```

```
D10*(MP+MV)-D9*MV^2*(C3*D9-C4*D10))*(RHOVX*FZUV-RHOVZ*FXUV)+(C4*MV^2*(

C4*CI5-CI4*D9)-CI4*(C4*D9*MV^2-CI4*(MP+MV))-CI9*(CI5*(MP+MV)-D9^2*MV^2

))*(FZU+COS(NQ8)^2*FZUV-SIN(NQ8)*COS(NQ8)*FXUV)+MV*(C3*CI4*(MP+MV)-CI9

*D10*(MP+MV)-C4*MV^2*(C3*D9-C4*D10))*(MU+RAP3*FXU+COS(NQ8)*(C6+RHOVX*(

RHOPX*RHOVZ*COS(NQ8)-RHOPX*RHOVX*SIN(NQ8)-RHOPZ*RHOVX*COS(NQ8)-RHOPZ*

RHOVZ*SIN(NQ8))/(RHOVX^2+RHOVZ^2))*FXUV-RAP1*FZU-COS(NQ8)*(C5-RHOVZ*(

RHOPX*RHOVZ*COS(NQ8)-RHOPX*RHOVX*SIN(NQ8)-RHOPZ*RHOVX*COS(NQ8)-RHOPZ*

RHOVZ*SIN(NQ8))/(RHOVX^2+RHOVZ^2))*FZUV))/CDEN1


ALONG[2,2] =
(MV^2*(C3*CI4*D9-CI9*D10*D9-C4*(C3*CI5-CI4*D10))*(FXW-SIN

        (NQ8)^2*FZUV-SIN(NQ8)*COS(NQ8)*FXUV)+(C4*MV^2*(C4*CI5-CI4*D9)-CI4*(C4*

        D9*MV^2-CI4*(MP+MV))-CI9*(CI5*(MP+MV)-D9^2*MV^2))*(FZW+SIN(NQ8)^2*FXUV

        -SIN(NQ8)*COS(NQ8)*FZUV)-MV*SIN(NQ8)*(C3*CI5*(MP+MV)-CI4*D10*(MP+MV)-

        D9*MV^2*(C3*D9-C4*D10))*(RHOVX*FZUV-RHOVZ*FXUV)-MV*(C3*CI4*(MP+MV)-CI9

        *D10*(MP+MV)-C4*MV^2*(C3*D9-C4*D10))*(RAP1*FZW+SIN(NQ8)*(C6+RHOVX*(RH

        OPX*RHOVZ*COS(NQ8)-RHOPX*RHOVX*SIN(NQ8)-RHOPZ*RHOVX*COS(NQ8)-RHOPZ*RH

        OVZ*SIN(NQ8))/(RHOVX^2+RHOVZ^2))*FXUV-MW-RAP3*FXW-SIN(NQ8)*(C5-RHOVZ*(

        RHOPX*RHOVZ*COS(NQ8)-RHOPX*RHOVX*SIN(NQ8)-RHOPZ*RHOVX*COS(NQ8)-RHOPZ*

        RHOVZ*SIN(NQ8))/(RHOVX^2+RHOVZ^2))*FZUV))/CDEN1


ALONG[2,3] =
-(((C4*MV^2*(C4*CI5-CI4*D9)-CI4*(C4*D9*MV^2-CI4*(MP+MV))-

        CI9*(CI5*(MP+MV)-D9^2*MV^2))*(C6*SIN(NQ8)*FXUV-D14-FZQ-C6*COS(NQ8)*FZ

        UV)-MV^2*(C3*CI4*D9-CI9*D10*D9-C4*(C3*CI5-CI4*D10))*(D13+FXQ+C6*SIN(

        NQ8)*FZUV+C6*COS(NQ8)*FXUV)-MV*(C3*CI5*(MP+MV)-CI4*D10*(MP+MV)-D9*MV^2

        *(C3*D9-C4*D10))*(D12*MV+C6*RHOVX*FZUV-C6*RHOVZ*FXUV)-MV*(C3*CI4*(MP+

        MV)-CI9*D10*(MP+MV)-C4*MV^2*(C3*D9-C4*D10))*(MQ+RAP3*FXQ+C6*(C6+RHOVX*
```

```
            (RHOPX*RHOVZ*COS(NQ8)-RHOPX*RHOVX*SIN(NQ8)-RHOPZ*RHOVX*COS(NQ8)-RHOPZ*

        RHOVZ*SIN(NQ8))/(RHOVX^2+RHOVZ^2))*FXUV-D11*MV-RAP1*FZQ-C6*(C5-RHOVZ*(

        RHOPX*RHOVZ*COS(NQ8)-RHOPX*RHOVX*SIN(NQ8)-RHOPZ*RHOVX*COS(NQ8)-RHOPZ*

        RHOVZ*SIN(NQ8))/(RHOVX^2+RHOVZ^2))*FZUV))/CDEN1


ALONG[2,4] =

-G*(MV^2*COS(NQ2)*(MP+MV)*(C3*CI4*D9-CI9*D10*D9-C4*(C3*

        CI5-CI4*D10))+C1*MV^2*(C3*CI5*(MP+MV)-CI4*D10*(MP+MV)-D9*MV^2*(C3*D9-

        C4*D10))+SIN(NQ2)*(MP+MV)*(C4*MV^2*(C4*CI5-CI4*D9)-CI4*(C4*D9*MV^2-CI4

        *(MP+MV))-CI9*(CI5*(MP+MV)-D9^2*MV^2))+MV^2*(C3*CI4*(MP+MV)-CI9*D10*(

        MP+MV)-C4*MV^2*(C3*D9-C4*D10))*(RHOPZ*COS(NQ2)-RHOPX*SIN(NQ2)-C2*(RHO

        PX*RHOVZ*COS(NQ8)-RHOPX*RHOVX*SIN(NQ8)-RHOPZ*RHOVX*COS(NQ8)-RHOPZ*RHO

        VZ*SIN(NQ8))/(RHOVX^2+RHOVZ^2)))/CDEN1


ALONG[2,5] =

RHOVZ*((C4*MV^2*(C4*CI5-CI4*D9)-CI4*(C4*D9*MV^2-CI4*(MP+

        MV))-CI9*(CI5*(MP+MV)-D9^2*MV^2))*(SIN(NQ8)*FXUV-COS(NQ8)*FZUV)-MV^2*(

        C3*CI4*D9-CI9*D10*D9-C4*(C3*CI5-CI4*D10))*(SIN(NQ8)*FZUV+COS(NQ8)*FXUV

        )-MV*(C3*CI5*(MP+MV)-CI4*D10*(MP+MV)-D9*MV^2*(C3*D9-C4*D10))*(RHOVX*

        FZUV-RHOVZ*FXUV)-MV*(C3*CI4*(MP+MV)-CI9*D10*(MP+MV)-C4*MV^2*(C3*D9-C4*

        D10))*((C6+RHOVX*(RHOPX*RHOVZ*COS(NQ8)-RHOPX*RHOVX*SIN(NQ8)-RHOPZ*RHO

        VX*COS(NQ8)-RHOPZ*RHOVZ*SIN(NQ8))/(RHOVX^2+RHOVZ^2))*FXUV-(C5-RHOVZ*(

        RHOPX*RHOVZ*COS(NQ8)-RHOPX*RHOVX*SIN(NQ8)-RHOPZ*RHOVX*COS(NQ8)-RHOPZ*

        RHOVZ*SIN(NQ8))/(RHOVX^2+RHOVZ^2))*FZUV))/CDEN1


ALONG[2,6] =

-(MV^2*(C3*CI4*D9-CI9*D10*D9-C4*(C3*CI5-CI4*D10))*(CF2-

        SIN(NQ8)*(FZTHERV-NU12*FZUV)-COS(NQ8)*(FXTHERV-NU12*FXUV))+(C4*MV^2*(
```

```
         C4*CI5-CI4*D9)-CI4*(C4*D9*MV^2-CI4*(MP+MV))-CI9*(CI5*(MP+MV)-D9^2*MV^2
         ))*(CF1+SIN(NQ8)*(FXTHERV-NU12*FXUV)-COS(NQ8)*(FZTHERV-NU12*FZUV))-MV*
         (C3*CI5*(MP+MV)-CI4*D10*(MP+MV)-D9*MV^2*(C3*D9-C4*D10))*(RHOVX*(FZTHE
         RV-NU12*FZUV)-C1*G*MV-RHOVZ*(FXTHERV-NU12*FXUV))-MV*(C3*CI4*(MP+MV)-
         CI9*D10*(MP+MV)-C4*MV^2*(C3*D9-C4*D10))*(CT2+(C6+RHOVX*(RHOPX*RHOVZ*
         COS(NQ8)-RHOPX*RHOVX*SIN(NQ8)-RHOPZ*RHOVX*COS(NQ8)-RHOPZ*RHOVZ*SIN(NQ8
         ))/(RHOVX^2+RHOVZ^2))*(FXTHERV-NU12*FXUV)-(C13*RHOPX*RHOVX*COS(NQ8)+
         C13*RHOPX*RHOVZ*SIN(NQ8)+C13*RHOPZ*RHOVZ*COS(NQ8)-C13*RHOPZ*RHOVX*SIN(
         NQ8)-C2*G*MV*(RHOPX*RHOVZ*COS(NQ8)-RHOPX*RHOVX*SIN(NQ8)-RHOPZ*RHOVX*
         COS(NQ8)-RHOPZ*RHOVZ*SIN(NQ8)))/(RHOVX^2+RHOVZ^2)-(C5-RHOVZ*(RHOPX*RH
         OVZ*COS(NQ8)-RHOPX*RHOVX*SIN(NQ8)-RHOPZ*RHOVX*COS(NQ8)-RHOPZ*RHOVZ*SIN
         (NQ8))/(RHOVX^2+RHOVZ^2))*(FZTHERV-NU12*FZUV)))/CDEN1


ALONG[3,1] =
(COS(NQ8)*(MP+MV)*(C3*D10*MV^2+C4*D9*MV^2-CI4*(MP+MV))*(
         RHOVX*FZUV-RHOVZ*FXUV)+MV*(D9*C3^2*MV^2-CI9*D9*(MP+MV)-C4*(C3*D10*MV^2
         -CI4*(MP+MV)))*(FXU+COS(NQ8)^2*FXUV+SIN(NQ8)*COS(NQ8)*FZUV)+MV*(D10*
         C4^2*MV^2-CI9*D10*(MP+MV)-C3*(C4*D9*MV^2-CI4*(MP+MV)))*(FZU+COS(NQ8)^2
         *FZUV-SIN(NQ8)*COS(NQ8)*FXUV)+(MP+MV)*(C3^2*MV^2+C4^2*MV^2-CI9*(MP+MV)
         )*(MU+RAP3*FXU+COS(NQ8)*(C6+RHOVX*(RHOPX*RHOVZ*COS(NQ8)-RHOPX*RHOVX*
         SIN(NQ8)-RHOPZ*RHOVX*COS(NQ8)-RHOPZ*RHOVZ*SIN(NQ8))/(RHOVX^2+RHOVZ^2))
         *FXUV-RAP1*FZU-COS(NQ8)*(C5-RHOVZ*(RHOPX*RHOVZ*COS(NQ8)-RHOPX*RHOVX*
         SIN(NQ8)-RHOPZ*RHOVX*COS(NQ8)-RHOPZ*RHOVZ*SIN(NQ8))/(RHOVX^2+RHOVZ^2))
         *FZUV))/CDEN1


ALONG[3,2] =
(MV*(D10*C4^2*MV^2-CI9*D10*(MP+MV)-C3*(C4*D9*MV^2-CI4*(
         MP+MV)))*(FZW+SIN(NQ8)^2*FXUV-SIN(NQ8)*COS(NQ8)*FZUV)+MV*(D9*C3^2*MV^2
```

```
       -CI9*D9*(MP+MV)-C4*(C3*D10*MV^2-CI4*(MP+MV)))*(FXW-SIN(NQ8)^2*FZUV-SIN
(NQ8)*COS(NQ8)*FXUV)-SIN(NQ8)*(MP+MV)*(C3*D10*MV^2+C4*D9*MV^2-CI4*(MP+
MV))*(RHOVX*FZUV-RHOVZ*FXUV)-(MP+MV)*(C3^2*MV^2+C4^2*MV^2-CI9*(MP+MV))
*(RAP1*FZW+SIN(NQ8)*(C6+RHOVX*(RHOPX*RHOVZ*COS(NQ8)-RHOPX*RHOVX*SIN(
NQ8)-RHOPZ*RHOVX*COS(NQ8)-RHOPZ*RHOVZ*SIN(NQ8))/(RHOVX^2+RHOVZ^2))*FX
UV-MW-RAP3*FXW-SIN(NQ8)*(C5-RHOVZ*(RHOPX*RHOVZ*COS(NQ8)-RHOPX*RHOVX*
SIN(NQ8)-RHOPZ*RHOVX*COS(NQ8)-RHOPZ*RHOVZ*SIN(NQ8))/(RHOVX^2+RHOVZ^2))
*FZUV))/CDEN1


ALONG[3,3] =
-(MV*(D10*C4^2*MV^2-CI9*D10*(MP+MV)-C3*(C4*D9*MV^2-CI4*(
          MP+MV)))*(C6*SIN(NQ8)*FXUV-D14-FZQ-C6*COS(NQ8)*FZUV)-(MP+MV)*(C3*D10*
          MV^2+C4*D9*MV^2-CI4*(MP+MV))*(D12*MV+C6*RHOVX*FZUV-C6*RHOVZ*FXUV)-MV*(
          D9*C3^2*MV^2-CI9*D9*(MP+MV)-C4*(C3*D10*MV^2-CI4*(MP+MV)))*(D13+FXQ+C6*
          SIN(NQ8)*FZUV+C6*COS(NQ8)*FXUV)-(MP+MV)*(C3^2*MV^2+C4^2*MV^2-CI9*(MP+
          MV))*(MQ+RAP3*FXQ+C6*(C6+RHOVX*(RHOPX*RHOVZ*COS(NQ8)-RHOPX*RHOVX*SIN(
          NQ8)-RHOPZ*RHOVX*COS(NQ8)-RHOPZ*RHOVZ*SIN(NQ8))/(RHOVX^2+RHOVZ^2))*FX
          UV-D11*MV-RAP1*FZQ-C6*(C5-RHOVZ*(RHOPX*RHOVZ*COS(NQ8)-RHOPX*RHOVX*SIN(
          NQ8)-RHOPZ*RHOVX*COS(NQ8)-RHOPZ*RHOVZ*SIN(NQ8))/(RHOVX^2+RHOVZ^2))*FZ
          UV))/CDEN1


ALONG[3,4] =
-G*MV*(MP+MV)*(C1*(C3*D10*MV^2+C4*D9*MV^2-CI4*(MP+MV))+
          SIN(NQ2)*(D10*C4^2*MV^2-CI9*D10*(MP+MV)-C3*(C4*D9*MV^2-CI4*(MP+MV)))+
          COS(NQ2)*(D9*C3^2*MV^2-CI9*D9*(MP+MV)-C4*(C3*D10*MV^2-CI4*(MP+MV)))+(
          C3^2*MV^2+C4^2*MV^2-CI9*(MP+MV))*(RHOPZ*COS(NQ2)-RHOPX*SIN(NQ2)-C2*(
          RHOPX*RHOVZ*COS(NQ8)-RHOPX*RHOVX*SIN(NQ8)-RHOPZ*RHOVX*COS(NQ8)-RHOPZ*
          RHOVZ*SIN(NQ8))/(RHOVX^2+RHOVZ^2)))/CDEN1
```

```
ALONG[3,5] =

RHOVZ*(MV*(D10*C4^2*MV^2-CI9*D10*(MP+MV)-C3*(C4*D9*MV^2-

        CI4*(MP+MV)))*(SIN(NQ8)*FXUV-COS(NQ8)*FZUV)-(MP+MV)*(C3*D10*MV^2+C4*

        D9*MV^2-CI4*(MP+MV))*(RHOVX*FZUV-RHOVZ*FXUV)-MV*(D9*C3^2*MV^2-CI9*D9*(

        MP+MV)-C4*(C3*D10*MV^2-CI4*(MP+MV)))*(SIN(NQ8)*FZUV+COS(NQ8)*FXUV)-(

        MP+MV)*(C3^2*MV^2+C4^2*MV^2-CI9*(MP+MV))*((C6+RHOVX*(RHOPX*RHOVZ*COS(

        NQ8)-RHOPX*RHOVX*SIN(NQ8)-RHOPZ*RHOVX*COS(NQ8)-RHOPZ*RHOVZ*SIN(NQ8))/(

        RHOVX^2+RHOVZ^2))*FXUV-(C5-RHOVZ*(RHOPX*RHOVZ*COS(NQ8)-RHOPX*RHOVX*SIN

        (NQ8)-RHOPZ*RHOVX*COS(NQ8)-RHOPZ*RHOVZ*SIN(NQ8))/(RHOVX^2+RHOVZ^2))*

        FZUV))/CDEN1


ALONG[3,6] =

-(MV*(D10*C4^2*MV^2-CI9*D10*(MP+MV)-C3*(C4*D9*MV^2-CI4*(

        MP+MV)))*(CF1+SIN(NQ8)*(FXTHERV-NU12*FXUV)-COS(NQ8)*(FZTHERV-NU12*FZUV

        ))+MV*(D9*C3^2*MV^2-CI9*D9*(MP+MV)-C4*(C3*D10*MV^2-CI4*(MP+MV)))*(CF2-

        SIN(NQ8)*(FZTHERV-NU12*FZUV)-COS(NQ8)*(FXTHERV-NU12*FXUV))-(MP+MV)*(

        C3*D10*MV^2+C4*D9*MV^2-CI4*(MP+MV))*(RHOVX*(FZTHERV-NU12*FZUV)-C1*G*

        MV-RHOVZ*(FXTHERV-NU12*FXUV))-(MP+MV)*(C3^2*MV^2+C4^2*MV^2-CI9*(MP+MV)

        )*(CT2+(C6+RHOVX*(RHOPX*RHOVZ*COS(NQ8)-RHOPX*RHOVX*SIN(NQ8)-RHOPZ*RHO

        VX*COS(NQ8)-RHOPZ*RHOVZ*SIN(NQ8))/(RHOVX^2+RHOVZ^2))*(FXTHERV-NU12*FX

        UV)-(C13*RHOPX*RHOVX*COS(NQ8)+C13*RHOPX*RHOVZ*SIN(NQ8)+C13*RHOPZ*RHOVZ

        *COS(NQ8)-C13*RHOPZ*RHOVX*SIN(NQ8)-C2*G*MV*(RHOPX*RHOVZ*COS(NQ8)-RHOPX

        *RHOVX*SIN(NQ8)-RHOPZ*RHOVX*COS(NQ8)-RHOPZ*RHOVZ*SIN(NQ8)))/(RHOVX^2+

        RHOVZ^2)-(C5-RHOVZ*(RHOPX*RHOVZ*COS(NQ8)-RHOPX*RHOVX*SIN(NQ8)-RHOPZ*

        RHOVX*COS(NQ8)-RHOPZ*RHOVZ*SIN(NQ8))/(RHOVX^2+RHOVZ^2))*(FZTHERV-NU12*

        FZUV)))/CDEN1
```

ALONG[4,1] = 0 ALONG[4,2] = 0 ALONG[4,3] = 1 ALONG[4,4] = 0

ALONG[4,5] = 0 ALONG[4,6] = 0 ALONG[5,1] =

-(COS(NQ8)*(MP+MV)*(CI5*(MP+MV)-D10^2*MV^2-D9^2*MV^2)*(

   RHOVX*FZUV-RHOVZ*FXUV)+MV*(CI4*D9*(MP+MV)-C3*D10*D9*MV^2-C4*(CI5*(MP+

   MV)-D10^2*MV^2))*(FXU+COS(NQ8)^2*FXUV+SIN(NQ8)*COS(NQ8)*FZUV)+MV*(CI4*

   D10*(MP+MV)-C4*D10*D9*MV^2-C3*(CI5*(MP+MV)-D9^2*MV^2))*(FZU+COS(NQ8)^2

   *FZUV-SIN(NQ8)*COS(NQ8)*FXUV)-(MP+MV)*(C3*D10*MV^2+C4*D9*MV^2-CI4*(MP+

   MV))*(MU+RAP3*FXU+COS(NQ8)*(C6+RHOVX*(RHOPX*RHOVZ*COS(NQ8)-RHOPX*RHOVX

   *SIN(NQ8)-RHOPZ*RHOVX*COS(NQ8)-RHOPZ*RHOVZ*SIN(NQ8))/(RHOVX^2+RHOVZ^2)

)*FXUV-RAP1*FZU-COS(NQ8)*(C5-RHOVZ*(RHOPX*RHOVZ*COS(NQ8)-RHOPX*RHOVX*

   SIN(NQ8)-RHOPZ*RHOVX*COS(NQ8)-RHOPZ*RHOVZ*SIN(NQ8))/(RHOVX^2+RHOVZ^2))

   *FZUV))/CDEN1

ALONG[5,2] =

(SIN(NQ8)*(MP+MV)*(CI5*(MP+MV)-D10^2*MV^2-D9^2*MV^2)*(RH

   OVX*FZUV-RHOVZ*FXUV)-MV*(CI4*D10*(MP+MV)-C4*D10*D9*MV^2-C3*(CI5*(MP+

   MV)-D9^2*MV^2))*(FZW+SIN(NQ8)^2*FXUV-SIN(NQ8)*COS(NQ8)*FZUV)-MV*(CI4*

   D9*(MP+MV)-C3*D10*D9*MV^2-C4*(CI5*(MP+MV)-D10^2*MV^2))*(FXW-SIN(NQ8)^2

   *FZUV-SIN(NQ8)*COS(NQ8)*FXUV)-(MP+MV)*(C3*D10*MV^2+C4*D9*MV^2-CI4*(MP+

   MV))*(RAP1*FZW+SIN(NQ8)*(C6+RHOVX*(RHOPX*RHOVZ*COS(NQ8)-RHOPX*RHOVX*

   SIN(NQ8)-RHOPZ*RHOVX*COS(NQ8)-RHOPZ*RHOVZ*SIN(NQ8))/(RHOVX^2+RHOVZ^2))

   *FXUV-MW-RAP3*FXW-SIN(NQ8)*(C5-RHOVZ*(RHOPX*RHOVZ*COS(NQ8)-RHOPX*RHOVX

   *SIN(NQ8)-RHOPZ*RHOVX*COS(NQ8)-RHOPZ*RHOVZ*SIN(NQ8))/(RHOVX^2+RHOVZ^2)

)*FZUV))/CDEN1

ALONG[5,3] =

-((MP+MV)*(CI5*(MP+MV)-D10^2*MV^2-D9^2*MV^2)*(D12*MV+C6*

   RHOVX*FZUV-C6*RHOVZ*FXUV)+MV*(CI4*D9*(MP+MV)-C3*D10*D9*MV^2-C4*(CI5*(

```
MP+MV)-D10^2*MV^2))*(D13+FXQ+C6*SIN(NQ8)*FZUV+C6*COS(NQ8)*FXUV)-MV*(

CI4*D10*(MP+MV)-C4*D10*D9*MV^2-C3*(CI5*(MP+MV)-D9^2*MV^2))*(C6*SIN(NQ8

)*FXUV-D14-FZQ-C6*COS(NQ8)*FZUV)-(MP+MV)*(C3*D10*MV^2+C4*D9*MV^2-CI4*(

MP+MV))*(MQ+RAP3*FXQ+C6*(C6+RHOVX*(RHOPX*RHOVZ*COS(NQ8)-RHOPX*RHOVX*

SIN(NQ8)-RHOPZ*RHOVX*COS(NQ8)-RHOPZ*RHOVZ*SIN(NQ8))/(RHOVX^2+RHOVZ^2))

*FXUV-D11*MV-RAP1*FZQ-C6*(C5-RHOVZ*(RHOPX*RHOVZ*COS(NQ8)-RHOPX*RHOVX*

SIN(NQ8)-RHOPZ*RHOVX*COS(NQ8)-RHOPZ*RHOVZ*SIN(NQ8))/(RHOVX^2+RHOVZ^2))

*FZUV))/CDEN1


ALONG[5,4] =

G*MV*(MP+MV)*(C1*(CI5*(MP+MV)-D10^2*MV^2-D9^2*MV^2)+SIN(

        NQ2)*(CI4*D10*(MP+MV)-C4*D10*D9*MV^2-C3*(CI5*(MP+MV)-D9^2*MV^2))+COS(

        NQ2)*(CI4*D9*(MP+MV)-C3*D10*D9*MV^2-C4*(CI5*(MP+MV)-D10^2*MV^2))-(C3*

        D10*MV^2+C4*D9*MV^2-CI4*(MP+MV))*(RHOPZ*COS(NQ2)-RHOPX*SIN(NQ2)-C2*(

        RHOPX*RHOVZ*COS(NQ8)-RHOPX*RHOVX*SIN(NQ8)-RHOPZ*RHOVX*COS(NQ8)-RHOPZ*

        RHOVZ*SIN(NQ8))/(RHOVX^2+RHOVZ^2)))/CDEN1


ALONG[5,5] =

RHOVZ*((MP+MV)*(CI5*(MP+MV)-D10^2*MV^2-D9^2*MV^2)*(RHOVX*

        FZUV-RHOVZ*FXUV)+MV*(CI4*D9*(MP+MV)-C3*D10*D9*MV^2-C4*(CI5*(MP+MV)-D10

        ^2*MV^2))*(SIN(NQ8)*FZUV+COS(NQ8)*FXUV)-MV*(CI4*D10*(MP+MV)-C4*D10*D9*

        MV^2-C3*(CI5*(MP+MV)-D9^2*MV^2))*(SIN(NQ8)*FXUV-COS(NQ8)*FZUV)-(MP+MV)

        *(C3*D10*MV^2+C4*D9*MV^2-CI4*(MP+MV))*((C6+RHOVX*(RHOPX*RHOVZ*COS(NQ8)

        -RHOPX*RHOVX*SIN(NQ8)-RHOPZ*RHOVX*COS(NQ8)-RHOPZ*RHOVZ*SIN(NQ8))/(RHO

        VX^2+RHOVZ^2))*FXUV-(C5-RHOVZ*(RHOPX*RHOVZ*COS(NQ8)-RHOPX*RHOVX*SIN(

        NQ8)-RHOPZ*RHOVX*COS(NQ8)-RHOPZ*RHOVZ*SIN(NQ8))/(RHOVX^2+RHOVZ^2))*FZ

        UV))/CDEN1
```

```
ALONG[5,6] =

-((MP+MV)*(CI5*(MP+MV)-D10^2*MV^2-D9^2*MV^2)*(RHOVX*(FZT
        HERV-NU12*FZUV)-C1*G*MV-RHOVZ*(FXTHERV-NU12*FXUV))-MV*(CI4*D10*(MP+MV)
        -C4*D10*D9*MV^2-C3*(CI5*(MP+MV)-D9^2*MV^2))*(CF1+SIN(NQ8)*(FXTHERV-NU
        12*FXUV)-COS(NQ8)*(FZTHERV-NU12*FZUV))-MV*(CI4*D9*(MP+MV)-C3*D10*D9*
        MV^2-C4*(CI5*(MP+MV)-D10^2*MV^2))*(CF2-SIN(NQ8)*(FZTHERV-NU12*FZUV)-
        COS(NQ8)*(FXTHERV-NU12*FXUV))-(MP+MV)*(C3*D10*MV^2+C4*D9*MV^2-CI4*(MP+
        MV))*(CT2+(C6+RHOVX*(RHOPX*RHOVZ*COS(NQ8)-RHOPX*RHOVX*SIN(NQ8)-RHOPZ*
        RHOVX*COS(NQ8)-RHOPZ*RHOVZ*SIN(NQ8))/(RHOVX^2+RHOVZ^2))*(FXTHERV-NU12*
        FXUV)-(C13*RHOPX*RHOVX*COS(NQ8)+C13*RHOPX*RHOVZ*SIN(NQ8)+C13*RHOPZ*RH
        OVZ*COS(NQ8)-C13*RHOPZ*RHOVX*SIN(NQ8)-C2*G*MV*(RHOPX*RHOVZ*COS(NQ8)-
        RHOPX*RHOVX*SIN(NQ8)-RHOPZ*RHOVX*COS(NQ8)-RHOPZ*RHOVZ*SIN(NQ8)))/(RHO
        VX^2+RHOVZ^2)-(C5-RHOVZ*(RHOPX*RHOVZ*COS(NQ8)-RHOPX*RHOVX*SIN(NQ8)-RH
        OPZ*RHOVX*COS(NQ8)-RHOPZ*RHOVZ*SIN(NQ8))/(RHOVX^2+RHOVZ^2))*(FZTHERV-
        NU12*FZUV)))/CDEN1


ALONG[6,1] = 0 ALONG[6,2] = 0 ALONG[6,3] = -1 ALONG[6,4] = 0
ALONG[6,5] = 1 ALONG[6,6] = 0


BLONG[1] =
(MV^2*(C4*CI4*D10-CI9*D10*D9-C3*(C4*CI5-CI4*D9))*FZDE+MV*(
        CI9*D9*(MP+MV)-C4*CI4*(MP+MV)-C3*MV^2*(C3*D9-C4*D10))*(RAP1*FZDE-MDE-
        RAP3*FXDE)+(C3*MV^2*(C3*CI5-CI4*D10)-CI4*(C3*D10*MV^2-CI4*(MP+MV))-CI9
        *(CI5*(MP+MV)-D10^2*MV^2))*FXDE)/CDEN1


BLONG[2] =
-(MV*(C3*CI4*(MP+MV)-CI9*D10*(MP+MV)-C4*MV^2*(C3*D9-C4*D10)
        )*(RAP1*FZDE-MDE-RAP3*FXDE)-MV^2*(C3*CI4*D9-CI9*D10*D9-C4*(C3*CI5-CI4*
```

```
        D10))*FXDE-(C4*MV^2*(C4*CI5-CI4*D9)-CI4*(C4*D9*MV^2-CI4*(MP+MV))-CI9*(

        CI5*(MP+MV)-D9^2*MV^2))*FZDE)/CDEN1
```

```
BLONG[3] =

-((MP+MV)*(C3^2*MV^2+C4^2*MV^2-CI9*(MP+MV))*(RAP1*FZDE-MDE-

        RAP3*FXDE)-MV*(D10*C4^2*MV^2-CI9*D10*(MP+MV)-C3*(C4*D9*MV^2-CI4*(MP+

        MV)))*FZDE-MV*(D9*C3^2*MV^2-CI9*D9*(MP+MV)-C4*(C3*D10*MV^2-CI4*(MP+MV)

        ))*FXDE)/CDEN1
```

```
BLONG[4] = 0 BLONG[5] =

-((MP+MV)*(C3*D10*MV^2+C4*D9*MV^2-CI4*(MP+MV))*(RAP1*FZDE-

        MDE-RAP3*FXDE)+MV*(CI4*D10*(MP+MV)-C4*D10*D9*MV^2-C3*(CI5*(MP+MV)-D9^2

        *MV^2))*FZDE+MV*(CI4*D9*(MP+MV)-C3*D10*D9*MV^2-C4*(CI5*(MP+MV)-D10^2*

        MV^2))*FXDE)/CDEN1
```

```
BLONG[6] = 0
```

For lateral/direction matrices:

```
ALAT[1,1] =

-((CI10*(CI1*CI6+CI3*CI7)+CI6*(CI1*CI3+CI2*CI6)+CI11*(CI1

        ^2-CI2*CI7))*FYV-MV*(CI10*(C9*CI1+CI3*RHOPX)-CI11*(C10*CI1+CI2*RHOPX)

        -CI6*(C10*CI3-C9*CI2))*(NV+RAP1*FYV)-MV*(CI11*(C10*CI7+CI1*RHOPX)-CI6

        *(C10*CI6+C9*CI1)-CI10*(C9*CI7-CI6*RHOPX))*(LV-RAP3*FYV))/(MV^2*(C9*

        CI1+CI10*RHOPX)*(C9*CI1+CI3*RHOPX)+MV^2*(C10*CI1+CI2*RHOPX)*(C9*CI6-

        CI11*RHOPX)+MV^2*(C10*CI3-C9*CI2)*(C9*CI7-CI6*RHOPX)+(CI1*CI6+CI10*

        CI7)*(C10*C9*MV^2-CI3*(MP+MV))-(CI1*CI11+CI10*CI6)*(C10*RHOPX*MV^2+

        CI1*(MP+MV))-(CI11*CI7-CI6^2)*(C10^2*MV^2-CI2*(MP+MV)))
```

```
ALAT[1,2] =
```

```
-((CI10*(CI1*CI6+CI3*CI7)+CI6*(CI1*CI3+CI2*CI6)+CI11*(CI1
          ^2-CI2*CI7))*(NU6*(MP+MV)+FYP)-C9*CLA2*NU6*MV^2-MV*(CI10*(C9*CI1+CI3*
          RHOPX)-CI11*(C10*CI1+CI2*RHOPX)-CI6*(C10*CI3-C9*CI2))*(MV*NU6*RHOPX+
          NP+RAP1*FYP)-MV*(CI11*(C10*CI7+CI1*RHOPX)-CI6*(C10*CI6+C9*CI1)-CI10*(
          C9*CI7-CI6*RHOPX))*(LP-C10*MV*NU6-RAP3*FYP))/(MV^2*(C9*CI1+CI10*RHOPX
          )*(C9*CI1+CI3*RHOPX)+MV^2*(C10*CI1+CI2*RHOPX)*(C9*CI6-CI11*RHOPX)+MV^
          2*(C10*CI3-C9*CI2)*(C9*CI7-CI6*RHOPX)+(CI1*CI6+CI10*CI7)*(C10*C9*MV^2
          -CI3*(MP+MV))-(CI1*CI11+CI10*CI6)*(C10*RHOPX*MV^2+CI1*(MP+MV))-(CI11*
          CI7-CI6^2)*(C10^2*MV^2-CI2*(MP+MV)))


ALAT[1,3] =

((CI10*(CI1*CI6+CI3*CI7)+CI6*(CI1*CI3+CI2*CI6)+CI11*(CI1^
          2-CI2*CI7))*(NU4*(MP+MV)-FYR)+MV*(CI11*(C10*CI7+CI1*RHOPX)-CI6*(C10*
          CI6+C9*CI1)-CI10*(C9*CI7-CI6*RHOPX))*(C10*MV*NU4+LR-RAP3*FYR)-C9*CLA2
          *NU4*MV^2-MV*(CI10*(C9*CI1+CI3*RHOPX)-CI11*(C10*CI1+CI2*RHOPX)-CI6*(
          C10*CI3-C9*CI2))*(MV*NU4*RHOPX-NR-RAP1*FYR))/(MV^2*(C9*CI1+CI10*RHOPX
          )*(C9*CI1+CI3*RHOPX)+MV^2*(C10*CI1+CI2*RHOPX)*(C9*CI6-CI11*RHOPX)+MV^
          2*(C10*CI3-C9*CI2)*(C9*CI7-CI6*RHOPX)+(CI1*CI6+CI10*CI7)*(C10*C9*MV^2
          -CI3*(MP+MV))-(CI1*CI11+CI10*CI6)*(C10*RHOPX*MV^2+CI1*(MP+MV))-(CI11*
          CI7-CI6^2)*(C10^2*MV^2-CI2*(MP+MV)))


ALAT[1,4] =

-G*COS(NQ2)*((MP+MV)*(CI10*(CI1*CI6+CI3*CI7)+CI6*(CI1*CI3
          +CI2*CI6)+CI11*(CI1^2-CI2*CI7))+C10*MV^2*(CI11*(C10*CI7+CI1*RHOPX)-
          CI6*(C10*CI6+C9*CI1)-CI10*(C9*CI7-CI6*RHOPX))-C9*CLA2*MV^2-RHOPX*MV^2
          *(CI10*(C9*CI1+CI3*RHOPX)-CI11*(C10*CI1+CI2*RHOPX)-CI6*(C10*CI3-C9*
          CI2)))/(MV^2*(C9*CI1+CI10*RHOPX)*(C9*CI1+CI3*RHOPX)+MV^2*(C10*CI1+CI2
          *RHOPX)*(C9*CI6-CI11*RHOPX)+MV^2*(C10*CI3-C9*CI2)*(C9*CI7-CI6*RHOPX)+
```

```
                   (CI1*CI6+CI10*CI7)*(C10*C9*MV^2-CI3*(MP+MV))-(CI1*CI11+CI10*CI6)*(C10
                   *RHOPX*MV^2+CI1*(MP+MV))-(CI11*CI7-CI6^2)*(C10^2*MV^2-CI2*(MP+MV)))


ALAT[1,5] =

D8*MV*(CI10*(CI1*CI6+CI3*CI7)+CI6*(CI1*CI3+CI2*CI6)+CI11*
                   (CI1^2-CI2*CI7)+C10*MV*(CI11*(C10*CI7+CI1*RHOPX)-CI6*(C10*CI6+C9*CI1)
                   -CI10*(C9*CI7-CI6*RHOPX))-C9*CLA2*MV-MV*RHOPX*(CI10*(C9*CI1+CI3*RHOPX
                   )-CI11*(C10*CI1+CI2*RHOPX)-CI6*(C10*CI3-C9*CI2)))/(MV^2*(C9*CI1+CI10*
                   RHOPX)*(C9*CI1+CI3*RHOPX)+MV^2*(C10*CI1+CI2*RHOPX)*(C9*CI6-CI11*RHOPX
                   )+MV^2*(C10*CI3-C9*CI2)*(C9*CI7-CI6*RHOPX)+(CI1*CI6+CI10*CI7)*(C10*
                   C9*MV^2-CI3*(MP+MV))-(CI1*CI11+CI10*CI6)*(C10*RHOPX*MV^2+CI1*(MP+MV))
                   -(CI11*CI7-CI6^2)*(C10^2*MV^2-CI2*(MP+MV)))


ALAT[1,6] =

-(CF1*(CI10*(CI1*CI6+CI3*CI7)+CI6*(CI1*CI3+CI2*CI6)+CI11*
                   (CI1^2-CI2*CI7))+MV*(CI11*(C10*CI7+CI1*RHOPX)-CI6*(C10*CI6+C9*CI1)-
                   CI10*(C9*CI7-CI6*RHOPX))*(CT1-C13*C4*B^2*TAN(NQ8)/(H*(RHOVX^2+RHOVZ^2
                   ))-C13*RHOPZ*(RHOVX*COS(NQ8)+RHOVZ*SIN(NQ8))/(RHOVX^2+RHOVZ^2))-CLA2*
                   MV*(C9*G*MV*SIN(NQ2)+C13*C4*B^2/(H*COS(NQ8)*(RHOVX^2+RHOVZ^2)))-MV*(
                   CI10*(C9*CI1+CI3*RHOPX)-CI11*(C10*CI1+CI2*RHOPX)-CI6*(C10*CI3-C9*CI2)
                   )*(NFAV1*RHOPX*COS(NQ8)+NFAV3*RHOPX*SIN(NQ8)+C13*C4*B^2/(H*(RHOVX^2+
                   RHOVZ^2))-C13*RHOPX*(RHOVX*COS(NQ8)+RHOVZ*SIN(NQ8))/(RHOVX^2+RHOVZ^2)
                   ))/(MV^2*(C9*CI1+CI10*RHOPX)*(C9*CI1+CI3*RHOPX)+MV^2*(C10*CI1+CI2*RH
                   OPX)*(C9*CI6-CI11*RHOPX)+MV^2*(C10*CI3-C9*CI2)*(C9*CI7-CI6*RHOPX)+(
                   CI1*CI6+CI10*CI7)*(C10*C9*MV^2-CI3*(MP+MV))-(CI1*CI11+CI10*CI6)*(C10*
                   RHOPX*MV^2+CI1*(MP+MV))-(CI11*CI7-CI6^2)*(C10^2*MV^2-CI2*(MP+MV)))


ALAT[2,1] =
```

```
(CLA6*MV*FYV-CLA7*(NV+RAP1*FYV)-(C9*MV^2*(C9*CI7-CI6*RHO
        PX)-CI11*(CI7*(MP+MV)-MV^2*RHOPX^2)-CI6*(C9*RHOPX*MV^2-CI6*(MP+MV)))*
        (LV-RAP3*FYV))/(MV^2*(C9*CI1+CI10*RHOPX)*(C9*CI1+CI3*RHOPX)+MV^2*(C10
        *CI1+CI2*RHOPX)*(C9*CI6-CI11*RHOPX)+MV^2*(C10*CI3-C9*CI2)*(C9*CI7-CI6
        *RHOPX)+(CI1*CI6+CI10*CI7)*(C10*C9*MV^2-CI3*(MP+MV))-(CI1*CI11+CI10*
        CI6)*(C10*RHOPX*MV^2+CI1*(MP+MV))-(CI11*CI7-CI6^2)*(C10^2*MV^2-CI2*(
        MP+MV)))
```

ALAT[2,2] =
```
(C9*MV*NU6*(CI6*(C10*RHOPX*MV^2+CI1*(MP+MV))-RHOPX*MV^2*(
        C9*CI1+CI3*RHOPX)-CI7*(C10*C9*MV^2-CI3*(MP+MV)))+CLA6*MV*(NU6*(MP+MV)
        +FYP)-CLA7*(MV*NU6*RHOPX+NP+RAP1*FYP)-(C9*MV^2*(C9*CI7-CI6*RHOPX)-CI
        11*(CI7*(MP+MV)-MV^2*RHOPX^2)-CI6*(C9*RHOPX*MV^2-CI6*(MP+MV)))*(LP-
        C10*MV*NU6-RAP3*FYP))/(MV^2*(C9*CI1+CI10*RHOPX)*(C9*CI1+CI3*RHOPX)+
        MV^2*(C10*CI1+CI2*RHOPX)*(C9*CI6-CI11*RHOPX)+MV^2*(C10*CI3-C9*CI2)*(
        C9*CI7-CI6*RHOPX)+(CI1*CI6+CI10*CI7)*(C10*C9*MV^2-CI3*(MP+MV))-(CI1*
        CI11+CI10*CI6)*(C10*RHOPX*MV^2+CI1*(MP+MV))-(CI11*CI7-CI6^2)*(C10^2*
        MV^2-CI2*(MP+MV)))
```

ALAT[2,3] =
```
(CLA7*(MV*NU4*RHOPX-NR-RAP1*FYR)-C9*MV*NU4*(CI6*(C10*RHO
        PX*MV^2+CI1*(MP+MV))-RHOPX*MV^2*(C9*CI1+CI3*RHOPX)-CI7*(C10*C9*MV^2-
        CI3*(MP+MV)))-CLA6*MV*(NU4*(MP+MV)-FYR)-(C9*MV^2*(C9*CI7-CI6*RHOPX)-
        CI11*(CI7*(MP+MV)-MV^2*RHOPX^2)-CI6*(C9*RHOPX*MV^2-CI6*(MP+MV)))*(C10
        *MV*NU4+LR-RAP3*FYR))/(MV^2*(C9*CI1+CI10*RHOPX)*(C9*CI1+CI3*RHOPX)+
        MV^2*(C10*CI1+CI2*RHOPX)*(C9*CI6-CI11*RHOPX)+MV^2*(C10*CI3-C9*CI2)*(
        C9*CI7-CI6*RHOPX)+(CI1*CI6+CI10*CI7)*(C10*C9*MV^2-CI3*(MP+MV))-(CI1*
        CI11+CI10*CI6)*(C10*RHOPX*MV^2+CI1*(MP+MV))-(CI11*CI7-CI6^2)*(C10^2*
```

```
           MV^2-CI2*(MP+MV)))


ALAT[2,4] =

-G*MV*COS(NQ2)*(CLA7*RHOPX-CLA6*(MP+MV)-C9*(CI6*(C10*RHO
           PX*MV^2+CI1*(MP+MV))-RHOPX*MV^2*(C9*CI1+CI3*RHOPX)-CI7*(C10*C9*MV^2-
           CI3*(MP+MV)))-C10*(C9*MV^2*(C9*CI7-CI6*RHOPX)-CI11*(CI7*(MP+MV)-MV^2*
           RHOPX^2)-CI6*(C9*RHOPX*MV^2-CI6*(MP+MV))))/(MV^2*(C9*CI1+CI10*RHOPX)*
           (C9*CI1+CI3*RHOPX)+MV^2*(C10*CI1+CI2*RHOPX)*(C9*CI6-CI11*RHOPX)+MV^2*
           (C10*CI3-C9*CI2)*(C9*CI7-CI6*RHOPX)+(CI1*CI6+CI10*CI7)*(C10*C9*MV^2-
           CI3*(MP+MV))-(CI1*CI11+CI10*CI6)*(C10*RHOPX*MV^2+CI1*(MP+MV))-(CI11*
           CI7-CI6^2)*(C10^2*MV^2-CI2*(MP+MV)))


ALAT[2,5] =

D8*MV*(CLA7*RHOPX-CLA6*MV-C9*(CI6*(C10*RHOPX*MV^2+CI1*(
           MP+MV))-RHOPX*MV^2*(C9*CI1+CI3*RHOPX)-CI7*(C10*C9*MV^2-CI3*(MP+MV)))-
           C10*(C9*MV^2*(C9*CI7-CI6*RHOPX)-CI11*(CI7*(MP+MV)-MV^2*RHOPX^2)-CI6*(
           C9*RHOPX*MV^2-CI6*(MP+MV))))/(MV^2*(C9*CI1+CI10*RHOPX)*(C9*CI1+CI3*
           RHOPX)+MV^2*(C10*CI1+CI2*RHOPX)*(C9*CI6-CI11*RHOPX)+MV^2*(C10*CI3-C9*
           CI2)*(C9*CI7-CI6*RHOPX)+(CI1*CI6+CI10*CI7)*(C10*C9*MV^2-CI3*(MP+MV))-
           (CI1*CI11+CI10*CI6)*(C10*RHOPX*MV^2+CI1*(MP+MV))-(CI11*CI7-CI6^2)*(
           C10^2*MV^2-CI2*(MP+MV)))


ALAT[2,6] =

-(CLA7*(NFAV1*RHOPX*COS(NQ8)+NFAV3*RHOPX*SIN(NQ8)+C13*C4*
           B^2/(H*(RHOVX^2+RHOVZ^2))-C13*RHOPX*(RHOVX*COS(NQ8)+RHOVZ*SIN(NQ8))/(
           RHOVX^2+RHOVZ^2))-CF1*CLA6*MV-(C9*G*MV*SIN(NQ2)+C13*C4*B^2/(H*COS(NQ8
           )*(RHOVX^2+RHOVZ^2)))*(CI6*(C10*RHOPX*MV^2+CI1*(MP+MV))-RHOPX*MV^2*(
           C9*CI1+CI3*RHOPX)-CI7*(C10*C9*MV^2-CI3*(MP+MV)))-(C9*MV^2*(C9*CI7-CI6
```

```
        *RHOPX)-CI11*(CI7*(MP+MV)-MV^2*RHOPX^2)-CI6*(C9*RHOPX*MV^2-CI6*(MP+

        MV)))*(CT1-C13*C4*B^2*TAN(NQ8)/(H*(RHOVX^2+RHOVZ^2))-C13*RHOPZ*(RHOVX

        *COS(NQ8)+RHOVZ*SIN(NQ8))/(RHOVX^2+RHOVZ^2)))/(MV^2*(C9*CI1+CI10*RHO

        PX)*(C9*CI1+CI3*RHOPX)+MV^2*(C10*CI1+CI2*RHOPX)*(C9*CI6-CI11*RHOPX)+

        MV^2*(C10*CI3-C9*CI2)*(C9*CI7-CI6*RHOPX)+(CI1*CI6+CI10*CI7)*(C10*C9*

        MV^2-CI3*(MP+MV))-(CI1*CI11+CI10*CI6)*(C10*RHOPX*MV^2+CI1*(MP+MV))-(

        CI11*CI7-CI6^2)*(C10^2*MV^2-CI2*(MP+MV)))
```

ALAT[3,1] =

```
(MV*(C9*(CI1*CI3+CI2*CI6)-CI11*(C10*CI1+CI2*RHOPX)-CI10*(

        C10*CI6-CI3*RHOPX))*FYV+(C9*MV^2*(C10*CI3-C9*CI2)+CI10*(C10*C9*MV^2-

        CI3*(MP+MV))-CI11*(C10^2*MV^2-CI2*(MP+MV)))*(NV+RAP1*FYV)-(CI11*(C10*

        RHOPX*MV^2+CI1*(MP+MV))-C9*MV^2*(C10*CI6+C9*CI1)-CI10*(C9*RHOPX*MV^2-

        CI6*(MP+MV)))*(LV-RAP3*FYV))/(MV^2*(C9*CI1+CI10*RHOPX)*(C9*CI1+CI3*

        RHOPX)+MV^2*(C10*CI1+CI2*RHOPX)*(C9*CI6-CI11*RHOPX)+MV^2*(C10*CI3-C9*

        CI2)*(C9*CI7-CI6*RHOPX)+(CI1*CI6+CI10*CI7)*(C10*C9*MV^2-CI3*(MP+MV))-

        (CI1*CI11+CI10*CI6)*(C10*RHOPX*MV^2+CI1*(MP+MV))-(CI11*CI7-CI6^2)*(

        C10^2*MV^2-CI2*(MP+MV)))
```

ALAT[3,2] =

```
(MV*(C9*(CI1*CI3+CI2*CI6)-CI11*(C10*CI1+CI2*RHOPX)-CI10*(

        C10*CI6-CI3*RHOPX))*(NU6*(MP+MV)+FYP)+(C9*MV^2*(C10*CI3-C9*CI2)+CI10*

        (C10*C9*MV^2-CI3*(MP+MV))-CI11*(C10^2*MV^2-CI2*(MP+MV)))*(MV*NU6*RHO

        PX+NP+RAP1*FYP)-C9*MV*NU6*(RHOPX*MV^2*(C10*CI3-C9*CI2)-CI1*(C10*C9*

        MV^2-CI3*(MP+MV))-CI6*(C10^2*MV^2-CI2*(MP+MV)))-(CI11*(C10*RHOPX*MV^2

        +CI1*(MP+MV))-C9*MV^2*(C10*CI6+C9*CI1)-CI10*(C9*RHOPX*MV^2-CI6*(MP+

        MV)))*(LP-C10*MV*NU6-RAP3*FYP))/(MV^2*(C9*CI1+CI10*RHOPX)*(C9*CI1+CI3

        *RHOPX)+MV^2*(C10*CI1+CI2*RHOPX)*(C9*CI6-CI11*RHOPX)+MV^2*(C10*CI3-
```

```
          C9*CI2)*(C9*CI7-CI6*RHOPX)+(CI1*CI6+CI10*CI7)*(C10*C9*MV^2-CI3*(MP+

          MV))-(CI1*CI11+CI10*CI6)*(C10*RHOPX*MV^2+CI1*(MP+MV))-(CI11*CI7-CI6^2

          )*(C10^2*MV^2-CI2*(MP+MV)))
```

```
ALAT[3,3] =
(C9*MV*NU4*(RHOPX*MV^2*(C10*CI3-C9*CI2)-CI1*(C10*C9*MV^2-

          CI3*(MP+MV))-CI6*(C10^2*MV^2-CI2*(MP+MV)))-MV*(C9*(CI1*CI3+CI2*CI6)-

          CI11*(C10*CI1+CI2*RHOPX)-CI10*(C10*CI6-CI3*RHOPX))*(NU4*(MP+MV)-FYR)-

          (CI11*(C10*RHOPX*MV^2+CI1*(MP+MV))-C9*MV^2*(C10*CI6+C9*CI1)-CI10*(C9*

          RHOPX*MV^2-CI6*(MP+MV)))*(C10*MV*NU4+LR-RAP3*FYR)-(C9*MV^2*(C10*CI3-

          C9*CI2)+CI10*(C10*C9*MV^2-CI3*(MP+MV))-CI11*(C10^2*MV^2-CI2*(MP+MV)))

          *(MV*NU4*RHOPX-NR-RAP1*FYR))/(MV^2*(C9*CI1+CI10*RHOPX)*(C9*CI1+CI3*

          RHOPX)+MV^2*(C10*CI1+CI2*RHOPX)*(C9*CI6-CI11*RHOPX)+MV^2*(C10*CI3-C9*

          CI2)*(C9*CI7-CI6*RHOPX)+(CI1*CI6+CI10*CI7)*(C10*C9*MV^2-CI3*(MP+MV))-

          (CI1*CI11+CI10*CI6)*(C10*RHOPX*MV^2+CI1*(MP+MV))-(CI11*CI7-CI6^2)*(

          C10^2*MV^2-CI2*(MP+MV)))
```

```
ALAT[3,4] =
G*MV*COS(NQ2)*((MP+MV)*(C9*(CI1*CI3+CI2*CI6)-CI11*(C10*

          CI1+CI2*RHOPX)-CI10*(C10*CI6-CI3*RHOPX))+C10*(CI11*(C10*RHOPX*MV^2+

          CI1*(MP+MV))-C9*MV^2*(C10*CI6+C9*CI1)-CI10*(C9*RHOPX*MV^2-CI6*(MP+MV)

          ))+RHOPX*(C9*MV^2*(C10*CI3-C9*CI2)+CI10*(C10*C9*MV^2-CI3*(MP+MV))-CI

          11*(C10^2*MV^2-CI2*(MP+MV)))-C9*(RHOPX*MV^2*(C10*CI3-C9*CI2)-CI1*(C10

          *C9*MV^2-CI3*(MP+MV))-CI6*(C10^2*MV^2-CI2*(MP+MV))))/(MV^2*(C9*CI1+

          CI10*RHOPX)*(C9*CI1+CI3*RHOPX)+MV^2*(C10*CI1+CI2*RHOPX)*(C9*CI6-CI11*

          RHOPX)+MV^2*(C10*CI3-C9*CI2)*(C9*CI7-CI6*RHOPX)+(CI1*CI6+CI10*CI7)*(

          C10*C9*MV^2-CI3*(MP+MV))-(CI1*CI11+CI10*CI6)*(C10*RHOPX*MV^2+CI1*(MP+

          MV))-(CI11*CI7-CI6^2)*(C10^2*MV^2-CI2*(MP+MV)))
```

```
ALAT[3,5] =

-D8*MV*(MV*(C9*(CI1*CI3+CI2*CI6)-CI11*(C10*CI1+CI2*RHOPX)

          -CI10*(C10*CI6-CI3*RHOPX))+C10*(CI11*(C10*RHOPX*MV^2+CI1*(MP+MV))-C9*

          MV^2*(C10*CI6+C9*CI1)-CI10*(C9*RHOPX*MV^2-CI6*(MP+MV)))+RHOPX*(C9*MV^

          2*(C10*CI3-C9*CI2)+CI10*(C10*C9*MV^2-CI3*(MP+MV))-CI11*(C10^2*MV^2-

          CI2*(MP+MV)))-C9*(RHOPX*MV^2*(C10*CI3-C9*CI2)-CI1*(C10*C9*MV^2-CI3*(

          MP+MV))-CI6*(C10^2*MV^2-CI2*(MP+MV))))/(MV^2*(C9*CI1+CI10*RHOPX)*(C9*

          CI1+CI3*RHOPX)+MV^2*(C10*CI1+CI2*RHOPX)*(C9*CI6-CI11*RHOPX)+MV^2*(C10

          *CI3-C9*CI2)*(C9*CI7-CI6*RHOPX)+(CI1*CI6+CI10*CI7)*(C10*C9*MV^2-CI3*(

          MP+MV))-(CI1*CI11+CI10*CI6)*(C10*RHOPX*MV^2+CI1*(MP+MV))-(CI11*CI7-

          CI6^2)*(C10^2*MV^2-CI2*(MP+MV)))


ALAT[3,6] =

-((C9*G*MV*SIN(NQ2)+C13*C4*B^2/(H*COS(NQ8)*(RHOVX^2+RHOVZ

          ^2)))*(RHOPX*MV^2*(C10*CI3-C9*CI2)-CI1*(C10*C9*MV^2-CI3*(MP+MV))-CI6*

          (C10^2*MV^2-CI2*(MP+MV)))-CF1*MV*(C9*(CI1*CI3+CI2*CI6)-CI11*(C10*CI1+

          CI2*RHOPX)-CI10*(C10*CI6-CI3*RHOPX))-(CI11*(C10*RHOPX*MV^2+CI1*(MP+

          MV))-C9*MV^2*(C10*CI6+C9*CI1)-CI10*(C9*RHOPX*MV^2-CI6*(MP+MV)))*(CT1-

          C13*C4*B^2*TAN(NQ8)/(H*(RHOVX^2+RHOVZ^2))-C13*RHOPZ*(RHOVX*COS(NQ8)+

          RHOVZ*SIN(NQ8))/(RHOVX^2+RHOVZ^2))-(C9*MV^2*(C10*CI3-C9*CI2)+CI10*(

          C10*C9*MV^2-CI3*(MP+MV))-CI11*(C10^2*MV^2-CI2*(MP+MV)))*(NFAV1*RHOPX*

          COS(NQ8)+NFAV3*RHOPX*SIN(NQ8)+C13*C4*B^2/(H*(RHOVX^2+RHOVZ^2))-C13*

          RHOPX*(RHOVX*COS(NQ8)+RHOVZ*SIN(NQ8))/(RHOVX^2+RHOVZ^2)))/(MV^2*(C9*

          CI1+CI10*RHOPX)*(C9*CI1+CI3*RHOPX)+MV^2*(C10*CI1+CI2*RHOPX)*(C9*CI6-

          CI11*RHOPX)+MV^2*(C10*CI3-C9*CI2)*(C9*CI7-CI6*RHOPX)+(CI1*CI6+CI10*

          CI7)*(C10*C9*MV^2-CI3*(MP+MV))-(CI1*CI11+CI10*CI6)*(C10*RHOPX*MV^2+

          CI1*(MP+MV))-(CI11*CI7-CI6^2)*(C10^2*MV^2-CI2*(MP+MV)))
```

```
ALAT[4,1] = 0 ALAT[4,2] = 1 ALAT[4,3] = TAN(NQ2) ALAT[4,4] = 0

ALAT[4,5] = 0 ALAT[4,6] = 0 ALAT[5,1] =

-(MV*(CI10*(C10*CI7+CI1*RHOPX)+CI6*(C10*CI1+CI2*RHOPX)+

         C9*(CI1^2-CI2*CI7))*FYV-(CI10*(C10*RHOPX*MV^2+CI1*(MP+MV))-C9*MV^2*(

         C10*CI1+CI2*RHOPX)-CI6*(C10^2*MV^2-CI2*(MP+MV)))*(NV+RAP1*FYV)-(C9*

         MV^2*(C10*CI7+CI1*RHOPX)-CI6*(C10*RHOPX*MV^2+CI1*(MP+MV))-CI10*(CI7*(

         MP+MV)-MV^2*RHOPX^2))*(LV-RAP3*FYV))/(MV^2*(C9*CI1+CI10*RHOPX)*(C9*

         CI1+CI3*RHOPX)+MV^2*(C10*CI1+CI2*RHOPX)*(C9*CI6-CI11*RHOPX)+MV^2*(C10

         *CI3-C9*CI2)*(C9*CI7-CI6*RHOPX)+(CI1*CI6+CI10*CI7)*(C10*C9*MV^2-CI3*(

         MP+MV))-(CI1*CI11+CI10*CI6)*(C10*RHOPX*MV^2+CI1*(MP+MV))-(CI11*CI7-

         CI6^2)*(C10^2*MV^2-CI2*(MP+MV)))


ALAT[5,2] =

-(MV*(CI10*(C10*CI7+CI1*RHOPX)+CI6*(C10*CI1+CI2*RHOPX)+

         C9*(CI1^2-CI2*CI7))*(NU6*(MP+MV)+FYP)-C9*MV*NU6*(RHOPX*MV^2*(C10*CI1+

         CI2*RHOPX)+CI1*(C10*RHOPX*MV^2+CI1*(MP+MV))+CI7*(C10^2*MV^2-CI2*(MP+

         MV)))-(CI10*(C10*RHOPX*MV^2+CI1*(MP+MV))-C9*MV^2*(C10*CI1+CI2*RHOPX)-

         CI6*(C10^2*MV^2-CI2*(MP+MV)))*(MV*NU6*RHOPX+NP+RAP1*FYP)-(C9*MV^2*(

         C10*CI7+CI1*RHOPX)-CI6*(C10*RHOPX*MV^2+CI1*(MP+MV))-CI10*(CI7*(MP+MV)

         -MV^2*RHOPX^2))*(LP-C10*MV*NU6-RAP3*FYP))/(MV^2*(C9*CI1+CI10*RHOPX)*(

         C9*CI1+CI3*RHOPX)+MV^2*(C10*CI1+CI2*RHOPX)*(C9*CI6-CI11*RHOPX)+MV^2*(

         C10*CI3-C9*CI2)*(C9*CI7-CI6*RHOPX)+(CI1*CI6+CI10*CI7)*(C10*C9*MV^2-

         CI3*(MP+MV))-(CI1*CI11+CI10*CI6)*(C10*RHOPX*MV^2+CI1*(MP+MV))-(CI11*

         CI7-CI6^2)*(C10^2*MV^2-CI2*(MP+MV)))


ALAT[5,3] =

(MV*(CI10*(C10*CI7+CI1*RHOPX)+CI6*(C10*CI1+CI2*RHOPX)+C9*
```

```
        (CI1^2-CI2*CI7))*(NU4*(MP+MV)-FYR)+(C9*MV^2*(C10*CI7+CI1*RHOPX)-CI6*(

        C10*RHOPX*MV^2+CI1*(MP+MV))-CI10*(CI7*(MP+MV)-MV^2*RHOPX^2))*(C10*MV*

        NU4+LR-RAP3*FYR)-C9*MV*NU4*(RHOPX*MV^2*(C10*CI1+CI2*RHOPX)+CI1*(C10*

        RHOPX*MV^2+CI1*(MP+MV))+CI7*(C10^2*MV^2-CI2*(MP+MV)))-(CI10*(C10*RHO

        PX*MV^2+CI1*(MP+MV))-C9*MV^2*(C10*CI1+CI2*RHOPX)-CI6*(C10^2*MV^2-CI2*

        (MP+MV)))*(MV*NU4*RHOPX-NR-RAP1*FYR))/(MV^2*(C9*CI1+CI10*RHOPX)*(C9*

        CI1+CI3*RHOPX)+MV^2*(C10*CI1+CI2*RHOPX)*(C9*CI6-CI11*RHOPX)+MV^2*(C10

        *CI3-C9*CI2)*(C9*CI7-CI6*RHOPX)+(CI1*CI6+CI10*CI7)*(C10*C9*MV^2-CI3*(

        MP+MV))-(CI1*CI11+CI10*CI6)*(C10*RHOPX*MV^2+CI1*(MP+MV))-(CI11*CI7-

        CI6^2)*(C10^2*MV^2-CI2*(MP+MV)))


ALAT[5,4] =

-G*MV*COS(NQ2)*((MP+MV)*(CI10*(C10*CI7+CI1*RHOPX)+CI6*(

        C10*CI1+CI2*RHOPX)+C9*(CI1^2-CI2*CI7))+C10*(C9*MV^2*(C10*CI7+CI1*RHO

        PX)-CI6*(C10*RHOPX*MV^2+CI1*(MP+MV))-CI10*(CI7*(MP+MV)-MV^2*RHOPX^2))

        -C9*(RHOPX*MV^2*(C10*CI1+CI2*RHOPX)+CI1*(C10*RHOPX*MV^2+CI1*(MP+MV))+

        CI7*(C10^2*MV^2-CI2*(MP+MV)))-RHOPX*(CI10*(C10*RHOPX*MV^2+CI1*(MP+MV)

        )-C9*MV^2*(C10*CI1+CI2*RHOPX)-CI6*(C10^2*MV^2-CI2*(MP+MV))))/(MV^2*(

        C9*CI1+CI10*RHOPX)*(C9*CI1+CI3*RHOPX)+MV^2*(C10*CI1+CI2*RHOPX)*(C9*

        CI6-CI11*RHOPX)+MV^2*(C10*CI3-C9*CI2)*(C9*CI7-CI6*RHOPX)+(CI1*CI6+CI

        10*CI7)*(C10*C9*MV^2-CI3*(MP+MV))-(CI1*CI11+CI10*CI6)*(C10*RHOPX*MV^2

        +CI1*(MP+MV))-(CI11*CI7-CI6^2)*(C10^2*MV^2-CI2*(MP+MV)))


ALAT[5,5] =

D8*MV*(MV*(CI10*(C10*CI7+CI1*RHOPX)+CI6*(C10*CI1+CI2*RHO

        PX)+C9*(CI1^2-CI2*CI7))+C10*(C9*MV^2*(C10*CI7+CI1*RHOPX)-CI6*(C10*RH

        OPX*MV^2+CI1*(MP+MV))-CI10*(CI7*(MP+MV)-MV^2*RHOPX^2))-C9*(RHOPX*MV^2

        *(C10*CI1+CI2*RHOPX)+CI1*(C10*RHOPX*MV^2+CI1*(MP+MV))+CI7*(C10^2*MV^2
```

```
        -CI2*(MP+MV)))-RHOPX*(CI10*(C10*RHOPX*MV^2+CI1*(MP+MV))-C9*MV^2*(C10*

        CI1+CI2*RHOPX)-CI6*(C10^2*MV^2-CI2*(MP+MV))))/(MV^2*(C9*CI1+CI10*RHO

        PX)*(C9*CI1+CI3*RHOPX)+MV^2*(C10*CI1+CI2*RHOPX)*(C9*CI6-CI11*RHOPX)+

        MV^2*(C10*CI3-C9*CI2)*(C9*CI7-CI6*RHOPX)+(CI1*CI6+CI10*CI7)*(C10*C9*

        MV^2-CI3*(MP+MV))-(CI1*CI11+CI10*CI6)*(C10*RHOPX*MV^2+CI1*(MP+MV))-(

        CI11*CI7-CI6^2)*(C10^2*MV^2-CI2*(MP+MV)))


ALAT[5,6] =
-(CF1*MV*(CI10*(C10*CI7+CI1*RHOPX)+CI6*(C10*CI1+CI2*RHOPX

            )+C9*(CI1^2-CI2*CI7))+(C9*MV^2*(C10*CI7+CI1*RHOPX)-CI6*(C10*RHOPX*MV^

            2+CI1*(MP+MV))-CI10*(CI7*(MP+MV)-MV^2*RHOPX^2))*(CT1-C13*C4*B^2*TAN(

            NQ8)/(H*(RHOVX^2+RHOVZ^2))-C13*RHOPZ*(RHOVX*COS(NQ8)+RHOVZ*SIN(NQ8))/

            (RHOVX^2+RHOVZ^2))-(C9*G*MV*SIN(NQ2)+C13*C4*B^2/(H*COS(NQ8)*(RHOVX^2+

            RHOVZ^2)))*(RHOPX*MV^2*(C10*CI1+CI2*RHOPX)+CI1*(C10*RHOPX*MV^2+CI1*(

            MP+MV))+CI7*(C10^2*MV^2-CI2*(MP+MV)))-(CI10*(C10*RHOPX*MV^2+CI1*(MP+

            MV))-C9*MV^2*(C10*CI1+CI2*RHOPX)-CI6*(C10^2*MV^2-CI2*(MP+MV)))*(NFAV1

            *RHOPX*COS(NQ8)+NFAV3*RHOPX*SIN(NQ8)+C13*C4*B^2/(H*(RHOVX^2+RHOVZ^2))

            -C13*RHOPX*(RHOVX*COS(NQ8)+RHOVZ*SIN(NQ8))/(RHOVX^2+RHOVZ^2)))/(MV^2*

            (C9*CI1+CI10*RHOPX)*(C9*CI1+CI3*RHOPX)+MV^2*(C10*CI1+CI2*RHOPX)*(C9*

            CI6-CI11*RHOPX)+MV^2*(C10*CI3-C9*CI2)*(C9*CI7-CI6*RHOPX)+(CI1*CI6+CI

            10*CI7)*(C10*C9*MV^2-CI3*(MP+MV))-(CI1*CI11+CI10*CI6)*(C10*RHOPX*MV^2

            +CI1*(MP+MV))-(CI11*CI7-CI6^2)*(C10^2*MV^2-CI2*(MP+MV)))


ALAT[6,1] = 0 ALAT[6,2] = -TAN(NQ8) ALAT[6,3] = -1 ALAT[6,4] = 0
ALAT[6,5] = 1/COS(NQ8) ALAT[6,6] = 0


BLAT[1] =
-((CI10*(CI1*CI6+CI3*CI7)+CI6*(CI1*CI3+CI2*CI6)+CI11*(CI1^2
```

```
     -CI2*CI7))*FYDR-MV*(CI10*(C9*CI1+CI3*RHOPX)-CI11*(C10*CI1+CI2*RHOPX)-
     CI6*(C10*CI3-C9*CI2))*(NDR+RAP1*FYDR)-MV*(CI11*(C10*CI7+CI1*RHOPX)-
     CI6*(C10*CI6+C9*CI1)-CI10*(C9*CI7-CI6*RHOPX))*(LDR-RAP3*FYDR))/(MV^2*
     (C9*CI1+CI10*RHOPX)*(C9*CI1+CI3*RHOPX)+MV^2*(C10*CI1+CI2*RHOPX)*(C9*
     CI6-CI11*RHOPX)+MV^2*(C10*CI3-C9*CI2)*(C9*CI7-CI6*RHOPX)+(CI1*CI6+CI
     10*CI7)*(C10*C9*MV^2-CI3*(MP+MV))-(CI1*CI11+CI10*CI6)*(C10*RHOPX*MV^2
     +CI1*(MP+MV))-(CI11*CI7-CI6^2)*(C10^2*MV^2-CI2*(MP+MV)))


BLAT[2] =
(MV*(CI11*(C10*CI7+CI1*RHOPX)-C9*(CI1*CI6+CI3*CI7)-CI6*(C10
          *CI6-CI3*RHOPX))*FYDR-(CI11*(C10*RHOPX*MV^2+CI1*(MP+MV))-C9*MV^2*(C9*
          CI1+CI3*RHOPX)-CI6*(C10*C9*MV^2-CI3*(MP+MV)))*(NDR+RAP1*FYDR)-(C9*MV^
          2*(C9*CI7-CI6*RHOPX)-CI11*(CI7*(MP+MV)-MV^2*RHOPX^2)-CI6*(C9*RHOPX*
          MV^2-CI6*(MP+MV)))*(LDR-RAP3*FYDR))/(MV^2*(C9*CI1+CI10*RHOPX)*(C9*CI1
          +CI3*RHOPX)+MV^2*(C10*CI1+CI2*RHOPX)*(C9*CI6-CI11*RHOPX)+MV^2*(C10*
          CI3-C9*CI2)*(C9*CI7-CI6*RHOPX)+(CI1*CI6+CI10*CI7)*(C10*C9*MV^2-CI3*(
          MP+MV))-(CI1*CI11+CI10*CI6)*(C10*RHOPX*MV^2+CI1*(MP+MV))-(CI11*CI7-
          CI6^2)*(C10^2*MV^2-CI2*(MP+MV)))


BLAT[3] =
(MV*(C9*(CI1*CI3+CI2*CI6)-CI11*(C10*CI1+CI2*RHOPX)-CI10*(
          C10*CI6-CI3*RHOPX))*FYDR+(C9*MV^2*(C10*CI3-C9*CI2)+CI10*(C10*C9*MV^2-
          CI3*(MP+MV))-CI11*(C10^2*MV^2-CI2*(MP+MV)))*(NDR+RAP1*FYDR)-(CI11*(
          C10*RHOPX*MV^2+CI1*(MP+MV))-C9*MV^2*(C10*CI6+C9*CI1)-CI10*(C9*RHOPX*
          MV^2-CI6*(MP+MV)))*(LDR-RAP3*FYDR))/(MV^2*(C9*CI1+CI10*RHOPX)*(C9*CI1
          +CI3*RHOPX)+MV^2*(C10*CI1+CI2*RHOPX)*(C9*CI6-CI11*RHOPX)+MV^2*(C10*
          CI3-C9*CI2)*(C9*CI7-CI6*RHOPX)+(CI1*CI6+CI10*CI7)*(C10*C9*MV^2-CI3*(
          MP+MV))-(CI1*CI11+CI10*CI6)*(C10*RHOPX*MV^2+CI1*(MP+MV))-(CI11*CI7-
```

```
        CI6^2)*(C10^2*MV^2-CI2*(MP+MV)))


BLAT[4] = 0 BLAT[5] =

-(MV*(CI10*(C10*CI7+CI1*RHOPX)+CI6*(C10*CI1+CI2*RHOPX)+C9*(

        CI1^2-CI2*CI7))*FYDR-(CI10*(C10*RHOPX*MV^2+CI1*(MP+MV))-C9*MV^2*(C10*

        CI1+CI2*RHOPX)-CI6*(C10^2*MV^2-CI2*(MP+MV)))*(NDR+RAP1*FYDR)-(C9*MV^2

        *(C10*CI7+CI1*RHOPX)-CI6*(C10*RHOPX*MV^2+CI1*(MP+MV))-CI10*(CI7*(MP+

        MV)-MV^2*RHOPX^2))*(LDR-RAP3*FYDR))/(MV^2*(C9*CI1+CI10*RHOPX)*(C9*CI1

        +CI3*RHOPX)+MV^2*(C10*CI1+CI2*RHOPX)*(C9*CI6-CI11*RHOPX)+MV^2*(C10*

        CI3-C9*CI2)*(C9*CI7-CI6*RHOPX)+(CI1*CI6+CI10*CI7)*(C10*C9*MV^2-CI3*(

        MP+MV))-(CI1*CI11+CI10*CI6)*(C10*RHOPX*MV^2+CI1*(MP+MV))-(CI11*CI7-

        CI6^2)*(C10^2*MV^2-CI2*(MP+MV)))


BLAT[6] = 0
```

APPENDIX D

PDS NONLINEAR SIMULATION[50]

Parafoil Dynamic Simulator (PDS) is originated from PARASIM that is a result of the Advanced Recovery System Guidance, Navigation and Control Model Development and Analysis Program developed by Boeing as a sub-contract of Pioneer Aerospace Corp. PARASIM is a high fidelity eight degrees-of-freedom two rigid body closed loop guidance, navigation and control (GN&C) computer simulation coded by standard Fortran-77. PARASIM simulates the flight of the Advanced Recovery System (ARS) parafoil and payload from steady glide after parafoil deployment, through the closed loop guided and controlled guide to a precise flared landing at the target.

NASA Johnson modified the PARASIM for X-38/CRV (Crew Return Vehicle) parafoil simulation for verifying the Parafoil Guidance Navigation & Control algorithm (PGNC). Mainly PDS has same structures of PARASIM, whereas the database is constructed for X-38/CRV parafoil and PGNC algorithm for X-38/CRV.

PDS simulates the flight of X-38/CRV parafoil from deploying stage, through steady glide and flare, to touchdown. The program feature an 8 degrees-of-freedom dynamics module linking two rigid bodies, the parafoil and the payload. The parafoil is modelled with 6 degrees-of-freedom and the payload rigid body may move relative to the parafoil rigid body in yaw and pitch about the load bar. The program was constructed using wind tunnel data, and validated by repeated drop test program of the scaled X-38/CRV. The simulation incorporates two-body dynamics, parafoil and payload aerodynamics, actuator and navigation sensor models, as well as guidance and control algorithms.

PDS used for the Buckeye simulation in this thesis is part of the PDS composed of two-body dynamics and their aerodynamics for open loop simulation. Guidance, navigation and control algorithms are deactivated for open loop simulation. During the Buckeye simulation it uses same aerodynamic database of the big parafoil for X-38/CRV with actual geometry of the Buckeye.

Input and Output of PDS The NAMELIST input is used for data initialization for PDS and the lists are summarized as follows:

- Start: Start-up state
- Sim: Simulation operations
- Design: Vehicle design parameters: weights, inertias, sizes, etc.
- Guid: Guidance mission data load parameters
- Nav: Guidance mission data load parameters
- Cont: Control mission data load parameters, winch parameters, manual control aray
- AeroPF: Parafoil aerodynamic coefficients
- AeroPL: Payload aerodynamics coefficients
- Winds: Wind and density dispersions

PDS outputs two trajectory text files such as PARA????.TRJ and PARA????.GGP where ???? is file name designator. Those are time history text files formatted for specific graphic plotter and lists. These output files can be converted to another format for a specific purpose.

VITA

Gi-Bong Hur, the first son of the late Sun Hur and Haengja Ko, was born on March 6, 1963 in Seogwipo, Korea. He has two sisters and a brother and married Eunju in 1992 and had a daughter Yoonjung in 1997 and a son Jaewon in 2001. He grew up in Seogwipo, Jeju and graduated from Namju High School in 1982. He attended Seoul National University and received a Bachelor of Science and Master degree in Industrial Engineering and Aerospace Engineering from Seoul National University, Korea in 1989. He was employed at the Agency for Defense Development in Korea as a senior research engineer, where he had been involved in the research of stability and control, simulation and flight test for the development of the basic and the advanced trainer aircraft from 1989 to 1999. He enrolled in the Department of Aerospace Engineering at Texas A&M University in College Station, Texas in 2000 and earned a Doctor of Philosophy degree in Aerospace Engineering from Texas A&M University in May 2005.

He can be reached at gbhur@yahoo.com. His permanent address is 115-101 Hyangchon Hyundai Apt., Dunsan-Dong, Seo-Ku, Daejeon, Korea.